



GENERATION GROWBOTS: MATERIALS, MECHANISMS, AND BIOMIMETIC DESIGN FOR GROWING ROBOTS

EDITED BY: Barbara Mazzolai, Ian Walker and Thomas Speck
PUBLISHED IN: Frontiers in Robotics and AI



frontiers

Frontiers eBook Copyright Statement

The copyright in the text of individual articles in this eBook is the property of their respective authors or their respective institutions or funders. The copyright in graphics and images within each article may be subject to copyright of other parties. In both cases this is subject to a license granted to Frontiers.

The compilation of articles constituting this eBook is the property of Frontiers.

Each article within this eBook, and the eBook itself, are published under the most recent version of the Creative Commons CC-BY licence.

The version current at the date of publication of this eBook is CC-BY 4.0. If the CC-BY licence is updated, the licence granted by Frontiers is automatically updated to the new version.

When exercising any right under the CC-BY licence, Frontiers must be attributed as the original publisher of the article or eBook, as applicable.

Authors have the responsibility of ensuring that any graphics or other materials which are the property of others may be included in the CC-BY licence, but this should be checked before relying on the CC-BY licence to reproduce those materials. Any copyright notices relating to those materials must be complied with.

Copyright and source acknowledgement notices may not be removed and must be displayed in any copy, derivative work or partial copy which includes the elements in question.

All copyright, and all rights therein, are protected by national and international copyright laws. The above represents a summary only. For further information please read Frontiers' Conditions for Website Use and Copyright Statement, and the applicable CC-BY licence.

ISSN 1664-8714

ISBN 978-2-88971-185-7

DOI 10.3389/978-2-88971-185-7

About Frontiers

Frontiers is more than just an open-access publisher of scholarly articles: it is a pioneering approach to the world of academia, radically improving the way scholarly research is managed. The grand vision of Frontiers is a world where all people have an equal opportunity to seek, share and generate knowledge. Frontiers provides immediate and permanent online open access to all its publications, but this alone is not enough to realize our grand goals.

Frontiers Journal Series

The Frontiers Journal Series is a multi-tier and interdisciplinary set of open-access, online journals, promising a paradigm shift from the current review, selection and dissemination processes in academic publishing. All Frontiers journals are driven by researchers for researchers; therefore, they constitute a service to the scholarly community. At the same time, the Frontiers Journal Series operates on a revolutionary invention, the tiered publishing system, initially addressing specific communities of scholars, and gradually climbing up to broader public understanding, thus serving the interests of the lay society, too.

Dedication to Quality

Each Frontiers article is a landmark of the highest quality, thanks to genuinely collaborative interactions between authors and review editors, who include some of the world's best academicians. Research must be certified by peers before entering a stream of knowledge that may eventually reach the public - and shape society; therefore, Frontiers only applies the most rigorous and unbiased reviews.

Frontiers revolutionizes research publishing by freely delivering the most outstanding research, evaluated with no bias from both the academic and social point of view. By applying the most advanced information technologies, Frontiers is catapulting scholarly publishing into a new generation.

What are Frontiers Research Topics?

Frontiers Research Topics are very popular trademarks of the Frontiers Journals Series: they are collections of at least ten articles, all centered on a particular subject. With their unique mix of varied contributions from Original Research to Review Articles, Frontiers Research Topics unify the most influential researchers, the latest key findings and historical advances in a hot research area! Find out more on how to host your own Frontiers Research Topic or contribute to one as an author by contacting the Frontiers Editorial Office: frontiersin.org/about/contact

GENERATION GROWBOTS: MATERIALS, MECHANISMS, AND BIOMIMETIC DESIGN FOR GROWING ROBOTS

Topic Editors:

Barbara Mazzolai, Italian Institute of Technology (IIT), Italy

Ian Walker, Clemson University, United States

Thomas Speck, University of Freiburg, Germany

Citation: Mazzolai, B., Walker, I., Speck, T., eds. (2021). Generation GrowBots: Materials, Mechanisms, and Biomimetic Design for Growing Robots. Lausanne: Frontiers Media SA. doi: 10.3389/978-2-88971-185-7

Table of Contents

04	<i>Editorial: Generation Growbots: Materials, Mechanisms, and Biomimetic Design for Growing Robots</i>
	Barbara Mazzolai, Ian Walker and Thomas Speck
07	<i>Pneumatic Coiling Actuator Inspired by the Awns of <i>Erodium cicutarium</i></i>
	Ryan Geer, Steven Iannucci and Suyi Li
17	<i>Mechanical Innovations of a Climbing Cactus: Functional Insights for a New Generation of Growing Robots</i>
	Patricia Soffiatti and Nick P. Rowe
31	<i>Artificial Venus Flytraps: A Research Review and Outlook on Their Importance for Novel Bioinspired Materials Systems</i>
	Falk J. Esser, Philipp Auth and Thomas Speck
44	<i>Plant Bioinspired Ecological Robotics</i>
	P. Adrian Frazier, Lorenzo Jamone, Kaspar Althoefer and Paco Calvo
53	<i>A General 3D Model for Growth Dynamics of Sensory-Growth Systems: From Plants to Robotics</i>
	Amir Porat, Fabio Tedone, Michele Palladino, Pierangelo Marcati and Yasmine Meroz
67	<i>Searching and Intertwining: Climbing Plants and GrowBots</i>
	James Gallentine, Michael B. Wooten, Marc Thielen, Ian D. Walker, Thomas Speck and Karl Niklas
81	<i>The Bio-Engineering Approach for Plant Investigations and Growing Robots. A Mini-Review</i>
	Barbara Mazzolai, Francesca Tramacere, Isabella Fiorello and Laura Margheri
90	<i>Design, Modeling, Control, and Application of Everting Vine Robots</i>
	Laura H. Blumenschein, Margaret M. Coad, David A. Haggerty, Allison M. Okamura and Elliot W. Hawkes
114	<i>Root Systems Research for Bioinspired Resilient Design: A Concept Framework for Foundation and Coastal Engineering</i>
	Elena Stachew, Thibaut Houette and Petra Gruber



Editorial: Generation Growbots: Materials, Mechanisms, and Biomimetic Design for Growing Robots

Barbara Mazzolai^{1*}, Ian Walker² and Thomas Speck³

¹Bioinspired Soft Robotics Laboratory, Istituto Italiano di Tecnologia, Genova, Italy, ²Department of Electrical and Computer Engineering, Clemson University, Clemson, SC, United States, ³Botanic Garden and Cluster of Excellence livMatS, University of Freiburg, Freiburg, Germany

Keywords: growing robotics, soft robotics, bioinspired robotics, biomimetic architecture, plant biology

Editorial on the Research Topic

Generation Growbots: Materials, Mechanisms, and Biomimetic Design for Growing Robots

Plants are the dominant life form on the planet, accounting for over 80% of its biomass (Thompson, 2018). Plants are adapted to and thrive in virtually all environments, both natural and human-adapted, across the globe. In achieving this widespread presence, plants exhibit a significant range of structures and operational strategies. On the one hand, many key aspects of plant biology remain imperfectly understood, and the possibilities for plant-inspired engineering remain largely unexplored. On the other hand, increasing interest in plant-inspired research can be observed in architecture and technology in general over the last decades (cf. Speck and Speck 2019). More recently, plants have also started to represent models in robotics (Mazzolai et al., 2010; Lastinger et al., 2019; Sadeghi et al., 2020; Wooten et al., 2018), especially for the design of systems that have to deal with unstructured environments and require advanced capabilities of soft interaction, adaptation, and self-morphing. With this view, the goal of this special issue is to illustrate the potential of identifying principles from plant growth and movement suitable for engineering, and the adaptation of those principles to the new emerging field of “growing” robots, or Growbots.

The field of robotics has expanded rapidly over the past 25 years. Important advances in robotic design, planning, locomotion, and manipulation have been inspired and driven by insights gained from biology, notably in the structure and behavior of animals. However, to date very little attention has been paid by roboticists to the multitude of “existence proofs” provided by plants.

In this Research Topic, which is based on the contributions presented at the 2019 Robotics Science and Systems (RSS) workshop “Generation GrowBots” (June 22, 2019 in Freiburg, Germany), we present a research topic of nine articles focused on the intersection of robotics and plant biology. The articles are authored by a highly interdisciplinary group of domain experts, bringing together natural scientists and engineers, including experts in material science, soft robotics, plant biology, and architecture to present new scientific discoveries on plants and technological advances relevant to continuum, soft, adaptable, and growing robots. Collectively, the articles are representative of the current state of the art in the emerging area of plant-inspired robotics. Trends, frontiers and potential applications for a variety of high-tech sectors are discussed.

Under the Research Topic “Generation GrowBots” contributing authors discuss the science and technologies of the new field of plant-inspired robotics and growing robotics, exploring the materials, mechanisms and behavioral strategies as the basis of a new paradigm for robot mobility inspired by

OPEN ACCESS

Edited and reviewed by:

Dahua Shou,
Hong Kong Polytechnic University,
China

*Correspondence:

Barbara Mazzolai
barbara.mazzolai@iit.it

Received: 19 May 2021

Accepted: 27 May 2021

Published: 15 June 2021

Citation:

Mazzolai B, Walker I and Speck T
(2021) Editorial: Generation Growbots:
Materials, Mechanisms, and
Biomimetic Design for
Growing Robots.
Front. Robot. AI 8:711942.
doi: 10.3389/frobt.2021.711942

the moving-by-growing ability of plants. Plants show unique capabilities of endurance and movement by growth. Growth allows plants to strongly adapt the body morphology to different environmental conditions, and to move in search for nutrients and light or for protection from harmful agents. Because of these features, together with plant biologists and materials scientists, engineers are deeply investigating the biomechanics, materials, energy efficiency mechanisms, and behavior of a variety of plant species, to take inspiration for the design of multi-functional and adaptable technologies, and for the development of a new class of low-mass, low-volume robots endowed with new and unprecedented abilities of movement. With their capability to better challenge unstructured and extreme environments, soft, self-morphing, growing machines will have potential applications in a variety of sectors, including the exploration and monitoring of archaeological sites, unknown/challenging terrestrial or extra-terrestrial areas, as well as novel technological systems for the advancement of future urban architectures.

The topics of the nine articles in the present issue on “Generation GrowBots” vary in focus, but all address the overall theme of plant-based movement and its potential adaptation to robots. Two articles (Gallentine et al.; Geer et al.) introduce new robotic structures based on curling structures in fruit awns and climbing plants. The two examples cover a huge size range. The biomimetic robotic manipulator presented by Geer et al. is inspired by the ultrastructure of the cell wall of awns showing a helical cellulose fiber arrangement which allows for humidity driven awn movement. The concepts for transfer to motile structure in robots presented by Gallentine et al. are based on the macroscopic structure and movement of liana stems and tendrils and the finding that many climbing plants use curling and/or twining of their stems or tendrils for stiffening (braided stems) or securing attachment (tendrils). They show that these systems represent interesting models for new types of climbing plant-inspired soft robots.

The nature of movement in plants, and the consequent implications for plant-inspired robots, are considered by Frazier et al., and models of plant growth aimed at implementation in robots are presented by Porat et al.. These two contributions prove that for a successful transfer of motion principles and movements in plants to soft robots and other types of soft machines, a thorough analysis of these movements in plants using a combination of experimental and modeling approaches are a prerequisite. Without a basic and quantitative understanding of the form-structure-function relation of the plant organs used as concept generators for moving GrowBots the potential of plant-inspired approach cannot fully be used.

Realizations of vine-inspired growing robots are described in (Blumenschein et al.), with review on recent work on robots that

“grow” via pressure-driven eversion, referred to as “everting vine robots,” due to a movement pattern that allows the soft systems to explore the environment. Designs based on eversion can extend over long distances (tens of meters), and offer numerous potential application novel to robotics.

Mechanical adaptations in climbing plants are considered by Soffiatti and Row, who analyzed the mechanics and underlying structure of a climbing cactus, which proves to be a suitable concept generator for shape adaptive and shape memory compound polymer materials systems which can be produced by additive manufacturing.

Root systems, a critical but generally neglected aspect of plant structures, are discussed in (Stachew et al.) as they offer promising strategies for the design of civil and coastal infrastructure, such as adaptivity, multi-functionality, self-healing, mechanical and chemical soil attachment. Using a biomimetic methodology, the work presents the potential of root-inspired designs for building foundations and coastal infrastructures that prevent soil erosion, anchor structures, penetrate soils, and provide natural habitat.

The research review by Esser et al. summarizes the current state of the art in constructing Artificial Venus Flytraps (AVTs), which represent iconic examples of plant-inspired soft machines. The article gives an outlook on the work done on AVTs in the Cluster of Excellence *livMatS*. AVTs are prime examples for shifting/blurring the boundaries between living and life-like but entirely technical systems (Speck and Speck, 2021). However, in addition to examining the question of dissolving this boundary the article offers some interesting potential applications for plant-inspired soft robots and building hulls in architecture.

Last but not least, as it has been 10 years since the publication of the first article looking at plants as a biomechatronic system and creating a bidirectional link between robotics and plant biology, the mini-review by Mazzolai et al. offers a brief overview of the fundamental aspects related to a bioengineering approach in plant-inspired robotics. The article analyses the works in which both biological and engineering aspects have been investigated, and highlights the key elements of plants that have been milestones in the pioneering field of growing robots.

We hope that the special issue will prove informational and inspirational to readers new to the topic, and also be a valuable resource for current and future researchers in the area.

AUTHOR CONTRIBUTIONS

All authors listed have made a substantial, direct, and intellectual contribution to the work and approved it for publication.

REFERENCES

- Lastinger, M. C., Verma, S., Kapadia, A. D., and Walker, I. D. (2019). “TREE: A Variable Topology, Branching Continuum Robot,” in *Proceedings IEEE International Conference on Robotics and Automation (ICRA)* (Montreal, Canada, 5365–5371. doi:10.1109/icra.2019.8794463
- Mazzolai, B., Laschi, C., Dario, P., Mugnai, S., and Mancuso, S. (2010). The Plant as a Biomechatronic System. *Plant Signaling Behav.* 5 (2), 90–93. doi:10.4161/psb.5.2.10457

- Sadeghi, A., Del Dottore, E., Mondini, A., and Mazzolai, B. (2020). Passive Morphological Adaptation for Obstacle Avoidance in a Self-Growing Robot Produced by Additive Manufacturing. *Soft Robotics* 7, 85–94. doi:10.1089/soro.2019.0025
- Speck, O., and Speck, T. (2021). Functional Morphology of Plants - a Key to Biomimetic Applications. *New Phytol.*, 17396. (in press). doi:10.1111/nph.17396
- Speck, T., and Speck, O. (2019). Quo Vadis plant Biomechanics: Old Wine in New Bottles or an Up-and-coming Field of Modern Plant Science? *Am. J. Bot.* 106 (11), 1399–1403. doi:10.1002/ajb2.1371
- Thompson, A. (2018). *Plants are the World's Dominant Life-form*. Scientific American.
- Wooten, M. B., Frazelle, C. G., Walker, I. D., Kapadia, A. D., and Lee, J. H. (2018). "Exploration and Inspection with Vine-Inspired Continuum Robot," in

Proceedings IEEE International Conference on Robotics and Automation (ICRA) (Brisbane, Australia). 5526–5533.

Conflict of Interest: The authors declare that the research was conducted in the absence of any commercial or financial relationships that could be construed as a potential conflict of interest.

Copyright © 2021 Mazzolai, Walker and Speck. This is an open-access article distributed under the terms of the Creative Commons Attribution License (CC BY). The use, distribution or reproduction in other forums is permitted, provided the original author(s) and the copyright owner(s) are credited and that the original publication in this journal is cited, in accordance with accepted academic practice. No use, distribution or reproduction is permitted which does not comply with these terms.



Pneumatic Coiling Actuator Inspired by the Awns of *Erodium cicutarium*

Ryan Geer, Steven Iannucci and Suyi Li*

Department of Mechanical Engineering, Clemson University, Clemson, SC, United States

This study examines the coiling and uncoiling motions of a soft pneumatic actuator inspired by the awn tissue of *Erodium cicutarium*. These tissues have embedded cellulose fibers distributed in a *tilted* helical pattern, which induces hygroscopic coiling and uncoiling in response to the daily changes in ambient humidity. Such sophisticated motions can eventually “drill” the seed at the tip of awn tissue into the soil: a drill bit in the plant kingdom. Through finite element simulation and experimental testing, this study examines a soft pneumatic actuator that has a similar reinforcing fiber layout to the *Erodium* plant tissue. This actuator, in essence, is a thin-walled elastomeric cylinder covered by tilted helical Kevlar fibers. Upon internal pressurization, it can exhibit a coiling motion by a combination of simultaneous twisting, bending, and extension. Parametric analyses show that the coiling motion characteristics are directly related to the geometry of tilted helical fibers. Notably, a moderate tilt in the reinforcing helical fiber leads to many coils of small radius, while a significant tilt gives fewer coils of larger radius. The results of this study can offer guidelines for constructing plant-inspired robotic manipulators that can achieve complicated motions with simple designs.

Keywords: plant motion, soft robotic actuator, tilted helix, coiling motion, reinforcing fiber

OPEN ACCESS

Edited by:

Barbara Mazzolai,
Italian Institute of Technology (IIT), Italy

Reviewed by:

Indrek Must,
University of Tartu, Estonia
Jinhan Jeon,
Robert Bosch (SEA) Pte Ltd,
Singapore

*Correspondence:

Suyi Li
suyil@clemson.edu

Specialty section:

This article was submitted to
Soft Robotics,
a section of the journal
Frontiers in Robotics and AI

Received: 02 December 2019

Accepted: 30 January 2020

Published: 18 February 2020

Citation:

Geer R, Iannucci S and Li S (2020)
Pneumatic Coiling Actuator Inspired
by the Awns of *Erodium cicutarium*.
Front. Robot. AI 7:17.
doi: 10.3389/frobt.2020.00017

1. INTRODUCTION

In our popular belief, plants are static and immobile, but this couldn't be further from the truth. Plants are capable of achieving many sophisticated motions—almost continuously—without any muscles or nerve systems (Burgert and Fratzl, 2009; Martone et al., 2010; Dumais and Forterre, 2012). These motions are central to plants' survival and fitness, and they vary drastically in terms of their actuation and control principle, physiological origin, magnitude, and speed. Some plant motions are reversible so they can serve as blueprints for engineering adaptive structures and robots (Forterre, 2013; Guo et al., 2015; Charpentier et al., 2017; Li and Wang, 2017). For example, the trap closing motion in Venus flytrap (*Dionaea muscipula*) is rapid enough to capture agile insect prey like the fruit flies, which are then digested as nutrition supplement (Forterre et al., 2005; Skotheim and Mahadevan, 2005). The Venus flytrap gains its speed from actively changing the turgor pressure in its motor cells and exploiting an embedded snap-through instability, and it has inspired many robotic grippers (Kim et al., 2014; Zhang et al., 2016; Wani et al., 2017) and adaptive cellular structures (Gramüller et al., 2015; Li and Wang, 2015b). On the other end of the speed spectrum is the pinecone opening motion. It is driven by tissue swelling and shrinking in response to the ambient humidity change (aka. hygroscopy), and a bimorph construction in the pinecone scales directs this swelling into bending to create the opening/closing motions (Dawson et al., 1997). The actuation principle and physiological features of pinecone have inspired new responsive materials (Erb et al., 2013; Wu et al., 2013; Wei et al., 2014; Sydney Gladman et al., 2016),

and building envelopes (Menges and Reichert, 2012; Holstov et al., 2015). Besides these reversible motions, plants can also move slowly and irreversibly, such as the growth of roots and tendrils. These growth motions have recently inspired a new family of robots with unique navigation and exploration capabilities (Sadeghi et al., 2014, 2017; Hawkes et al., 2017; Nahar et al., 2017). Even to this day, we are still discovering new examples of plant motions and developing engineered systems based on the lessons from them.

In this study, we focus on a particularly intriguing plant motion: coiling in the seed awn of *Erodium Cicutarium* plant and its relatives (Stamp, 1984). The long and slender appendage tissues of their seed can coil and uncoil in response to the diurnal humidity cycle. Such a repetitive motion, combined with the angled bristles on the seed and along the side of the awn, can eventually bury the seed into the soil for germination (Evangelista et al., 2011) (**Figure 1A**). The key ingredient to achieving this coiling is in the plant cell walls. That is, the walls of the *Erodium* awn cells have reinforcing cellulose fibers arranged in a *tilted helical* pattern (**Figure 1B**) so that the longitudinal axis of the helical fibers does not align with the cell axis. As a result, when the ambient humidity drops, plant tissues in the *Erodium* awn would shrink in volume due to hygroscopy, and their tilted helical fibers can direct this shrinking into a coiling motion (Abraham et al., 2012; Aharoni et al., 2012; Abraham and Elbaum, 2013; Elbaum and Abraham, 2014; Jung et al., 2014; Zhao et al., 2017). Similarly, the awn would uncoil when humidity increases, essentially creating a “drill bit” in the plant kingdom.

While the role of tilted helical geometry in the *Erodium* seed coiling are well-studied, we haven't seen much efforts of applying this design in nature to the engineered systems. Indeed, many plant-inspired soft actuators are available and can exploit carefully designed reinforcing fibers to achieve sophisticated motions. For example, pneumatically pressurized tubes with reinforcing fibers in the *standard* helical pattern have shown pre-programmed twisting and elongation (Li and Wang, 2012, 2015a; Bishop-Moser and Kota, 2015; Connolly et al., 2015, 2017). Hydrogel-based bimorph materials with uniformly distributed fibers or stripes could bend or twist in response to different ambient stimuli (Wan et al., 2018). However, their relatively simple reinforcing fibers are not sufficient to create coiling—a combination of twisting *and* bending—unless we add strain-limiting layers (Polygerinos et al., 2015) or a third fiber (Bishop-Moser and Kota, 2013; Uppalapati and Krishnan, 2018) to the standard helical fibers, or use multiple fluidic chambers (Martinez et al., 2013). These are not as simple and elegant as the tilted helix design in *Erodium*.

Therefore, the objective of this study is to design and test a pneumatically driven soft actuator that can mimic the coiling motion using tilted helical reinforcing fibers. Instead of using the hygroscopic actuation principle like in the *Erodium* plant, we choose pneumatics to ensure a rapid response time, which is crucial for the targeted application of this actuator: soft robotic manipulation. This concept of pneumatic coiling actuator using tilted helical fiber was initially proposed in an earlier paper by the authors (Geer and Li, 2018a), however, it only demonstrated the feasibility obtaining coiling motion without carefully examining

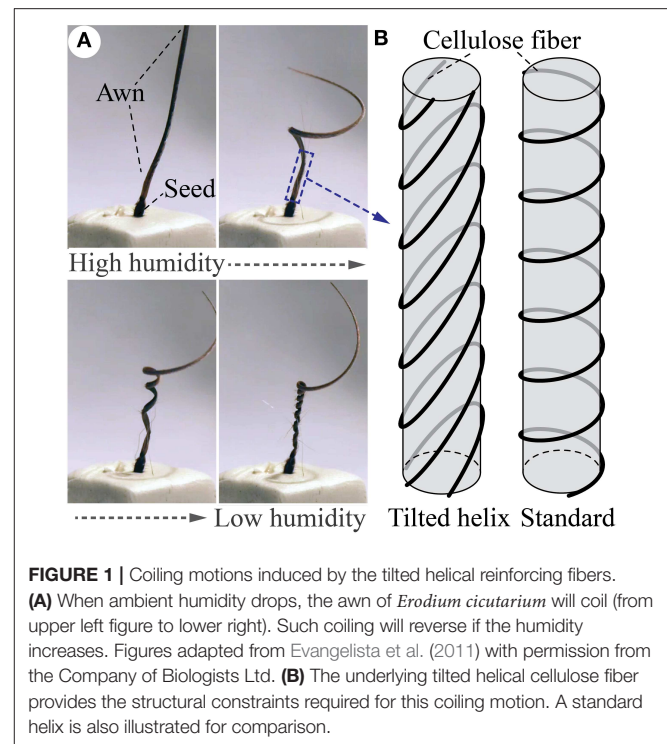


FIGURE 1 | Coiling motions induced by the tilted helical reinforcing fibers. **(A)** When ambient humidity drops, the awn of *Erodium cicutarium* will coil (from upper left figure to lower right). Such coiling will reverse if the humidity increases. Figures adapted from Evangelista et al. (2011) with permission from the Company of Biologists Ltd. **(B)** The underlying tilted helical cellulose fiber provides the structural constraints required for this coiling motion. A standard helix is also illustrated for comparison.

the connections between actuator design and corresponding motion. Therefore, this paper particularly focuses on establishing the correlation between the pneumatically-driven coiling motion characteristics and the design of tilted helical fibers. To this end, we fabricate prototypes of the plant-inspired actuator by casting thin-walled elastomeric tubes using 3D printed molds and then wrap Kevlar fibers around them according to the prescribed tilted helical geometry. Experimental validations on these prototypes reveal that the coiling deformation is strongly correlated to the tilt angle. Further parametric analyses based on finite element simulations show that a moderate tilt in the reinforcing helical fiber leads to many coils of small radius, while a significant tilt gives fewer coils of larger radius. Results of this study can offer guidelines for new soft robotic components capable of prescribed coiling motions for object manipulation or field exploration.

The rest of this paper is organized as follows. Section 2 briefly summarizes the design of plant-inspired coiling actuator and how the tilt in helical fiber can generate a combination of bending and twisting. Section 3 details the fabrication and testing of proof-of-concept prototypes. Section 4 discusses the results of a parametric study that elucidates the correlation between tilt helix design and coiling motion characteristics. Finally, section 5 ends this paper with a summary and conclusion.

2. COILING ACTUATOR DESIGN

The plant-inspired coiling actuator is essentially a pneumatically actuated, thin-walled tube reinforced by tilted helical fibers (**Figure 2**). The two ends of this tube are sealed and connected to the pressurized air supply. The tube has a total length of L and

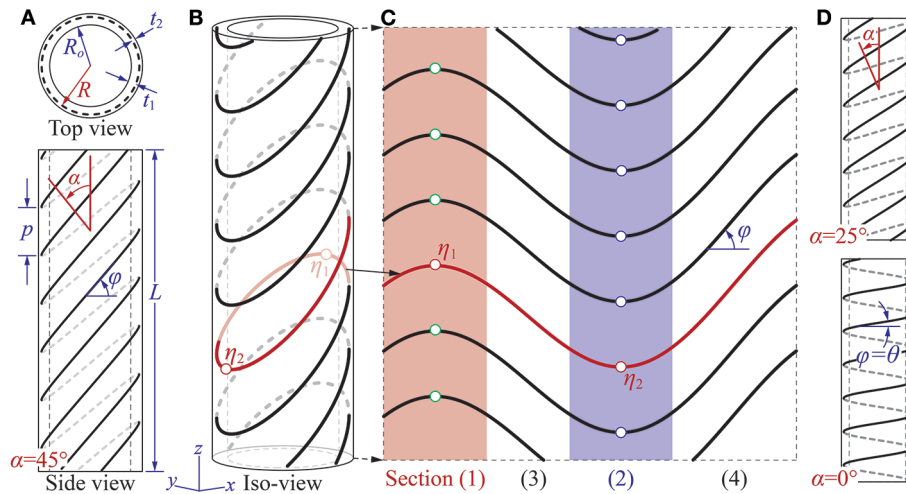


FIGURE 2 | Design of the plant-inspired coiling actuator. **(A)** Top-view and side-view of the actuator showing the multi-layered construction and different design parameters. In this particular illustration, $\alpha = 45^\circ$ and $\theta = 6^\circ$. **(B)** The iso-parametric view. **(C)** The geometry of reinforcing fiber if its cylindrical surface is cut and unwrapped into a flat surface. The four sections discussed in the main text are highlighted. **(D)** Side views of two different actuator designs with two different tilt angles. If $\alpha = 0^\circ$, the reinforcing fiber has a standard helix shape, so $\varphi = \theta$ according to Equation (5).

inner radius of R_i , and its thin wall—made of highly stretchable elastomeric materials—consists of two layers with thickness t_1 and t_2 , respectively. The reinforcing fibers are between these two layers, and their geometry follows the equations

$$x = R \cos \eta, \quad (1)$$

$$y = R \sin \eta, \quad (2)$$

$$z = \frac{p}{2\pi} \eta + A \cos \eta, \quad (3)$$

where x , y , and z are the coordinates of a point on the tilted helix. R is the helix radius ($R = R_o + t_1$), p is the helix pitch, and η is the parameter representing the helix length. The variable A directly defines the tilt angle α of the helix in that

$$\alpha = \tan^{-1} \left(\frac{A}{R} \right). \quad (4)$$

If $\alpha = 0$, the tilted helix becomes a *standard helix* so that $z = (p\eta)/(2\pi)$ (**Figure 2D**). When the tube has only one family of standard helical fibers, it exhibits a combination of twisting and elongation under internal pressure (Bishop-Moser and Kota, 2015; Connolly et al., 2015, 2017). The magnitude of such twisting is “programmable” by prescribing the ratio between helical radius R and pitch p . One can also use more complicated helical patterns to enrich the corresponding motion. For example, combining two standard helices with different pitches can offer more freedom for programming the twisting motions. Combining two standard helices of the same pitch but opposite winding directions (aka. one right-handed and the other left-handed) can eliminate twisting so that only elongation or contraction is obtainable (Bishop-Moser and Kota, 2015; Polygerinos et al., 2015; Connolly et al., 2017). The standard helix, however, is fundamentally *axisymmetric* in that it repeats itself

after being rotated by any angles along its longitudinal axis. So it is incapable of generating any non-axisymmetric motions like bending unless we intentionally break this axisymmetry.

The introduction of tilt angle α can effectively eliminate the axisymmetry, so it is the crucial design factor that enables the bending and eventually coiling motions. In the standard helix, z coordinate increases monotonically as η increases, but this is not true in the tilted helix. By defining φ as the angle between reinforcing fiber and cylinder circumference (**Figure 2**), one can use trigonometry to show that

$$\tan \varphi = \frac{\partial z}{R \partial \eta} = \frac{p}{2\pi R} - \tan \alpha \sin \eta = \tan \theta - \tan \alpha \sin \eta, \quad (5)$$

where θ is the fiber angle of the corresponding standard helix. Assuming $\alpha > \theta$, one can then find two sets of critical points (η_1 , η_2) along the tilted helix by solving $\varphi = 0$ in Equation (5) so that

$$\eta_1 = \sin^{-1} \left(\frac{p}{2\pi R \tan \alpha} \right) + 2n\pi, \quad (6)$$

$$\eta_2 = -\sin^{-1} \left(\frac{p}{2\pi R \tan \alpha} \right) + (2n+1)\pi, \quad (7)$$

where n is an integer. One can then *intuitively* understand how this tilted helical geometry can generate the combination of bending and twisting by dividing it into four sections shown as (1), (2), (3), and (4) in **Figure 2C**. Section (1) and (2) correspond to $\eta \in [\eta_1 - \pi/4, \eta_1 + \pi/4]$ and $\eta \in [\eta_2 - \pi/4, \eta_2 + \pi/4]$, respectively. The reinforcing fibers in these two sections are concave or convex curves that are perpendicular to the tube axis at their center points. Thus, one can deduce that these two sections are primarily responsible for generating the bending motion. On the other hand, sections (3) and (4) are between sections (1) and (2), and the reinforcing fibers in these two sections are similar to the standard helical fibers. That is, they

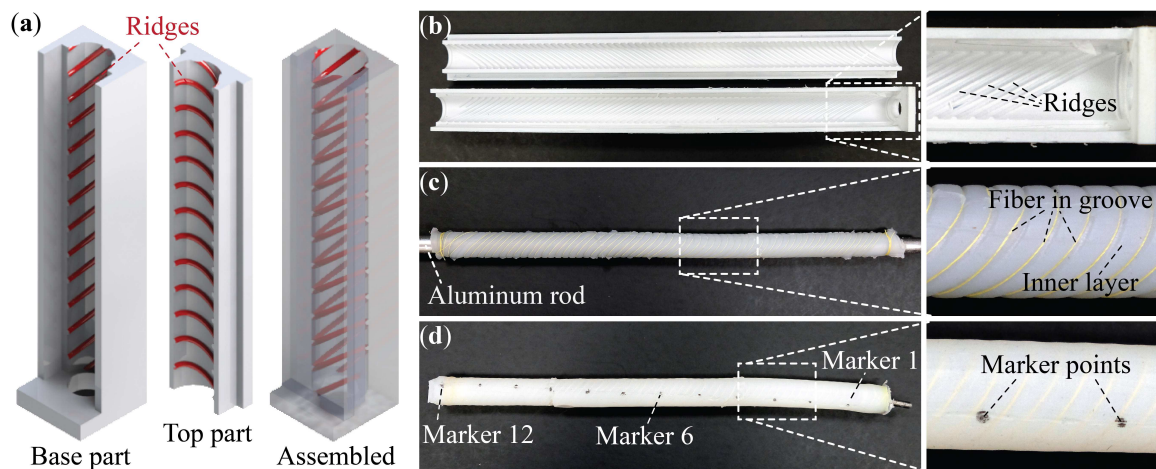


FIGURE 3 | Fabrication of the plant-inspired coiling actuator. **(a)** CAD models of a section of the primary molds. The ridges for fiber placement are highlighted. **(b)** The finished primary molds from 3D printer. **(c)** The assembly consists of an aluminum rod, cured inner layer, and wrapped Kevlar fiber. **(d)** A finished coiling actuator. The end adaptor for pressurized air supply and the markers for displacement measurement are highlighted. Note that for every marker shown in this picture, there is another one on the opposite side behind the actuator body.

show an oblique angle with respect to the tube axis. Thus, one can deduce that these two sections are primarily responsible for generating the twisting motion. The fiber orientations in these four sections change significantly if the tilt angle α changes, so the following experimental study focuses on the correlations between α and the coiling motion.

3. PROOF-OF-CONCEPT TESTING

To verify that the tilted helix can indeed generate coiling motion by a combination of testing and bending, we fabricate and test three proof-of-concept prototypes of different tilt angles: $\alpha = 41^\circ$, 51° , and 61° . The fabrication method is adapted from the previous studies in soft robotic actuators (Polygerinos et al., 2015; Geer and Li, 2018b) and includes three consecutive steps: (1) designing and 3D printing molds, (2) tube casting and fiber wrapping, and (3) creating end caps for pressure sealing (Figure 3).

The first step is to construct two sets of molds according to the coiling actuator design. One is for creating the inner layer shown in Figure 3a, and we refer them as the “primary mold.” The other set of “external molds” are for the outer layer to keep the reinforcing fiber in place. All molds are made in an Object Connect 350 3D Printer using Nylon material. The primary molds have protruding ridges distributed in the tilted helix pattern to create grooves in the casted inner layer (Figures 3b,c). These grooves, which are 0.25 mm in radius, can facilitate the fiber wrapping in the next step.

In the second step, we cast the inner layer of the coiling actuator using the primary molds, an aluminum rod of a 6.4 mm radius, and a vacuum-degassed mixture of DragonSkin 10 Slow silicon rubber (from Smooth-on). After curing at room temperature, we remove the primary molds and manually wrapped the Kevlar fiber (0.035 mm in diameter, from McMaster Carr) along the exposed grooves (Figure 3c). Then we place this

TABLE 1 | Baseline design parameters and material properties of the coiling actuators in experimental study and finite element simulations.

Parameter	Value
Inner radius (R_o)	6.4 mm
Inner layer thickness (t_1)	1.7 mm
Outer layer thickness (t_2)	1.8 mm
Pitch (p)	10 mm
Underlying standard helix angle (θ)	11.1°
Tilt angle α	41° , 51° , and 61°
Total length including end plugs	339 mm
Effective length without end plugs (L)	305 mm
Kevlar fiber stiffness (E_f)	31.6 GPa
Kevlar fiber Poisson's ratio (ν)	0.36
Odgen model material properties	$\mu_1 = 9.11 \times 10^{-4}$ MPa, $\alpha_1 = 5.88$ $\mu_2 = 6.75 \times 10^{-2}$ MPa, $\alpha_2 = 1.45$

assembly into the external molds and cast the outer layer using the same DragonSkin 10 rubber mixture.

In the third and final step, we remove the external molds and aluminum rod from the finished actuator tube, and then dip the tube ends into an uncured rubber mixture for 5–10 min to create the end caps. After curing, we insert a vented screw into one cap and connected it to the pneumatic pressure supply (Figure 3d). Detailed design parameters of these prototypes are in Table 1. It is worth emphasizing that the finished prototypes have two evenly-spaced tilted helix fibers to ensure sufficient fiber coverage.

We hang the finished actuator vertically and fix its upper end to a custom made aluminum frame, then use a DC voltage/pressure transducer to pressurize the actuator from 0 to 82.7 kPa with an increment step of 20.7 kPa (Controlair Type

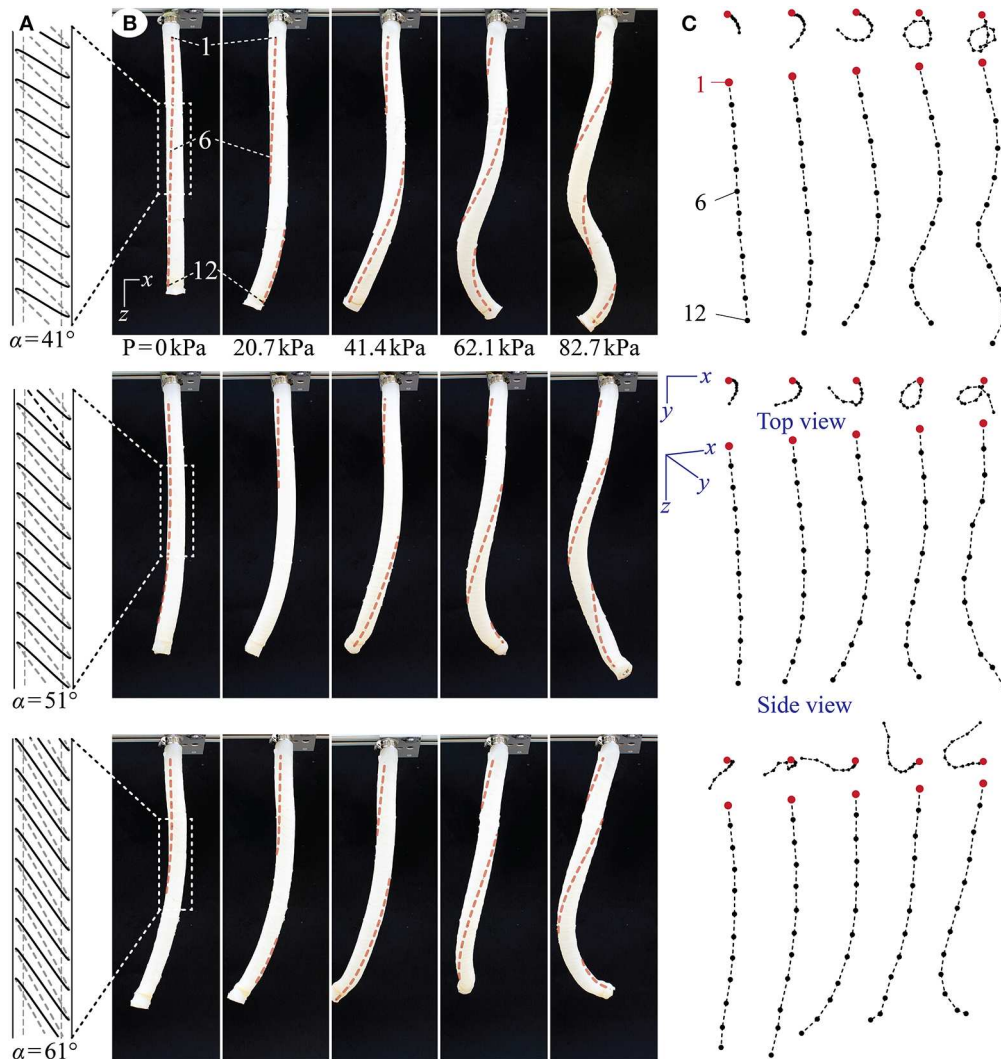


FIGURE 4 | Proof-of-concept test results from the actuator prototypes with $\alpha = 41^\circ$ (top row), 51° (middle row), and 61° (bottom row). **(A)** To-scale schematic drawing of the tilted reinforcing fiber geometry. Only one string of fiber is shown here for visual clarity, but the actuator prototypes each has two strings of evenly spaced fibers to ensure sufficient coverage. **(B)** The actuator prototypes at different pressure levels. To better illustrate the twisting motion in these pictures, we added dashed lines to connect the marker points on the actuator surface. **(C)** The approximated motion of the actuator longitudinal axes based on the depth camera readings. The cameras have limited accuracy, so they generate small and random errors when recording the marker position in the y-axis. Therefore, the center axis can seem non-smooth on some occasions. This error, however, does not hinder us from understanding the overall coiling motion characteristics.

900-ELA E/P pressure transducer and Tenma 72-2690 DC power supply). To measure the actuator deformation accurately, we custom made a motion tracking system by placing two motion depth cameras at the opposite sides of the coiling actuator (Intel Realsense Depth Camera D415). We draw twelve pairs of marker points, labeled as 1–12, on the actuator surface so that each pair lies on the opposite side (**Figure 3d**). In this way, the motion track cameras can record these marker point positions in 3D space, and the averaged results of these twelve pairs can reflect the motion of the actuator longitudinal axis.

Figure 4 summarizes the deformation of the pressurized coiling actuators (also see the **Supplemental Video 1**). As the internal pressure increases, all actuator prototypes exhibit a

unique “elongate and coil” motion through a combination of elongation, bending, and twisting. Moreover, these actuators primarily show elongation and bending at low pressure, and when the pressure increases beyond a threshold value ($\sim 41 \text{ kPa}$), twisting emerges rapidly and drives the actuator bodies into different coil shapes. This non-uniform appearance of various deformations reflects the non-linear elastic properties of DragonSkin silicon rubber.

Moreover, by comparing the deformations between different actuator prototypes, one can observe a strong influence of the tilt angle on the coiling motion. If the tilt angle α is small, the actuator deforms into a thin coil with a relatively small radius. On the other hand, if the tilt angle α is large, the actuator deforms

with a relatively larger coiling radius. Since the actuator length is the same, the coiling radius is inversely related to the number of completed coils. That is, while the actuator prototype with $\alpha = 41^\circ$ manages to complete more than one and a half coils, the one with $\alpha = 61^\circ$ can only achieve about a half coil.

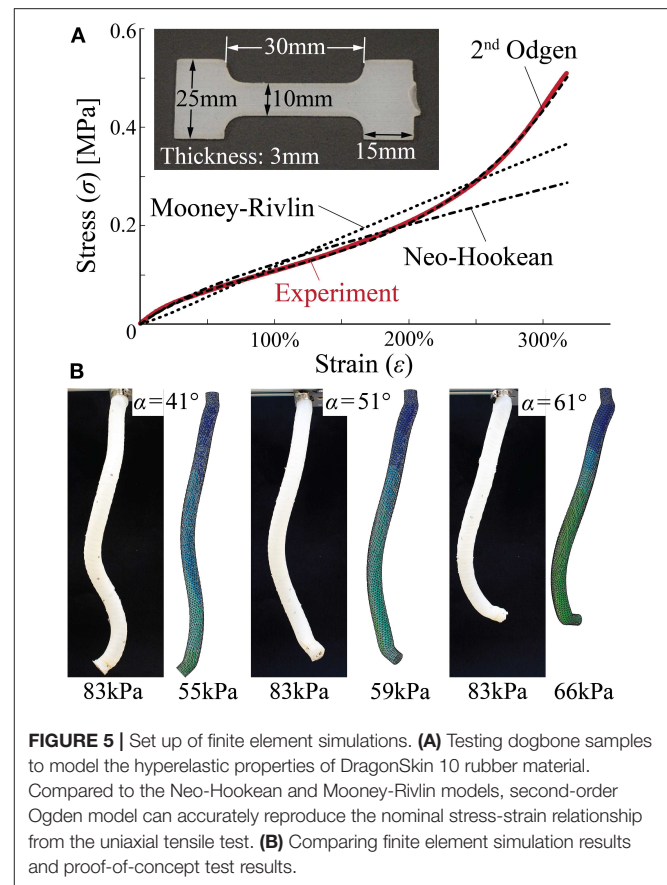
It is worthwhile to discuss the differences between the coiling motion exhibited by these engineered actuators and the motion of *Erodium* awn tissues shown in **Figure 1**. Firstly, although these two systems have similar tilted helical reinforcing fiber design, they differ in the actuation principles. The plant tissue achieves coiling by hygroscopic shrinking, while the engineered actuators achieve coiling by pneumatic expansion. As a result, their motion characteristics have some differences. In particular, the longitudinal elongation shown by the coiling actuators is the result of the pneumatic pressurization, but the *Erodium* tissue does not exhibit any significant elongation or contraction. Secondly, the scaling between the engineered actuator and *Erodium* tissues are quite different. That is, the plant tissue has much slender shape. If we reduce the radius of the pneumatic actuator, we would likely observe a more prominent bending component like in the plant tissues because of the smaller bending stiffness. However, the correlations between the actuator radius, length, and title fiber design are strongly non-linear, as indicated by relevant studies on the plant tissue (Aharoni et al., 2012). We chose the scale of these pneumatic actuators to ensure manufacturability based on the 3D-printed mold and manual fiber wrapping method.

4. THE INFLUENCES OF TILTED HELIX GEOMETRY ON COILING MOTION

To further understand the influence of tilted helical fiber geometry on coiling motion, we conduct two finite element simulations using ABAQUSTM. The first simulation aims to validate the correlation between tilt angle and coiling observed in the experiments, while the second simulation explores the tilted helix design space more comprehensively.

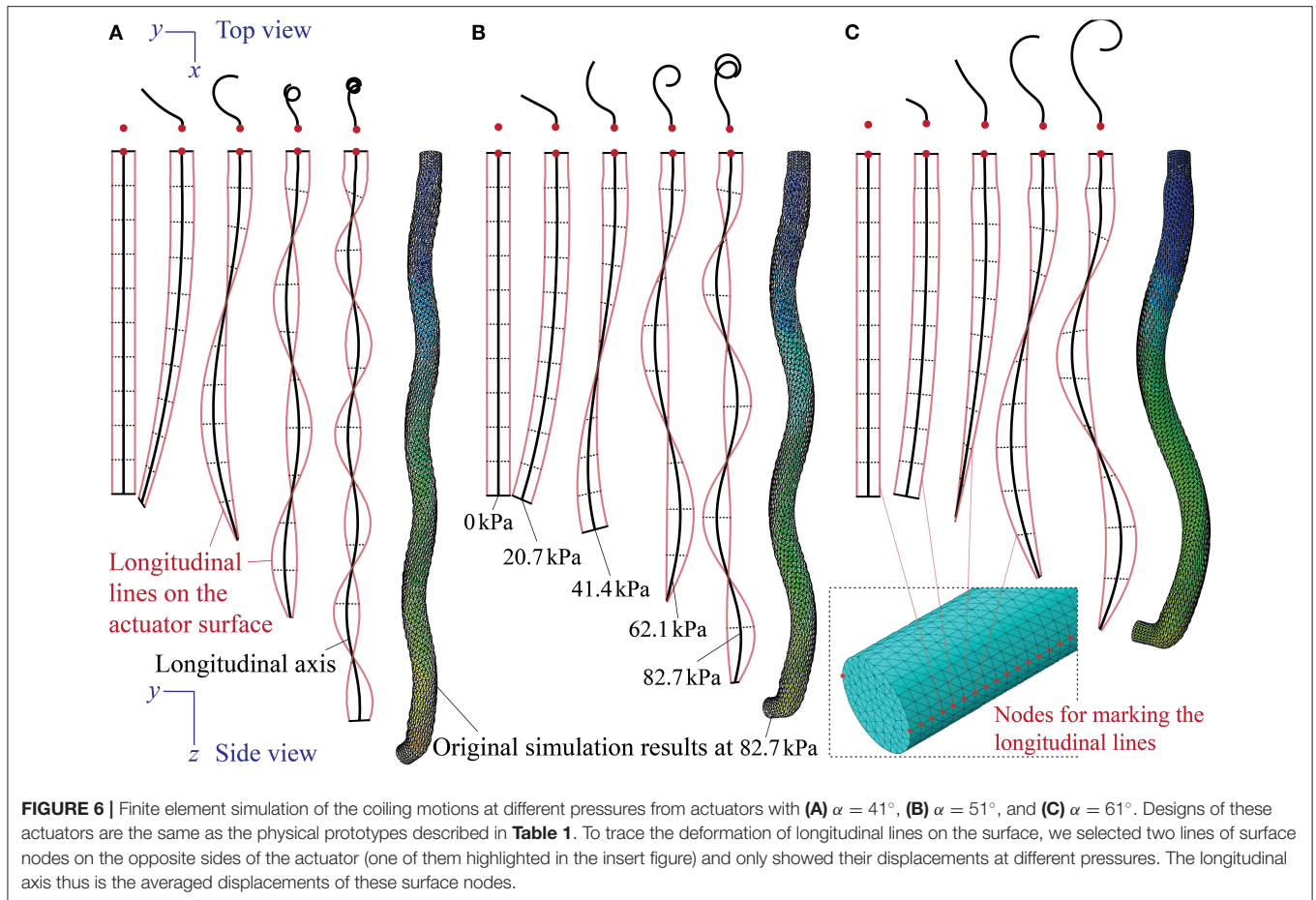
In the first simulation, we construct finite element models according to the prototype design parameters in **Table 1**, and hung the actuator vertically by applying fixed boundary conditions at its upper end. Quadratic and tetrahedral elements (C3D10H) are used to mesh the two layers of the actuator wall separately, and the hybrid formulation is adopted to avoid volume locking since the silicon rubber material is assumed incompressible. We mesh the reinforcing fibers by quadratic beam elements (B32), apply tie constraints between the fiber and inner layer, and then merge the outer layer to the inner layer.

The DragonSkin 10 silicon rubber used for constructing the actuator wall is strongly hyperelastic, so it is challenging to obtain an accurate description of its non-linear elastic properties. To this end, we cast a dogbone specimen using 3D printed molds (**Figure 5A**) and measure its reaction force under stretch on a universal testing machine (Instron 1125, 325% of maximum strain). We fit different hyperelastic material models to the measured nominal stress-strain relationship, and the second-order Ogden model can give the best agreement throughout



the deformation range (**Figure 5**). The fitted material properties, together with the elastic properties of the Kevlar fiber, are summarized in **Table 1**.

The finite element models are able to reproduce the elongation and coiling motions observed in the proof-of-concept tests. That is, the actuator deformations predicted by the numerical simulations agree with the experimental observation well (**Figure 5B**). However, these agreements occur at different pressures in that numerical simulations predicted smaller pressures to achieve similar coiling. There can be a few causes for this discrepancy. The first probable cause is errors in the property modeling of DragonSkin 10 material. Fitting the uniaxial test data alone cannot guarantee the accuracy of the second-order Ogden model, and one can significantly improve the model by using additional tests, such as a bi-axial stretch test. However, these further tests require sophisticated equipment that are not available to the authors. The second probable cause is the fabrication imperfections. Since the actuator prototype assembly is manual, many defects can occur like reinforcing fiber misalignment, entrapped air bubbles in the DragonSkin rubber, and residual stress from removing the aluminum rod that caused the prototype to bend slightly even without pressure. Despite the quantitative differences, the numerical simulations confirm the experimentally-observed correlation between tilt angle and coiling motion. That is, a



small tilt angle α generates a significant elongation and small coiling radius so that the actuator can complete a relatively large number of coils. While a large tilt angle gives less elongation and larger coiling radius, so a relatively smaller amount of coils are achieved (Figure 6).

By using the finite element model, we conduct a parametric study to further examine the relationship between the tilted reinforcing helix design and coiling motion. In this study, we simulate the actuator deformations based on different combinations of tilt angles ($\alpha = 21, 31, 41, 51$, and 61°) and pitches ($p = 8, 10$, and 12 mm), and Figure 7 summarizes the results when the internal pressure is 69 kPa. All other actuator design parameters and material properties remain the same as those listed in Table 1. Here, the range of title angles and pitches are chosen carefully to ensure manufacturability. We find that when the tilt angle is bigger than 61° , it becomes quite challenging to wrap the reinforcing Kevlar fiber into the grooves of the actuator inner layer. A pitch bigger than 12 mm would leave too much space between the adjacent fibers (i.e., low fiber coverage); as a result, the rubber-like DragonSkin material between the fibers can bulge under pressure, leading to excessive and localized deformation. It is worth emphasizing that all of the actuators have two strings of evenly spaced reinforcing fibers to ensure sufficient coverage.

The simulation results, shown in Figure 7, reveals that the experimentally observed correlation between tilt angle and coiling motion applies to different pitches. That is, for the same pitch, the actuator can complete several coils of small radius if the tilt angle is low, but fewer coils of larger radius as the title angle increases. We further examined this trend by comparing the averaged twist and curvature of different actuators. Here, the twist refers to rotation of the cross-sections of the coiling actuator about its longitudinal axis. Denote \mathbf{d}_i and \mathbf{d}_{i+1} as the adjacent diameter vectors, each defined by two surface nodes on the opposite side of the deformed actuator (insert in Figure 7C). The local twist is

$$\tau_i = \frac{\cos^{-1}(\mathbf{d}_i \cdot \mathbf{d}_{i+1})}{d\eta}, \quad (8)$$

where $d\eta$ is the distance between these two diameter vectors at the *initially undeformed configuration*. The localized curvature is,

$$\kappa_i = \frac{\|\mathbf{t}'_i \times \mathbf{t}''_i\|}{\|\mathbf{t}'_i\|^3}, \quad (9)$$

where \mathbf{t}_i is the tangent vector of the deformed longitudinal axis (insert in Figure 7C), and “ $'$ ” is the derivative with respect to

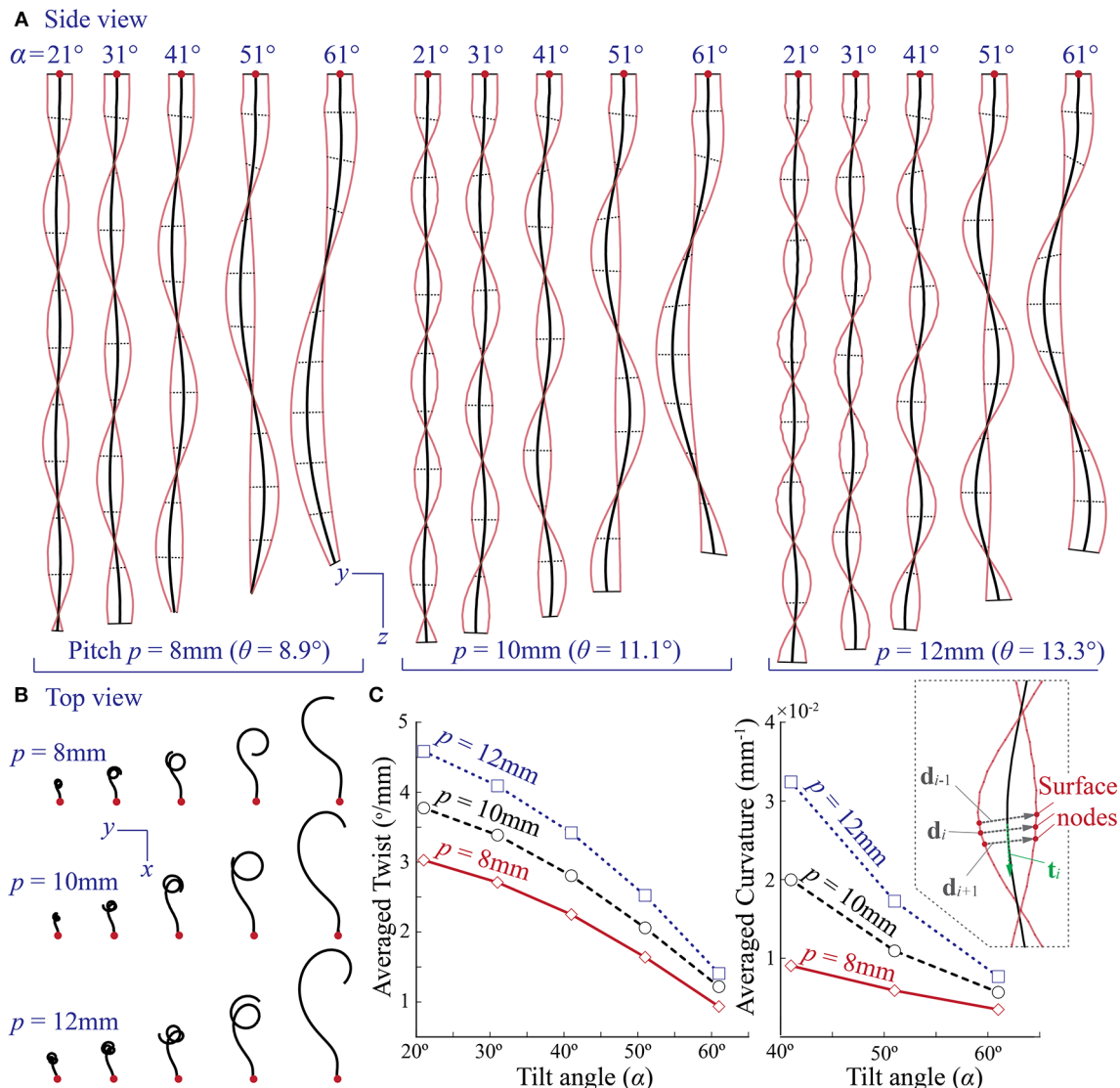


FIGURE 7 | Design parametric study using finite element simulations. **(A,B)** Simulated external shapes of different coiling actuators with various combinations of reinforcing helix tilt angle (α) and pitch (p). All of them are subjected to the same internal pressure at 69 kPa. **(C)** The correlation between the averaged actuator twist, curvature, and tilted helix design parameters based on FEA results. The insert figure on the right illustrates the method of calculating local twist and curvature.

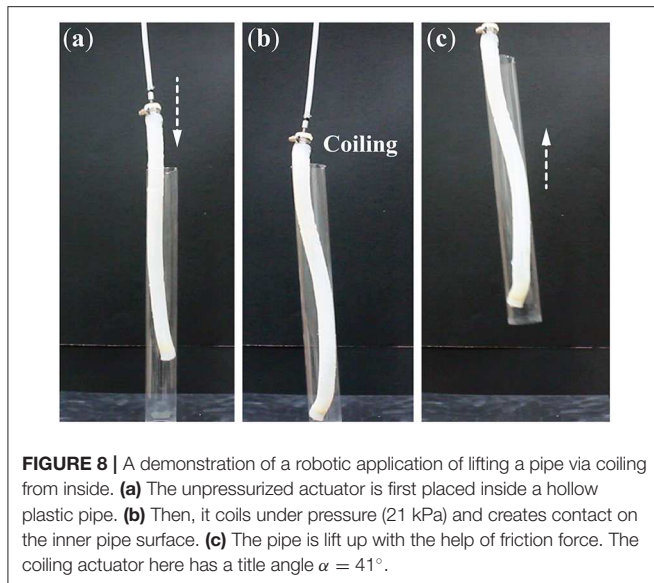
the initially undeformed configuration. Then, the local twist and curvature of the center half of the deformed actuator are averaged to avoid the boundary effects from the two end plugs.

The averaged results, shown in **Figure 7C**, indicate that both the twist and curvature decrease as the tilt angle α increases. Moreover, a larger pitch seems to amplify both twist and curvature; as a result, the actuator with a larger pitch can complete more coils.

5. SUMMARY AND DISCUSSION

Inspired by the sophisticated motions shown in the awn of *Erodium* plant seeds, we examine pneumatic actuators capable of generating coiling motion—a combination of twisting and

bending. These actuators are essentially thin-walled elastomeric tubes reinforced by tilted helical fibers, which closely resemble the cellulose fiber distributions in the *Erodium* seed awn. However, instead of operating based on the hygroscopic principle like in plants, these actuators use pneumatics to ensure fast response time so that they are suitable for robotic applications. Several actuator prototypes of different fiber tilt angles are fabricated using 3D printed molds, and they manage to achieve coiling. The magnitude of helical tilt angle plays a crucial role in creating the coiling motion because this helical tilt causes the actuator to bend, which is not possible from the standard helical reinforcing fiber. Experimental results reveal that actuators with a smaller tilt angle show significant elongation and can achieve several coils of small radius; while those with a large tilt angle typically



make fewer, large radius coils. We also construct finite element models to simulate the coiling. The numerical simulations confirm the correlation between tilt angle and coiling motion characteristics despite the discrepancies in terms of motion magnitude. With this finite element model, we are able to conduct a more comprehensive parametric study by combining different helical tilt angles and pitches. We find that the experimentally observed correlation between tilt angle and coiling applies to different helical pitches, and increasing this pitch would amplify the actuator twisting, leading to more coils of smaller radius. Therefore, one can effectively program the coiling characteristics by carefully designing the reinforcing tilted helix geometry.

The elongation and coiling motion exhibited by these plant-inspired actuators are unique and can open up new capabilities in soft robotic manipulation. For example, coiling can be used to manipulate long and slender shaped objects better than simple twisting or bending actuators (like from inside the pipe shown

in (Figure 8 and Supplemental Video 2). So these actuators might have potential applications in bio-medical applications like assistive care or rehabilitation. One could also possibility use these actuators to achieve drilling into porous media just like the Erodium tissue, so that we can use these actuators for field exploration or environment monitoring. The results of this study could provide physical insights and a design guideline for future implementations.

DATA AVAILABILITY STATEMENT

The datasets generated for this study are available on request to the corresponding author.

AUTHOR CONTRIBUTIONS

RG and SL conceived the research topic. RG conducted the fabrication, experimentation, and finite element simulation. SL conducted the data analysis and presentation. SI assisted the experiment design and data acquisition. All contributed to the manuscript draft.

ACKNOWLEDGMENTS

The authors acknowledge the support from Clemson University through startup funding and CECAS Dean's Faculty Fellow Award.

SUPPLEMENTARY MATERIAL

The Supplementary Material for this article can be found online at: <https://www.frontiersin.org/articles/10.3389/frobt.2020.00017/full#supplementary-material>

Supplemental Video 1 | Coiling motion of the plant-inspired actuators with different helix tilt angles.

Supplemental Video 2 | A demonstration of slender object handling using coiling motion.

REFERENCES

- Abraham, Y., and Elbaum, R. (2013). Hygroscopic movements in Geraniaceae: the structural variations that are responsible for coiling or bending. *New Phytol.* 199, 584–594. doi: 10.1111/nph.12254
- Abraham, Y., Tamburu, C., Klein, E., Dunlop, J. W. C., Fratzl, P., Raviv, U., et al. (2012). Tilted cellulose arrangement as a novel mechanism for hygroscopic coiling in the stork's bill awn. *J. R. Soc. Interface* 9, 640–647. doi: 10.1098/rsif.2011.0395
- Aharoni, H., Abraham, Y., Elbaum, R., Sharon, E., and Kupferman, R. (2012). Emergence of spontaneous twist and curvature in non-Euclidean rods: application to erodium plant cells. *Phys. Rev. Lett.* 108:238106. doi: 10.1103/PhysRevLett.108.238106
- Bishop-Moser, J., and Kota, S. (2013). "Towards snake-like soft robots: design of fluidic fiber-reinforced elastomeric helical manipulators," in *IEEE/RSJ International Conference on Intelligent Robots and Systems* (Tokyo), 5021–5026.
- Bishop-Moser, J., and Kota, S. (2015). Design and modeling of generalized fiber-reinforced pneumatic soft actuators. *IEEE Trans. Robot.* 31, 536–545. doi: 10.1109/TRO.2015.2409452
- Burgert, I., and Fratzl, P. (2009). Actuation systems in plants as prototypes for bioinspired devices. *Philos. Trans. R. Soc. A Math. Phys. Eng. Sci.* 367, 1541–1557. doi: 10.1098/rsta.2009.0003
- Charpentier, V., Hannequart, P., Adriaenssens, S., Baverel, O., Viglino, E., and Eisenman, S. (2017). Kinematic amplification strategies in plants and engineering. *Smart Mater. Struct.* 26:063002. doi: 10.1088/1361-665X/aa640f
- Connolly, F., Polygerinos, P., Walsh, C. J., and Bertoldi, K. (2015). Mechanical programming of soft actuators by varying fiber angle. *Soft Robot.* 2, 26–32. doi: 10.1089/soro.2015.0001
- Connolly, F., Walsh, C. J., and Bertoldi, K. (2017). Automatic design of fiber-reinforced soft actuators for trajectory matching. *Proc. Natl. Acad. Sci. U.S.A.* 114, 51–56. doi: 10.1073/pnas.1615140114
- Dawson, C., Vincent, J. F. V., and Rocca, A.-M. (1997). How pine cones open. *Nature* 390, 668–668. doi: 10.1038/377745

- Dumais, J., and Forterre, Y. (2012). "Vegetable dynamics": the role of water in plant movements. *Annu. Rev. Fluid Mech.* 44, 453–478. doi: 10.1146/annurev-fluid-120710-101200
- Elbaum, R., and Abraham, Y. (2014). Insights into the microstructures of hygroscopic movement in plant seed dispersal. *Plant Sci.* 223, 124–133. doi: 10.1016/j.plantsci.2014.03.014
- Erb, R. M., Sander, J. S., Grisch, R., and Studart, A. R. (2013). Self-shaping composites with programmable bioinspired microstructures. *Nat. Commun.* 4:1712. doi: 10.1038/ncomms2666
- Evangelista, D., Hotton, S., and Dumais, J. (2011). The mechanics of explosive dispersal and self-burial in the seeds of the filaree, *Erodium cicutarium* (Geraniaceae). *J. Exp. Biol.* 214, 521–529. doi: 10.1242/jeb.050567
- Forterre, Y. (2013). Slow, fast and furious: understanding the physics of plant movements. *J. Exp. Bot.* 64, 4745–4760. doi: 10.1093/jxb/ert230
- Forterre, Y., Skotheim, J. M., Dumais, J., and Mahadevan, L. (2005). How the Venus flytrap snaps. *Nature* 433, 421–425. doi: 10.1038/nature03185
- Geer, R., and Li, S. (2018a). "Examining the coiling motion of soft actuators reinforced with tilted helix fibers," in *ASME Conference on Smart Materials, Adaptive Structures and Intelligent Systems* (San Antonio, TX), 2018–8038.
- Geer, R., and Li, S. (2018b). "Examining the coiling motion of soft actuators reinforced with tilted helix fibers," in *ASME Conference on Smart Materials, Adaptive Structures and Intelligent Systems* (San Antonio, TX), V002T06A005.
- Grammüller, B., Köke, H., and Hühne, C. (2015). Holistic design and implementation of pressure actuated cellular structures. *Smart Mater. Struct.* 24:125027. doi: 10.1088/0964-1726/24/12/125027
- Guo, Q., Dai, E., Han, X., Xie, S., Chao, E., and Chen, Z. (2015). Fast nastic motion of plants and bioinspired structures. *J. R. Soc. Interface* 12:20150598. doi: 10.1098/rsif.2015.0598
- Hawkes, E. W., Blumenschein, L. H., Greer, J. D., and Okamura, A. M. (2017). A soft robot that navigates its environment through growth. *Sci. Robot.* 2:eaan3028. doi: 10.1126/scirobotics.aan3028
- Holstov, A., Bridgens, B., and Farmer, G. (2015). Hygroscopic materials for sustainable responsive architecture. *Construct. Build. Mater.* 98, 570–582. doi: 10.1016/j.conbuildmat.2015.08.136
- Jung, W., Kim, W., and Kim, H. Y. (2014). Self-burial mechanics of hygroscopically responsive awns. *Integr. Compar. Biol.* 54, 1034–1042. doi: 10.1093/icb/icu026
- Kim, S. W., Koh, J. S., Lee, J. G., Ryu, J., Cho, M., and Cho, K. J. (2014). Flytrap-inspired robot using structurally integrated actuation based on bistability and a developable surface. *Bioinspir. Biomim.* 9:036004. doi: 10.1088/1748-3182/9/3/036004
- Li, S., and Wang, K. W. (2012). On the dynamic characteristics of biological inspired multicellular fluidic flexible matrix composite structures. *J. Intell. Mater. Syst. Struct.* 23, 291–300. doi: 10.1177/1045389X11424218
- Li, S., and Wang, K. W. (2015a). Architectural synthesis and analysis of dual-cellular fluidic flexible matrix composites for multifunctional metastructures. *J. Mech. Des.* 137:041402. doi: 10.1115/1.4029516
- Li, S., and Wang, K. W. (2015b). Fluidic origami with embedded pressure dependent multi-stability: a plant inspired innovation. *J. R. Soc. Interface* 12:20150639. doi: 10.1098/rsif.2015.0639
- Li, S., and Wang, K. W. (2017). Plant-inspired adaptive structures and materials for morphing and actuation: a review. *Bioinspir. Biomim.* 12:011001. doi: 10.1088/1748-3190/12/1/011001
- Martinez, R. V., Branch, J. L., Fish, C. R., Jin, L., Shepherd, R. F., Nunes, R. M. D., et al. (2013). Robotic tentacles with three-dimensional mobility based on flexible elastomers. *Adv. Mater.* 25, 205–212. doi: 10.1002/adma.201203002
- Martone, P. T., Boller, M., Burgert, I., Dumais, J., Edwards, J., Mach, K., et al. (2010). Mechanics without muscle: biomechanical inspiration from the plant world. *Integr. Compar. Biol.* 50, 888–907. doi: 10.1093/icb/icq122
- Menges, A., and Reichert, S. (2012). Material capacity: embedded responsiveness. *Archit. Des.* 82, 52–59. doi: 10.1002/ad.1379
- Nahar, D., Yanik, P. M., and Walker, I. D. (2017). "Robot tendrils: long, thin continuum robots for inspection in space operations," in *IEEE Aerospace Conference* (Big Sky, MT), 16932680.
- Polygerinos, P., Wang, Z., Overvelde, J. T. B., Galloway, K. C., Wood, R. J., Bertoldi, K., et al. (2015). Modeling of soft fiber-reinforced bending actuators. *IEEE Trans. Robot.* 31, 778–789. doi: 10.1109/TRO.2015.2428504
- Sadeghi, A., Mondini, A., and Mazzolai, B. (2017). Toward self-growing soft robots inspired by plant roots and based on additive manufacturing technologies. *Soft Robot.* 4, 211–223. doi: 10.1089/soro.2016.0080
- Sadeghi, A., Tonazzini, A., Popova, L., and Mazzolai, B. (2014). A novel growing device inspired by plant root soil penetration behaviors. *PLoS ONE* 9:e90139. doi: 10.1371/journal.pone.0090139
- Skotheim, J. M., and Mahadevan, L. (2005). Physical limits and design principles for plant and fungal movements. *Science* 308, 1308–1310. doi: 10.1126/science.1107976
- Stamp, N. E. (1984). Self-burial behaviour of *Erodium cicutarium* seeds. *J. Ecol.* 72:611. doi: 10.2307/2260070
- Sydney Gladman, A., Matsumoto, E. A., Nuzzo, R. G., Mahadevan, L., and Lewis, J. A. (2016). Biomimetic 4D printing. *Nat. Mater.* 15, 413–418. doi: 10.1038/nmat4544
- Uppalapati, N. K., and Krishnan, G. (2018). Towards pneumatic spiral grippers: modeling and design considerations. *Soft Robot.* 5, 695–709. doi: 10.1089/soro.2017.0144
- Wan, G., Jin, C., Trase, I., Zhao, S., and Chen, Z. (2018). Helical structures mimicking chiral seedpod opening and tendril coiling. *Sensors* 18:2973. doi: 10.3390/s18092973
- Wani, O. M., Zeng, H., and Priimagi, A. (2017). A light-driven artificial flytrap. *Nat. Commun.* 8:15546. doi: 10.1038/ncomms15546
- Wei, Z., Jia, Z., Athas, J., Wang, C., Raghavan, S. R., Li, T., et al. (2014). Hybrid hydrogel sheets that undergo pre-programmed shape transformations. *Soft Matter* 10, 8157–8162. doi: 10.1039/C4SM01299B
- Wu, Z. L., Moshe, M., Greener, J., Therien-Aubin, H., Nie, Z., Sharon, E., et al. (2013). Three-dimensional shape transformations of hydrogel sheets induced by small-scale modulation of internal stresses. *Nat. Commun.* 4:1586. doi: 10.1038/ncomms2549
- Zhang, Z., Chen, D., Wu, H., Bao, Y., and Chai, G. (2016). Non-contact magnetic driving bioinspired Venus flytrap robot based on bistable anti-symmetric CFRP structure. *Compos. Struct.* 135, 17–22. doi: 10.1016/j.compstruct.2015.09.015
- Zhao, C., Liu, Q., Ren, L., Song, Z., and Wang, J. (2017). A 3D micromechanical study of hygroscopic coiling deformation in *Pelargonium* seed: from material and mechanics perspective. *J. Mater. Sci.* 52, 415–430. doi: 10.1007/s10853-016-0341-6

Conflict of Interest: The authors declare that the research was conducted in the absence of any commercial or financial relationships that could be construed as a potential conflict of interest.

Copyright © 2020 Geer, Iannucci and Li. This is an open-access article distributed under the terms of the Creative Commons Attribution License (CC BY). The use, distribution or reproduction in other forums is permitted, provided the original author(s) and the copyright owner(s) are credited and that the original publication in this journal is cited, in accordance with accepted academic practice. No use, distribution or reproduction is permitted which does not comply with these terms.



Mechanical Innovations of a Climbing Cactus: Functional Insights for a New Generation of Growing Robots

Patricia Soffiatti^{1*} and Nick P. Rowe²

¹ Department of Botany, Federal University of Parana State (UFPR), Curitiba, Brazil, ² AMAP, Univ Montpellier, CIRAD, CNRS, INRAE, IRD, Montpellier, France

OPEN ACCESS

Edited by:

Barbara Mazzolai,
Italian Institute of Technology (IIT), Italy

Reviewed by:

Heiko Hamann,
University of Lübeck, Germany
Cosimo Della Santina,
Massachusetts Institute of
Technology, United States

*Correspondence:

Patricia Soffiatti
psoffiatti.ufpr@gmail.com

Specialty section:

This article was submitted to
Soft Robotics,
a section of the journal
Frontiers in Robotics and AI

Received: 13 December 2019

Accepted: 20 April 2020

Published: 09 June 2020

Citation:

Soffiatti P and Rowe NP (2020)
Mechanical Innovations of a Climbing
Cactus: Functional Insights for a New
Generation of Growing Robots.
Front. Robot. AI 7:64.
doi: 10.3389/frobt.2020.00064

Climbing plants are being increasingly viewed as models for bioinspired growing robots capable of spanning voids and attaching to diverse substrates. We explore the functional traits of the climbing cactus *Selenicereus setaceus* (Cactaceae) from the Atlantic forest of Brazil and discuss the potential of these traits for robotics applications. The plant is capable of growing through highly unstructured habitats and attaching to variable substrates including soil, leaf litter, tree surfaces, rocks, and fine branches of tree canopies in wind-blown conditions. Stems develop highly variable cross-sectional geometries at different stages of growth. They include cylindrical basal stems, triangular climbing stems and apical star-shaped stems searching for supports. Searcher stems develop relatively rigid properties for a given cross-sectional area and are capable of spanning voids of up to 1 m. Optimization of rigidity in searcher stems provide some potential design ideas for additive engineering technologies where climbing robotic artifacts must limit materials and mass for curbing bending moments and buckling while climbing and searching. A two-step attachment mechanism involves deployment of recurved, multi-angled spines that grapple on to wide ranging surfaces holding the stem in place for more solid attachment via root growth from the stem. The cactus is an instructive example of how light mass searchers with a winged profile and two step attachment strategies can facilitate traversing voids and making reliable attachment to a wide range of supports and surfaces.

Keywords: biomechanics, climbing cactus, indeterminate growth, light architecture, searcher, soft robotics, two-step attachment

INTRODUCTION

Plants have recently become a focus of interest as potential bioinspired models for soft robotics (Mazzolai et al., 2014; Walker, 2015; Mazzolai, 2017; Del Dottore et al., 2018). Plants offer a rich source of potential innovations because of (i) their many kinds of growth and movement by growth (ii) their modular construction and strategically positioned functional structures and specialized organs and (iii) their morphological and functional plasticity—in particular their ability to make simple changes in developmental to profoundly change structural properties and functionality. The combination of these life history processes bestows high levels of adaptability in biological contexts and thus offers a wide adaptive potential for technological applications. Climbing plants possess a number of traits that can deal with many environmental challenges that other kinds of robot cannot (Walker, 2015). The approach seeking bioinspiration from the whole organism and its life history

and adaptive strategies has recently been coined as an “organism-inspired” approach as opposed to inspiration on finer cellular and molecular levels (Del Dottore et al., 2018).

Research on different plant growth forms and life histories has highlighted the architectural e.g., (Barthélémy and Caraglio, 2007), developmental e.g., (Speck and Rowe, 1999; Bateman, 2002), and mechanical e.g., (Rowe and Speck, 2005) diversity of different plant growth forms and the mechanisms that underline them. Climbing plants represent some of the most developmentally complex and potentially plastic growth forms (Rowe, 2018). They have highly indeterminate growth patterns, exceptionally variable stem mechanics and highly adaptive behavior as erect “searchers” or creeping, climbing or pendulous stems (Putz and Mooney, 1991). The climbing habits have evolved many times in plants (Gentry, 1991) and their stem morphology, biomechanics, climbing modes, attachment organs, roots, and anatomy are immensely diverse. Climbing plants are now providing a lot of choice for bioinspired technologies in robotics (Mehling et al., 2006; Wooten and Walker, 2016, 2018; Fiorello et al., 2018, 2019, 2020; Wooten et al., 2018; Must et al., 2019).

Over recent decades, plant biomechanics research has explored much of the diversity of form and function in both living and fossil plants and has documented the structural novelties that have appeared during evolution e.g., (Speck and Rowe, 2001). Today, plant biomechanics is an intrinsic part of the research for bioinspired technological solutions. Many of these investigations have yielded fascinating insight into the functioning of individual plant structures and organs at all scales and hierarchical levels, many of which could be of potential interest for bioinspired applications in robotics. This has proved an important source of bioinspiration in many applications: light weight fabricated plant stem-like organizations (Milvich et al., 2006); self-repairing and self-healing structures and technologies (Huss et al., 2018a,b; Speck et al., 2018; Yang et al., 2018); sealing foam for pneumatic systems based on the strategy found in the stems of *Aristolochia* (Busch et al., 2010; Rampf et al., 2011, 2013). The variety of attachment structures and organs of climbing plants is remarkable and has a great potential for bioinspired anchoring devices (Melzer et al., 2010; Bauer et al., 2011; Andrews and Badyal, 2014; Gallenmuller et al., 2015; Burris et al., 2018; Fiorello et al., 2018, 2019; Must et al., 2019). Plant surfaces have also offered inspiration for several technological applications for the creation of self-cleaning and water-repellent materials (Neinhuis and Barthlott, 1997; Koch and Barthlott, 2009; Latthe et al., 2014; Barthlott et al., 2017).

Bioinspired studies based on plants are now increasingly turning toward soft robotic applications (Mazzolai et al., 2014; Mazzolai, 2017). A turning point is that movement via adaptive growth is being integrated into bioinspired designs for artifacts to grow and move by artificial growth and movements like plant stems (Hawkes et al., 2017), tendrils (Must et al., 2019), tendril and searcher like structures (Mehling et al., 2006; Wooten and Walker, 2018; Wooten et al., 2018) and roots (Sadeghi et al., 2014, 2016; Del Dottore et al., 2019). The approach also considers how plants develop and adapt their modes of growth and varying stem stiffness and rigidity

to locate supports as well as attaching and climbing on different substrates.

Plant biodiversity provides a diverse tableau from which to choose potential kinds of bioinspired robotic behavior. Furthermore, convergent and parallel evolution has provided a wide choice of different biological models—different “ways” of being a root or stem or tree or climbing plant. Steven Vogel summarized nicely the fact that convergence can be a source of confusion for evolutionary biologists but a bonus for bioinspired research: “for the biologist and evolutionist convergence is a fascinating... problem, for the bioinspired researcher, convergence and diversity is a... gift” (Vogel, 2003).

Cacti are well-known for their remarkable adaptations to arid and semi-arid conditions (Gibson and Nobel, 1986), resulting in a reduced structural organization, where leaves are absent and succulent stems take over photosynthesis and provide storage, in parallel with support and water conduction. The focus of this study is a root-climbing cactus, a rather unusual growth form that shows truly indeterminate growth with behavioral and morphological shifts that change according to the kind of 3-dimensional environment. The combination of succulence, creeping and climbing is rare in such plants. Previous studies have shown how upright cactus stems have unusual anatomies but can still attain relatively large sizes and heights (Niklas et al., 1999). Furthermore, certain very rare forms have an adapted organization for creeping along the ground (Niklas et al., 2003).

Many climbing plant stems are merely millimeters in diameter during searching and initial climbing. Scaling up geometries and properties will be necessary if biological principles from diminutive plants are to be applied to robotic artifacts constrained by size limits of available technologies. This is especially crucial for reaching across voids and avoiding buckling. Scaled-up structures must be still capable of adaptively keeping on course toward the desired support e.g., (Del Dottore et al., 2019) and minimizing constructional cost and mass in terms of energy and materials. We investigated developmental changes of a cactus species that develops a large diameter stem via primary growth of soft tissues. These reach a similar size (centimeters in diameter) as some current robotic artifacts e.g., (Sadeghi et al., 2014, 2016).

In this paper we outline an approach for identifying functional traits of a climbing plant in its natural habitat and how these are linked to the biomechanics and basic organization of the stem. To our knowledge this is the first account of the life history of a climbing cactus that includes biomechanical observations. Our goal was to identify its behavioral characteristics that allow it to navigate through highly unstructured, heterogeneous and even moving environment. In this first paper we highlight the key developmental features, how the plant deploys them and provide a summary of features that can be examined and potentially integrated into technological projects.

MATERIALS AND METHODS

Selenicereus setaceus (Cactaceae) is a climbing cactus with succulent, leafless stems occurring in dry coastal formations of

Atlantic Forest in Southern Brazil. Plant stems were collected from the “Restinga” coastal lowland dry forests in Armação dos Buzios town (22° 44′ 49″ S, 41° 52′ 54″ W, 174 km from Rio de Janeiro city), Rio de Janeiro State. The region is composed of a mosaic of vegetation types and the climate is typically warm and dry. The so-called “Restinga forests” are lowland dry forests composed of trees and shrubs, where *S. setaceus* is a common component.

We outline a methodological approach, which can serve as a working model for detecting biological traits for potential technical solutions in robotics. The methodology can be viewed as several steps: (a) Observing the ecological context and variability of functional traits in the natural habitat such as searching, climbing and creeping behavior. All of these represent potentially interesting features for enabling robotic artifacts to traverse different kinds of terrain and crossing voids. (b) We then outline how the mechanical properties of these different behaviors are modified by different combinations of tissues during growth and development. This step is of interest for adapting and fine-tuning properties via simple changes in geometry and material composition. (c) We then compare the relative “cost” of different mechanical solutions by comparing rigidity and stiffness with the carbon content or biomass that has been attributed by the plant for different roles. (D) Finally, we list the biological functions and discuss their relevance for bioinspired robotics research using, as far as possible, a biologically non-technical language. This overall approach represents just one example of how the study of a biological system might be focused on the search for functional attributes useful for novel technologies for robotics applications.

Ecological Observations

We made observations at ~12 sites where *S. setaceus* was common and presented its full range of growth phases from creeping and climbing to searching stems. Our main aim was to gather observations about its growth through complex three-dimensional spaces from forest floor, to low level branches and scrub to climbing stems on tree trunks and as searcher stems emerging from the forest margin and tree canopies. We measured the reach of 34 vertical to horizontal searcher stems as the length of stem segment from the last supported point on the host vegetation to the apex of the searcher. We did not include stems that had reached or passed their maximum length as self-supporting axes.

Mechanical Tests and Macro Anatomy

Three different types of stem were collected from natural sites for the mechanical tests and kept in humid conditions prior to the measurements. Three-point bending tests (Vincent, 1990) were carried out on the stems using a portable Instron machine (In-Spec 2200, Instron Corporation, Norwood, MA, USA; <http://www.instron.com>). The study included a total of 127 stem segments: 36 basal stem segments that were approximately cylindrical in cross-section (from 25 individuals); 62 stem segments that were approximately triangular in cross-section (from 32 individuals) and 34 apical “searcher” stems that were approximately star-shaped in cross-section (from 28 individuals).

We obtained a span-to-depth ratio of 20–30 after tests were taken to determine the minimum span to depth ratio necessary to minimize the influence of shear on the measured bending (Vincent, 1990).

Flexural rigidity (EI) is the resistance of the stem to a bending force. This parameter is the product of the axial second moment of area (I) (cross section dimensions and shape), and the elastic modulus (E) of the stem.

$$\text{Flexural rigidity} = E^*I \quad (1)$$

Stem flexural rigidity (Nmm^2) was calculated as:

$$EI = L^3 * b / 48 \quad (2)$$

where L is the distance (mm) between the supports in three-point bending and b is the slope of the force-deflection curve (Nmm^{-1}).

The second moment of area (I) is a geometrical property of a cross section that describes the spatial distribution of areas within the section with reference to the centroid and neutral axis in bending.

The cross-sections of stems showed highly complex cross-section geometries that varied from circular to triangular to highly winged or star-shaped. Following each mechanical test, we prepared three transverse slices from the middle 5 cm portion of each tested stem segment, each slice was then orientated in the direction of the applied force during the test and then photographed. Image analysis software “Optimas”, V.6.5.172, Media Cybernetics, Inc., Rockville, MD, USA was then used to trace the transverse outlines of each slice and a macro (courtesy of T. Almeras, Montpellier) was then used to calculate the second moment of area of each stem shape.

Young’s modulus is the stiffness of a material, defined as the slope of the linear region in a stress-strain curve. It is a parameter used for homogeneous solid materials. Taking into consideration that plant stems are significantly anisotropic structures composed of different tissues with distinct properties, the concept of a Young’s modulus refers here to a composite structure in bending. In the literature it has been previously referred as a “structural” Young’s modulus (Speck and Rowe, 1999).

Young’s modulus in bending E (MNm^{-2}) was obtained using the following formula:

$$E = EI/I \quad (3)$$

where EI (Nmm^2) is the flexural rigidity of the stem (Equation 1) and I (mm^4) is the axial second moment of area of the stem calculated using Image analysis software.

Dry Matter Content and Dry Matter Concentration

A fresh portion of each tested stem was used to calculate the dry matter content [DMC, dry mass (mg)/fresh mass (g)] and the dry matter concentration (D , dry mass/volume), also called density (Pérez-Harguindeguy et al., 2013). For the volume calculation we used the weight-displacement method (Hughes, 2005). We first

obtained the fresh weight using a digital balance. The sample was then attached to a fine needle and immersed in a water-filled container placed on a digital balance without touching the walls of the container. The weight of the water displaced was measured, which corresponds to the volume of the sample in cm^3 . For the dry weight, we left the sample to dry in a laboratory oven under forced-air ventilation for ca. 15 days, until reaching a constant weight. With the obtained values we calculated the DMC and the D for comparing the different stems biomass. We used a total of 90 stem segments: 32 circular, 35 triangular and 23 star-shaped.

Statistical Analysis

All quantitative data were analyzed using non-parametric Kruskal-Wallis tests, followed by Dunn's *post hoc* tests (Siegel and Castellan, 1988) in software Statistica (StatSoft, Inc., 2013). Non-parametric tests were chosen for comparing cross-sectional areas, second moments of area, flexural rigidity and Young's modulus between the stem types—circular, triangular, and star-shaped. We elected to use the non-parametric K-W test followed by the relatively conservative *post-hoc* Dunn's test because: (a) some of the tested parameters were not normally distributed for each stem category, (b) degrees of variance for some parameters were not very homogeneous (as is often the case for geometrical and mechanical values), and (c) because of difficulties of sampling equivalent numbers for each stem type. Finally, from a biologically point of view, non-parametric rank-based comparisons are arguably more suitable for comparisons of stem properties that are developmentally ranked rather than as elements belonging to separate entities.

RESULTS

Ecology and Phases of Growth

Selenicereus setaceus exists commonly as a climbing plant in the “Restinga forest” of southern coastal Brazil. It shows highly variable behavior according to the age and position of the plant and in relation to its immediate environment (Figures 1A–H). It was observed on a wide variety of substrates: creeping along the forest floor (Figure 1H), climbing among canopy branches of scrub and trees (Figure 1A) and climbing up tree trunks to 8 m high (Figure 1F). Older, basal stems are circular to elliptical in cross-section with a smooth, brown to green surface (Figure 1G). They gave rise to the green, photosynthetic climbing stems. These stems are triangular to rounded triangular in cross section—often producing roots which adhere to a wide range of surfaces. Younger stem branches we termed “searchers” (Figure 1B) are light green photosynthetic stems bearing spines. These have a “winged,” triangular to star-shaped cross-section and often emerge from trees to cross gaps toward neighboring supports. All categories of stem bear groups of recurved spines. In the young tips of growing stems, spines are initially pointing apically and flattened against the stem (Figure 1D); during development they become generally recurved and point in several directions (Figure 1C).

Two-Step Attachment Strategy

This species employs a “two-step” attachment strategy. In a first step, the clusters of lateral spines (2–5 mm long) act as grappling hooks which fix the searching and climbing stem in place (Figure 2 arrow 1). The groups of 3 to five spines per group and their arrangement on the three angled stem ridges are highly effective for initial adhesion in a wide range of three dimensionally structured environments from laterally clinging to tree trunks and branches (Figure 2 arrow 1), small diameter twigs in the moving tree canopy as well as friable soil surfaces and even stone and concrete objects. Our field observations in a range of environments suggest that this spine attachment serves to mechanically stabilize and fix long searcher stems that would otherwise risk sliding away from supports during early stages of climbing growth. The Restinga forest is a coastal, predominantly wind-exposed environment and we observed that spine attachment was likely important for retaining attachment and stability for stems climbing into the finer branches of trees and scrub.

In a second step (Figure 2 arrow 2) stems that have already been stabilized by hooks and that are held in place become more firmly attached to the support via roots that emerge from the stem surface and grow over the surface of the support entering any fissures or spaces. Stems that are held firmly in place in this way can then continue growth apically without the risk of bending or twisting away from the support and falling to the ground.

Stem Biomechanics and Geometry

Stems differed in mechanical properties, cross-sectional geometry and tissue composition (Figures 3A–D, 4–6). Generally, flexural rigidity (EI) was higher (for a given stem size) in basal, circular stems ($641,683 \pm 1,081,766 \text{ Nmm}^2$) than both triangular climbing stems ($177,804 \pm 172,821 \text{ Nmm}^2$) and apical searcher stems ($376,712 \pm 664,598 \text{ Nmm}^2$) ($P < 0.05$) (Figure 4).

This pattern was also observed in terms of Young's modulus with rounded stems showing higher values of Young's modulus ($328 \pm 115 \text{ MNm}^{-2}$) than younger climbing ($214 \pm 143 \text{ MNm}^{-2}$) and searcher stems ($114 \pm 64 \text{ MNm}^{-2}$) (Figure 5). Second moment of area varied significantly from older basal rounded stems ($1875 \pm 2720 \text{ mm}^4$) and was significantly smaller in triangular stems ($799 \pm 780 \text{ mm}^4$) but tended to be larger in the star-shaped searcher axes ($3322 \pm 3190 \text{ mm}^4$) (Figures 3B, 4–5). Star-shaped stems reached high values of rigidity (EI) approaching that of circular stems due their high values of second moment of area resulting from their winged geometry (Figure 4). We calculated by how much the circular, triangular and star-shaped cross-sections increased in second moment of area compared with theoretical, exactly circular cross-sectional areas for each stem (Table 1). Star-shaped stems showed a significant increase in second moment of area of 67% compared with an equivalent circular model, while triangular and circular stems showed much lower increases of 30 and 27%, respectively (Table 1). In general, the stems present relatively low values of stiffness (E), where triangular stems present intermediate values between circular (highest) and star shape stems (lowest) (Figures 3C, 5).

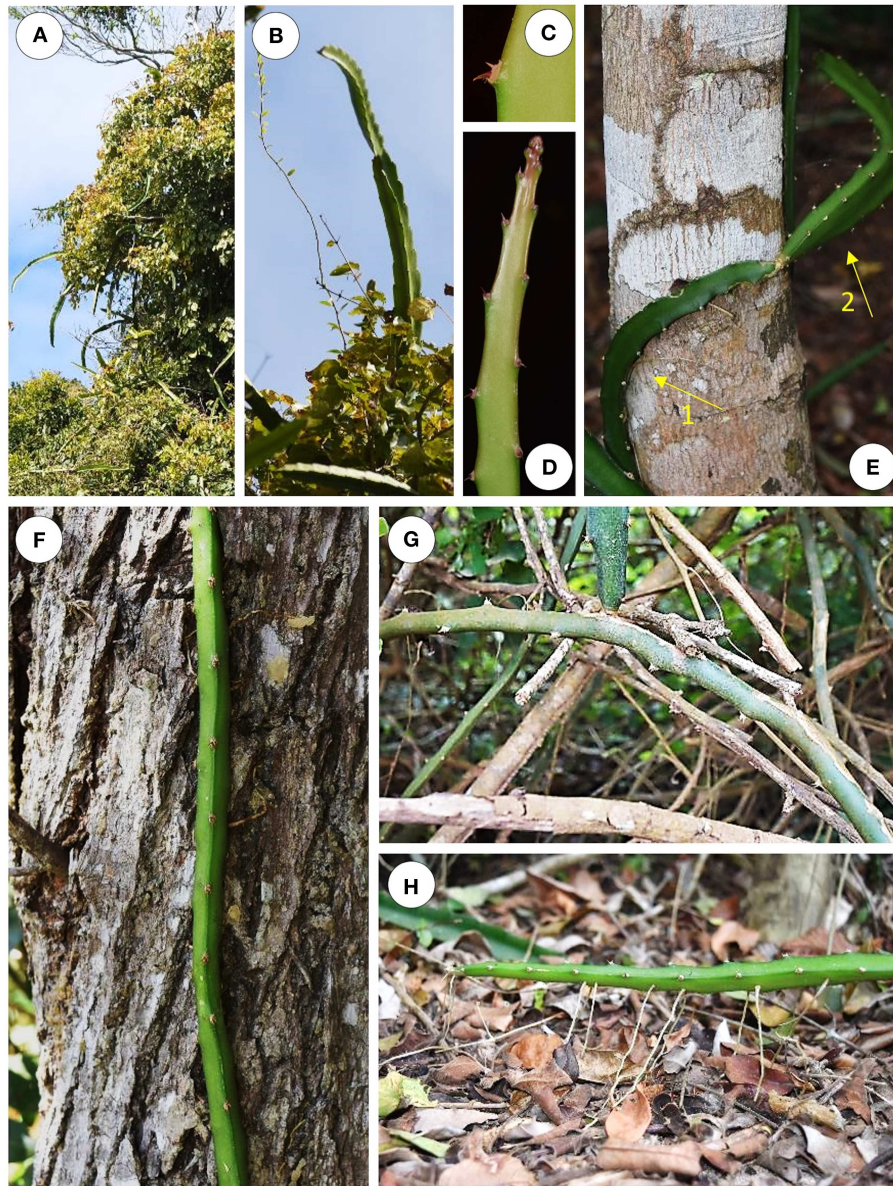


FIGURE 1 | Growth habits of *Selenicereus setaceus* (Cactaceae). **(A)** The species is a tree climber and young apical stems are adapted as “searchers” and emerge from the tree branches. **(B)** Searchers have a star-shaped or winged profile and can grow vertically or horizontally in search of supports. **(C)** Detail of multi-angled clusters of recurved spines; these occur along the edges of three-ridged stems. **(D)** Young searcher apex: spines are initially pointing toward the tip and flattened against the stem; they become recurved during later development and are deployed so as to attach in several directions. **(E)** Triangular root-climbing stems partly coiling around a tree trunk; the more basal portion of the stem is attached by spines and roots to the trunk (arrow 1) while the apex is searching freely (arrow 2). **(F)** A triangular stem climbing up a tree trunk initially deployed recurved hooks that grappled onto the support prior to the development of stronger anchorage by roots. **(G)** Older, basal cylindrical stem traversing complex understory of surrounding stems and branches. **(H)** Roots also attach to the soil at ground level.

Tissue Composition and Dry Matter Content

Tissue contributions to cross-sectional area (% *A*) and second moment of area (% *I*) varied significantly between different stem types (Table 2). All stem types had a large proportion of cortex (including outer collenchyma, epidermis and/or periderm), especially star-shaped stems, which showed 88% of the total cross-sectional area occupied by these tissues. Dissection of

stems for mechanical tests indicated that the soft cortex exuded high levels of hydrogel-like mucilage that expanded in contact with water. Older circular stems showed the highest percentage cross-sectional areas of wood cylinder reaching 15%, while the wood cylinder in triangular and star-shaped stems reached only 5 and 4%, respectively of the cross-sectional area. The percentage of pith area did not vary significantly between stem shapes.



FIGURE 2 | Two-step attachment strategy. The climbing cactus employs a two-step strategy for attaching to a variety of substrates. (1) Initial grappling-steadying attachment using clusters of recurved spines (arrow 1) fixing the plant stem in place while it grows and (2) Solid anchoring using lateral roots (arrow 2) in addition to resource gathering (e.g., water). The strategy is of interest for growing robots as it will allow a device to hook on to the surrounding unstructured environment providing temporary support (bracing) for growth and securing a more solid fixation even in potentially moving (e.g., wind-buffed) environments. White arrows indicate clusters of multi-angled, recurved spines, which are themselves arranged at multi-angles on the plant stem (top right), and roots invading the crevices on the tree surface (bottom right).

Tissue contributions to second moment of area varied significantly between stem types (Table 2). The contribution of cortex (including outer collenchyma, epidermis and/or periderm) dominated the second moments of area in all stems, reaching 94% in circular stems, 98% in triangular and 99% in star-shaped stems. In contrast, wood cylinder contribution was very low, only 5% in circular stems, 1% in triangular stems and <1% in the star shape stems. The pith showed <1% of contribution in all stem types.

All values for dry matter content, density and percentage of biomass were significantly different between the stem types (Table 3). Biomass content was highest in circular basal stems because of the higher amount of denser, lignified wood and presence of a periderm.

DISCUSSION

The Climbing Cactus as a New Concept Generator for Growing and Climbing Robot Technologies

The stem biomechanics in climbing and searching stems of this plant are characterized by a light-biomass architecture of thin-walled tissue which needs to be turgescient to retain stiffness. Basal

(circular) parts of the plant are constructed of stiffer tissues than more apical parts. This organization differs mechanically from many vines and lianas in which basal segments are highly flexible (Speck and Rowe, 1999; Speck et al., 2003; Rowe et al., 2004, 2006; Rowe and Speck, 2005). The combination of succulence and turgescence, searchers with star-shaped geometries as well as a two-step attachment strategy, provides a novel combination of functional traits that might be considered as potential innovations for new climbing plant-like robots. We discuss these as concept generators in terms of overall organization, reaching across voids and attachment (Box 1).

Life History and Terrain

Reaching across voids and efficient, secure attachment will be essential functions for growing robots that are designed to climb and thereby successfully negotiate three dimensionally unstructured, chaotic and even moving environments. Such a design strategy is interesting for applications where the targeted terrain is heterogeneous or not fully known. Potential applications that have been cited for such tasks include: reconnaissance and data gathering following landslides and earthquakes, archaeological investigations of buried/dangerous sites such as wells, ecological and agricultural measuring, surveillance in diverse and unpredictable habitats and space and planetary exploration and maintenance.

Figure 7 summarizes some of the key features that contribute to this life-history at the habitat scale with a highly heterogeneous terrain. (A) Stems start growth rooted in the soil. (B) Early growth as circular to triangular stems can rove and climb across soil, rocks, and tree trunks using spines for initially attaching to these different substrates. (C) Searcher stems develop when the growing tip meets voids and stems develop an optimized geometry to increase rigidity. (D) A two-step attachment strategy ensures initial stabilization via hooks followed by strong attachment via fibrous adhesive roots.

We propose that useful insight for new innovations in robotics can be made by considering entire life-histories of different climbing plant species—how combinations of different functional traits integrate and are adapted for a specific kind of “robotic niche.” We think that this approach should be possibly just as useful as choosing specific functions and structures drawn from parts of a climbing plant life history. For example, the combination of robust (diameter in cm rather than mm), cheaply constructed searcher stems equipped with two kinds of attachment organ is evidently suited for extremely heterogeneous unstructured terrain, soil, rocks, tree trunks and fine branches and leaves with voids of up to 1.5 meters. Other kinds of climbing plant life history such as stem twining or tendril climbing will not be able to navigate and attach to such a heterogeneous range of supports since they are best adapted to attach to a 3-dimensional environment of cylinders (tree branches). It has long been known since Darwin’s experiments and from ecological studies ever since that certain kinds of attachment are limited to certain kinds of support (Darwin, 1867; Peñalosa, 1982; Hegarty, 1991; Gianoli, 2015).

The climbing cactus shows a strong ability to grow through very unstructured and heterogeneous environments by attaching

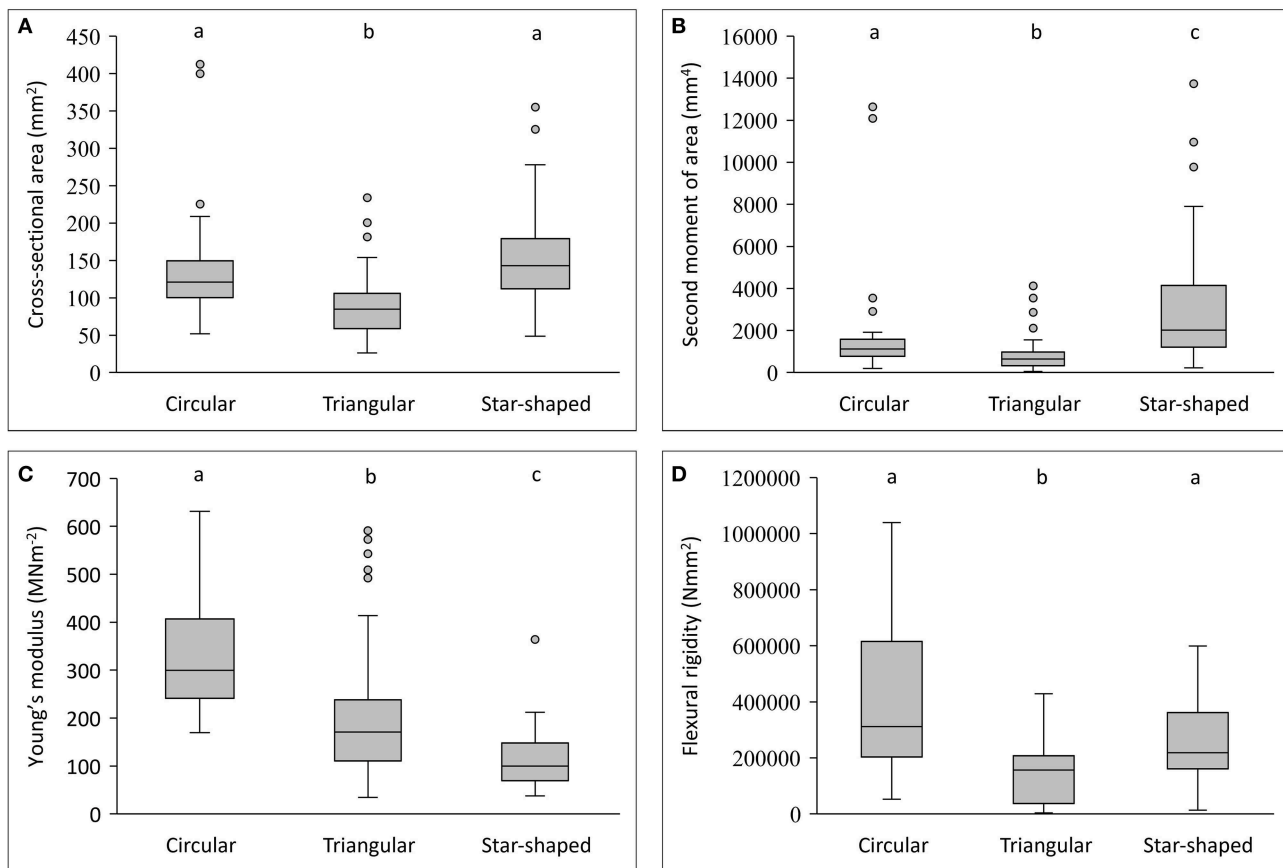


FIGURE 3 | Box plots of geometry and mechanical properties of stem types in *Selenicereus setaceus* (circular, triangular and star-shaped). **(A)** Cross-sectional areas (mm²): circular and star-shaped stems have similar cross-sectional areas that are generally larger than climbing triangular stems. **(B)** Second moment of areas (mm⁴): star-shaped stems show the largest second moment of areas for an equivalent surface area due to their highly winged shape. **(C)** Young's modulus (MNm⁻²): stems decrease in stiffness from old (circular) to young stems (star-shaped). **(D)** Comparison of flexural rigidity (Nmm⁻²): star-shaped stems reach a high rigidity, approaching the values for circular stems but retain a "light" structural organization. Inner lines: medians; boxes: 25th and 75th percentiles; whiskers: max and min values; excluding outliers: circles (not depicted in **D**); small letters show significant differences (Dunn's *post hoc* test) between median values of stem types.

to a very wide range of supports and being able to cross voids of about a meter in length. We propose that these life history traits can provide possible functional innovations for designing robots that are required to navigate through unstructured terrains.

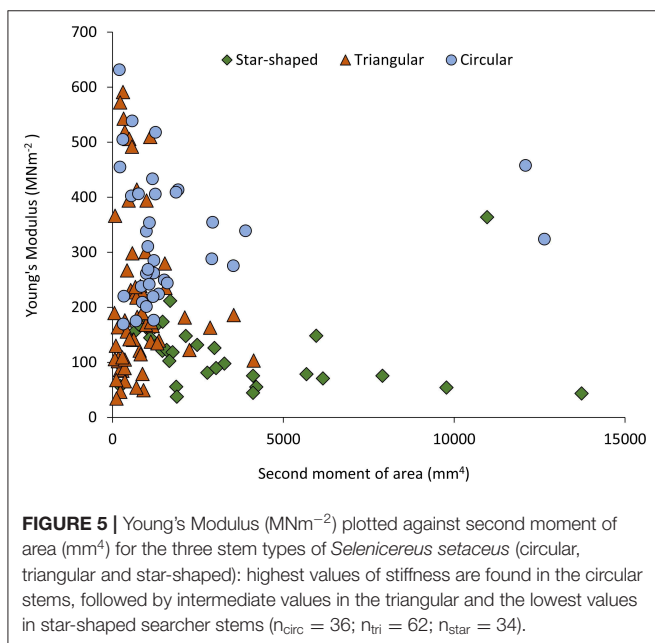
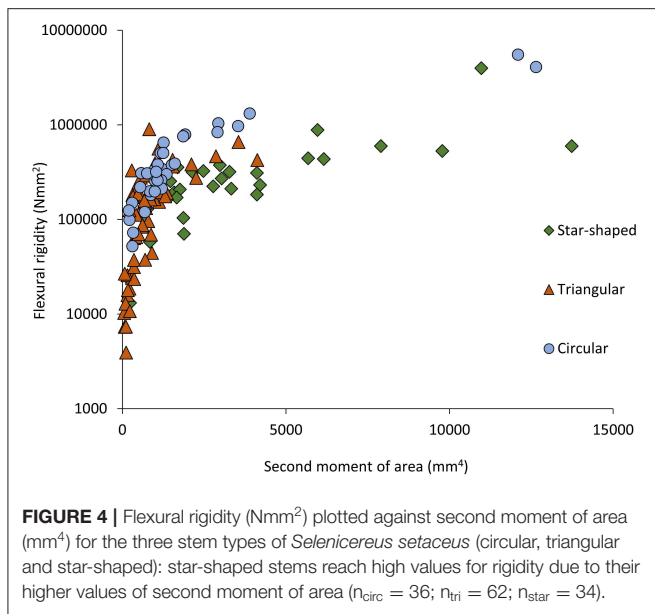
Crossing Voids

Ensuring reach across spaces via growth represents a significant challenge for plants as well as robotic artifacts. Recent studies have made great progress in developing growing root-like robots for movement in soil (Sadeghi et al., 2014, 2016) and for movements comparable to climbing plant stems in air and in relation to supports (Del Dottore et al., 2019). These approaches require potentially different behaviors and technological innovations. Movements in and through soil media require negotiating and growth-by-bending around and between obstacles (rocks and solid substrates) and this has required adaptive behavior of the additive engineering process for artificial root lengthening (Sadeghi et al., 2014, 2017).

The searcher stems of the climbing cactus described here indicate that maximal rigidity using low density materials can be optimized by developing (a) a highly lobed cross-section rather

than a more typical cylindrical organization in stems that need to cross-gaps (**Figure 6**) and a relatively "simple" combination of tissue layers with minimal secondary radial growth. This kind of organization provides a simple biological model for additive growth technologies (3D printing, electron spinning and expanding polymer, hydrogel or foam-based materials). It offers a way of modulating rigidity without complex secondary radial growth or the equivalent of longitudinally continuous fiber composite materials (the equivalents of wood and fiber tissue) for robotic "stems" to traverse gaps and voids to over a meter at this scale. If additive manufacturing technologies can construct different layers of materials having different mechanical properties such as a thin stiff outer skin and a bulking but light inner "tissue" in the forms of lobed cross-sections this would go some way to providing high rigidity for the minimum mass, as well as reducing problems of bending and torsion moments and "cost" of material production in terms of energy.

Our study did not enable us to resolve what might be the stimulus or trigger, either internal or extrinsic, that initiates geometrical and mechanical changes from circular to star-shaped. However, our observations of young "small"



diameter individuals in well-lit forest floor situations suggest that light might be a factor governing this rather than ontogeny. It is also possible that the response might also be due to bending moments when growth exceeds the length of a support. Interestingly, lack of a support (presence of a void) and presence of light coincide in many natural situations here such as the edge of the forest or forest gaps. The shift to a winged cross-section optimizing light capture and rigidity as an adaptive response would be an interesting aspect to investigate more closely. It would also be of further interest to observe the behavior on encountering voids in dark situations.

Our observations indicated that low biomass stems are capable of navigating by “steering” toward, along, around and away from

obstacles during first to second steps of the attachment phase (**Figure 1E** arrow 1, arrow 2). The ability to change direction while still retaining flexural stability is a crucial functional trait for searchers of climbing plants. In the cactus this likely depends on geometrical and material optimization below the growing apex. In artificial systems such changes will likely depend on the kind of growing mechanism—either immediately behind the apex such as apical additive manufacturing devices, or by other processes which influence (modify or add to) the stem after the “artificial” tissues have been formed. Ongoing studies on the *Selenicereus* anatomy, morphology and mechanics will investigate to what extent soft tissues modulate bending of the stem for adaptive growth (**Box 1**).

As pointed out above, one of the aims of developing movement by growth artifacts is the ability to negotiate navigate and climb through unstructured environments where the kinds of terrain are possibly far more heterogeneous than a system of cylindrical supports. Many climbing plants that do not fully twine can develop open hook-like stem curvatures that shape their surface for better adherence to broad surfaces like trees via micro-hooks or roots. The cactus described here appears to make such movements in relation to large diameter supports (**Figure 1E**). We suggest that this kind of “interactive growth” which does not require full twining might be an effective means by which “searching” robotic artifacts might align with encountered supports in order to deploy attachment mechanisms.

Finally, stems need to ensure rigidity and minimize mass in order to avoid dangerous bending moments that interfere with the desired directional growth via Euler buckling or worse sudden dramatic failure from local buckling. Artificial additive systems using an apical head are thus significantly end loaded and this is very different from most plant searchers in the biological world, which are nearly always tapered from base to apex with minimal end loading. This poses challenges for technologies using additive manufacturing if the mechanism (a) imparts significant end loading that increases bending and torsional moments or (b) is unable to mimic “secondary growth” of plants that adaptively increase rigidity below the apex. Keeping searcher stems light, rigid and optimized in terms of mass and end loading might mitigate against risks of buckling and enable search over wider voids.

Two-Step Attachment

Unlike artificial root-like growth (Sadeghi et al., 2017) climbing, growing artifacts will possibly require alternative “adaptive” reactions in the transition from searching/spanning to attaching to “obstacles” rather than avoiding them (Walker, 2015). In the natural world there is probably not one single mode of attachment in climbing plants that will function in all habitats and on all supports. Attachment of growing robotic artifacts is a challenging prospect in environments with voids of different and unknown distances and with obstacles and supports of different, sizes, shapes, and surface properties. For example, stem twining and tendrill twining organs are an appealing

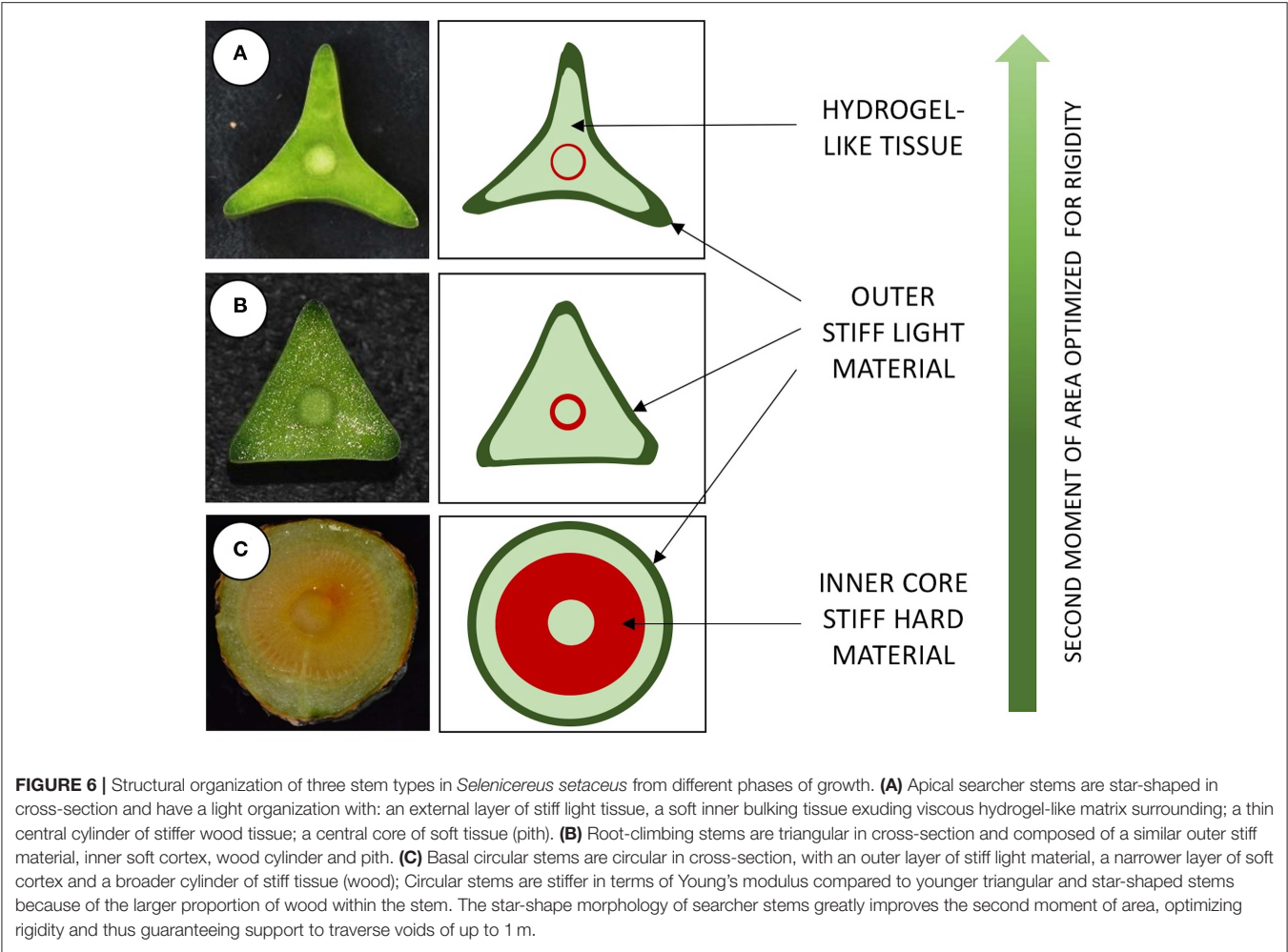


TABLE 1 | Cross sectional areas and second moments of area (*I*) of a circle of equivalent area and second moment of area (*I*) measured using the Image software Optimas of three stems types of *Selenicereus setaceus*: circular, triangular and star-shaped (means) ($n_{\text{circ}} = 36$; $n_{\text{tri}} = 62$; $n_{\text{star}} = 34$).

Stem type cross-section	Total cross sectional area (mm ²)	<i>I</i> for a circle of equivalent area (mm ⁴)	<i>I</i> measured (mm ⁴)	Percentage gain in <i>I</i> (%)
Circular	136.22	1477.46	1875.31	26.93
Triangular	87.70	614.56	798.33	29.90
Star-shaped	157.08	1967.86	3322.25	68.83

biological phenomenon for technical transfer e.g. (Must et al., 2019). However, among climbing plants, twining is highly constrained to the size and diameter of the support—i.e., slender, approximately cylindrical objects. Such mechanisms might not easily attach to flat or blocky objects or to friable or granular unconsolidated substrates. Climbing artifacts will likely need a more “generalized” or more “adaptive” system of attachment if they are to navigate through heterogeneous environments.

The cactus deploys a two-step attachment strategy (Figure 7) where clusters of sharp spines, are deployed on the stem in different orientations, each cluster bearing 3 to 5 spines, which are in turn deployed in different directions. This represents a multi-directional grappling system (Figure 7) and is effective

on (i) narrow springy branches of shrubs and trees even in wind-blown environments, (ii) smooth or rough bark surfaces of trees, (iii) rock and concrete surfaces and (iv) soil and leaf litter surfaces. The engagement of sharp spines creates an initial grappling attachment that will prevent the stem from falling during continued growth and consequent shifts of weight distribution. It gives the plant “time” to deploy the slower growth of the root system to attach more firmly adjacent to the attached hooks (Figures 2 arrow 2, 7). The second step involves initialization of root growth from the stem followed by further root growth onto, into or around a large variety of supports differing in geometry and surface properties (soil, rock, on and around and within the crevices of bark surfaces).

TABLE 2 | Percentage contribution of tissues to cross-sectional area (CSA) and second moment of area (*I*) of three stems types of *Selenicereus setaceus*: circular, triangular and star-shaped (means ± standard deviations, tested with Kruskal-Wallis (*P* < 0.001) and Dunn's *post hoc* tests (*P* < 0.05).

Stem type cross-section	Cortex and epidermis/peridermis	Wood cylinder	Pith
Contribution to CSA (%)			
Circular	77.49 (±6.33) ^A	14.71 (±6.40) ^A	7.79 (±2.39) ^A
Triangular	86.29 (±4.28) ^B	4.75 (±1.42) ^B	8.96 (±3.61) ^A
Star-shaped	88.03 (±2.16) ^C	4.38 (±0.67) ^C	7.59 (±1.64) ^A
Contribution to <i>I</i> (%)			
Circular	94.07 (±2.93) ^A	5.17 (±2.96) ^A	0.77 (±0.34) ^A
Triangular	98.05 (±1.03) ^B	1.08 (±0.54) ^B	0.86 (±0.57) ^A
Star-shaped	98.56 (±0.71) ^C	0.81 (±0.35) ^C	0.63 (±0.37) ^A

Different letters indicate significant differences between groups (*n* = 10).

TABLE 3 | Dry matter content, density and percentage of biomass of three stem types of *Selenicereus setaceus*: circular, triangular and star-shaped (means ± standard deviations).

Stem type cross-section	Dry matter content (mg.g ⁻¹)	Density (g.cm ⁻³)	Percentage of biomass
Circular	154.13 (± 41.81) ^A	0.15 (± 0.04) ^A	15.41 (±4.18) ^A
Triangular	108.33 (± 24.06) ^B	0.1 (± 0.02) ^B	10.83 (±2.41) ^B
Star-shaped	90.41 (±41.21) ^C	0.09 (± 0.04) ^C	9.0 (± 4.12) ^C

Tested with Kruskal-Wallis (*P* < 0.001) and Dunn's *post hoc* tests (*P* < 0.05). Different letters indicate significant differences between groups (*n*_{circ} = 32; *n*_{tri} = 35; *n*_{star} = 23).

BOX 1 Overview of biological structures and their biological functions in heterogeneous environments, mechanical organization across the plant body and conceptual applications for growing robotic artifacts.			
Biological structure	Biological function in habitat	Mechanical organization	Concept for applications
Stem geometry circular, triangular to star-shaped	For adapting stem profiles for modulating mechanical properties and creeping, climbing and searching, while minimizing physiological and material “costs.”	Gradient of profile geometries from circular (base) to deeply lobed at apex optimized for rigidity in searcher stems.	Growth process adapts profiles for different phases of growth and navigation. e.g., load-bearing searchers with optimized star-shapes using light material architectures.
Reflexed multi-directional spine clusters	Grappling on highly variable shapes and sizes of support and substrate. Step 1 attachment for initial steadying and bracing for facilitating solid attachment (step 2).	Smart (preformed) deployment from folded position at stem tip to open and multi-directional clusters lower down stem.	Incorporation of multi-directional grappling clusters arranged in different directions for attachment to diverse shapes, sizes and substrates. Programmable actuation of hook deployment and geometry.
Aerial climbing roots from stem surface	For solidly attaching climbing stem to many kinds of support and surface. (step 2 attachment for secure attachment and anchoring, bracing for supporting further growth at apex).	Roots invading and adhering to surfaces and crevices (exact mechanisms under study).	Integrate artificial “secondary growth and attachment processes” e.g., “second step” attachment and adhesion following initial steadying. For ensuring support/bracing for growing robot body through unpredictable supports and voids.

The initial attachment is therefore “passive” (there is little or no active movement of spines following their deployment from the apex—but see below) with “pre-formed” structures (the spines are developed on the surface of the stem automatically and not in response to a nearby support or other stimulus such as gravity or shade). The second attachment by roots is an “active” growth process that needs to be triggered and its slow but secure attachment is relatively slow compared to the passive engagement of sharp spines. Passive and active attachment mechanisms are found widely throughout the biological diversity

of climbing plants, they are also functionally linked to kinds of niche, especially the presence of short or wide voids and the arrangement and density of supports.

We suggest that multi attachment systems could be an invaluable design strategy for climbing artifacts, particularly in highly unstructured environments with extreme diversity of supports—just as we see in the natural range of situations for the climbing cactus (**Box 1, Figure 7**).

Hook and spine-inspired structures have been a rich and general source of bioinspiration for attachment strategies e.g.,

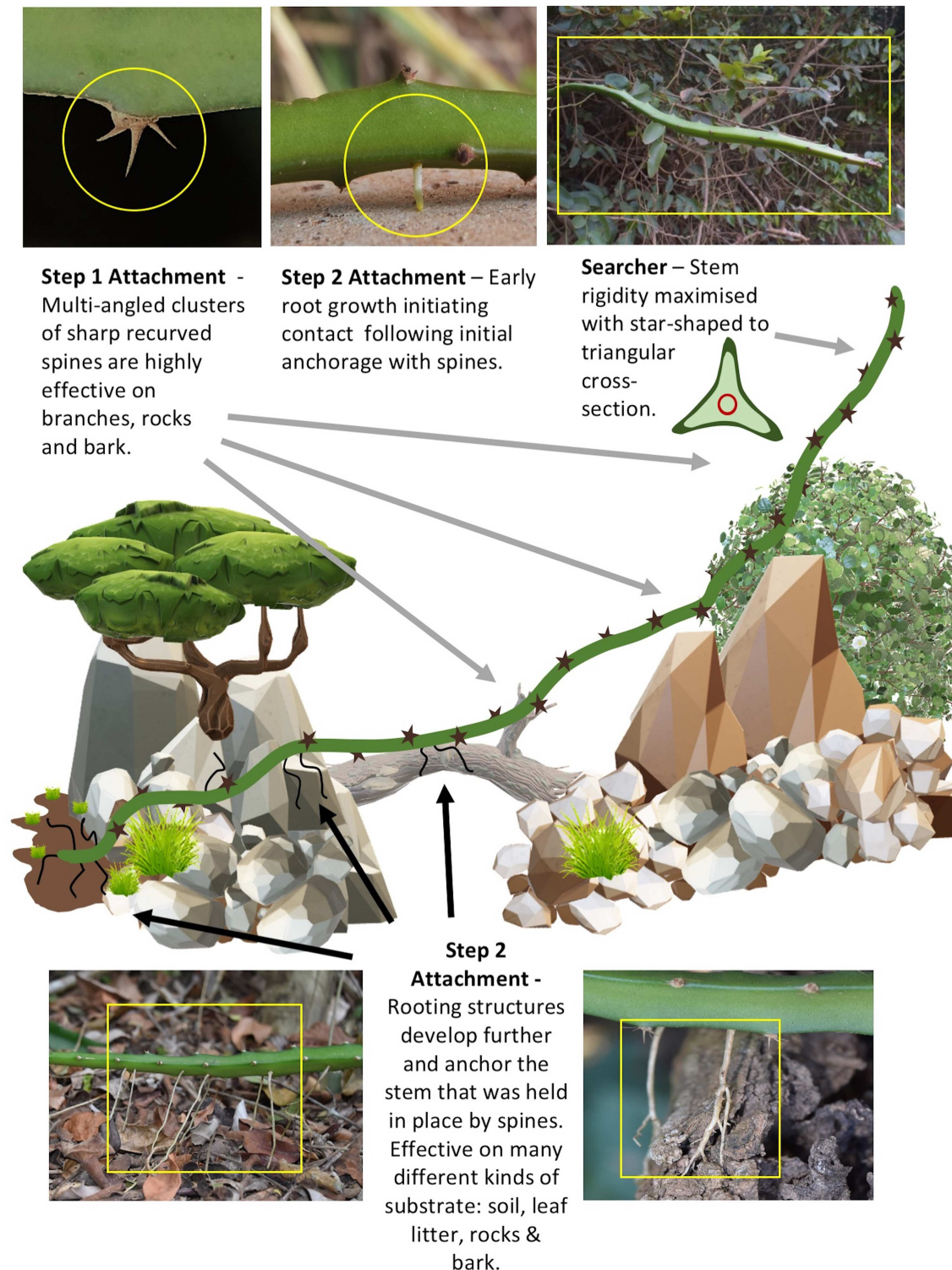


FIGURE 7 | Depiction of growth mode and two-step attachment strategy of (*Selenicereus setaceus*) in traversing (roving, climbing and searching) through a highly unstructured environment with highly variable support substrates. Step 1: Multi-angled clusters of multi-angled recurved spines (top left) initiate preliminary anchoring (steading) in relation to many different geometrical supports (flat, curved, large-thin cylinders, and substrates (hard rocks and cement, friable bark, leaves and soil). Stems held “in place” in otherwise potentially unstable positions during climbing and roving allow slower but more permanent attachment by roots to be initiated and (Continued)

FIGURE 7 | make a first contact with a substrate (top center). Step 2: Roots grow and firmly anchor the stem to several kinds of substrates e.g., soil and leaf litter (lower left) and hard rocks/cement surfaces, tree surfaces such as bark (lower right). Grappling using spines is very effective especially in complex moving environments (like branches and leaves of other plants in the surrounding vegetation). Following initial and then firm attachment the stem can continue to explore across voids and uneven terrain but is now protected from falling away from its desired position as additive growth adds more mass and bending moments that would otherwise cause a fall. The searcher axes (top right) maximizes rigidity by developing a highly winged cross-section enabling the light-mass structure to cross voids of up to 1 m. It deploys further multi-angled hooks for further initial contact and anchoring to apparently most kinds of support in this habitat. These two mechanisms of attachment (fast and slow) ensure that this climbing plant (unlike many other climbing plants with higher support substrate specificity) can continuously grow and climb into a very wide range of habitats. The mechanisms therefore serve as a model for robotic artifacts that with design requirements for “highly diverse” support geometries and substrate properties.

(Gorb, 2008; Voigt et al., 2012; Gallenmuller et al., 2015). Grappling devices for climbing plant-inspired robotic devices have already been implemented in continuum robotic artifacts that can grapple onto supports (Wooten and Walker, 2018) and help anchor the device and support it for its continued searching and functioning. The notion of bracing in robotics (Book et al., 1984; Walker, 2015) has probably been played out many times in the diversification of climbing plants at variable scales of organization. Mechanisms that promote “early adherence” and “steadying” of adjacent structures before more solid attachment are probably common in climbing plants and are probably of great importance especially in perturbed environments. Darwin commented on the probable “early” attachment of small radius twining stems that were efficient in windy conditions for a twining species (Darwin, 1867; Gianoli, 2015). Even much smaller -scale adhesion mechanisms probably entail multi-step mechanisms, for example in highly specialized sticky pads of *Parthenocissus tricuspidata* (Boston Ivy) where small hook structures probably steady the deployment of sticky pads near their support (Steinbrecher et al., 2011). New technologies may potentially play an important role in mimicking these multi-step mechanisms, which climbing plants use to ensure functionality in unstructured and perturbed environments (**Box 1**).

Spines of the cactus are forward pointing and in a “folded away” position near the searching apex (**Figure 1D**). Further below the apex they change in position to become recurved and multi-angled. Technologies now exist for fabricating and modulating artificial hook properties (stiffness) and geometries (angle of curvature) (Fiorello et al., 2018, 2019) using Direct Laser Lithography (DLL), micro molding of PDSM, among others, and incorporated nano particle actuation. Such possibilities might be feasible for “pre-formed” spine attachment on robotic bodies. Based on our observations of *Selenicereus* such technologies might be useful for deploying hook-like structures so as to avoid snagging on to obstacles during extensional growth and be deployed following extension and in the vicinity of supports (Wooten and Walker, 2018). This kind of hook movement prior to deployment for attachment is known in other climbing plants such as the highly effective acanthophylls (modified hook-like leaflets) in the climbing palms (Isnard and Rowe, 2008).

The root adhesion system in *Selenicereus* follows initial hook attachment and firmly anchors segments of stem to a range of support substrates. Root attaching mechanisms are well described for English ivy and also entail a multi-step mechanism of passive and active processes at the micro to nano scale (Melzer et al., 2010, 2012). To our knowledge, as yet there is no published account of “growth-like” technologies that

could mimic this kind of attachment in either apical additive engineering growth artifacts or pre-formed, telescoping/everting and continuum technologies.

In *Selenicereus* the apex “decides” which stem geometry and which tissue properties are best adapted for the requirements at the apex. It also produces hooks in a “pre-deployed” geometry. As in many climbing plants “second step processes” including secondary radial growth of the wood cylinder and growth of attachment root meristems laterally are crucial for fine-tuning rigidity and deploying strong and stable growth-mediated attachment by roots. These second-step processes are absolutely crucial for maintaining reach, minimizing end-load effects and providing secure and safe rather than risky or temporary attachment when the plant has found a support. A challenge for growing robotic designs will be to integrate multi-step growth and attachment devices along the “grown” part of the artificial stem as in many climbing plants such as the climbing cactus described here. A fascinating breakthrough in climbing plant robotics would be to enable such “secondary growth” and “deployment functions,” either by pre-forming structures that could be actuated during later development (such as the spines here) or embed structure in the additive manufacturing process that can be later triggered and capable of extendable growth for attachment or modifying properties of the stem.

Further research on the spine architecture and their deployment as well as the strength and attachment properties of the *Selenicereus* root system will afford more information on how such traits can be translated into technological concepts and technologies.

DATA AVAILABILITY STATEMENT

The datasets generated for this study are available on request to the corresponding author.

AUTHOR CONTRIBUTIONS

PS and NR both conceived of the project, carried out the field and technical research, conceived of technical modifications for mechanical measurements in the field, analyzed the data, and wrote the manuscript.

FUNDING

This work was supported by Grant Agreement number: 824074—GrowBot—H2020-FETPROACT-2018-2020/H2020-FETPROACT-2018-01.

ACKNOWLEDGMENTS

We thank staff at the UMR AMAP and the University of Parana State for technical assistance during this study and we thank Edson and Edmea Soffiatti for logistic support during field work. This project has received funding from

the European Union's Horizon 2020 research and innovation programme under grant agreement no. 824074. We thank our two reviewers and editors for their comments which have greatly improved this manuscript. NR also acknowledges Prof. Ian Walker for a recent, fruitful discussion during the course of this project.

REFERENCES

- Andrews, H. G., and Badyal, J. P. S. (2014). Bioinspired hook surfaces based on a ubiquitous weed (*Galium aparine*) for dry adhesion. *J. Adhes. Sci. Technol.* 28, 1243–1255. doi: 10.1080/01694243.2014.891435
- Barthélémy, D., and Caraglio, Y. (2007). Plant architecture: a dynamic, multilevel and comprehensive approach to plant form, structure and ontogeny. *Ann. Bot.* 99, 375–407. doi: 10.1093/aob/mcl260
- Barthlott, W., Mail, M., Bhushan, B., and Koch, K. (2017). Plant surfaces: structures and functions for biomimetic innovations. *NanoMicro. Lett.* 9:23. doi: 10.1007/s40820-016-0125-1
- Bateman, R. M. (2002). "Generating and filtering major phenotypic novelties: neoGoldschmidtian saltation revisited," in *Developmental Genetics and Plant Evolution*, eds Q.C.B. Cronk, R.M. Bateman and J.A. Hawkins (London: Taylor and Francis), 109–159. doi: 10.1201/9781420024982.ch7
- Bauer, G., Klein, M. C., Gorn, S., Speck, T., Voigt, D., and Gallenmüller, F. (2011). Always on the bright side – the climbing mechanism of *Galium aparine*. *Proc. R. Soc. B* 287, 2233–2238. doi: 10.1098/rspb.2010.2038
- Book, W. J., Le, S., and Sangveraphunsiri, V. (1984). "The bracing strategy for robot operation," in: *5th Symposium on Theory and Practice of Robots and Manipulators* (Udine, Italy). doi: 10.1007/978-1-4615-9882-4_20
- Burris, J. N., Lenaghan, S. C., and Stewart, C. N. Jr. (2018). Climbing plants: attachment adaptations and bioinspired innovations. *Plant Cell. Rep.* 37, 565–574. doi: 10.1007/s00299-017-2240-y
- Busch, S., Seidel, R., Speck, O., and Speck, T. (2010). Morphological aspects of self-repair of lesions caused by internal growth stresses in stems of *Aristolochia macrophylla* and *Aristolochia ringens*. *Proc. R. Soc. B. Biol. Sci.* 277, 2113–2120. doi: 10.1098/rspb.2010.0075
- Darwin, C. (1867). On the movements and habits of climbing plants. *J. Linn. Soc. Bot.* 9, 1–118. doi: 10.1111/j.1095-8339.1865.tb00011.x
- Del Dottore, E., Mondini, A., Sadeghi, A., and Mazzolai, B. (2019). Characterization of the growing from the tip as robot locomotion strategy. *Front. Robot. AI* 6:45. doi: 10.3389/frobt.2019.00045
- Del Dottore, E., Sadeghi, A., Mondini, A., Mattoli, V., and Mazzolai, B. (2018). Toward growing robots: a historical evolution from cellular to plant-inspired robotics. *Front. Robot. AI* 5:16. doi: 10.3389/frobt.2018.00016
- Fiorello, I., Del Dottore, E., Tramacere, F., and Mazzolai, B. (2020). Taking inspiration from climbing plants: methodologies and benchmarks -a review. *Bioinspir. Biomim.* 15:031001. doi: 10.1088/1748-3190/ab7416
- Fiorello, I., Meder, F., Tricinci, O., Filippeschi, C., and Mazzolai, B. (2019). "Rose-inspired micro-device with variable stiffness for remotely controlled release of objects in robotics," in *Biomimetic and Biohybrid Systems. Living Machines 2019*, eds U. Martinez-Hernandez, V. Vouloutsis, A. Mura, M. Mangan, M. Asada, T.J. Prescott, and P. F. M. J. Verschure (Cham: Springer International Publishing), 122–133. doi: 10.1007/978-3-030-24741-6_11
- Fiorello, I., Tricinci, O., Mishra, A. K., Tramacere, F., Filippeschi, C., and Mazzolai, B. (2018). "Artificial system inspired by climbing mechanism of galium aparine fabricated via 3D laser lithography," in *Biomimetic and Biohybrid Systems. Living Machines 2018. Lecture Notes in Computer Science*, eds V. Vouloutsis, J. Halloy, A. Mura, M. Mangan, N. Lepora, T. J. Prescott, and P. F. M. J. Verschure (Cham: Springer International Publishing), 168–178. doi: 10.1007/978-3-319-95972-6_18
- Gallenmüller, F., Feus, A., Fiedler, K., and Speck, T. (2015). Rose prickles and asparagus spines - different hook structures as attachment devices in climbing plants. *PLoS ONE* 10:e0143850. doi: 10.1371/journal.pone.0143850
- Gentry, A. G. (1991). "The distribution and evolution of climbing plants," in *The Biology of Vines*, eds F.E. Putz and H.A. Mooney (Cambridge: Cambridge University Press), 73–97.
- Gianoli, E. (2015). The behavioural ecology of climbing plants. *AoB Plants* 7:plv013. doi: 10.1093/aobpla/plv013
- Gibson, A. C., and Nobel, P. S. (1986). *The Cactus Primer*. Cambridge: Harvard University Press. doi: 10.4159/harvard.9780674281714
- Gorb, S. (2008). Biological attachment devices: exploring nature's diversity for biomimetics. *Philos. Trans. A* 366, 1557–1574. doi: 10.1098/rsta.2007.2172
- Hawkes, E. W., Blumenschein, L. H., Greer, J. D., and Okamura, A. M. (2017). A soft robot that navigates its environment through growth. *Sci. Robot.* 2:eaan3028. doi: 10.1126/scirobotics.aan3028
- Hegarty, E. E. (1991). "Vine-host interactions," in *The Biology of Vines*, eds F.E. Putz and H.A. Mooney (Cambridge: Cambridge University Press), 357–375. doi: 10.1017/CBO9780511897658.015
- Hughes, S. W. (2005). Archimedes revisited: a faster, better, cheaper method of accurately measuring the volume of small objects. *Phys. Educ.* 40, 468–474. doi: 10.1088/0031-9120/40/5/008
- Huss, J. C., Schoeppler, V., Merritt, D. J., Best, C., Maire, E., Adrien, J., et al. (2018a). Climate-dependent heat-triggered opening mechanism of banksia seed pods. *Adv. Sci.* 5:1700572. doi: 10.1002/advs.201700572
- Huss, J. C., Spaeker, O., Gierlinger, N., Merritt, D. J., Miller, B. P., Neinhuis, C., et al. (2018b). Temperature-induced self-sealing capability of *Banksia* follicles. *J. R. Soc. Interface* 15:20180190. doi: 10.1098/rsif.2018.0190
- Isnard, S., and Rowe, N. P. (2008). The climbing habit in palms: biomechanics of the cirrus and flagellum. *Am. J. Bot.* 95, 1538–1547. doi: 10.3732/ajb.0700005
- Koch, K., and Barthlott, W. (2009). Superhydrophobic and superhydrophilic plant surfaces: an inspiration for biomimetic materials. *Phil. Trans. R. Soc. A* 367, 14871509. doi: 10.1098/rsta.2009.0022
- Latthe, S. S., Terashima, C., Nakata, K., and Fujishima, A. (2014). Superhydrophobic surfaces developed by mimicking hierarchical surface morphology of lotus leaf. *Molecules* 19, 4256–4283. doi: 10.3390/molecules19044256
- Mazzolai, B. (2017). "Plant inspired growing robots," in *Soft Robotics: Trends, Applications and Challenges*, eds C. Laschi, J. Rossiter, F. Lida, M. Cianchetti, and L. Margheri (Springer International Publishing AG), 2017.
- Mazzolai, B., Beccai, L., and Mattoli, V. (2014). Plants as model in biomimetics and biorobotics: new perspectives. *Front. Bioeng. Biotechnol.* 2, 1–5. doi: 10.3389/fbioe.2014.00002
- Mehling, J. S., Diftler, M. A., Chu, M., and Valvo, M. (2006). "A minimally invasive tendril robot for in-space inspection," in *The First IEEE/RAS-EMBS International Conference on Biomedical Robotics and Biomechatronics, 2006 BioRob2006* (Pisa, Italy).
- Melzer, B., Seidel, R., Steinbrecher, T., and Speck, T. (2012). Biomechanics of the attachment system of English Ivy (*Hedera helix*): properties and structure of attachment roots in relation to the climbing substrate. *J. Exp. Bot.* 63, 191–201. doi: 10.1093/jxb/err260
- Melzer, B., Steinbrecher, T., Seidel, R., Kraft, O., Schwaiger, R., and Speck, T. (2010). The attachment strategy of English ivy: a complex mechanism acting on several hierarchical levels. *J. R. Soc. Interface* 7, 1383–1389. doi: 10.1098/rsif.2010.0140
- Milvich, M., Speck, T., Speck, O., Stegmaier, T., and Planck, H. (2006). Biomimetics and technical textiles: solving engineering problems with the help of nature's wisdom. *Am. J. Bot.* 93, 1455–1465. doi: 10.3732/ajb.93.10.1455
- Must, I., Sinibaldi, E., and Mazzolai, B. (2019). A variable-stiffness tendril-like soft robot based on reversible osmotic actuation. *Nat. Com.* 10:344. doi: 10.1038/s41467-018-08173-y
- Neinhuis, C., and Barthlott, W. (1997). Characterization and distribution of water-repellent, self-cleaning plant surfaces. *Ann. Bot.* 79, 667–677. doi: 10.1006/anbo.1997.0400

- Niklas, K. J., Molina-Freaner, F., and Tinoco-Ojanguren, C. (1999). Biomechanics of the columnar cactus *Pachycereus pringlei*. *Am. J. Bot.* 86, 767–775. doi: 10.2307/2656697
- Niklas, K. J., Molina-Freaner, F. O., Tinoco-Ojanguren, C., Hogan, C. J. Jr., and Paolillo, D. J. Jr. (2003). On the mechanical properties of the rare endemic cactus *Stenocereus eruca* and the related species *S. gummosus*. *Am. J. Bot.* 90, 663–674. doi: 10.3732/ajb.90.5.663
- Peñalosa, J. (1982). Morphological specialization and attachment success in two twining lianas. *Am. J. Bot.* 69, 1043–1045. doi: 10.1002/j.1537-2197.1982.tb13348.x
- Pérez-Harguindeguy, N., Díaz, S., Garnier, E., Lavorel, S., Poorter, H., Jaureguiberry, P., et al. (2013). New handbook for standardised measurement of plant functional traits worldwide. *Aust. J. Bot.* 61, 167–234. doi: 10.1071/BT12225
- Putz, F. E., and Mooney, H. A. (1991). *The Biology of Vines*. Cambridge: Cambridge University Press. doi: 10.1017/CBO9780511897658
- Rampf, M., Speck, O., Speck, T., and Luchsinger, R. H. (2011). Self-repairing membranes for inflatable structures inspired by a rapid wound sealing process of climbing plants. *J. Bionic Eng.* 8, 242–250. doi: 10.1016/S1672-6529(11)60028-0
- Rampf, M., Speck, O., Speck, T., and Luchsinger, R. H. (2013). Investigation of a fast mechanical self-repair mechanism for inflatable structures. *Int. J. Eng. Sci.* 63, 61–70. doi: 10.1016/j.ijengsci.2012.11.002
- Rowe, N. P. (2018). Lianas. *Curr. Biol.* 28, 249–252. doi: 10.1016/j.cub.2018.01.028
- Rowe, N. P., Isnard, S., Gallenmüller, F., and Speck, T. (2006). “Diversity of mechanical architectures in climbing plants: an ecological perspective,” in *Ecology and Biomechanics: a Mechanical Approach to the Ecology of Animals and Plants*, eds A. Herrel, T. Speck, and N.P. Rowe (Boca Raton, FL: Taylor and Francis), 35–59. doi: 10.1201/9781420001594.ch2
- Rowe, N. P., Isnard, S., and Speck, T. (2004). Diversity of mechanical architectures in climbing plants: an evolutionary perspective. *J. Plant Growth Regul.* 23, 108–128. doi: 10.1007/s00344-004-0044-0
- Rowe, N. P., and Speck, T. (2005). Plant growth forms: an ecological and evolutionary perspective. *New Phytol.* 166, 61–72. doi: 10.1111/j.1469-8137.2004.01309.x
- Sadeghi, A., Mondini, A., Del Dottore, E., Mattoli, V., Beccai, L., Taccola, S., et al. (2016). A plant-inspired robot with soft differential bending capabilities. *Bioinspir. Biomim.* 12:015001. doi: 10.1088/1748-3190/12/1/015001
- Sadeghi, A., Mondini, A., and Mazzolai, B. (2017). Toward self-growing soft robots inspired by plant roots and based on additive manufacturing technologies. *Soft Robot.* 4, 211–223. doi: 10.1089/soro.2016.0080
- Sadeghi, A., Tonazzini, A., Popova, L., and Mazzolai, B. (2014). A novel growing device inspired by plant root soil penetration behaviors. *PLoS ONE* 9:e90139. doi: 10.1371/journal.pone.0090139
- Siegel, S., and Castellan, N. J. (1988). *Nonparametric Statistics for the Behavioural Sciences*. New York, NY: McGraw-Hill Book Company.
- Speck, O., Schlechtendahl, M., Borm, F., Kampowski, T., and Speck, T. (2018). Humidity-dependent wound sealing in succulent leaves of *Delosperma cooperi*—An adaptation to seasonal drought stress. *Beilstein J. Nanotechnol.* 9, 175–186. doi: 10.3762/bjnano.9.20
- Speck, T., and Rowe, N. P. (1999). “A quantitative approach for analytically defining growth form and habit in living and fossil plants,” in *The Evolution of Plant Architecture*, eds M.H. Kurmann and A.R. Hemsley (Kew: Royal Botanic Gardens), 447–479.
- Speck, T., and Rowe, N. P. (2001). “Plant growth forms and biomechanics,” in *Palaeobiology II*, eds D.E.G. Briggs and P.R. Crowther (Oxford: Blackwell Science), 379–384. doi: 10.1002/9780470999295.ch89
- Speck, T., Rowe, N. P., Civeyrel, L., Classen-Bockhoff, R., Neinhuis, C., and Spatz, H.-C. (2003). “The potential of plant biomechanics in functional biology and systematics,” in *Deep Morphology: Toward a Renaissance of Morphology in Plant Systematics*, eds T.F. Stuessy, V. Mayer, and E. Hörandl (Königstein: Koeltz), 241–271.
- Steinbrecher, T., Beuchle, G., Melzer, B., Speck, T., Kraft, O., and Schwaiger, R. (2011). Structural development and morphology of the attachment system of *Parthenocissus tricuspidata*. *Int. J. Plant Sci.* 172, 1120–1129. doi: 10.1086/662129
- Vincent, J. F. V. (1990). *Structural Biomaterials*. New Jersey: Princeton University Press.
- Vogel, S. (2003). *Comparative Biomechanics: Life's Physical World*. Princetown and Oxford: Princeton University.
- Voigt, D., Karguth, A., and Gorb, S. (2012). Shoe soles for the gripping robot: searching for polymer-based materials maximising friction. *Rob Auton Syst.* 60, 1046–1055. doi: 10.1016/j.robot.2012.05.012
- Walker, I. D. (2015). “Biologically inspired vine-like and tendril-like robots,” in *Science and Information Conference (SAI)* (London). doi: 10.1109/SAI.2015.7237221
- Wooten, M., Frazelle, C., Walker, I. D., Kapadia, A., and Lee, J. H. (2018). “Exploration and inspection with vine-inspired continuum robots,” in *2018 IEEE International Conference on Robotics and Automation (ICRA)* (Brisbane, QLD). doi: 10.1109/ICRA.2018.8461132
- Wooten, M., and Walker, I. D. (2016). “Circumnutation: from plants to robots,” in *From Animals to Animats 14. SAB 2016*, eds E. Tuci, A. Giagkos, M. Wilson, and J. Hallam (Cham: Springer International Publishing), 1–11. doi: 10.1007/978-3-319-43488-9_1
- Wooten, M., and Walker, I. D. (2018). Vine inspired continuum tendril robots and circumnutations. *Robotics* 7:58. doi: 10.3390/robotics7030058
- Yang, Y., Davydovich, D., Hornat, C. C., Liu, X., and Urban, M. U. (2018). Leaf-inspired self-healing polymers. *Chem* 4, 1–9. doi: 10.1016/j.chempr.2018.06.001

Conflict of Interest: The authors declare that the research was conducted in the absence of any commercial or financial relationships that could be construed as a potential conflict of interest.

Copyright © 2020 Soffiatti and Rowe. This is an open-access article distributed under the terms of the Creative Commons Attribution License (CC BY). The use, distribution or reproduction in other forums is permitted, provided the original author(s) and the copyright owner(s) are credited and that the original publication in this journal is cited, in accordance with accepted academic practice. No use, distribution or reproduction is permitted which does not comply with these terms.



Artificial Venus Flytraps: A Research Review and Outlook on Their Importance for Novel Bioinspired Materials Systems

Falk J. Esser^{1,2,3*}, Philipp Auth¹ and Thomas Speck^{1,2,3,4}

¹ Plant Biomechanics Group and Botanic Garden, University of Freiburg, Freiburg, Germany, ² Cluster of Excellence livMatS @FIT, Freiburg Center for Interactive Materials and Bioinspired Technologies, University of Freiburg, Freiburg, Germany, ³ Freiburg Center for Interactive Materials and Bioinspired Technologies (FIT), Freiburg, Germany, ⁴ FMF, Freiburg Materials Research Center, University of Freiburg, Freiburg, Germany

OPEN ACCESS

Edited by:

Matteo Cianchetti,
Sant'Anna School of Advanced
Studies, Italy

Reviewed by:

Donato Romano,
Sant'Anna School of Advanced
Studies, Italy
Arri Priimagi,
Tampere University, Finland

*Correspondence:

Falk J. Esser
falk.esser@biologie.uni-freiburg.de

Specialty section:

This article was submitted to
Soft Robotics,
a section of the journal
Frontiers in Robotics and AI

Received: 27 February 2020

Accepted: 05 May 2020

Published: 08 July 2020

Citation:

Esser FJ, Auth P and Speck T (2020)
Artificial Venus Flytraps: A Research
Review and Outlook on Their
Importance for Novel Bioinspired
Materials Systems.
Front. Robot. AI 7:75.
doi: 10.3389/frobt.2020.00075

Bioinspired and biomimetic soft machines rely on functions and working principles that have been abstracted from biology but that have evolved over 3.5 billion years. So far, few examples from the huge pool of natural models have been examined and transferred to technical applications. Like living organisms, subsequent generations of soft machines will autonomously respond, sense, and adapt to the environment. Plants as concept generators remain relatively unexplored in biomimetic approaches to robotics and related technologies, despite being able to grow, and continuously adapt in response to environmental stimuli. In this research review, we highlight recent developments in plant-inspired soft machine systems based on movement principles. We focus on inspirations taken from fast active movements in the carnivorous Venus flytrap (*Dionaea muscipula*) and compare current developments in artificial Venus flytraps with their biological role model. The advantages and disadvantages of current systems are also analyzed and discussed, and a new state-of-the-art autonomous system is derived. Incorporation of the basic structural and functional principles of the Venus flytrap into novel autonomous applications in the field of robotics not only will inspire further plant-inspired biomimetic developments but might also advance contemporary plant-inspired robots, leading to fully autonomous systems utilizing bioinspired working concepts.

Keywords: artificial Venus flytrap, artificial, materials systems, biomimetics, demonstrators, embodied intelligence

INTRODUCTION

In the last decade, the topics of soft robotics and soft machines have tremendously grown as research fields. The field of compliant robots has grown tremendously from the early beginnings of compliant-like actuation for bioinspired robots fitted with McKibben muscles in the early 1950's and 1960's (Agerholm and Lord, 1961; Schulte Jr H. F., 1961). The hard but inflatable McKibben muscles paved the way for inflatable and flexible micro-actuators (Baldur and Blach, 1985; Suzumori et al., 1991), which made compliant actuators considerably smaller, inspiring the development of flexible continuum robots, with Robinson and Davies (1999) highlighting the state of the art, and further to flexible silicone-based robots such as the iconic multigait soft robot of Shepherd et al. (2011). Bridging the

gap from compliant to fully flexible autonomous soft machines, systems were developed such as Kim's autonomous meshworm (Seok et al., 2010; Kim et al., 2013) or the now iconic entirely soft, autonomous robot "octobot" by Wehner et al. (2016). Spanning decades, the research achieved a transition from hard robots with soft actuation to entirely soft systems. These systems were made possible by utilizing various smart and partially soft materials as actuators, such as liquid crystal elastomers (LCEs) (Wani et al., 2017), shape memory alloys (SMAs) (Kim et al., 2013), and polymers (Mather et al., 2009; Behl et al., 2013; Meng and Li, 2013; Besse et al., 2017), electroactive polymers (e.g., DEA, Pelrine et al., 2000; Wang et al., 2019, and IPMC, Shahinpoor, 2011), and materials with thermal (Behl et al., 2013), and humidity responsiveness such as hydrogel (Athas et al., 2016). The newest systems are capable not only of soft actuation but also of "soft sensing" by utilizing soft materials such as conductive elastomers or silicones and/or soft and flexible channels filled with liquid metals (e.g., EGaln, consisting of a mixture of gallium, indium, and tin) forming soft sensors (Kumar et al., 2019). Materials systems are also available, functioning as stretchable electroluminescent skin; these are able to emit light actively, sense deformation, and withstand surface expansion of over 600% (Larson et al., 2016; Zhou et al., 2019). Such extraordinary developments enable a new age of sensing and environment-adaptive robots.

A novel field of soft robotics and soft machines has also emerged within the last few years, namely, that of plant-inspired robotics, focusing on the implementation of the functional principles of plants. These systems utilize structural and functional principles of plants to move, harvest energy, and sense the environment. Plants in particular are well-suited as models for adaptable materials systems that consist of hierarchically structured materials systems with various functions that span several orders of magnitude and that show adaptations to changing environmental conditions, for example, through growth processes and material restructuring.

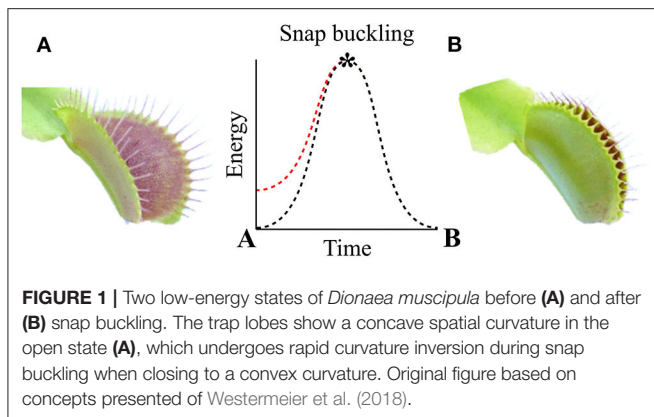
Since plants are sedentary photoautotrophic organisms with the ability to self-reproduce organic molecules (through photosynthesis), locomotion is not strictly necessary. If environmental conditions change, they adapt by changing their physiology and behavior in order to improve their interception of solar radiation and their uptake of ions from the air and the soil, respectively. By means of the exploration and colonization of habitats, plants are able to overcome obstacles, penetrate into hard media, and even move within it, for example, roots within soil (Roy and Bassham, 2014; Sadeghi et al., 2014, 2017). Sensing, selection processes, and reactions to changing conditions are accomplished in plants without a central control unit (i.e., a brain). This raises the possibilities of using plants as role models for autonomous robots whereby the complexity of the overall system can be reduced by eliminating the need for a central control unit and replacing it with a distributed, plant-like, cue-sensitive system that reacts only to certain stimuli.

Currently, soft robotic systems are available based on plant organs such as tendrils, roots, and leaves (Laschi et al., 2017; Wang et al., 2018; Must et al., 2019; Mazzolai et al., 2020). The leaf-inspired systems are particularly interesting not only as role

models for energy harvesters (Liu et al., 2016; Jie et al., 2018; Meder et al., 2018, 2020) but also for fast motions in examples of soft machines inspired by carnivorous plants (Esser et al., 2019). The carnivorous plants *Dionaea muscipula* (Venus flytrap) and *Aldrovanda vesiculosa* (waterwheel plant) have inspired a number of biomimetic robots and facade shading systems for elastic architecture during the last decade (Schleicher et al., 2015; Körner et al., 2018; Knippers et al., 2019). Darwin (1875) was fascinated by *D. muscipula* and called it "one of the most wonderful plants in the world." Therefore, it is not surprising that many attempts have been made to create an artificial trap inspired by the movements of the *D. muscipula*.

The natural habitats of the biological role model for these systems, namely, *D. muscipula*, are nutrient-poor environments such as bogs. To meet its nutrient demands, it catches small arthropods and digests them within its traps. One plant can grow up to 10 leaves with traps that are ~20 mm long, each consisting of two lobes. The lobes are connected via a midrib, with three to four trigger hairs being present on the inside of each lobe. Trap closure is triggered when prey enters the trap and stimulates at least one of the trigger hairs inside the trap twice within a certain time frame (20–30 s at room temperature, Hodick and Sievers, 1989). Water displacement followed by the release of stored elastic energy takes place, leading to the closing movement of the trap leaves within 0.1–0.5 s (Forterre et al., 2005; Poppinga et al., 2018). Trap lobes that are open and ready to snap have a typical concave spatial curvature (as seen from the outside) and undergo rapid curvature inversion releasing the stored energy (snap buckling) when closing. Therefore, the leaves can be described as bistable systems with two low-energy states (Figure 1) (Poppinga and Joyeux, 2011; Westermeier et al., 2018; Sachse et al., under revision). The energy consumption of *D. muscipula* for one trap closure is ~300 μmol ATP, equivalent to 9.66 J (Jaffe, 1973) (ATP hydrolysis consumes roughly 30.5 kJ/mol (Rosing and Slater, 1972). Reopening, after prey capture and digestion, occurs over 1–2 days Fagerberg and Howe, 1996; Volkov et al., 2014; Poppinga et al., 2016, 2018). It is controlled either by irreversible growth processes (Ashida, 1934) or by hydrostatic pressure changes within the lobes (Markin et al., 2008). In comparison, the trap closure of its carnivorous sister species, the waterwheel plant *A. vesiculosa*, utilizes active hydraulics, elastic relaxation, and kinematic amplification via midrib bending deformation (Westermeier et al., 2018), whereas the Venus flytrap employs an initial hydraulic deformation, followed by elastic instability (Sachse et al., under revision). The various mechanical principles for snapping are related to physical limits such as trap size and tissue thickness, which both fundamentally differ in the two traps types (Westermeier et al., 2018, 2019). The kinematic coupling of the midrib bending and trap closure has inspired the development of the Flectofold facade shading system, which incorporates a bioinspired kinetic curved-line folding system with distinct flexible hinge zones actuated with pneumatic cushion bending the midrib (Körner et al., 2018; Saffarian et al., 2019).

The unique functions of the Venus flytrap are of significant interest for biomimetic robotics, as indicated by the development of various artificial Venus flytraps (AVFTs) over the last



25 years (Figure 2). One of the first macroscopic systems was driven by DC motors (Venus flytrap robot) and developed by Yang et al. (2012) who transferred the theoretical models of prey capture into a first fully functional technological demonstrator for a detailed description of the biological role model, the reader is referred to papers by Forterre et al. (2005), Markin et al. (2008), Volkov et al. (2008, 2014), Yang et al. (2010, 2012), Poppinga et al. (2018), and Sachse et al. (under revision). The models theoretically describe the trap closure after prey detection by *D. muscipula*. Most other AVFT systems were soft robots based on smart materials systems, spanning from LCE-based systems of a few millimeters in size (Kohlmeyer and Chen, 2013; Wani et al., 2017) (Figure 3F) to more macroscopic designs driven by heat produced photothermally (Figure 2F) (Lim et al., 2017) or via joule heating (Figure 3B) (Kim et al., 2014; Lim et al., 2017). Other systems were actuated by magnetism and electricity (Figure 3A) (Shahinpoor and Thompson, 1995; Shahinpoor, 2011; Schmied et al., 2017) or pressurized air (Temirel et al., 2016; Pal et al., 2019) (Figure 3E) or were based on hydrogels activated via enzymes (Athas et al., 2016) and moisture (Lee et al., 2010; Fan et al., 2019) (Figure 3D). In addition, the aforementioned designs for applications in architecture can be scaled up to span widths of several meters such as in the Flectofold actuators for facade shading inspired by the trapping movement of the waterwheel plant *A. vesiculosa* (Körner et al., 2018; Saffarian et al., 2019). Furthermore, snap buckling, as seen in and inspired by the Venus flytrap, has been used in various applications from snap-through transitions in optical devices (Holmes and Crosby, 2007) to bistable buckling beam actuators for mechanical memories, micro-relays, micro-valves, optical switches, or digital micro-mirrors in, for example, MEMS systems (Saif and Taher, 2000; Park and Hah, 2008; Shankar et al., 2013).

The AVFT systems differ in their basic composition markedly from one another. In order to achieve better comparability, AVFT systems, representing the current state of the art, are categorized in terms of their actuation mode (Figure 3). In the following, we provide an overview of existing AVFT systems, highlight their advantages/disadvantages, and compare their performances, by using values from literature (providing that data are available) (Table 1). All AVFT systems should meet

certain general conditions and requirements to be classified as an AVFT; these include actuation after a certain trigger, a certain closure time, snap buckling movement of the lobes, and reversibility. Influencing factors for these systems are costs for production and operation, weight, size, geometry, feasible temperature range, trigger parameters, energy consumptions, produced forces, and robustness. The following parameters are used for a comparison of AVFT systems not only among themselves but also with the biological role model: actuation type, sensing capabilities, usage of the snap buckling principle, lobe closure time, input/requirements for actuation, and reversibility of closure (Table 1). The comparison draws attention to current shortcomings and possible novel application fields of AVFT systems.

CHARACTERISTICS OF THE AVFT SYSTEMS (ACTUATION, DESIGN, AND FUNCTIONALITY)

As a common basis for a comparison, we describe here the characteristics of the various AVFT systems. A focus on the actuation mode, material composition, and lobe closure (movement and time) of the various AVFT systems has also enabled us to compare the systems with the biological role model.

Like most soft robots, two pneumatically driven AVFT systems exist that are also triggered by pneumatic actuation. Temirel et al. (2016) have developed a pneumatically driven 3D-printed AVFT (Figure 3E, 1). This system incorporates a touch sensor that is connected to a pneumatic controller. In sensing an object by touch, the shutoff valve is triggered, and the AVFT closes within 8 s; it reopens when pressure is applied. An increase in “trap lobe” displacement correlates with an increase of applied pressure (Temirel et al., 2016). Another pneumatic artificial trap presented by Pal et al. (2019) (Figure 3E, 2) is based on prestressed soft actuators (PSAs) and performs closing movements in 0.05 s. This is achieved through the release of stored elastic energy in different segments of the trap, namely, the spatially curved lobes and the prestressed backbone. Like the biological role model, *D. muscipula*, the artificial lobes invert their curvature from concave to convex while closing. The backbone that connects the two lobes consists of three layers, a prestressed silicon layer (which stores elastic energy) with the activation air chamber, a folded strain-limiting layer in the middle, and another silicon layer at the bottom with a second pneumatic channel for reopening of the AVFT. When pressurizing the activation air chamber, the folded strain-limiting layer is flattened, resulting in a decrease in flexural rigidity of the segment until the PSA “snaps” and the AVFT closes. The snapping motion can be reversed when pressure is applied to the lower pneumatic chamber, reopening the trap, and refolding the crease in the strain-limiting layer (Pal et al., 2019). As in other artificial traps, the pneumatically actuated trap does not feature a separated sensor and has to be activated manually.

One of the greatest advantages of the current AVFT systems is the possible contactless actuation, although most systems need to

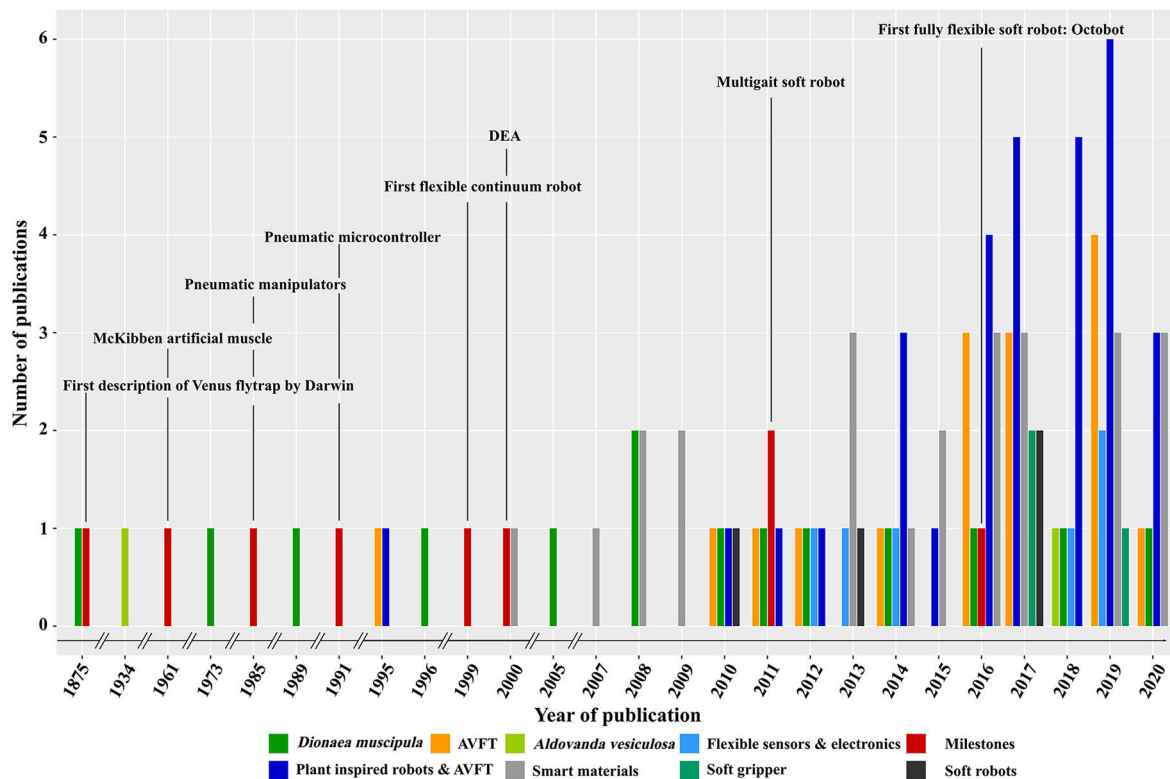


FIGURE 2 | Bibliographic overview of cited publications, highlighting the number of cited publications concerning research about Venus flytraps, *Aldrovanda vesiculosa*, smart materials (*inter alia*: unit cells, logical metamaterials, and self-healing materials), flexible sensors and electronics, soft robots, and plant-inspired robotics including AVFT over the last 145 years since the first description of the Venus flytrap by Darwin in 1875. The numbers are set into relation to noteworthy milestones within these fields. AVFTs were developed within the last 25 years. Shahinpoor and Thompson (1995) were the first to consider theoretically developing an AVFT based on IPMC, and in 2011, Shahinpoor published a paper on an actual IPMC-based AVFT. Within the last decade, publication numbers have risen from one in 2010 to five in 2019, highlighting the growing interest in AVFT systems as platforms or showcases for novel materials developments.

be triggered, like the pneumatic systems, by human input, such as the magnetically actuated artificial flytraps that use carbon-fiber-reinforced prepreg (CFRP) cylindrical shells as “leaves” and that are manually actuated with an electromagnet (**Figure 3A**) (Zhang et al., 2016, 2019). After activation of the electromagnet, the repulsive force between the electromagnet and a permanent magnet, which is attached to the outer leaf rim, triggers a snapping motion. The leaves have a positive curvature in the x-axis and no curvature in the y-axis. After actuation, closure is achieved within 0.2 s, whereas the curvature changes to a positive curvature along the y-axis and zero curvature along the x-axis (Zhang et al., 2016). Moreover, SMA springs are used to actuate a similar AVFT system based on CFRP lobes (**Figure 3B**) (Kim et al., 2014). When actuated by electric current, heat is generated within the material via joule heating, which causes the spring to change its structural phase from martensite to austenite and to shorten (Kumar and Lagoudas, 2008). Hereby, enough force is generated to overcome the crest of the potential energy hill of the system and results in a snapping movement that closes the artificial trap in 0.1 s. By using a second SMA spring as an antagonist, the process can be reversed (Kim et al., 2014). Both

systems use external actuators attached to the lobes to drive the closure.

In using smart materials as a base material, AVFT system lobes have been developed that directly react to a stimulus with movement; in the case of the following examples of electroactive polymers as actuators, the stimulus is electrically based. One smart material type used to create artificial traps is a substance composed of ionic electroactive polymer metal composites (IPMCs) (**Figure 3C**) (Shahinpoor, 2011; Shi et al., 2012). The multilayer material performs bending movements when exposed to an electric field. Whereas, positive charges can move inside the polymer, negative charges are located at an immobile backbone that impedes their ability to move, causing a separation of charges in the electric field (Shahinpoor, 2011). Dissolved cations move within the material, dragging solvent along and causing one side of the material to swell and the opposite side to shrink. Furthermore, IPMCs can generate a small output current. When the material is bent by external force, the solvent is displaced, and the resulting charge separation generates the current. Based on this principle, the IPMCs can be used as bending sensors. Artificial traps made of IPMC attain closing times of around 0.5 s

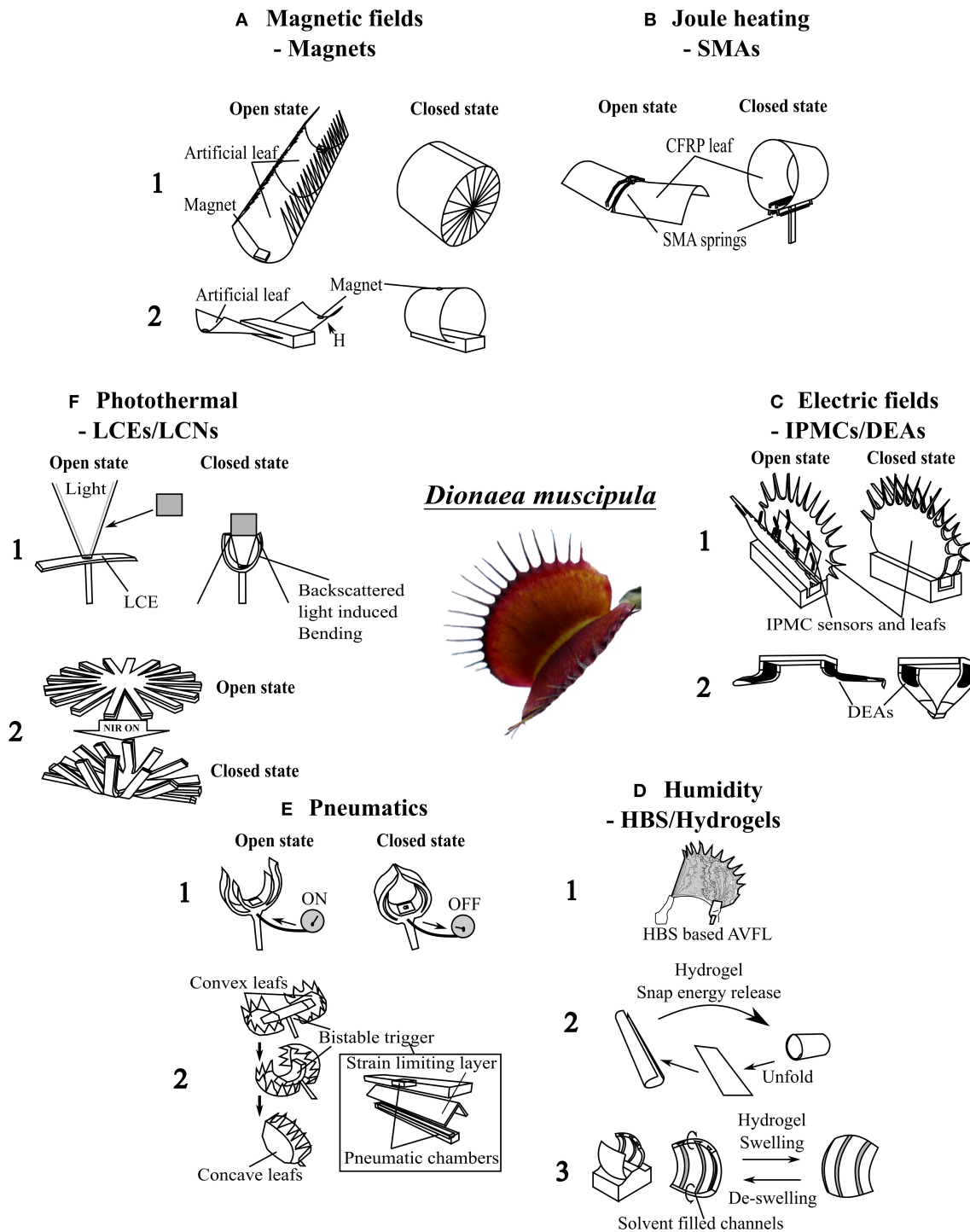













FIGURE 3 | Overview of artificial Venus flytrap systems (AVFTs) categorized by actuation mode. Center: The biological role model *Dionea muscipula*; its basic build and functionalities were abstracted into various AVFT systems. **(A)** Electromagnetic systems: (1) Electromagnetic CFRP-based AVFT (Zhang et al., 2016); (2) electromagnetic CFRP-based gripper (Zhang et al., 2019). **(B)** Heat-driven SMA-based AVFT (Kim et al., 2014). **(C)** IPMC-based systems: (1) IPMC-based AVFT with artificial trigger hairs (Shahinpoor, 2011); (2) DEA-based AVFT with a fast gripping motion (Wang et al., 2019). **(D)** Humidity-driven systems: (1) HBS-based humidity change-driven AVFT (Lunni et al., 2020); (2) hydrogel-based water- and temperature-triggered AVFT (Fan et al., 2019); (3) Hydrogel-based solvent-triggered doubly curved system [adapted from Lee et al. (2010)]. **(E)** Pneumatic systems: (1) 3D-printed pneumatic AVFT (Temirel et al., 2016); (2) silicone-based AVFT (Pal et al., 2019). **(F)** Photothermally driven systems: (1) LCE-based AVFT (Wani et al., 2017); (2) NIR-light-triggered AVFT (Lim et al., 2017). Sketches of the AVFTs are all originals based on the concepts presented in the mentioned references.

TABLE 1 | Comparison of AVFTs with the biological role model with respect to various parameters.

Schematic	Type	Actuation	Sensing	Snap buckling	Closing time	Input/requirements for actuation	Reversibility
	<i>Dionea muscipula</i>	Stimulation of trigger hairs results in active water displacement	Touch-sensitive trigger hairs	Yes	0.1–0.5 s [1]	~300 μ mol ATP (at standard conditions equals 9.66 J) [2]	Yes
	Magnet	Electromagnet	No sensor/actuated manually	Yes (no spatial inversion of configuration)	0.1 s [3]	Repulsive force by the electromagnet 0.06–41.46 N [3,4]	No/manually
	SMA	Electric current/joule heating	No sensor/actuated manually	Yes (no spatial inversion of configuration)	0.1 s [5]	Closing: 12.4 J for 4.5 s reopening: 48 J for 10 s [5]	Yes
	IPMC	Electric field/voltage	Touch-sensitive IPMC-based trigger hairs [6]/proximity sensors [7]	No	0.05 s [7]	4–9 V of input voltage [6,7]	Yes
	DEA	Voltage	No sensor /actuated manually	Yes	0.17 s [8]	6 kV, 7.7 mA for 0.04 s	Yes
	Hydroscopic bistable sheet	Swelling of hydroscopic layer	Inherent to the material	Yes	0.5 s [9]	Rise of relative humidity of 30%	Yes
	Hydrogel	Water with various temperatures	Inherent to the material	Yes (no spatial inversion of configuration)	30 s needed from contact with stimulus, <1 s for snapping [10]	Water with a temperature difference of 40 K [10]	Yes
	Hydrogel	Solvent	Inherent to the material	Yes	3.6 s needed from contact with stimulus, 0.012 s for snapping [11]	Solvent [11]	Yes
	Pneumatic	Pressurized air	No sensor /actuated manually	Yes	0.05 s [12]	0.35–0.7 bar [12]	Yes
	Photothermal—LCE	Light with certain wavelength	Inherent to the material	No	0.2 s [13]	Light with wavelength of 488 nm and intensity of 0.3 W [13]	Yes
	Photothermal—PEDOT/PDMS	Near-infrared light	Inherent to the material	No	~4 s [14]	Light with wavelength of 80 nm and intensity of 910 mW cm ⁻² [14]	Yes

Sketches of the AVFTs are all originals based on the concepts presented in mentioned references.

References: [1] Forterre et al. (2005), [2] Jaffe (1973), [3] Zhang et al. (2019), [4] Zhang et al. (2016) [5] Kim et al. (2014), [6] Shahinpoor (2011), [7] Shi et al. (2012), [8] Wang et al. (2019), [9] Lunni et al. (2020), [10] Fan et al. (2019), [11] Lee et al. (2010), [12] Pal et al. (2019), [13] Wani et al. (2017), [14] Lim et al. (2017).

and feature a separated sensor made of the same material that connects input signals via an amplifying circuit with the actuator (Shahinpoor, 2011). These sensors are used to trigger the IPMC bending motion. Similar to IPMCs, dielectric elastomer actuators (DEAs), another type of electroactive polymers, react to an applied voltage. DEAs convert electrical energy into mechanical work. A DEA is a compliant capacitor in which a passive elastomer film is sandwiched between two compliant electrodes.

When a voltage difference is applied between the electrodes, the opposite electrodes attract each other because of electrostatic forces (Maxwell stress) (Pelrine et al., 2000). The elastomer film is compressed in a vertical direction and expands in a lateral direction; this expansion actuates a bistable system. Wang et al. (2019) have applied this principle to actuate an AVFT gripper based on parabolic PET foil framing. On each side of the frame, a DEA is attached with a center electrode within the frame,

connecting both DEAs. The system can be switched from one stable minimal energy state to another by manually applying a short high-voltage impulse ($V = 6$ kV, $I = 7.7$ mA for 0.04 s) (Wang et al., 2019). The DEAs attached to the bistable frame snap within 0.17 s, closing and opening the AVFT gripper. The total energy consumption for each grasping movement amounts here to ~ 0.14 J (with 0.003 s of charging time of the actuator; Wang et al., 2019). After snapping, no energy is needed to hold the position. The system has no sensing capabilities and requires manual triggering.

Human input is not the only means that can be used to trigger AVFT systems. Changes of environmental conditions such as humidity or temperature have been employed as input, for example, for hydrogel-based artificial traps (**Figure 3D**) (Fan et al., 2019; Lunni et al., 2020). These systems are based on composite (Fan et al., 2019) or hybrid hydrogels (Athas et al., 2016), utilizing various swelling behaviors and coefficients of the building components under variable environmental and triggering conditions for movement. Within hydrogels, sensing (e.g., sensing and reacting to changes in humidity) and acting (bending, folding, and snapping movement caused by swelling) are combined in one structural system. Athas et al. (2016) constructed, with a hybrid hydrogel, a rudimentary analog of the Venus flytrap, consisting of two flat gels as “leaves” connected via a folding hydrogel as a hinge or “midrib.” When exposed to a certain quantity of enzyme (50 U/ml collagenase), the hinge bends, and the leaves close within 50 min. The system of Fan et al. (2019) is faster in comparison and can perform a rapid snapping motion (< 1 s) along the transversal axis. However, first, it has to be initialized by heating it in a water bath from 20 to 60°C and then keeping it at 60°C for 10 min; only after this treatment is the system ready to perform a fast snapping motion (**Figure 3D**, 2). The actuator is based on a reduced graphene oxide/PDMAEMA composite. By polymerizing the monomers with UV light from only one side, the light-exposed side features higher chain density and cross-linking density than the other side. When the actuator is submerged in water at 20°C and when the water temperature is raised to 60°C, the flat composite sheet bends toward the high-density side along the longitudinal axis; because of the shrinking of the high-density side, the system accumulates potential energy as stresses within the material. When placed back into water at 20°C, it takes 30 s to reverse the rollup motion slightly, followed by a fast snapping motion along the transversal axis (< 1) (Fan et al., 2019). After snapping, the reopening through gradually unrolling back to a flat state takes 60 min in water at 20°C. In contrast to these two rather slow systems, Lee et al. (2010) have developed a 3D polymeric device that snaps open in response to a solvent within 3.6 s and is able to snap close again. The system consists of two 3D-printed, doubly curved hydrogel sheets connected via a flat hydrogel sheet forming a table-like structure (**Figure 3D**). Lee et al. used poly(ethylene glycol) diacrylate (PEGDA) as a base material to produce this π -shaped structure via 3D hydrogel printing. On the inside of the convex sheets lie three parallel-aligned channels with a trapezoidal cross section for solvent transport. When solvent comes into contact with a sheet, it is transported within the microfluidic channel network by capillary action over the entire length of the sheet. Local

swelling around the aligned channels causes the doubly curved device to bend only along the vertical axis (Lee et al., 2010). Thereby, the elastic sheet is only stretched along one axis storing elastic energy (attributable to the bending–stretching coupling of the doubly curved plate geometry, Lee et al., 2010). Through further swelling, the sheet deforms and passes through the energy barrier. Stored elastic energy is instantaneously released and converted into kinetic energy; as a result, an outwardly directed snap buckling opening occurs (Lee et al., 2010). During drying and de-swelling, the system reverses its movement and snaps back into its original shape. The whole opening and closing process takes places within 5 s. The snapping motion of the sheets in the de-swelling phase takes 12 ms. The system releases 25.5 nJ of energy during the snapping motion and, thus, is able to propel itself 7 mm into the air (Lee et al., 2010). This system is able to snap open and close in response to solvent as stimuli. A purely humidity-responsive AVFT leaf based on a hygroscopic bistable sheet (HBS) system has been developed by Lunni et al. (2020) (**Figure 3D**). The system consists of a pre-stretched passive layer of polydimethylsiloxane (PDMS) and a hygroscopic active layer of electrospun polyethylene oxide (PEO) nanofibers. The PEO swells in response to a rise of environmental humidity of around 30%. The coupling between the hygroscopic material and the passive layer causes a curvature reduction of the system until it snaps within 0.5 s (Lunni et al., 2020). The initial state can be restored by reducing the humidity.

In contrast to the above systems, light-driven monolithic LCE-based artificial traps have sensing and actuating mechanisms combined in one material (**Figure 3F**). When an LCE-based AVFT is exposed to light of a certain wavelength, a cis-trans-isomerization of photoactive molecules within the LCE leads to a change in length of the top layer and therefore to a bending motion and a closure within 0.2 s. After the light source is removed, the actuator returns to its original shape (Wani et al., 2017). The LCE actuators are also temperature responsive. If the energy provided by a heat source is sufficient to trigger the isomerization, bending occurs even without light. This heat-driven motion is also reversible. Wani et al. (2018) presented a second demonstrator that uses liquid crystal networks (LCNs) as photo actuators whose reaction can be controlled and modified by light and humidity. By using these humidity-controlled photo-actuators, an artificial nocturnal flower was developed that closed during the day (conditions: low humidity levels and high light levels) and opened at night (conditions: no light and high humidity levels). The LCN humidity-gated photo-actuators could be actuated with lower light intensities than their photothermal LCE actuator counterparts (Wani et al., 2017, 2018). Another photothermal AVFT, developed by Lim et al. (2017), is actuated via near-infrared (NIR) light at a wavelength of 808 nm (**Figure 3F**, 2). This bimorph structure consists of a photothermal PEDOT layer and a soft PDMS layer. A heat pocket inside the structure is created by exploiting the photothermal properties of PEDOT. When actuated by NIR light, bending occurs, and the trap closes in < 4 s and reopens when the infrared light source is removed. This system shows reversibility but not the typical snapping motion of the Venus flytrap.

COMPARISON OF AVFT

To evaluate such systems in direct comparison to *D. muscipula* and to determine whether they are truly AVFTs, one can imagine using a Turing test (Pinar Saygin et al., 2000). Turing's aim was to provide a method to assess whether or not a machine can "play the imitation game." A tester has to determine if either a human or a computer program has given him an answer to a question. If the tester is not able to distinguish the human from the machine, then the machine or program can be viewed as having an artificial intelligence (Pinar Saygin et al., 2000). Within such a test involving the AVFT, distinguishing criteria would include the basic functionalities, appearance, and behavior of the artificial vs. the biological model. The biological role is able to harvest and store energy from the environment, to sense and compute sensed information, and to react accordingly. For example, the plant can sense prey and close its lobes in reaction to triggers but can also sense damage and repair or discard the damaged part. The general Bauplan of the two lobes with sensors and harvesting structures have to be fulfilled. If all these criteria are met, one should not be able to distinguish the artificial from the real Venus flytrap in its reactions and mode of functioning. The target performance of the truly artificial system would be defined as being able to sense "prey," respond to it with flap closure, adapt to a changing environment, and harvest and store energy, if the general Bauplan and appearance of the biological role model is maintained.

The comparison provided within this review is a first baseline for such a Turing test concerning functionalities. As none of the systems is currently able to harvest and store energy from the environment, we focus here on the key features characterizing the closing motion of the biological Venus flytrap and AVFT systems. These are highlighted in **Table 1**, enabling a more direct comparison of the systems and directly showing whether the state-of-the-art systems are capable of meeting the requirements of an AVFT: actuation after a certain trigger and with a certain closure time, type of movement (snap buckling), and reversibility. Of note here is that a comparison involving the input or required energy for actuation is only possible and feasible in specific cases because of the variable energy forms and inputs used for the actuation.

The magnetically driven and SMA systems are based on the same basic principal and material, namely, CFRP cylindrical shells as "leaves" that perform a curvature change within 0.1 s when actuated manually. The closing speed is within the range of the biological role model. These systems do not have sensory capabilities, nor is the curvature change a spatial inversion as seen in *D. muscipula*. The initial configuration can be restored in the SMA-based system by an antagonist function. Low force and energy are required to initiate the snap buckling within the systems. The SMA requires slightly more energy for closure than *D. muscipula* (12.4 J, (Kim et al., 2014), vs. 9.66 J in the natural system, Jaffe, 1973).

Being able to be triggered by changing environmental conditions, the hydrogel-based, HBS-based, and photothermal systems have a sensing capability inherent to their composition. Their base material reacts to humidity/moisture (HBS and

hydrogel), light (LCEs), and temperature changes with a conformational change within the material. The LCN nocturnal flower (Wani et al., 2018) utilizes all triggering conditions (humidity, light, and temperature) but is also far removed from the biological role model as no curvature change, snap buckling, or fast actuation (1.8–9 s for closure) occurs. In contrast, the hydrogel-based system developed by Fan et al. (2019) is able to perform a fast snapping motion but shows a long initialization phase to snapping (30 s from stimulation with a temperature change of 40 K). Moreover, the jumping hydrogel of Lee et al. (2010) has an initialization phase, in which elastic energy is built up over 3.6 s through controlled swelling, until the system snaps open within 12 ms. Via de-swelling, the system snaps close again, releasing stored energy, and propelling the system into the air. The HBS-based system of Lunni et al. (2020) represents a system that is able to perform a fast (0.5 s) and reversible snapping motion in correspondence to a humidity change of 30%. This system performs the fastest moisture-driven motion without an initialization phase of all of the AVFTs and resembles the biological role model not only in appearance but also in motion. The LCE-based AVFT by Wani et al. (2017) can be triggered via a change in environmental conditions, but the system resembles a Venus flytrap only in a purely reactive way by being able to "sense" its "prey." If "prey" enters the space between the lobes, it reflects the emitted light of the central rod, illuminating the LCE lobes, which then bend and catch the "prey" within 0.2 s. This system can also be utilized as a gripper, automatically gripping an object whenever it lies between the lobes. The energy required to activate the systems is again far removed from the biological role model (temperature change of 40 K and light of an NIR laser at 0.3–1.1 W with an intensity of 980 mW cm⁻²). The PEDOT/PDMS bimorph-based AVFT of Lim et al. (2017) cannot be considered an AVFT in the proper sense, as the system incorporates none of the basic principles or predefined requirements. However, the system highlights the possibility of usage underwater and as an oscillator or light-driven motor.

The pneumatic system developed by Pal et al. (2019) is able to change the curvature of its lobes, perform a snap buckling motion, and close within 0.05 s, making it faster than the biological role model. The system has no sensors, but by using antagonistic pneumatic chambers, the motion can be reversed. The low-energy fast AVFT gripper system developed by Wang et al. (2019) is based on DEAs. Via the combination of a bistable parabolic-shaped PET foil backbone, the DEA can switch within 0.17 s from one stable state to another actuated by a short electrical impulse resulting in low-energy consumption (~0.14 J). Like the biological role model, the system does not require energy to be held during an open or closed state. On the basis of the transfer of movement principles, these two systems represent the most sophisticated AVFT systems developed so far.

The only system incorporating a sensing system similar to that of the biological role model is the IPMC-based AVFT of Shahinpoor (2011). The IPMC trigger hairs are attached to the IPMC lobes and connected to a solid-state relay. When the trigger hairs are deflected by an object, an electrical signal is generated, which is used to activate a small dynamic voltage generator actuating the IPMC lobes (Shahinpoor, 2011). However, neither

curvature change nor snap buckling is performed within the closure movement.

None of the above-described system transfers all principles of *D. muscipula* into an artificial system. Of note here however is that the aim of most of these studies was not to transfer the principles fully into one system but to highlight a novel actuator, material, or bistable system and to build with it a system that resembles a Venus flytrap. To transfer all essential principles behind a *D. muscipula*, one needs to develop a system that is able not only to snap and move like the role model but also to sense its environment and “prey,” to make a decentralized decision to capture “prey,” and to harvest energy both via prey capture and from the environment.

ENVISIONING A TRUE AVFT AS AN INSPIRATION FOR LIVING ADAPTIVE MATERIALS SYSTEMS AND NOVEL TECHNOLOGIES

The presented AVFT systems highlight the great potential that lies within bioinspired and especially plant-inspired soft machines in the field of adaptive and autonomous systems. Some of the systems are able to sense changes in the environmental conditions or approaching “prey” and react to them via actuation. These “trapping” reactions are achieved via electricity, thermally, pneumatically, or magnetically, or by humidity-change-driven actuators. In this way, systems are constructed that can harvest energy from the environment for the actuation in the case of the humidity-driven and photothermally driven systems.

The above-described material-wise, often sophisticated, systems inspired our low-cost, low-energy, fast-moving, simplified AVFT system (Esser et al., 2019). This system highlights the status quo of AVFT actuation within one system and is currently being characterized. The basic geometry of the snap traps of the Venus flytrap (*D. muscipula*) and waterwheel plant (*A. vesiculosa*) (Poppinga et al., 2018; Westermeier et al., 2018, 2019; Sachse et al., under revision) was abstracted in a compliant foil demonstrator with two triangular lobes connected via a rigid backbone with two ears for actuation (Figure 4B). By applying a force to the ears and bending them down, the geometrically connected lobes are made to close (Figure 4D). The movement can be actuated pneumatically (Figure 4C, 1), thermally (through SMAs) (Figure 4C, 2), or magnetically (Figure 4C, 3), and a hydrogel-based locking mechanism can be incorporated into the system (Figure 4C, 4). The system can snap shut (Venus flytrap) or continuously bend to close (waterwheel plant) like its biological role models and is able to snap open in a snap buckling motion of its backbone. Through the hydrogel and specifically designed 3D-printed backbones, the system can be held in the snap-opened state, until the system is initialized via a stimulus combination of humidity and temperature.

This snap trap demonstrator is considered to be a baseline for the development of a true AVFT. The final system will be able to react to certain triggers, adapt to the environment, and

harvest energy to maintain its homeostasis, implying that the energy demand of the actuation systems is lower or equal to the provided energy from the harvester and storage structures. In order to attain this, materials are needed that are able to sense, react, and adapt to the environment (Walther, 2019). These should be able not only to adapt but also to learn and to transition from one stable energy state to another. They must be able to cope with local triggers and convert them into global answers or adaptations. As in nature, the materials and systems need self-healing properties and damage-sensing and damage-control capabilities. These might be achieved via chemically or catalyst-based and diffusion-based information transfer, as in the stimulus and immune responses of plants (Spoel and Dong, 2012). Additionally, a decentralized decision-making process should be incorporated that decides the time to act and the specific stimulus for action. To achieve autonomy in these systems, energy must be harvested from the environment and stored and distributed within the system. The system should also be sustainable and easily recycled to conform to the agenda 2030 of sustainable development (Colglazier, 2015).

In our opinion, a multilayer materials-based system is best suited to cope with all these requirements and specifications. The outer layers should be compliant self-healing foils, safeguarding inner systems from harsh environments and repairing any damage occurring during use. These layers should contain an intermediary layer of stimulus-computing metamaterials with embedded energy-harvesting and storage materials systems. Of note here, stresses, strains, and deformations must be deflected or guided around the energy-generating regions within this layer. The central actuation layer should consist either of an environmentally triggerable active material connected to the environment directly or of sensors lying on the outer layers and gaining the energy for actuation from the harvesters. These systems would be able to adapt to changing weather conditions by altering the lobe curvature for better light incidence; to adapt to variable “prey” dimension by altering their inner structure to achieve stiffening, elongation, or higher flexibility; and to heal damage caused by prey or harsh conditions. The technology to build the components for such a compliant multilayer system is partially available today. Currently, self-healing foils (Hönes et al., 2017), flexible sensors, and electronic circuits (Lu and Kim, 2014; Majidi, 2018; Kumar et al., 2019), solar batteries (Zhong et al., 2017), and, as shown above, smart actuators can be produced using, for example, multiphoton lithography (Malinauskas et al., 2009; Vaezi et al., 2013; Meza et al., 2014, 2015), wafer technology (Kim et al., 2012; Segev-Bar and Haick, 2013), spray coating (Kent et al., 2020), and 3D and 4D printing (Kumar et al., 2019; Ma et al., 2019). Nevertheless, one challenge that remains open is the combination of all these components into one multi-materials system. Therefore, the development of a fully functional AVFT with the aforementioned specifications will involve the development of novel materials systems. These systems will enable the manufacture of a new phase of self-sensing and environment-adaptive robots. Such advancements will lead to innovative technologies, as unprecedented types of materials systems will have to be developed for their production.

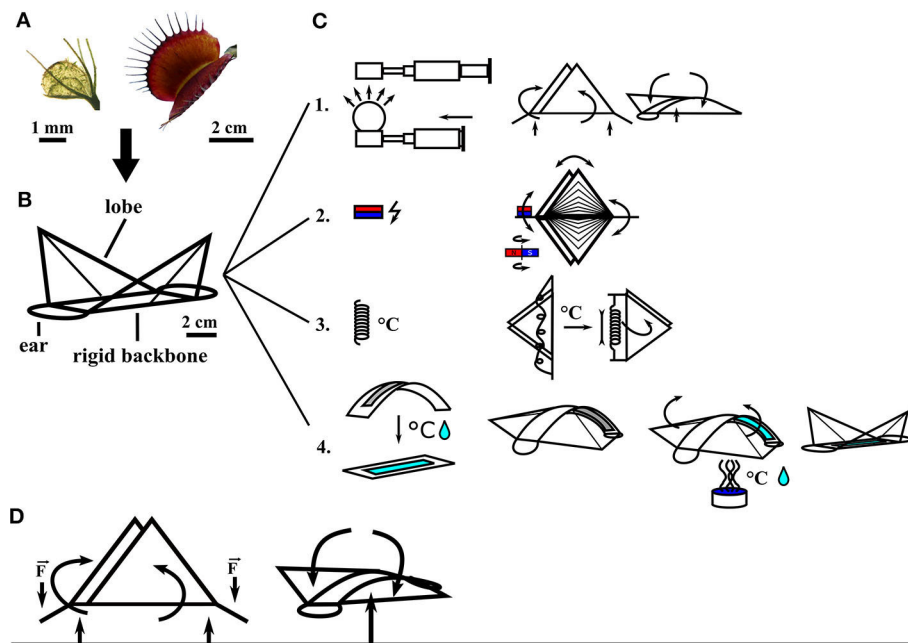


FIGURE 4 | Compliant foil AVFTs with four different actuation modes. Biological role models *Aldrovanda vesiculosa* (left) and *Dionaea muscipula* (right) **(A)** are abstracted into a compliant foil system **(B)** with two lobes, two ears for actuation, and a rigid backbone. Various movement actuators **(C)**: (1) Pressurized pneumatic cushion (left) pushes the backbone upwards, closing the lobes (middle); when pressure is applied via a central cushion, the backbone bends, and the AVFTs snap open (right). (2) Magnetic field actuation of closure movement; a permanent magnet is attached to one ear and actuated via a rotating magnetic field bending the ear up and down, closing and opening the AVFT, respectively. (3) An SMA spring is attached to the ears behind the backbone; when the SMA is heated in a contact-free manner via a rise in environmental temperature, the spring contracts, closing the AVFT. (4) Via specifically designed 3D-printed backbones coated with hydrogel (left), the system can be held in the snap-opened state, until the system is initialized via a stimulus combination of humidity and temperature (right). **(D)** Movement principle of the AVFT system: bending down the ears closes the lobes, and the system snaps open by bending the backbone.

FUTURE APPLICATION OF AVFT AS A NOVEL GRIPPING TECHNOLOGY

In robotics, an artificial flytrap can serve as a deployable structure, such as gripper or energy harvester, which can be attached to a fixed structure to perform independent functions and to increase overall system flexibility and adaptation (Yang et al., 2012). A first glimpse of these possible usages is given by the CFRP- and DEMES-based AVFT gripper systems from Wang et al. (2019) and Zhang et al. (2019) consisting of DEMES-based and CFRP-based smart materials systems, respectively. However, one shortcoming of these systems is that the materials cannot adapt to the gripped object. Because of their flexibility, they do not destroy the payload but unfortunately also do not adapt to it to achieve a better grip. In order to use AVFT as low-energy grippers, robust materials with adjustable stiffness are required that are able to actuate the system consistently and to adapt, on demand, their stiffness to the requirements of the payload. A material combination that might be able to meet these requirements is a combination of soft elastomers with fluidic channels filled with liquid metals or low-melting-point alloys (LMPAs), as are used for soft sensors (Yufei et al., 2017). Sensor hairs consisting of triboelectric materials or IPMCs (Shahinpoor, 2011) might be used to identify payload properties and trigger an adaption process within the material of the gripper lobe. LMPA integrated into the lobe material might stiffen and

thus strengthen the materials system via on-demand temperature changes, liquefaction, or curing. A combination of adaptive stiffening materials with flexible miniaturized energy harvesters such as photo-batteries or material immanent triboelectric and thermoelectric harvesters should enable the next generation of grippers to act as autonomous systems.

For plant-inspired robotics, these systems could be employed as attachment, manipulation, or energy-harvesting structures within harsh environments. In order to enable such systems to cope with harsh environmental conditions, these systems must run with low wear and low to no maintenance requirements because of, for example, their low complexity. To achieve this, the proposed systems should be able to repair damage and heal themselves, as their natural role models do (Speck and Speck, 2019). The incorporation of a dissolvable sacrificial layer (SL) underneath the outer layer of the multilayer would be a possible solution (Hönes et al., 2017). If the outer layer is damaged, the SL would be exposed and dissolved by moisture or atmospheric gases (oxidation), which would remove the support for the damaged layer, detaching it and renewing the functional surface of the outer layer.

A combination of the aforementioned principles and functionalities will lead to autonomous low-energy systems with embodied energy and intelligence or with morphological computation (Paul, 2006; Polygerinos et al., 2017). As in nature, these systems will achieve tasks not via the high computational

power of today's robots but via their material composition, which will enable the system to start/stop moving or to grasp by design rather than by following a computer program. This achievement will reduce system complexity and maintenance requirements. A few examples of soft grippers able to adapt to the payload are indeed available and are capable of, for example, grasping a flower or an egg because of stiffness differences (Ilievski et al., 2011; Krahn et al., 2017; Wang et al., 2018). This principle has been inspired by the natural design of combined sensor and actuator systems (e.g., muscles) in animals (Paul, 2006; Polygerinos et al., 2017). For the design of materials systems that embody intelligence and are able to learn and transfer information, unit-cell-based mesostructured, and metamaterials systems with simple logical structuring might be employed (Grigorovitch and Gal, 2015; Meza et al., 2015; Haghpanah et al., 2016; Raney et al., 2016; Paoletti et al., 2017; Guseinov et al., 2020; Jin et al., 2020). Research into and the development of biomimetic artificial systems, such as AVFT systems, should lead to the creation of lifelike, adaptive, autonomous materials systems. In turn, these materials will spawn novel technologies such as autonomous grippers and resilient, adaptive, and low-maintenance solar harvesters for plant-inspired robots and self-charging sensors, smart phones, or electric vehicles, plus energy harvesters and adaptive shading for low-energy buildings and sustainable architecture.

AUTHOR CONTRIBUTIONS

TS and FE initiated and supervised the study. FE and PA performed the data collection from literature and wrote the first draft of the manuscript. All authors designed, performed,

evaluated the study, critically revised, and approved the final version of the manuscript.

FUNDING

This work was funded by the Deutsche Forschungsgemeinschaft (DFG, German Research Foundation) under Germany's Excellence Strategy—EXC-2193/1-390951807.

ACKNOWLEDGMENTS

In addition to the funding within the framework of the cluster of excellence *livMatS*, TS is also grateful for funding for applications in architecture within the collaborative research project “Bio-inspirierte elastische Materialsysteme und Verbundkomponenten für nachhaltiges Bauen im 21ten Jahrhundert (BioElast)” within the Zukunftsoffensive IV Innovation und Exzellenz—Aufbau und Stärkung der Forschungsinfrastruktur im Bereich der Mikro- und Nanotechnologie sowie der neuen Materialien of the State Ministry of Baden-Wuerttemberg for Sciences, Research, and Arts. We thank the University of Freiburg for funding the article-processing charge via the University of Freiburg funding program Open Access Publishing. The work in the field for growing soft robotics was funded by the European Community within the project “GrowBot: Toward a new generation of plant-inspired growing artifacts (EU-H2020-FETPROACT).” We thank Dr. Simon Poppinga and many colleagues within the framework of the cluster of excellence Living Materials Systems (*livMatS*) and within GrowBot for fruitful discussion.

REFERENCES

- Agerholm, M., and Lord, A. (1961). The “artificial muscle” of McKibben. *Lancet* 277, 660–661. doi: 10.1016/S0140-6736(61)91676-2
- Ashida, J. (1934). Studies on the leaf movement of *Aldrovanda vesiculosa*. *Shokubutsugaku Zasshi* 51, 505–513.
- Athas, J. C., Nguyen, C. P., Zarket, B. C., Gargava, A., Nie, Z., and Raghavan, S. R. (2016). Enzyme-triggered folding of hydrogels: toward a mimic of the Venus flytrap. *ACS Appl. Mater. Interfaces* 8, 19066–19074. doi: 10.1021/acsami.6b05024
- Baldur, R., and Blach, W. (1985). *Inflatable Manipulator*. Society of Manufacturing Engineers.
- Behl, M., Kratz, K., Noechel, U., Sauter, T., and Lendlein, A. (2013). Temperature-memory polymer actuators. *Proc. Natl. Acad. Sci.* 110, 12555–12559. doi: 10.1073/pnas.1301895110
- Besse, N., Rosset, S., Zarate, J. J., and Shea, H. (2017). Flexible active skin: Large reconfigurable arrays of individually addressed shape memory polymer actuators. *Adv. Mater. Technol.* 2:1700102. doi: 10.1002/admt.201700102
- Colglazier, W. (2015). Sustainable development agenda: 2030. *Science* 349, 1048–1050. doi: 10.1126/science.aad2333
- Darwin, C. (1875). *Insectivorous Plants*. London: John Murray.
- Esser, F., Scherag, F. D., Poppinga, S., Westermeier, A., Mylo, M. D., Kampowski, T., et al. (2019). “Adaptive biomimetic actuator systems reacting to various stimuli by and combining two biological snap-trap mechanics,” in *Biomimetic and Biohybrid Systems. 8th International Conference*, eds U. Martinez-Hernandez, V. Vouloutsis, A. Mura, M. Mangan, M. Asada, T. J. Prescott et al. (Cham: Springer), 114–121. doi: 10.1007/978-3-030-24741-6
- Fagerberg, W. R., and Howe, D. G. (1996). A quantitative study of tissue dynamics in Venus's flytrap *Dionaea muscipula* (Droseraceae). II. Trap reopening. *Am. J. Botany* 83, 836–842. doi: 10.1002/j.1537-2197.1996.tb12775.x
- Fan, W., Shan, C., Guo, H., Sang, J., Wang, R., Zheng, R., et al. (2019). Dual-gradient enabled ultrafast biomimetic snapping of hydrogel materials. *Sci. Adv.* 5:eav7174. doi: 10.1126/sciadv.aav7174
- Forterre, Y., Skotheim, J. M., Dumais, J., and Mahadevan, L. (2005). How the Venus flytrap snaps. *Nature* 433, 421–425. doi: 10.1038/nature03185
- Grigorovitch, M., and Gal, E. (2015). The local response in structures using the Embedded Unit Cell Approach. *Comput. Struct.* 157, 189–200. doi: 10.1016/j.compstruc.2015.05.006
- Guseinov, R., McMahan, C., Pérez, J., Daraio, C., and Bickel, B. (2020). Programming temporal morphing of self-actuated shells. *Nat. Commun.* 11, 1–7. doi: 10.1038/s41467-019-14015-2
- Haghpanah, B., Salari-Sharif, L., Pourrajab, P., Hopkins, J., and Valdevit, L. (2016). Multistable shape-reconfigurable architected materials. *Adv. Mater.* 28, 7915–7920. doi: 10.1002/adma.201601650
- Hodick, D., and Sievers, A. (1989). On the mechanism of trap closure of Venus flytrap (*Dionaea muscipula* Ellis). *Planta* 179, 32–42. doi: 10.1007/BF00395768
- Holmes, D. P., and Crosby, A. J. (2007). Snapping surfaces. *Adv. Mater.* 19, 3589–3593. doi: 10.1002/adma.200700584
- Hönes, R., Kondrashov, V., and Rühe, J. (2017). Molting materials: restoring superhydrophobicity after severe damage via snakeskin-like shedding. *Langmuir* 33, 4833–4839. doi: 10.1021/acs.langmuir.7b00814
- Ilievski, F., Mazzeo, A. D., Shepherd, R. F., Chen, X., and Whitesides, G. M. (2011). Soft robotics for chemists. *Angewandte Chemie* 50, 1890–1895. doi: 10.1002/anie.201006464

- Jaffe, M. J. (1973). The role of ATP in mechanically stimulated rapid closure of the Venus's flytrap. *Plant Physiol.* 51, 17–18. doi: 10.1104/51.1.17
- Jie, Y., Jia, X., Zou, J., Chen, Y., Wang, N., Wang, Z. L., et al. (2018). Natural leaf made triboelectric nanogenerator for harvesting environmental mechanical energy. *Adv. Energy Mater.* 8:3133. doi: 10.1002/aenm.201703133
- Jin, L., Khajetourian, R., Mueller, J., Rafsanjani, A., Tournat, V., Bertoldi, K., et al. (2020). Guided transition waves in multistable mechanical metamaterials. *Proc. Natl. Acad. Sci. U. S. A.* 117:201913228. doi: 10.1073/pnas.1913228117
- Kent, T. A., Ford, M. J., Markvicka, E. J., and Majidi, C. (2020). Soft actuators using liquid crystal elastomers with encapsulated liquid metal Joule heaters. *Multifunct. Mater.* 3, 1–10. doi: 10.1088/2399-7532/ab835c
- Kim, D., Wang, S., Keum, H., Ghaffari, R., Kim, Y., Tao, H., et al. (2012). Thin, flexible sensors and actuators as “instrumented” surgical sutures for targeted wound monitoring and therapy. *Small* 8, 3263–3268. doi: 10.1002/smll.201200933
- Kim, S., Koh, J., Lee, J., Ryu, J., Cho, M., and Cho, K. (2014). Flytrap-inspired robot using structurally integrated actuation based on bistability and a developable surface. *Bioinspir. Biomim.* 9:36004. doi: 10.1088/1748-3182/9/3/036004
- Kim, S., Laschi, C., and Trimmer, B. (2013). Soft robotics: a bioinspired evolution in robotics. *Trends Biotechnol.* 31, 287–294. doi: 10.1016/j.tibtech.2013.03.002
- Knippers, J., Schmid, U., and Speck, T. (2019). *Biomimetics for Architecture. Learning From Nature*. Basel: Birkhäuser Verlag.
- Kohlmeyer, R. R., and Chen, J. (2013). Wavelength-selective, IR light-driven hinges based on liquid crystalline elastomer composites. *Angewandte Chemie* 52, 9234–9237. doi: 10.1002/anie.201210232
- Körner, A., Born, L., Mader, A., Sachse, R., Saffarian, S., Westermeier, A. S., et al. (2018). Flectofold—a biomimetic compliant shading device for complex free form facades. *Smart Mater. Struct.* 27:17001. doi: 10.1088/1361-665X/aa9c2f
- Krahn, J. M., Fabbro, F., and Menon, C. (2017). A soft-touch gripper for grasping delicate objects. *IEEE/ASME Trans. Mechatron.* 22, 1276–1286. doi: 10.1109/TMECH.2017.2663322
- Kumar, K. S., Chen, P., and Ren, H. (2019). A review of printable flexible and stretchable tactile sensors. *Research* 2019:3018568. doi: 10.34133/2019/3018568
- Kumar, P. K., and Lagoudas, D. C. (2008). “Introduction to shape memory alloys,” in *Shape Memory Alloys. Modeling and Engineering Applications*, ed D.C. Lagoudas (New York, NY: Springer), 1–51. doi: 10.1007/978-0-387-47685-8_1
- Larson, C., Peele, B., Li, S., Robinson, S., Totaro, M., Beccai, L., et al. (2016). Highly stretchable electroluminescent skin for optical signaling and tactile sensing. *Science* 351, 1071–1074. doi: 10.1126/science.aac5082
- Laschi, C., Rossiter, J., Iida, F., Cianchetti, M., Margheri, L., and Mazzolai, B. (2017). *Plant-Inspired Growing Robots. Soft Robotics: Trends, Applications and Challenges*. Cham: Springer International Publishing.
- Lee, H., Xia, C., and Fang, N. X. (2010). First jump of microgel; actuation speed enhancement by elastic instability. *Soft Matter* 6:4342. doi: 10.1039/c0sm00092b
- Lim, H., Park, T., Na, J., Park, C., Kim, B., and Kim, E. (2017). Construction of a photothermal Venus flytrap from conductive polymer bimorphs. *NPG Asia Mater.* 9:e399. doi: 10.1038/am.2017.101
- Liu, C., Colón, B. C., Ziesack, M., Silver, P. A., and Nocera, D. G. (2016). Water splitting-biosynthetic system with CO₂ reduction efficiencies exceeding photosynthesis. *Science* 352, 1210–1213. doi: 10.1126/science.aaf5039
- Lu, N., and Kim, D. (2014). Flexible and stretchable electronics paving the way for soft robotics. *Soft Robotics* 1, 53–62. doi: 10.1089/soro.2013.0005
- Lunni, D., Cianchetti, M., Filippeschi, C., Sinibaldi, E., and Mazzolai, B. (2020). Plant-inspired soft bistable structures based on hygroscopic electrospun nanofibers. *Adv. Mater. Interfaces* 7:1901310. doi: 10.1002/admi.201901310
- Ma, S., Zhang, Y., Wang, M., Liang, Y., Ren, L., and Ren, L. (2019). Recent progress in 4D printing of stimuli-responsive polymeric materials. *Sci. China Technol. Sci.* 63, 532–544. doi: 10.1007/s11431-019-1443-1
- Majidi, C. (2018). Soft-matter engineering for soft robotics. *Adv. Mater. Technol.* 4:1800477. doi: 10.1002/admt.201800477
- Malinauskas, M., Purlys, V., Rutkauskas, M., and Gadonas, R. (2009). “Two-photon polymerization for fabrication of three-dimensional micro- and nanostructures over a large area,” in *Micromachining Microfabrication Process Technology XIV. SPIE MOEMS-MEMS: Micro- and Nanofabrication*, ed M. A. Maher, J. C. Chiao, P. J. Resnick (San Jose, CA: SPIE), 72040C.
- Markin, V. S., Volkov, A. G., and Jovanov, E. (2008). Active movements in plants. *Plant Signaling Behav.* 3, 778–783. doi: 10.4161/psb.3.10.6041
- Mather, P. T., Luo, X., and Rousseau, I. A. (2009). Shape memory polymer research. *Ann. Rev. Mater. Res.* 39, 445–471. doi: 10.1146/annurev-matsci-082908-145419
- Mazzolai, B., Mondini, A., Dottore, E. D., and Sadeghi, A. (2020). “Self-growing adaptable soft robots,” in *Mechanically Responsive Materials for Soft Robotics*, ed H. Koshima (Weinheim: Wiley-VCH), 363–394. doi: 10.1002/9783527822201.ch15
- Meder, F., Must, I., Sadeghi, A., Mondini, A., Filippeschi, C., Beccai, L., et al. (2018). Energy conversion at the cuticle of living plants. *Adv. Functional Mater.* 28:6689. doi: 10.1002/adfm.201806689
- Meder, F., Thielen, M., Mondini, A., Speck, T., and Mazzolai, B. (2020). Living plant-based generators for multidirectional wind energy conversion. *Energy Technol.* 8, 1–9. doi: 10.1002/ente.202000236
- Meng, H., and Li, G. (2013). A review of stimuli-responsive shape memory polymer composites. *Polymer* 54, 2199–2221. doi: 10.1016/j.polymer.2013.02.023
- Meza, L. R., Das, S., and Greer, J. R. (2014). Strong, lightweight, and recoverable three-dimensional ceramic nanolattices. *Science* 345, 1322–1326. doi: 10.1126/science.1255908
- Meza, L. R., Zelhofer, A. J., Clarke, N., Mateos, A. J., Kochmann, D. M., and Greer, J. R. (2015). Resilient 3D hierarchical architected metamaterials. *Proc. Natl. Acad. Sci. U. S. A.* 112, 11502–11507. doi: 10.1073/pnas.1509120112
- Must, I., Sinibaldi, E., and Mazzolai, B. (2019). A variable-stiffness tendril-like soft robot based on reversible osmotic actuation. *Nat. Commun.* 10, 1–8. doi: 10.1038/s41467-018-08173-y
- Pal, A., Goswami, D., and Martinez, R. V. (2019). Elastic energy storage enables rapid and programmable actuation in soft machines. *Adv. Functional Mater.* 30. doi: 10.1002/adfm.201906603
- Paoletti, P., Jones, G. W., and Mahadevan, L. (2017). Grasping with a soft glove: intrinsic impedance control in pneumatic actuators. *J. Royal Soc. Interface* 14:867. doi: 10.1098/rsif.2016.0867
- Park, S., and Hah, D. (2008). Pre-shaped buckled-beam actuators: theory and experiments. *Sensors Actuat. A Phys.* 148, 186–192. doi: 10.1016/j.sna.2008.07.009
- Paul, C. (2006). Morphological computation: a basis for the analysis of morphology and control requirements. *Robot. Autonomous Syst.* 54, 619–630. doi: 10.1016/j.robot.2006.03.003
- Pelrine, R., Kornbluh, R., Pei, Q., and Joseph, J. (2000). High-speed electrically actuated elastomers with strain greater than 100%. *Science* 287, 836–839. doi: 10.1126/science.287.5454.836
- Pinar Saygin A., and Cicekli, I., Akman, V. (2000). Turing test: 50 years later. *Minds Machines* 10, 463–518. doi: 10.1023/A:1011288000451
- Polygerinos, P., Correll, N., Morin, S. A., Mosadegh, B., Onal, C. D., Petersen, K., et al. (2017). Soft Robotics: review of fluid-driven intrinsically soft devices; manufacturing, sensing, control, and applications in human-robot interaction. *Adv. Eng. Mater.* 19:16. doi: 10.1002/adem.201700016
- Poppinga, S., Bauer, U., Speck, T., and Volkov, A. G. (2018). “Motile traps,” in *Carnivorous Plants: Physiology, Ecology, and Evolution*, ed Aaron Ellison and Lubomir Adamec (Oxford: Oxford University Press), 180–193.
- Poppinga, S., and Joyeux, M. (2011). Different mechanics of snap-trapping in the two closely related carnivorous plants *Dionaea muscipula* and *Aldrovanda vesiculosa*. *Phys. Rev. E* 84, 041928–041935. doi: 10.1103/PhysRevE.84.041928
- Poppinga, S., Kampowski, T., Metzger, A., Speck, O., and Speck, T. (2016). Comparative kinematical analyses of Venus flytrap (*Dionaea muscipula*) snap traps. *Beilstein J. Nanotechnol.* 7, 664–674. doi: 10.3762/bjnano.7.59
- Raney, J. R., Nadkarni, N., Daraio, C., Kochmann, D. M., Lewis, J. A., and Bertoldi, K. (2016). Stable propagation of mechanical signals in soft media using stored elastic energy. *Proc. Natl. Acad. Sci. U. S. A.* 113, 9722–9727. doi: 10.1073/pnas.1604838113
- Robinson, G., and Davies, J. B. C. (1999). “Continuum robots—a state of the art,” in *Proceedings. 1999 IEEE International Conference on Robotics and Automation, May 10–15, 1999, Marriott Hotel, Renaissance Center, Detroit, MI: International Conference on Robotics and Automation, Piscataway, NJ: Robotics and Automation Society; IEEE Service Center*, 2849–2854.
- Rosing, J., and Slater, E. C. (1972). The value of ΔG° for the hydrolysis of ATP. *Biochim. Biophys. Acta.* 267, 275–290. doi: 10.1016/0005-2728(72)90116-8
- Roy, R., and Bassham, D. C. (2014). Root growth movements: waving and skewing. *Plant Sci.* 221–222, 42–47. doi: 10.1016/j.plantsci.2014.01.007

- Sadeghi, A., Mondini, A., and Mazzolai, B. (2017). Toward self-growing soft robots inspired by plant roots and based on additive manufacturing technologies. *Soft Robotics* 4, 211–223. doi: 10.1089/soro.2016.0080
- Sadeghi, A., Tonazzini, A., Popova, L., and Mazzolai, B. (2014). A novel growing device inspired by plant root soil penetration behaviors. *PLoS ONE* 9:e90139. doi: 10.1371/journal.pone.0090139
- Saffarian, S., Born, L., Körner, A., Mader, A., Westermeier, A. S., Poppinga, S., et al. (2019). “From pure research to biomimetic products: the Flectofold facade shading device,” in eds Jan Knippers, Ulrich Schmid, and Thomas Speck, *Biomimetics for Architecture: Learning From Nature*, (Birkhäuser Verlag, Basel), 42–51.
- Saif, M., and Taher, A. (2000). On a tunable bistable MEMS-theory and experiment. *J. Microelectromech. Syst.* 9, 157–170. doi: 10.1109/84.846696
- Schleicher, S., Lienhard, J., Poppinga, S., Speck, T., and Knippers, J. (2015). A methodology for transferring principles of plant movements to elastic systems in architecture. *Computer-Aided Design* 60, 105–117. doi: 10.1016/j.cad.2014.01.005
- Schmied, J. U., Le Ferrand, H., Ermanni, P., Studart, A. R., and Arrieta, A. F. (2017). Programmable snapping composites with bio-inspired architecture. *Bioinspiration Biomimetics* 12:26012. doi: 10.1088/1748-3190/aa5efd
- Schulte, Jr, H. F. (1961). “The characteristics of the McKibben artificial muscle,” in *The Application of External Power in Prosthetics and Orthotics* (Washington, DC: National Academy of Sciences - National Research Council) 94–115.
- Segev-Bar, M., and Haick, H. (2013). Flexible sensors based on nanoparticles. *ACS Nano* 7, 8366–8378. doi: 10.1021/nn402728g
- Seok, S., Onal, C. D., Wood, R., Rus, D., and Kim, S. (2010). “Peristaltic locomotion with antagonistic actuators in soft robotics,” in *2010 IEEE International Conference on Robotics and Automation. Anchorage, Alaska, May 3–8, 2010: 50 Years of Robotics. 2010 IEEE International Conference on Robotics and Automation (ICRA 2010). Anchorage, AK, 5/3/2010–5/7/2010* (Piscataway, NJ: IEEE), 1228–1233.
- Shahinpoor, M. (2011). Biomimetic robotic Venus flytrap (*Dionaea muscipula* Ellis) made with ionic polymer metal composites. *Bioinspir. Biomim.* 6:46004. doi: 10.1088/1748-3182/6/4/046004
- Shahinpoor, M., and Thompson, M. S. (1995). The Venus Flytrap as a model for a biomimetic material with built-in sensors and actuators. *Mater. Sci. Eng. C* 2, 229–233. doi: 10.1016/0928-4931(95)00105-0
- Shankar, M. R., Smith, M. L., Tondiglia, V. P., Lee, K. M., McConney, M. E., Wang, D. H., et al. (2013). Contactless, photoinitiated snap-through in azobenzene-functionalized polymers. *Proc. Natl. Acad. Sci. U. S. A.* 110, 18792–18797. doi: 10.1073/pnas.1313195110
- Shepherd, R. F., Ilievski, F., Choi, W., Morin, S. A., Stokes, A. A., Mazzeo, A. D., et al. (2011). Multigait soft robot. *Proc. Natl. Acad. Sci. U. S. A.* 108, 20400–20403. doi: 10.1073/pnas.1116564108
- Shi, L., Guo, S., Kudo, H., and Asaka, K. (2012). “Development of a Venus flytrap-inspired robotic flytrap,” in *2012 IEEE International Conference on Robotics and Biomimetics (ROBIO). 2012 IEEE International Conference on Robotics and Biomimetics (ROBIO)* (Guangzhou: IEEE), 551–556.
- Speck, O., and Speck, T. (2019). An overview of bioinspired and biomimetic self-repairing materials. *Biomimetics* 4:26. doi: 10.3390/biomimetics4010026
- Spoel, S. H., and Dong, X. (2012). How do plants achieve immunity? Defence without specialized immune cells. *Nat. Rev. Immunol.* 12, 89–100. doi: 10.1038/nri3141
- Suzumori, K., Iikura, S., and Tanaka, H. (1991). “Flexible microactuator for miniature robots,” in *IEEE Micro Electro Mechanical Systems. An Investigation of Micro Structures, Sensors, Actuators, Machines, and Robots: Proceedings, Nara, Japan, 30 January–2 February 1991. IEEE Micro Electro Mechanical Systems. Nara, Japan, 30 Jan.–2 Feb. 1991. IEEE Workshop on Micro Electro Mechanical Systems* (New York, NY: Institute of Electrical and Electronics Engineers), 204–209.
- Temirel, M., Yenilmez, B., Knowlton, S., Walker, J., Joshi, A., and Tasoglu, S. (2016). Three-dimensional-printed carnivorous plant with snap trap. *3D Printing Additive Manufacturing* 3, 244–251. doi: 10.1089/3dp.2016.0036
- Vaezi, M., Seitz, H., and Yang, S. (2013). A review on 3D micro-additive manufacturing technologies. *Int. J. Adv. Manufacturing Technol.* 67, 1721–1754. doi: 10.1007/s00170-012-4605-2
- Volkov, A. G., Adesina, T., Markin, V. S., and Jovanov, E. (2008). Kinetics and mechanism of *Dionaea muscipula* trap closing. *Plant Physiol.* 146, 694–702. doi: 10.1104/107.108241
- Volkov, A. G., Forde-Tuckett, V., Volkova, M. I., and Markin, V. S. (2014). Morphing structures of the *Dionaea muscipula* Ellis during the trap opening and closing. *Plant Signaling Behav.* 9:27793. doi: 10.4161/psb.27793
- Walther, A. (2019). Viewpoint: from responsive to adaptive and interactive materials and materials systems: a roadmap. *Adv. Mater.* 32:e1905111. doi: 10.1002/adma.201905111
- Wang, W., Li, C., Cho, M., and Ahn, S. (2018). Soft tendril-inspired grippers: shape morphing of programmable polymer-paper bilayer composites. *ACS Appl. Mater. Interfaces* 10, 10419–10427. doi: 10.1021/acsami.7b18079
- Wang, Y., Gupta, U., Parulekar, N., and Zhu, J. (2019). A soft gripper of fast speed and low energy consumption. *Sci. China Technol. Sci.* 62, 31–38. doi: 10.1007/s11431-018-9358-2
- Wani, O. M., Verpaalen, R., Zeng, H., Priimagi, A., and Schenning, A. P. H. J. (2018). An Artificial nocturnal flower via humidity-gated photoactuation in liquid crystal networks. *Adv. Mater.* 31:1805985. doi: 10.1002/adma.201805985
- Wani, O. M., and Zeng, H., Priimagi, A. (2017). A light-driven artificial flytrap. *Nat. Commun.* 8:15546. doi: 10.1038/ncomms15546
- Wehner, M., Truby, R. L., Fitzgerald, D. J., Mosadegh, B., Whitesides, G. M., Lewis, J. A., et al. (2016). An integrated design and fabrication strategy for entirely soft, autonomous robots. *Nature* 536, 451–455. doi: 10.1038/nature19100
- Westermeier, A. S., Poppinga, S., Körner, A., Born, L., Sachse, R., Saffarian, S., et al. (2019). “No joint ailments: how plants move and inspire technology,” in *Biomimetics for Architecture: Learning from Nature*, eds J. Knippers, U. Schmid, T. Speck (Basel: Birkhäuser Verlag), 32–41.
- Westermeier, A. S., Sachse, R., Poppinga, S., Vögele, P., Adamec, L., Speck, T., et al. (2018). How the carnivorous waterwheel plant (*Aldrovanda vesiculosa*) snaps. *Proc. Royal Soc. London Biol. Sci.* 285:12. doi: 10.1098/rspb.2018.0012
- Yang, R., Lenaghan, S. C., Li, Y., Oi, S., and Zhang, M. (2012). “Mathematical modeling, dynamics analysis and control of carnivorous plants,” in *Signaling and Responses*, ed A. G. Volkov (Heidelberg: Springer), 63–83. doi: 10.1007/978-3-642-29110-4-3
- Yang, R., Lenaghan, S. C., Zhang, M., and Xia, L. (2010). A mathematical model on the closing and opening mechanism for Venus flytrap. *Plant Signaling Behav.* 5, 968–978. doi: 10.4161/psb.5.8.12136
- Yufei, H., Tianmiao, W., Xi, F., Kang, Y., Ling, M., Juan, G., et al. (2017). “A variable stiffness soft robotic gripper with low-melting-point alloy,” in *Proceedings of the 36th Chinese Control Conference. July 26–28, 2017*, eds T. Liu, Q. Zhao and Chinese Control Conference (Dalian, China. Piscataway, NJ: IEEE), 6781–6786.
- Zhang, Z., Chen, D., Wu, H., Bao, Y., and Chai, G. (2016). Non-contact magnetic driving bioinspired Venus flytrap robot based on bistable anti-symmetric CFRP structure. *Composite Structures* 135, 17–22. doi: 10.1016/j.compstruct.2015.09.015
- Zhang, Z., Li, X., Yu, X., Chai, H., Li, Y., Wu, H., et al. (2019). Magnetic actuation bionic robotic gripper with bistable morphing structure. *Composite Structures* 229:111422. doi: 10.1016/j.compstruct.2019.111422
- Zhong, Y., Xia, X., Mai, W., Tu, J., and Fan, H. J. (2017). Integration of energy harvesting and electrochemical storage devices. *Adv. Mater. Technol.* 2:1700182. doi: 10.1002/admt.201700182
- Zhou, Y., Zhao, C., Wang, J., Li, Y., Li, C., Zhu, H., et al. (2019). Stretchable high-permittivity nanocomposites for epidermal alternating-current electroluminescent displays. *ACS Mater. Lett.* 1, 511–518. doi: 10.1021/acsmaterialslett.9b00376

Conflict of Interest: The authors declare that the research was conducted in the absence of any commercial or financial relationships that could be construed as a potential conflict of interest.

Copyright © 2020 Esser, Auth and Speck. This is an open-access article distributed under the terms of the Creative Commons Attribution License (CC BY). The use, distribution or reproduction in other forums is permitted, provided the original author(s) and the copyright owner(s) are credited and that the original publication in this journal is cited, in accordance with accepted academic practice. No use, distribution or reproduction is permitted which does not comply with these terms.



Plant Bioinspired Ecological Robotics

P. Adrian Frazier^{1,2}, Lorenzo Jamone³, Kaspar Althoefer³ and Paco Calvo^{1*}

¹ MINTLab - Minimal Intelligence Lab, Universidad de Murcia, Murcia, Spain, ² Center for the Ecological Study of Perception and Action University of Connecticut, Storrs, CT, United States, ³ Centre for Advanced Robotics @ Queen Mary (ARQ), School of Electronic Engineering and Computer Science, Queen Mary University of London, London, United Kingdom

Plants are movers, but the nature of their movement differs dramatically from that of creatures that move their whole body from point A to point B. Plants grow to where they are going. Bio-inspired robotics sometimes emulates plants' growth-based movement; but growing is part of a broader system of movement guidance and control. We argue that ecological psychology's conception of "information" and "control" can simultaneously make sense of what it means for a plant to navigate its environment and provide a control scheme for the design of ecological plant-inspired robotics. In this effort, we will outline several control laws and give special consideration to the class of control laws identified by tau theory, such as time to contact.

Keywords: bioinspired robotics, ecological psychology, plant signaling and behavior, endogenous control, tau theory

OPEN ACCESS

Edited by:

Barbara Mazzolai,
Italian Institute of Technology (IIT), Italy

Reviewed by:

Luigi Manfredi,
University of Dundee, United Kingdom
Marc Thielen,
University of Freiburg, Germany

*Correspondence:

Paco Calvo
fjcalvo@um.es

Specialty section:

This article was submitted to
Soft Robotics,
a section of the journal
Frontiers in Robotics and AI

Received: 07 March 2020

Accepted: 08 May 2020

Published: 14 July 2020

Citation:

Frazier PA, Jamone L, Althoefer K and
Calvo P (2020) Plant Bioinspired
Ecological Robotics.
Front. Robot. AI 7:79.
doi: 10.3389/frobt.2020.00079

INTRODUCTION

Bioinspired robotics and artificial intelligence has taken various forms, including genetic algorithms, artificial life, and evolutionary robotics (Langton, 1986; Mitchell, 1996; Doncieux et al., 2015); behavior-based and situated robotics (Steels et al., 1995; Arkin, 1998); swarm robotics (Romanishin et al., 2013); morphological computation and soft robotics (Paul, 2006; Pfeifer et al., 2014; Laschi et al., 2016), and others (Calvo and Gomila, 2008). Plants have inspired advances in the material sciences (Mazzolai et al., 2010; Szyndler et al., 2013; Guo et al., 2015; Lucarotti et al., 2015; Voigt et al., 2015) and novel forms of movement based on regeneration, accretion, and eversion (Sadeghi et al., 2014, 2017; Sadeghi et al., 2014, Sadeghi et al., 2017, Greer et al., 2019 Putzu et al., 2018). Elaborate "plantoid" robots come equipped with tree-like branches, leaves, and sensorized, bendable roots, which emulate to some degree the distributed foraging exhibited by plants (Sadeghi et al., 2017). Others have taken inspiration from plant nanoparticles and adhesives (Burris et al., 2018).

Much plant-inspiration remains to be discovered (Vidoni et al., 2015; Wahby et al., 2018) beyond "copying innovations" (Burris et al., 2018). For one thing, innovations along the aforementioned lines resort to pulling out the same bag of tricks that animal researchers have exploited in the past (e.g., materials, morphologies, adhesive nanoproperties, and other biochemical mechanisms), if only rehearsed with plants rather than animal models. But plant bio-inspiration doesn't reduce to transferring biomimetic successes from the animal to the plant kingdom, either in systems and synthetic biology or in molecular and cell biology. Put bluntly, it is not the synthetic gadgets themselves that we are after here. It is rather the grasping and climbing behaviors, the way in which the approaching maneuvers may be controlled, and not their attachment mechanisms or their smart biomimesis.

In what follows, we highlight a role for ecological psychology in both plant science and plant-based robotics. In particular, we explain how successful movement requires an organism (and a robot) to be informed by the very environment as to where to go about. A plant-inspired ecological robot is a robot that can tune to the structure that the surrounding energy media provides. To do so, we suggest, robots could be engineered to exploit the same type of control laws that plants exploit. It is our hope that a plant-inspired ecological robotics will allow researchers to pay due consideration to some new challenges, and opportunities, for robotics and artificial intelligence.

PLANT MOVEMENT

As with animals, plants *move* (Darwin and Darwin, 1880; Mugnai et al., 2007; Riviere et al., 2017). They do so to access information about their environments and engage in adaptive interactions with them (Isnard and Silk, 2009; Carello et al., 2012; Gianoli, 2015). But as rooted creatures, plants cannot get up and flee when threatened, if needed (Trewavas, 2017; Calvo et al., 2020). Their survival strategies can in fact vary dramatically. Extremophytes, such as *Anastatica hierochuntica* (the Rose of Jericho, a somewhat distant relative of the Brassicaceae family of the plant model *Arabidopsis thaliana*) exhibits a high degree of metabolism-based tolerance to extreme heat, lack of Nitrogen, or to a salty environment (Eshel et al., 2017). But not all strategies reduce to evolving a resilient metabolism. Plants, for instance, can survive by extending themselves over as much terrain and in as many directions as they can gain access to (Gianoli et al., 2012). If a line of growth gets cut off, enough redundancy exists to compensate (Trewavas, 2014). But the foregoing is unlikely to succeed if it proceeds at random. Slow movement time and irreversibility means that the plant can ill-afford to rely on chance alone. Through action, plants are able to sample the environment and tune to information with an adaptive value (Calvo and Friston, 2017). This is especially true of climbing plants (Darwin, 1875), like *Phaseolus vulgaris* (Millet et al., 1988; Badot et al., 1990; Millet and Badot, 1996), the so-called “common bean,” which take big risks by extending themselves upward with little in the way of a supportive trunk. They grow tendrils that sway and whip around in ovular cycles until grabbing hold of something (Caré et al., 1998), providing support for continued upward expansion. While the temptation exists to imagine this process in terms of random ballistic projections, there is reason to believe that such is not the case (Calvo et al., 2017a), nor should it be.

To be successful, plant movement must be informed about where to go by the environment (Carello et al., 2012). The plant control system, like that of any organism, is sensitive to an array of different biotic and abiotic energy media and their structuring, ranging from electromagnetic fields to chemical diffusion gradients, vibrations in air and water, and deformations of its own proprioceptive surfaces (Balusška et al., 2006; Brenner et al., 2006; Bastien et al., 2013, 2015; Dumais, 2013; Calvo et al., 2016; Choi et al., 2016; Gilroy et al., 2016; Huber and Bauerle, 2016). If a plant needs a climbable surface, and if a nearby climbable rod structures ambient light in a way that is *specific* to its climbability, then the plant does not have to guess about where to go (Gibson, 1966, 1979; Carello et al., 2012; Turvey,

2019). Climbability, in this case, would be a function of plant-rod properties, such as distance between plant and rod, stalk-strength, tendril length, curl-tightness, and so on. Assuming all this to be the case, a control law would exist relating the plant's getting-to-climbable-surface relevant activities to the light and its getting-to-climbable-surface-relevant structure. If the plant can tune its activities to that structure, then it can capitalize on it and extend its capacity to exploit the sunlight. Whatever the structure in whatever informational media are involved in climbing and nutation, exploiting control laws has numerous advantages over a blind trial and error. For instance, a control law specifying the rate of approach to the rod would allow the plant to manage inertial forces and avoid bouncing off the rod (Lee, 1998). For the plant-inspired roboticist, this also means offloading control to the environment. As an analogy, consider a six-legged robot moving through a field of debris. If the legs are springy, as with RHex (Altendorfer et al., 2001), then the robot can bounce its way from one side to the other. The debris itself, in its interactions with the legs, will cause the bouncing, all without any computing or explicit instructions. Similar morphological-dynamical coupling can be found with, for instance, bio-tensegrity (Turvey and Fonseca, 2014) and reflexes (Dickinson et al., 2000). Control laws go deeper than purely morphological-dynamical coupling and offer the creature and robot alike the opportunity to *act in advance of acting*.

ECOLOGICAL PSYCHOLOGY

Ecological psychology (Gibson, 1966, 1979) was meant to contrast with cognitive psychology in that the emphasis of analysis is the organism-environment relationship, rather than the organism's thoughts. Several more recent theories centering embodiment, embeddedness/situatedness, and enaction have adopted a similar stance (Richardson et al., 2008; Froese and Di Paolo, 2011). Increasingly, these perspectives are making their way into robotics, given that robots are bodied and need to get around in cluttered environments and realize goals (Duchon et al., 1998; Jamone et al., 2016; Zech et al., 2017). For ecological psychologists, the what-is-perceived is not a category of thing, like “rod,” but a climbable surface. In this case, “climbable” is an affordance and “climbing” is an effectivity. Before questions of control can be answered, the roboticist needs to consider whether its robot can do the task at hand. Is the robot a climber? Can it climb? And is climbing available to do? Less trivial is determining if the affordance is specified in the lawfully structured energies to which it is sensitive. An oceanic protist that feeds on photosynthetic bacteria needs to get to the ocean surface. How does it know where to go? If it has a light sensitive pigment coupled to its swimming apparatus, then it should swim so as to increase stimulation of the pigment, because sunlight forms light gradients near the ocean surface (Swenson and Turvey, 1991). The light gradient specifies that food is available (because it is day) and where to go to get it. It is “information about” the location of photosynthetic bacteria. The relationship between swimming and the light gradient is, as previously mentioned, a control law.

Information and Control Laws

The key principle behind ecological psychology's conception of "specifying (or lawful) information" is that the various ambient energy media surrounding an organism are structured by the dynamics of its environment. At a given point of observation (PO), a set of relations exists between the PO and the field, as well as between the sub-fields defined by local distributions of ambient energy. As either the location of a PO or that of an object in the environment is transformed, so too is the set of relations. An organism differs from a generic PO in that it can only access so much of the field—it has a perspective. Nevertheless, the story is similar to that of the PO. As the organism's perspective (or position of an object in the environment) changes, so too do relations within the subfield. Some relations change systematically, while others remain constant (X changes in size relative to Y, but X is always above Y, relative to the direction of gravity). Most importantly, a relationship between transformations of an organism's perspective are directly related to transformations of the relations between distributions of energy in the sub-field (or, respectively, the PO and the field). The latter constitute "lawful information" about the former. Processes that generate transformations of the organism's perspective constitute the "control structure." Mathematically, control and information are duals, akin to the relationship between points and lines, where two points define a line, and two intersecting lines define a point (Shaw and Turvey, 1981). Control is governed by transformations of the relations between energy distributions in the sub-field, i.e., information. And transformations of the information present in the sub-field are determined by transformations of perspective, i.e., control. When this is the case, a control law exists. The ability for an organism (or robot) to attune its activities to these laws is what makes transformations of energy informative.

The Outfielder Problem

The Chapman strategy (Chapman, 1968) for catching a flyball illustrates the foregoing. Think of an imaginary screen placed at some distance from an outfielder as the batter hits a flyball in their direction. The projection $h(t)$ of the ball on the screen at a given time t is

$$h = \frac{Y(t)_{ball} - Y(t)_{po}}{X(t)_{ball} - X(t)_{po}},$$

where (X_{ball}, Y_{ball}) and (X_{po}, Y_{po}) are the position of the ball and outfielder (respectively) in an inertial coordinate system (see **Figure 1A**). The *optical acceleration* (OA) is \ddot{h} , the second derivative. Control laws, in this situation, arise from the following (see **Figure 1B**):

1. If $\ddot{h} = 0$, the ball will intercept the PO.
2. If $\ddot{h} > 0$, the ball will fly over the PO.
3. If $\ddot{h} < 0$, the ball will land in front of the PO.

This means different things depending on whether the outfielder is moving or stationary. If the latter, then the outfielder (1) is positioned to catch the ball, (2) needs to run backwards, or (3) needs to run forwards. If moving at constant velocity in the same direction as the ball, the outfielder (1) is running at

the right speed to catch the ball, (2) needs to run at a faster constant velocity, and (3) needs to run at a slower constant velocity. In both cases, the strategy is cancellation of the optical acceleration (Michaels and Oudejans, 1992; McLeod and Dienes, 1993; Rozendaal and van Soest, 2003). The following dynamical law describes this scenario when $\ddot{h} = 0$ throughout the ball's trajectory (Rozendaal and van Soest, 2003):

$$\ddot{X}_{po} = \ddot{X}_{ball} - \frac{X_{ball,po}}{Y_{ball}} \ddot{Y}_{ball} - 2\dot{X}_{ball,po} \left(\frac{\dot{X}_{ball,po}}{X_{ball,po}} - \frac{\dot{Y}_{ball}}{Y_{ball}} \right).$$

The behavior of the PO under this dynamical law, generally, is initially high acceleration settling into constant velocity, which is consistent with the empirically observed tendency to do the same near interception. The stationary case described earlier suggests a somewhat different strategy, which is to accelerate not at all, backwards, or forwards (respectively). The same strategy can be applied more generally, where constant velocity (near interception of the ball) of the PO is no longer assumed, so that $\ddot{X}_{po} = -\kappa\dot{h}$. The gain κ is positive under circumstances where both times the ball crosses the outfielder's line of site, it is out in front of the outfielder. This is reversed if the outfielder faces the opposite direction (among other cases; see Rozendaal and van Soest, 2003, for details).

Optical Flow Fields and the Optical Push

An *optic field* consists of a packed nesting of reflected-light optical cones extending out from a single PO to all the edges and textures around it (see **Figure 2**). If the PO changes, or something in the environment changes in relation to the PO, the distribution of optical cones is transformed systematically. This change in distribution constitutes an *optic flow field* (OFF). Note that, as with catching a flyball, the PO need not be occupied by an eyeball or sensor on a creature or robot—it could just as well be a particle of dust. Nevertheless, an observer's perspective is limited by their embodied constitution, including their ocular apparatus, to only a portion of the OFF, the *visible optic flow field* (VOFF). The VOFF, embedded as it is in the OFF and defined as it is as a relation between the organism (its PO) and the objects in its environment, manifests a number of control laws. To adumbrate a few of them: moving forward expands the VOFF; moving backward contracts it; moving sideways translates it. The distribution of optical cones for an object moving toward the PO (at rest) will expand while the rest of the field remains the same; or, if the PO is also in motion, the object's optical cones will expand more rapidly, and it will occlude some of the others. Objects hidden behind others will introduce accrete or delete cones as it comes in and out of view. And so on (Gibson, 1979).

To get an idea of how control laws involving the optic flow field work, consider the hanging room experiment (Lee and Aronson, 1974). While standing still in a room without moving objects, the OFF will remain constant in all its relations. The VOFF will shift around with the viewer's saccades, but again, all relations in the distribution of cones will remain the same across saccadic transformations. This constancy is information about both the viewer and the environment's objects: namely, that neither is moving. Thus, if the "goal" is to remain standing still, the relationship between the OFF and the control

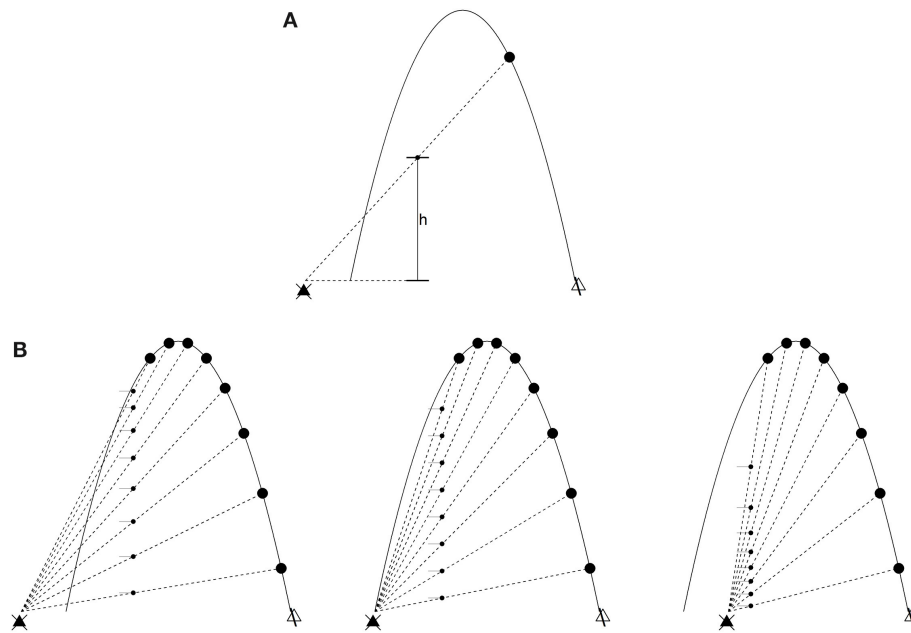


FIGURE 1 | The outfielder problem. The ball (in low-friction conditions) flies in a parabolic trajectory. The large dots are time slices of such a trajectory, and the black triangle on the left is the point of observation (the outfielder's line of sight). **(A)** The optical variable h is the distance between the outfielder's line of sight and a projection of the ball at an arbitrary position x . Optical acceleration is \ddot{h} , the second derivative of h . **(B)** Left: decreasing optical acceleration. The ball will land in front of the outfielder if they do not run forward. Middle: zero optical acceleration. The outfielder will intercept the ball's trajectory. Right: increasing optical acceleration. The ball will land behind the outfielder.

structure embodied by the viewer is this: maintain constant OFF. If the entire OFF were to suddenly expand or contract, then this would imply that the viewer is moving forwards or backwards, respectively. Under normal circumstances, this is “specifying information” about the viewer's movement and the environment's lack of movement. Being dual with control, it also specifies *what to do* (Shaw and Turvey, 1981). If the OFF expands, move backward (to keep it constant), and move forward if it contracts (Lee and Lishman, 1975). The sliding room experiment subverts the usual relations, at least in part, by suspending the walls and ceiling of a room just above the floor, so that the room can move without moving the participant—at least, not physically. Moving the room *did* result in an “optic push,” explicable in terms of the foregoing control law. “Push” is used here because the response to the moving room is like that of a push, probably due to the mismatch between the moving room and a non-moving floor. Participants tripped backwards when the room moved toward them, and forwards when away. Children and inebriated adults fell over entirely. And again, this is without a physical push.

Tau (τ) Guidance

Tau is the ratio $\tau(X, t) = X(t) / \dot{X}(t)$, which describes the time to close gap X , given the current rate of closure. In the case of control systems, the gap is between the current PO and a final (goal) PO. Rate $\dot{\tau}(X(t))$ (alias, “tau dot”) can be used to guide controlled collisions and collision avoidance. Tau dot specifies whether the PO will make contact with a target, given the current

rate of deceleration. Stopping *just at or before* colliding with an object requires stabilizing $\dot{\tau}$ to $\dot{\tau} \leq 1/2$. As with the OA and OFF, the gap X and its rate of closure \dot{X} are constituted in the relationship between a PO and an object. Unlike OA and OFF, X and \dot{X} cannot be detected. On the other hand, $\rho(t) = 1/\tau(t) = \dot{X}(t)/X(t)$, a proportion of the rate of change to the current size of the gap, *can* be detected (Lee, 1998). In the case where final PO is also moving, synchronizing the closing of the two gaps means keeping their respective ρ in constant proportion, $\rho(X, t) = \lambda_{X,Y} \rho(Y, t)$, where X and Y are the two gaps, and $\lambda_{X,Y}$ is a scaling factor setting the relative velocity curve. In the case of action guided by a gap closure with constant acceleration from rest, the rho $\rho(X, t) = \lambda_{X,G} \rho_G(G, t, T_G)$, where T_G is the time it takes to close the guiding gap G , and $\rho_G(G, t, T_G) = 2t/(t^2 - T_G^2)$. The equivalence means that ρ_G prescribes the value of $\lambda_{X,G}$. In the case of a guiding gap D with constant deceleration, $\rho_D(D, t, T_D) = 2/(t - T_D)$ (Lee, 2018).

Moving beyond gaps between organism and environment, tau guidance provides a general scheme for control constituted by managing the opening and closing of gaps of all sorts, including pressure, angle, distance, and others (Lee et al., 2009). Information about gap closures can be found in relative rates of change ρ in *power* (its magnitude), whether found in ambient energy media, stimulation of sensory organs, or flows of electrochemical energy in a nervous or *phytonervous* system (Calvo et al., 2017b; Lee, 2018). Similarly, with parameters of the efferent circuits, effectors, and action on the environment. None of this is to say that the organism *knows* anything

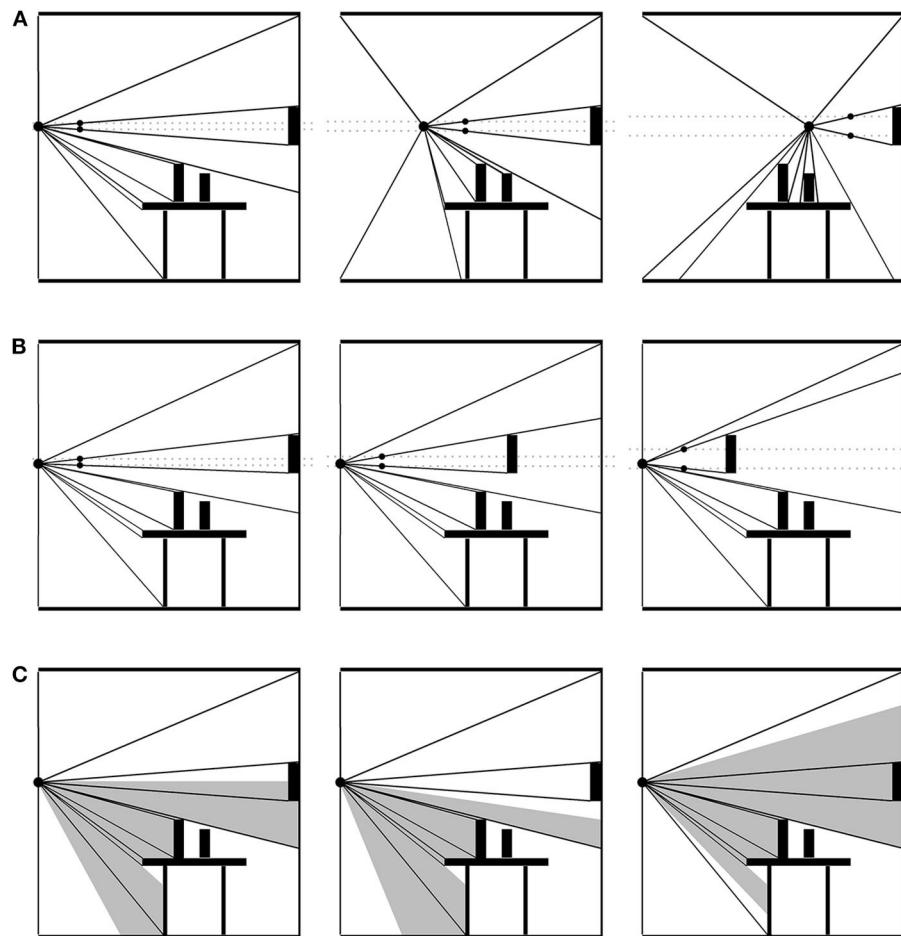


FIGURE 2 | Optical flow field (OFF). A packed nesting of optical cones extends out from the point of observation to each surface. The OFF is structured by changes in surface details both large and small. **(A)** The point of observation (PO) moving across the scene. The gray, dashed lines illustrate the increasingly wide cone extending from the PO to the wall decoration. The black arrow points out a cone gradually disappearing as its surface disappears. The gray arrow points out cones accreting into the OFF as the PO approaches. Information about the environment's stationarity and the PO's non-stationarity is in the collective expansion and contraction of the field. **(B)** The point of observation remains stationary, but the wall decoration moves toward it. The change in the decoration's cone relative to the non-change in the rest of the field specifies that the object is moving and not the PO. **(C)** When the PO is an organism's line of sight, their particular embodiment will determine how much of the OFF is visible. Additional information about head movements, orientation, and location exists in the visible OFF.

about the powers, energies, or gaps anymore than a cat chasing and eating a mouse knows anything about its protein content. The control system generates gaps and ρ 's, even as its gaps and ρ 's are transformed by the environment. The control system *generates* information. And control laws exist where other parts of the control system are governed by it. As such, these information-generating ρ 's amount to prescriptions for any other ρ 's tied up in the interaction. Again, control is constituted in the coordination and synchronization of ρ 's.

TAU GUIDANCE OF PLANT NUTATION

Plant nutation is neither wholly endogenously nor wholly exogenously controlled, and it remains an open question

whether nutation itself is due to internal oscillations, gravity-driven processes, or some combination of the two (Johnsson and Heathcote, 1973; Brown et al., 1990; Hejnowicz and Sievers, 1995; Johnsson et al., 1999; Charzewska and Zawadzki, 2006; Stolarz, 2009). The nutating tendril reaches out in all directions, taking stimulation at its receptors from the various structured energy fields in its environment. Stimulation at the sense organs is transformed into a variety of other energies, such as turgor pressure; flows of phytohormones and a number of other growth factors resulting in auxin redistribution and growth changes (Weisenseel and Meyer, 1997); and changes in electrical potential and ion transmission (Volkov, 2012). Much of this process takes place in dividing, meristematic embryological structures and courtesy of “rapid-long distance electrical and calcium signaling” (Choi et al., 2016) throughout the plant vascular system, has its effect

in patterns of elongation and differentiation (Waddington, 1966) that underlie plant flexible, adaptive behavior (Calvo and Keijzer, 2011; Calvo et al., 2020).

Suppose that as the tendril makes its way around, nothing changes about the ambient energy media to which the plant has access. Stimulation of the sensory organs is constant. Perhaps the plant is surrounded by a climbable surface, but even so, the environment says nothing about where to go to get to it. The plant's nutation will go on, but undirected. On the other hand, there might be a tree branch. The plant will whip itself *toward* the branch, but *away* from the shade. The difference can be understood in terms of the ratio of red to far-red and blue to green light (Ballaré and Pierik, 2017)—the lower the ratio, the more shade from other plants, as they will have already absorbed the red and blue. Whatever the case, the plant's shade-avoidance movements will generate differences of stimulation at the plant's sensory organs, or gaps in stimulus power. And, when encountering these gaps, flows of phytohormone and other growth factors will generate auxin flows with yet further gaps, and so on, each process informed by its context of unequal distributions of power and their equalization.

Control Laws Redux

Theory in ecological psychology is primarily concerned with interactive success. What are the necessary conditions for repeatable, reliable, successful encounters with the world? This is a matter that brings the entire ecosystem into focus—no organism can get by without reliable access to its environment. And no species comes into existence in a world where it has to do guess work and make inferences for more than a very small number of its activities. The layout of an environment and its lawfully structured energy media contain information, so the hypothesis goes, about *what to do*. As mentioned previously, control and lawful information are duals, they both define and entail one another (Shaw and Turvey, 1981).

The gap closures of tau theory may well be the most bountiful source of control laws in nature. The first gap any of us deal with in life is that between our own bodies and the floor or bed as we struggle against gravity. Indeed, the rate of closure of that gap is the ultimate prescriptive, guiding gap when we fall, as whatever action we take to reduce its damage must take place within it. Arguably, the optical flow field is a special case of tau-theoretic gap closure, as the changing distribution of optical cones can easily be conceived of as a packed nesting of opening and closing gaps. The chapman strategy involves the closing of not only the gap between ball and glove and ball and outfielder, but the closing in on a constant velocity, and so on.

CONCLUSION

The preceding discussion suggests a reconsideration of what the challenges for robotics and artificial intelligence

really are. Movement by growth, for instance, raises new questions. Artificial move-by-growing systems already exist (Mazzolai et al., 2010; Mazzolai et al., 2011), but can they explore their surrounds by growth? What about movement by exploration-guided growth? To ask such questions is to break with common intuitions centered narrowly around animals and their brains. It suggests that plants are like animals in being competent, agentic creatures capable of pursuing and realizing outcomes. And yet they differ from animals in being *brainless* and *morphologically plastic*, extending their surfaces outward, spatially and fractally. These facts suggest a need to rethink how we conceptualize agency.

The reader may be willing to admit that between organism or robot and environment, the control law is king, but once getting *inside* the thing, what then? A temptation exists to “scale up” with a hybrid between ecological and classical designs. For instance, Google bought Boston Dynamics. The former is known for world class artificial intelligence, and the latter state-of-the-art movement systems making heavy use of dynamics in their control structures. Perhaps the engineers at Google hoped to integrate them, as is the most logical conclusion if one assumes the body is a physical structure subject to the forces and flows of the real world, but the mind is some kind of computer. This partnership did not last long—why not? Our claim is that such endeavors are ill conceived in the first place. Organisms evolved their capabilities in dynamic, physical environments, impinged upon by a variety of forces, flows, and structured energy media. The organism need not guess about what to do most of the time, instead, it must *resonate* with what is already there (Raja, 2018, 2020; Fultot et al., 2019; Golonka and Wilson, 2019). The scheme is one of modulation of endogenous activity: *process informing*, rather than *information processing* (cf. Bickhard, 2015a,b; Fultot et al., 2019). The organism “tunes into” *lawful* information, and in doing so, *generates* information internally and further tunes its activities to *it*. In the case of tau theory, this means tau coupling. As the organism (robot) moves, it transforms stimulation at the sensors, generating gaps and taus/rhos. If the tau/rho in the environment prescribes tau/rho of a movement, then by picking up source power, stimulus power, then neural/phytoneural power, each tau/rho acts as a prescription for the next, an ensemble of coordinating degrees of freedom.

The foregoing provides a sampling of the richness available to a robotics and artificial intelligence for future research via ecological psychology and an emerging dialogue with neuroscience. Further models of “higher level” psychology exist within and around ecological psychology, such as direct learning (Jacobs and Michaels, 2007), resonance-based perceptual learning (Raja, 2019), and a wide array of others developed in interactivist theory (Bickhard and Richie, 1983; Bickhard, 1993, 2009, 2015a,b; Bickhard and Terveen, 1996).

AUTHOR CONTRIBUTIONS

PC conceived the original idea. PC and PF devised the project, the main conceptual ideas, and proof outline. PF worked out the technical details and wrote the manuscript in consultation with PC, LJ, and KA. All authors provided feedback and helped shape the manuscript.

REFERENCES

- Altendorfer, R., Moore, N., Komsuoglu, H., Buehler, M., Brown, H. B., McMordie, D., et al. (2001). RHex: a biologically inspired hexapod runner. *Auton. Robots* 11, 207–213. doi: 10.1023/A:1012426720699
- Arkin, R. C. (1998). *Behavior-Based Robotics*. Cambridge, MA: MIT Press.
- Badot, P.-M., Melin, D., and Garrec, J. P. (1990). Circumnutation in *Phaseolus vulgaris* L. II. Potassium content in the free-moving part of the shoot. *Plant Physiol. Biochem.* 28, 123–130.
- Ballaré, C. L., and Pierik, R. (2017). The shade-avoidance syndrome: multiple signals and ecological consequences. *Plant Cell Environ.* 40, 2530–2543. doi: 10.1111/pce.12914
- Balusška, F., Mancuso, S., and Volkmann, D. (2006). *Communication in plants: Neuronal aspects of plant life*. Berlin: Springer-Verlag. doi: 10.1007/978-3-540-28516-8
- Bastien, R., Bohr, T., Moulia, B., and Douady, S. (2013). Unifying model of shoot gravitropism reveals proprioception as a central feature of posture control in plants. *Proc. Natl. Acad. Sci. U.S.A.* 110, 755–760. doi: 10.1073/pnas.1214301109
- Bastien, R., Douady, S., and Moulia, B. (2015). A unified model of shoot tropism in plants: photo-, gravi- and proprioception. *PLoS Comput. Biol.* 11:e1004037. doi: 10.1371/journal.pcbi.1004037
- Bickhard, M. H. (1993). Representational content in humans and machines. *J. Exp. Theor. Artif. Intell.* 5, 285–333. doi: 10.1080/09528139308953775
- Bickhard, M. H. (2009). The interactivist model. *Synthese* 166, 547–591. doi: 10.1007/s11229-008-9375-x
- Bickhard, M. H. (2015a). Toward a model of functional brain processes I: central nervous system functional micro-architecture. *Axiomathes* 25, 217–238. doi: 10.1007/s10516-015-9275-x
- Bickhard, M. H. (2015b). Toward a model of functional brain processes II: central nervous system functional macro-architecture. *Axiomathes* 25, 377–407. doi: 10.1007/s10516-015-9276-9
- Bickhard, M. H., and Richie, D. M. (1983). *On the Nature of Representation*. New York, NY: Praeger.
- Bickhard, M. H., and Terveen, L. (1996). *Foundational Issues in Artificial Intelligence and Cognitive Science: Impasse and Solution*, Vol. 109. Amsterdam: Elsevier.
- Brenner, E. D., Stahlberg, R., Mancuso, S., Vivanco, J. M., Baluška, F., and van Volkenburgh, E. (2006). Plant neurobiology: an integrated view of plant signaling. *Trends Plant Sci.* 11, 413–419. doi: 10.1016/j.tplants.2006.06.009
- Brown, A. H., Chapman, D. K., Lewis, R. F., and Venditti, A. L. (1990). Circumnutations of sunflower hypocotyls in satellite orbit. *Plant Physiol.* 94, 233–238. doi: 10.1104/pp.94.1.233
- Burris, J. N., Lenaghan, S. C., and Stewart, C. N. (2018). Climbing plants: attachment adaptations and bioinspired innovations. *Plant Cell Rep.* 37, 565–574. doi: 10.1007/s00299-017-2240-y
- Calvo, P., Baluška, F., and Sims, A. (2016). 'Feature detection' vs. 'predictive coding' models of plant behavior. *Front. Psychol.* 7:1505. doi: 10.3389/fpsyg.2016.01505
- Calvo, P., and Friston, K. (2017). Predicting green: really radical (plant) predictive processing. *J. R. Soc. Interface* 14:20170096. doi: 10.1098/rsif.2017.0096
- Calvo, P., Gagliano, M., Souza, G. M., and Trewavas, A. J. (2020). Plants are intelligent: here's how. *Ann. Bot.* 125, 11–18. doi: 10.1093/aob/mcz155
- Calvo, P., and Gomila, A. (2008). *Handbook of Cognitive Science: An Embodied Approach*. Amsterdam: Elsevier Science.

FUNDING

This research is partially supported by the Office of Naval Research Global (Award # N62909-19-1-2015) to PF and PC, and by the EPSRC UK (with projects MAN3, EP/S00453X/1, and NCNR, EP/R02572X/1) to LJ and KA.

- Calvo, P., and Keijzer, F. (2011). Plants: adaptive behavior, root-brains, and minimal cognition. *Adaptive Behav.* 11, 155–171. doi: 10.1177/1059712311409446
- Calvo, P., Raja, V., and Lee, D. (2017a). Guidance of circumnutation of climbing bean stems: an ecological exploration. *bioRxiv* 122358. doi: 10.1101/122358
- Calvo, P., Sahi, V. P., and Trewavas, A. (2017b). Are plants sentient? *Plant Cell Environ.* 40, 2858–2869. doi: 10.1111/pce.13065
- Caré, A. F., Nefed'ev, L., Bonnet, B., Millet, B., and Badot, P.-M. (1998). Cell elongation and revolving movement in *Phaseolus vulgaris* L. twining shoots. *Plant Cell Physiol.* 39, 914–921. doi: 10.1093/oxfordjournals.pcp.a029454
- Carello, C., Vaz, D., Blau, J. J. C., and Petrusz, S. C. (2012). Unnerving intelligence. *Ecol. Psychol.* 24, 241–264. doi: 10.1080/10407413.2012.702628
- Chapman, S. (1968). Catching a baseball. *Am. J. Phys.* 36, 868–870. doi: 10.1119/1.1974297
- Charzewska, A., and Zawadzki, T. (2006). Circadian modulation of circumnutation length, period, and shape in *Helianthus annuus*. *J. Plant Growth Regl.* 25, 324–331. doi: 10.1007/s00344-006-0042-5
- Choi, W.-G., Hilleary, R., Swanson, S. J., Kim, A.-H., and Gilroy, S. (2016). Rapid-long distance electrical and calcium signalling in plants. *Ann. Rev. Plant Biol.* 67, 287–307. doi: 10.1146/annurev-arplant-043015-112130
- Darwin, C. (1875). *The Movements and Habits of Climbing Plants*. London: John Murray. doi: 10.5962/bhl.title.55239
- Darwin, C., and Darwin, F. (1880). *The Power of Movement in Plants*. London: John Murray. doi: 10.5962/bhl.title.102319
- Dickinson, M. H., Farley, C. T., Full, R. J., Koehl, M. A., Kram, R., and Lehman, S. (2000). How animals move: an integrative view. *Science* 288, 100–106. doi: 10.1126/science.288.5463.100
- Doncieux, S., Bredeche, N., Mouret, J.-B., and Eiben, A. E. (2015). Evolutionary robotics: what, why, and where to. *Front. Robot. AI* 2:4. doi: 10.3389/frobt.2015.00004
- Duchon, A. P., Kaelbling, L. P., and Warren, W. H. (1998). Ecological robotics. *Adaptive Behav.* 6, 473–507. doi: 10.1177/105971239800600306
- Dumais, J. (2013). Beyond the sine law of plant gravitropism. *Proc. Natl. Acad. Sci. U.S.A.* 110, 391–392. doi: 10.1073/pnas.1219974110
- Eshel, G., Shaked, R., Kazachkova, Y., Khan, A., Eppel, A., Cisneros, A., et al. (2017). *Anastatica hierochuntica*, an *Arabidopsis* Desert relative, is tolerant to multiple abiotic stresses and exhibits species-specific and common stress tolerance strategies with its halophytic relative, *Eutrema (Thellungiella) salsugineum*. *Front. Plant Sci.* 7:1992. doi: 10.3389/fpls.2016.01992
- Froese, T., and Di Paolo, E. A. (2011). The enactive approach: theoretical sketches from cell to society. *Pragmat. Cogn.* 19, 1–36. doi: 10.1075/pc.19.1.01fro
- Fultot, M., Frazier, P. A., Turvey, M. T., and Carello, C. (2019). What are nervous systems for? *Ecol. Psychol.* 31, 218–234. doi: 10.1080/10407413.2019.1615205
- Gianoli, E. (2015). The behavioural ecology of climbing plants. *AoB PLANTS* 7:plv013. doi: 10.1093/aobpla/plv013
- Gianoli, E., Saldaña, A., and Jiménez-Castillo, M. (2012). Ecophysiological traits may explain the abundance of climbing plant species across the light gradient in a temperate rainforest. *PLoS ONE* 7:e38831. doi: 10.1371/journal.pone.0038831
- Gibson, J. J. (1966). *The Senses considered as Perceptual Systems*. Boston, MA: Houghton Mifflin.
- Gibson, J. J. (1979). *The Ecological Approach to Visual Perception*. Boston, MA: Houghton Mifflin.

- Gilroy, S., Bialasek, M., Suzuki, N., Goórecka, M., Devireddy, A. R., Karpiniński, S., et al. (2016). ROS, calcium, and electric signals: key mediators of rapid systemic signaling in plants. *Plant Physiol.* 171, 1606–1615 doi: 10.1104/pp.16.00434
- Golonka, S., and Wilson, A. D. (2019). Ecological representations. *Ecol. Psychol.* 31, 235–253. doi: 10.1080/10407413.2019.1615224
- Greer, J. D., Morimoto, T. K., Okamura, A. M., and Hawkes, E. W. (2019). A soft, steerable continuum robot that grows via tip extension. *Soft Robot.* 6, 95–108. doi: 10.1089/soro.2018.0034
- Guo, Q., Dai, E., Han, X., Xie, S., Chao, E., and Chen, Z. (2015). Fast nastic motion of plants and bioinspired structures. *J. R. Soc. Interface* 12:20150598. doi: 10.1098/rsif.2015.0598
- Hejnowicz, Z., and Sievers, A. (1995). Proton efflux from the outer layer of the peduncle of tulip in gravitropism and circumnutation. *Bot. Acta* 108, 7–13. doi: 10.1111/j.1438-8677.1995.tb00825.x
- Huber, A. E., and Bauerle, T. L. (2016). Long-distance plant signaling pathways in response to multiple stressors: the gap in knowledge. *J. Exp. Bot.* 67, 2063–2079. doi: 10.1093/jxb/erw099
- Isnard, S., and Silk, W. K. (2009). Moving with climbing plants from charles darwin's time into the 21st century. *Am. J. Bot.* 96, 1205–1221. doi: 10.3732/ajb.0900045
- Jacobs, D. M., and Michaels, C. F. (2007). Direct learning. *Ecol. Psychol.* 19, 321–349. doi: 10.1080/10407410701432337
- Jamone, L., Ugur, E., Cangelosi, A., Fadiga, L., Bernardino, A., Piater, J., et al. (2016). Affordances in psychology, neuroscience, and robotics: a survey. *IEEE Trans. Cogn. Dev. Syst.* 10, 4–25. doi: 10.1109/TCDS.2016.2594134
- Johnsson, A., and Heathcote, D. (1973). Experimental evidence and models on circumnutations. *Z. Pflanzenphysiol.* 70, 371–405. doi: 10.1016/S0044-328X(73)80117-5
- Johnsson, A., Jansen, C., Engelmann, W., and Schuster, J. (1999). Circumnutations without gravity: a two-oscillator model. *J. Gravit. Physiol.* 6, 9–12.
- Langton, C. G. (1986). Studying artificial life with cellular automata. *Physica D* 22, 120–149. doi: 10.1016/0167-2789(86)90237-X
- Laschi, C., Mazzolai, B., and Bianchetti, M. (2016). Soft robotics: technologies and systems pushing the boundaries of robot abilities. *Sci. Robot.* 1:eaah3690. doi: 10.1126/scirobotics.aah3690
- Lee, D. N. (1998). Guiding movement by coupling taus. *Ecol. Psychol.* 10, 221–250. doi: 10.1207/s15326969eco103&4_4
- Lee, D. N. (2018). How organisms guide their actions. *Preprints* 2018050458. doi: 10.20944/preprints201805.0458.v1
- Lee, D. N., and Aronson, E. (1974). Visual proprioceptive control of standing in human infants. *Atten. Percept. Psychophys.* 15, 529–532. doi: 10.3758/BF03199297
- Lee, D. N., Bootsma, R. J., Frost, B. J., Land, M., and Regan, D. (2009). General tau theory: evolution to date. Special Issue: landmarks in perception. *Perception* 38, 837–858. doi: 10.1068/pmklee
- Lee, D. N., and Lishman, J. R. (1975). Visual proprioceptive control of stance. *J. Human Mov. Stud.* 1, 87–95
- Lucarotti, M. T., Sadeghi, A., Mazzolai, B., and Beccai, L. (2015). Revealing bending and force in a soft body through a plant root inspired approach. *Sci. Rep.* 5:8788. doi: 10.1038/srep08788
- Mazzolai, B., Laschi, C., Dario, P., Mugnai, S., and Mancuso, S. (2010). The plant as a biomechatronic system. *Plant Signal. Behav.* 5, 90–93. doi: 10.4161/psb.5.2.10457
- Mazzolai, B., Mondini, A., Corradi, P., Laschi, C., Mattoli, V., Sinibaldi, E., et al. (2011). A miniaturized mechatronic system inspired by plant roots for soil exploration. *IEEE/ASME Trans. Mech.* 16, 201–212. doi: 10.1109/TMECH.2009.2038997
- McLeod, P., and Dienes, Z. (1993). Running to catch the ball. *Nature.* 362:23. doi: 10.1038/362023a0
- Michaels, C. F., and Oudejans, R. O. D. (1992). The optics and actions of catching fly balls: zeroing out optical acceleration. *Ecol. Psychol.* 4, 199–222. doi: 10.1207/s15326969eco0404_1
- Millet, B., and Badot, P.-M. (1996). “The revolving movement mechanism in phaseolus. New approaches to old questions,” in *Vistas on Biorhythmicity*. eds H. Greppin, R. Degli Agosti, and M. Bonzon (Geneva: University of Geneva Press), 77–98).
- Millet, B., Melin, D., and Badot, P.-M. (1988). Circumnutation in *Phaseolus vulgaris*. I., Growth, osmotic potential and cell ultrastructure in the free-moving part of the shoot. *Physiol. Plant.* 72, 133–138. doi: 10.1111/j.1399-3054.1988.tb06634.x
- Mitchell, M. (1996). *An Introduction to Genetic Algorithms*. Cambridge, MA: MIT Press.
- Mugnai, S., Azzarello, E., Masi, E., Pandolfi, C., and Mancuso, S. (2007). “Nutation in plants,” in *Rhythms in Plants: Phenomenology, Mechanisms, and Adaptive Significance*. eds S. Mancuso, and S. Shabala (Berlin, Germany: Springer), 77–79.
- Paul, C. (2006). Morphological computation: a basis for the analysis of morphology and control requirements. *Robot. Auton. Syst.* 54, 619–630. doi: 10.1016/j.robot.2006.03.003
- Pfeifer, R., Lungarella, M., and Sporns, O. (2014). “The synthetic approach to embodied cognition: a primer,” in *Handbook of Cognitive Science: An Embodied Approach*. eds P. Calvo, and T. Gomila (San Diego, CA: Elsevier), 121–138.
- Putzu, F., Abrar, T., and Althoefer, K. (2018). Plant-inspired soft pneumatic eversion robot. *IEEE Int. Conf. Biomed. Robot. Biomech.* 1327–1332. doi: 10.1109/BIOROB.2018.8487848
- Raja, V. (2018). A theory of resonance: towards an ecological cognitive architecture. *Minds Mach.* 28, 29–51. doi: 10.1007/s11023-017-9431-8
- Raja, V. (2019). From metaphor to theory: the role of resonance in perceptual learning. *Adapt. Behav.* 27, 405–421. doi: 10.1177/1059712319854350
- Raja, V. (2020). Resonance and radical embodiment. *Synthese* 1–29. doi: 10.1007/s11229-020-02610-6
- Richardson, M., Shockley, K., Fajen, B. R., Riley, M. A., and Turvey, M. (2008). “Ecological psychology: six principles for an embodied-embedded approach to behavior,” in *Handbook of Cognitive Science: An Embodied Approach*. eds P. Calvo, and T. Gomila (San Diego, CA: Elsevier), 161–187. doi: 10.1016/B978-0-08-046616-3.00009-8
- Riviere, M., Derr, J., and Douady, S. (2017). Motions of leaves and stems, from growth to potential use. *Physiol. Biol.* 14:051001. doi: 10.1088/1478-3975/aa5945
- Romanishin, J. W., Gilpin, K., and Rus, D. (2013). “M-blocks: momentum-driven magnetic modular robots,” *Intelligent Robots and Systems (IROS) 2013 IEEE/RSJ International Conference*, Tokyo, 4288–4295.
- Rozendaal, L. A., and van Soest, A. J. (2003). Optical acceleration cancellation: a viable interception strategy? *Biol. Cybern.* 89, 415–425. doi: 10.1007/s00422-002-0393-3
- Sadeghi, A., Mondini, A., and Mazzolai, B. (2017). Toward self-growing soft robots inspired by plant roots and based on additive manufacturing technologies. *Soft Robot.* 4, 211–223. doi: 10.1089/soro.2016.0080
- Sadeghi, A., Tonazzini, A., Popova, L., and Mazzolai, B. (2014). A novel growing device inspired by plant root soil penetration behaviors. *PLoS ONE* 9:e90139. doi: 10.1371/journal.pone.0090139
- Shaw, R., and Turvey, M. T. (1981). “Coalitions as models for ecosystems: a realist perspective on perceptual organization,” in *Perceptual Organization*. eds M. Kubovy, and J. R. Pomerantz (Hillsdale: Lawrence Erlbaum Associates), 343–415. doi: 10.4324/9781315512372-11
- Steels, L., and Brooks, R. A., (Eds.). (1995). *The Artificial Life Route to Artificial Intelligence: Building Embodied Situated Agents*. Hillsdale: Lawrence Erlbaum Associates Inc.
- Stolarz, M. (2009). Circumnutation as a visible plant action and reaction. *Plant Signal. Behav.* 4, 380–387. doi: 10.4161/psb.4.5.8293
- Swenson, R., and Turvey, M. T. (1991). Thermodynamic reasons for perception-action cycles. *Ecol. Psychol.* 3, 317–348. doi: 10.1207/s15326969eco0304_2
- Szyndler, M. W., Haynes, K. F., Potter, M. F., Corn, R. M., and Loudon, C. (2013). Entrapment of bed bugs by leaf trichomes inspires microfabrication of biomimetic surfaces. *J. R. Soc. Interface* 10:20130174. doi: 10.1098/rsif.2013.0174
- Trewavas, A. J. (2014). *Plant Behaviour and Intelligence*. Oxford: Oxford UP. doi: 10.1093/acprof:oso/9780199539543.001.0001
- Trewavas, A. J. (2017). The foundations of plant intelligence. *Interface Focus* 7:20160098. doi: 10.1098/rsfs.2016.0098
- Turvey, M. T. (2019). *Lectures on Perception: an Ecological Perspective*. New York, NY: Routledge. doi: 10.4324/9780429443879

- Turvey, M. T., and Fonseca, S. T. (2014). The medium of haptic perception: a tensegrity hypothesis. *J. Motor Behav.* 46, 143–187. doi: 10.1080/00222895.2013.798252
- Vidoni, R., Mimmo, T., and Pandolfi, C. (2015). Tendril-based climbing plants to model, simulate and create bio-inspired robotic systems. *J. Bionic Eng.* 12, 250–262. doi: 10.1016/S1672-6529(14)60117-7
- Voigt, D., Konrad, W., and Gorb, S. (2015). A universal glue: underwater adhesion of the secretion of the carnivorous flypaper plant *Roridula gorgonias*. *Interface Focus* 5:20140053. doi: 10.1098/rsfs.2014.0053
- Volkov, A. G. (ed.). (2012). *Plant Electrophysiology. Signaling and Responses*. Berlin: Springer. doi: 10.1007/978-3-642-29110-4
- Waddington, C. H. (1966). *Principles of Development and Differentiation*. London: MacMillan.
- Wahby, M., Heinrich, M. K., Hofstadler, D. N., Neufeld, E., Kuksin, I., Zahadat, P., et al. (2018). Autonomously shaping natural climbing plants: a bio-hybrid approach. *R. Soc. Open Sci.* 5:180296. doi: 10.1098/rsos.180296
- Weisenseel, M. H., and Meyer, A. J. (1997). Bioelectricity, gravity and plants. *Planta* 203, S98–108. doi: 10.1007/PL00008122
- Zech, P., Haller, S., Lakani, S. R., Ridge, B., Ugur, E., and Piater, J. (2017). Computational models of affordance in robotics: a taxonomy and systematic classification. *Adapt. Behav.* 25, 235–271. doi: 10.1177/1059712317726357

Conflict of Interest: The authors declare that the research was conducted in the absence of any commercial or financial relationships that could be construed as a potential conflict of interest.

Copyright © 2020 Frazier, Jamone, Althoefer and Calvo. This is an open-access article distributed under the terms of the Creative Commons Attribution License (CC BY). The use, distribution or reproduction in other forums is permitted, provided the original author(s) and the copyright owner(s) are credited and that the original publication in this journal is cited, in accordance with accepted academic practice. No use, distribution or reproduction is permitted which does not comply with these terms.



A General 3D Model for Growth Dynamics of Sensory-Growth Systems: From Plants to Robotics

Amir Porat¹, Fabio Tedone², Michele Palladino², Pierangelo Marcati² and Yasmine Meroz^{3*}

¹ Faculty of Exact Sciences, School of Physics, Tel Aviv University, Tel Aviv, Israel, ² Gran Sasso Science Institute, L'Aquila, Italy, ³ Faculty of Life Sciences, School of Plant Sciences and Food Security, Tel Aviv University, Tel Aviv, Israel

OPEN ACCESS

Edited by:

Thomas Speck,
University of Freiburg, Germany

Reviewed by:

Manfred Bischoff,
University of Stuttgart, Germany
Karl J. Niklas,
Cornell University, United States
Wilfried Konrad,
University of Tübingen, Germany

*Correspondence:

Yasmine Meroz
jazz@tauex.tau.ac.il

Specialty section:

This article was submitted to
Soft Robotics,
a section of the journal
Frontiers in Robotics and AI

Received: 16 April 2020

Accepted: 03 June 2020

Published: 05 August 2020

Citation:

Porat A, Tedone F, Palladino M, Marcati P and Meroz Y (2020) A General 3D Model for Growth Dynamics of Sensory-Growth Systems: From Plants to Robotics. *Front. Robot. AI* 7:89. doi: 10.3389/frobt.2020.00089

In recent years, there has been a rise in interest in the development of self-growing robotics inspired by the moving-by-growing paradigm of plants. In particular, climbing plants capitalize on their slender structures to successfully negotiate unstructured environments while employing a combination of two classes of growth-driven movements: tropic responses, growing toward or away from an external stimulus, and inherent nastic movements, such as periodic circumnutations, which promote exploration. In order to emulate these complex growth dynamics in a 3D environment, a general and rigorous mathematical framework is required. Here, we develop a general 3D model for rod-like organs adopting the Frenet-Serret frame, providing a useful framework from the standpoint of robotics control. Differential growth drives the dynamics of the organ, governed by both internal and external cues while neglecting elastic responses. We describe the numerical method required to implement this model and perform numerical simulations of a number of key scenarios, showcasing the applicability of our model. In the case of responses to external stimuli, we consider a distant stimulus (such as sunlight and gravity), a point stimulus (a point light source), and a line stimulus that emulates twining of a climbing plant around a support. We also simulate circumnutations, the response to an internal oscillatory cue, associated with search processes. Lastly, we also demonstrate the superposition of the response to an external stimulus and circumnutations. In addition, we consider a simple example illustrating the possible use of an optimal control approach in order to recover tropic dynamics in a way that may be relevant for robotics use. In all, the model presented here is general and robust, paving the way for a deeper understanding of plant response dynamics and also for novel control systems for newly developed self-growing robots.

Keywords: plant tropism, circumnutation, self-growing robots, plant-inspired robotics, control system, optimal control, growth

1. INTRODUCTION

Though the field of robotics has long been inspired from the capabilities of biological organisms, it is only recently that the plant world has become a source of inspiration, particularly due to the ability of plants to continuously change their morphology and functionality by growing, thus adapting to a changing environment (Del Dottore et al., 2016; Laschi and Mazzolai, 2016; Mazzolai et al., 2016). A new class of plant-inspired robots has emerged, based on the

moving-by-growing capabilities of plants. Some recent examples include: (i) a tendril robot developed at NASA's Johnson Space Center, which is a slender manipulator composed of multiple bending segments (Mehling et al., 2006), (ii) a vine-bot that elongates its body at the tip by skin eversion, growing in a pre-determined form (Hawkes et al., 2017), (iii) plantoid robots inspired by plant roots, based on additive manufacturing technologies (Sadeghi et al., 2014, 2017; Del Dottore et al., 2016), and (iv) FIBERBOTS, based on the addition of fiber and resin (Kayser et al., 2019). Though these are impressive accomplishments, these robots are currently limited in their control systems and autonomy. The challenge lies in the fact that the morphology of such self-growing robots changes over time and is therefore not known in advance. Furthermore, in the future, such robots are expected to perform autonomously in unstructured scenarios, including achieving locomotion in uncertain terrains involving obstacles and voids, as well as the manipulation of unknown objects. Therefore, the development of a control system is not trivial and cannot be based on existing control systems of classic predefined robotic structures.

Plants, on the other hand, excel at these types of tasks. Though plants exhibit a variety of types of movements as part of their interaction with their environment (Darwin, 1880; Jost and Gibson, 1907; Ruhland, 1959; Hart, 1990; Forterre, 2013), here we focus on the relevant growth-driven movements of rod-like organs, such as shoots and roots. Such growth-driven movements are generally classified as either *nastic* or *tropic* (Rivière et al., 2017). Nastic movements are due to internal drivers, such as the inherent periodic movement of plants called circumnutations, sometimes associated with search processes. Tropisms are the growth-driven responses of a plant in the direction of a stimulus, such as a plant shoot growing toward a source of light or away from the direction of gravity (Darwin, 1880; Gilroy and Masson, 2007; Rivière et al., 2017). Tropic responses are based on three main processes: (i) sensing of a directional external stimulus by specialized biosensors, (ii) transduction of signals within the plant, leading to the redistribution of the growth hormone auxin, resulting in (iii) an anisotropic growth pattern that reorients the organ toward or away from a given stimulus.

In order to emulate these complex growth dynamics in a 3D environment in a way that is meaningful from the robotics standpoint, a general mathematical framework is required. Recently developed models of growth-driven plant dynamics are limited to specific aspects of tropisms or circumnutations. Bastien et al. have developed models for tropism in 2D, such as the AC (Bastien et al., 2013, 2015) and ACE (Bastien et al., 2014) models, addressing the influence of growth, and identifying the requirement of a *restoring force* called proprioception, whereby a plant can dampen the curving dynamics according to how curved it is (Bastien et al., 2013; Hamant and Mouliat, 2016). Bressan et al. (2017) developed a model based on a similar formalism, but not accounting for growth explicitly as the driver of dynamics and achieving stable dynamics by controlling the growth-zone and sensitivity rather than proprioception. Another model focuses on circumnutations in 3D (Bastien and Meroz, 2016) but disregarding tropic responses. These models disregard elastic responses, implicitly

assuming that no forces or torques act on the organs. Recently, efforts have been made to consider elastic responses in specific scenarios, namely incorporating gravitational forces in the case of gravitropism (Chelakkot and Mahadevan, 2017) and in the case of circumnutations (Agostinelli et al., 2020).

Here, we present a general and rigorous mathematical framework of a rod-like growing organ whose dynamics are driven by both internal and external cues. Though this model is inspired by plant responses, it is not based on biological details and is therefore relevant to any rod-like organisms that respond to signals via growth, such as neurons and fungi. The model does not include elastic responses, but the mathematical framework we adopt here allows a natural integration of elasticity, which we plan to do in future work. The paper is organized as follows: section 2 describes the dynamical equations of our model based on a 3D description of an organ in the Frenet-Serret formalism, implementing differential growth as the driver of movement, and relating external and internal signals. In section 3, we present the numerical method required to implement this model, and in section 4, we perform numerical simulations of a number of key case examples, including responses to external stimuli, such as a distant stimulus, a point stimulus, and a line stimulus, as well as circumnutations (the response to an internal oscillatory cue). We also present an example where we superimpose two different types of cues, namely the response to an external stimulus and circumnutations. Lastly, in section 5, we consider a simple example illustrating the possible use of an optimal control approach in order to recover tropic dynamics in a way which may be amenable to robotics use.

2. GOVERNING EQUATIONS

In this section, we develop the dynamical equations that form the basis of our model. We first introduce a 3D description of an organ in the Frenet-Serret formalism and then detail the implementation of growth and differential growth as the driver of movement. Finally, we relate external and internal signals to differential growth, which drives the desired movement. We then show that our model is a generalization that consolidates different aspects of existing models, allowing the characteristic time and length scales of our model to be identified and discussed.

2.1. 3D Description of an Organ

We model an elongated rod-like organ as a curved cylinder with radius R , described by its centerline that follows a curve in 3D. We denote the location of the centerline from the origin of a Cartesian frame of reference as $\vec{r}(s, t)$, where t is time, and s is its arc-length, which runs along the organ, taking the value $s = 0$ at the base and $s = L$ at the apical tip, equal to the total length (see **Figure 1A**). In order to describe the dynamics of the centerline with respect to local stimuli, we begin by defining a local frame of reference using the Frenet-Serret framework (Goriely, 2017). Using the Frenet-Serret formulas for a 3D curve parameterization, as shown in **Figure 1A**, we can

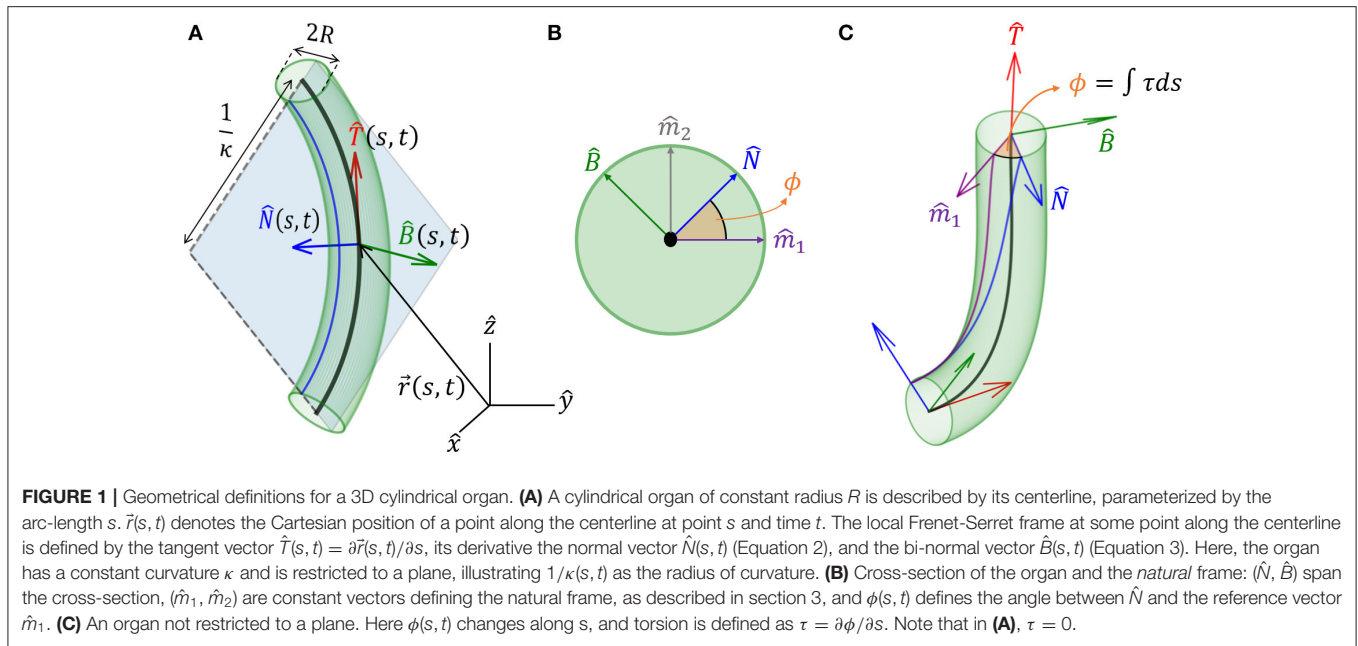


FIGURE 1 | Geometrical definitions for a 3D cylindrical organ. **(A)** A cylindrical organ of constant radius R is described by its centerline, parameterized by the arc-length s . $\vec{r}(s, t)$ denotes the Cartesian position of a point along the centerline at point s and time t . The local Frenet-Serret frame at some point along the centerline is defined by the tangent vector $\hat{T}(s, t) = \partial \vec{r}(s, t) / \partial s$, its derivative the normal vector $\hat{N}(s, t)$ (Equation 2), and the bi-normal vector $\hat{B}(s, t)$ (Equation 3). Here, the organ has a constant curvature κ and is restricted to a plane, illustrating $1/\kappa(s, t)$ as the radius of curvature. **(B)** Cross-section of the organ and the *natural* frame: (\hat{N}, \hat{B}) span the cross-section, (\hat{m}_1, \hat{m}_2) are constant vectors defining the natural frame, as described in section 3, and $\phi(s, t)$ defines the angle between \hat{N} and the reference vector \hat{m}_1 . **(C)** An organ not restricted to a plane. Here $\phi(s, t)$ changes along s , and torsion is defined as $\tau = \partial \phi / \partial s$. Note that in **(A)**, $\tau = 0$.

define the tangent vector at arc-length s as:

$$\hat{T}(s, t) = \frac{\partial}{\partial s} \vec{r}(s, t), \quad (1)$$

where \hat{T} is a unit vector, from the definition of the arc-length (Goriely, 2017). The second derivative of \vec{r} can be written as:

$$\frac{\partial^2}{\partial s^2} \vec{r}(s, t) = \frac{\partial}{\partial s} \hat{T}(s, t) = \kappa(s, t) \hat{N}(s, t), \quad (2)$$

where κ is the local curvature of the curve, and \hat{N} is the respective normal vector. We note that when $\kappa = 0$, \hat{N} is not defined, in which case we adopt a related local frame described in section 3. Since $|\frac{\partial}{\partial s} \vec{r}| = |\hat{T}| = 1$, taking the derivative of $\hat{T} \cdot \hat{T} = 1$ yields $2\hat{T} \cdot \frac{\partial \hat{T}}{\partial s} = 0$, meaning that $\hat{T} \perp \frac{\partial \hat{T}}{\partial s}$, i.e., we have $\hat{T} \perp \hat{N}$. The curvature equals the inverse of the radius of curvature, and the normal vector \hat{N} points to the center of the circle with that radius. The third unit vector in the Frenet-Serret framework is the bi-normal vector $\hat{B}(s, t)$, which creates an orthogonal basis in 3D, as illustrated in **Figure 1A**:

$$\hat{B} = \hat{T} \times \hat{N}. \quad (3)$$

For the sake of legibility, we interchangeably omit writing the explicit dependence of variables on (s, t) , i.e., when we write \hat{T} , we mean $\hat{T}(s, t)$.

The Frenet-Serret framework describes the change in this local frame of reference as a function of the arc-length s (Goriely,

2017):

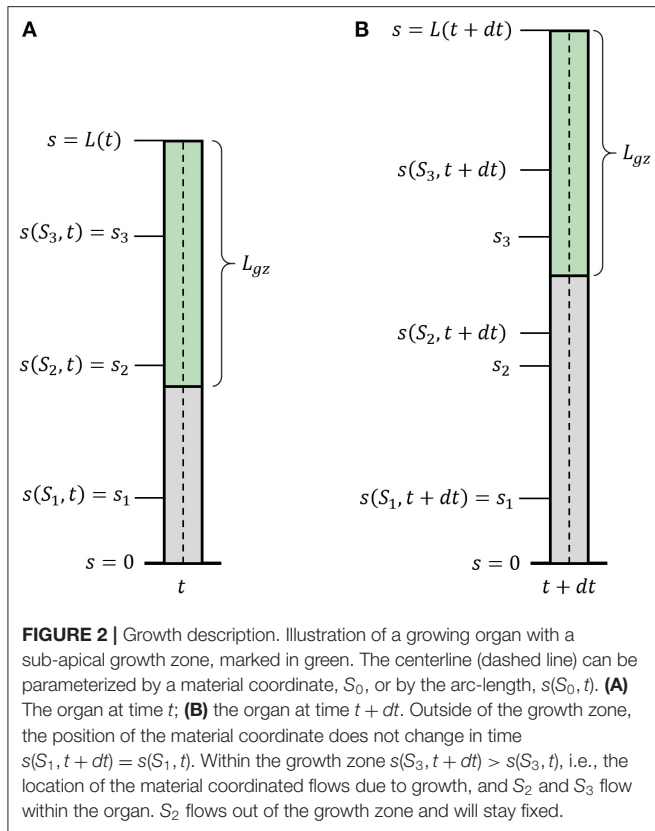
$$\begin{aligned} \frac{\partial}{\partial s} \hat{T} &= \kappa \hat{N} \\ \frac{\partial}{\partial s} \hat{N} &= -\kappa \hat{T} + \tau \hat{B} \\ \frac{\partial}{\partial s} \hat{B} &= -\tau \hat{N}, \end{aligned} \quad (4)$$

so that the local coordinate system changes accordingly along the curve. Here, $\kappa(s, t)$ is the curvature and $\tau(s, t)$ is the torsion of the centerline, describing rotations in the (\hat{N}, \hat{B}) plane leading to a non-planar centerline, as illustrated in **Figures 1B,C**. We now define ϕ , the angle between \hat{N} and arbitrarily chosen fixed direction \hat{m}_1 (Bishop, 1975; Langer and Singer, 1996; Bastien and Meroz, 2016). The change in the direction of \hat{N} along the curve yields the torsion $\tau(s, t)$ (see **Figure 1C**):

$$\tau(s, t) = \frac{\partial}{\partial s} \phi(s, t). \quad (5)$$

2.2. Modeling Growth and Differential Growth

We now introduce growth, using similar definitions to those introduced in Silk (1989), Bastien et al. (2014), and Goriely (2017). We define S_0 as the arc-length of the initial centerline of the organ, and the current arc length $s(S_0, t)$ as the evolution of the point S_0 in time, with initial conditions $s(S_0, t = 0) = S_0$. One can think of the arc-length $s(S_0, t)$ as describing the flow of the initial point S_0 due to the growth of all previous parts of the organ (see **Figure 2**). Therefore, assuming that the organ does not shrink, $s(S_0, t)$ monotonically increases over time. This growth-induced flow within the organ motivates us to use definitions from fluid dynamics, in which the parameter S_0 can be thought

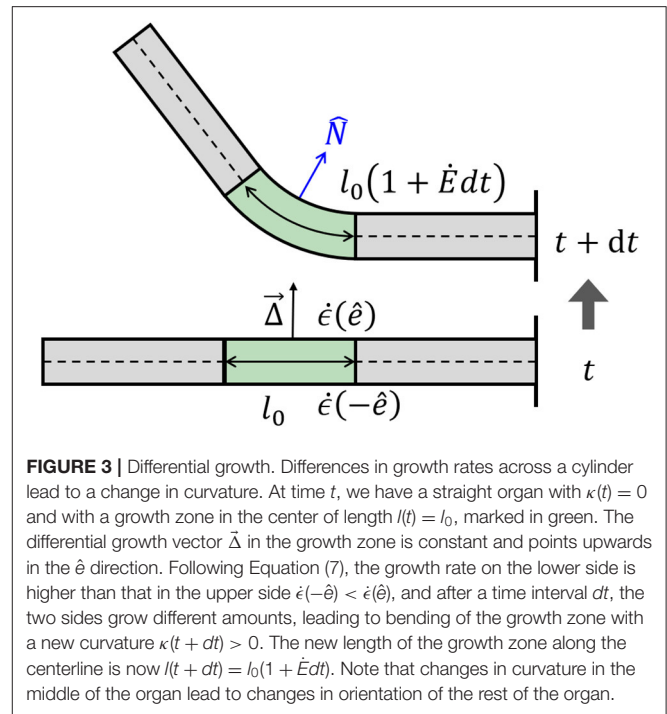


of as the Lagrangian, referential, or material coordinate and s as the Eulerian or spatial coordinate (Goriely, 2017). Using regular conventions of continuum mechanics, we define the local velocity of point s as the accumulation of the growth that occurs in previous parts of the organ:

$$\frac{ds}{dt} = v(s, t) = \int_0^s \dot{E}(u, t) du, \quad (6)$$

where $\dot{E}(s, t)$ is the local growth rate, representing a combination of the effect of the addition of new cells and their elongation. We define the length of the active growth-zone of a growing organ L_{gz} as the length over which the growth rate $\dot{E}(s, t)$ is non-zero. Without loss of generality, here we will consider the common case where growth is confined to a finite sub-apical growth-zone: $L - L_{gz} \leq s \leq L$, as shown in **Figure 2**. However, the growth zone may be defined along any other relevant section of the organ, for example when considering internodal growth. We note that as opposed to Lagrangian quantities (functions of S_0), the time derivative of Eulerian fields [functions of $s(S_0, t)$] incurs an additional convection term. We use the convention of material derivatives for the total time derivative, namely: $D/Dt \equiv \partial/\partial t + v\partial/\partial s$.

As mentioned in the Introduction, plant tropisms are the growth-driven reorientation of plant organs due to a directional stimulus, such as light, gravity, or water gradient. In particular, the reorientation of the plant organ is due to differential growth, i.e., one side of the cylindrical organ grows at a higher rate than



the other side, resulting in a curved organ. Following Bastien and Meroz (2016), we consider an infinitesimal cross-section of a cylindrical organ and define the differential growth rate in a direction \hat{e} as the difference in growth rate $\dot{\epsilon}$ on either side, normalized by their sum:

$$\Delta(\hat{e}) = \frac{\dot{\epsilon}(-\hat{e}) - \dot{\epsilon}(\hat{e})}{\dot{\epsilon}(-\hat{e}) + \dot{\epsilon}(\hat{e})}. \quad (7)$$

Following this definition, for $\Delta(\hat{e}) > 0$, the organ grows faster in direction $-\hat{e}$ and the organ bends in direction \hat{e} (see **Figure 3**). We now define the differential growth vector, which is in the direction of the active reorientation:

$$\vec{\Delta} = \Delta(\hat{N})\hat{N} + \Delta(\hat{B})\hat{B}. \quad (8)$$

In order to describe the active reorientation of an entire organ, we relate the shape of the organ and its growth dynamics, expressed by the dynamics of its local curvature, $D(\kappa\hat{N})/Dt$, to the differential growth term $\vec{\Delta}$ (Bastien and Meroz, 2016), resulting in:

$$\begin{aligned} \frac{D}{Dt}\kappa &= \frac{\dot{E}}{R}\vec{\Delta} \cdot \hat{N} \\ \kappa \frac{D}{Dt}\phi &= \frac{\dot{E}}{R}\vec{\Delta} \cdot \hat{B}, \end{aligned} \quad (9)$$

where the equations have been linearized by assuming that the radius of curvature $1/\kappa$ is always larger than the radius of the organ ($\kappa R \ll 1$). For a detailed calculation, see **Appendix A**. These equations are similar to those developed in (Bastien and Meroz, 2016), where the differential growth vector represented the

internal cues related to circumnutations. Given an expression for the differential growth vector $\vec{\Delta}(s, t)$ and an initial configuration, the dynamics can be integrated completely. The form of $\vec{\Delta}(s, t)$ is dictated by either internal cues (circumnutations) or external stimuli, as discussed in the following section.

2.3. Relating External and Internal Signals to Differential Growth

In the last section, we represented the anisotropic growth pattern by the local differential growth vector $\vec{\Delta}(s, t)$. An external signal is translated to a specific growth pattern thanks to signal-specific biosensors and biochemical signal transduction mechanisms. Here, we reduce these complex processes to a sensitivity or gain function that maps the external signal to a growth response and directly governs the differential growth vector.

Environmental signals can be mathematically described as fields. For example, vector fields describe light and gravity, while a scalar field describes the concentration of water or nutrients, and the direction of increasing concentrations is again described by a vector field of the gradients. Lastly, tensor fields may describe stress and strain; however, we will not discuss these here since our model does not include elasticity. Here we focus on vector fields, where we can write the directional stimulus in the form $\vec{I}(\vec{r}) \equiv I(\vec{r})\hat{n}(\vec{r})$, where $I(\vec{r})$ is the magnitude of the stimulus at a point \vec{r} in space, and $\hat{n}(\vec{r})$ is its direction. For example, in the case of an infinitely distant stimulus, such as light or gravity, the stimulus magnitude and direction are constant in space, i.e., $\vec{I}(\vec{r}) = I_0\hat{n}$. In the case of a chemical concentration gradient, a possible form would be $\vec{I}(\vec{r}) = \vec{\nabla}c(\vec{r})$, though the sensed magnitude may depend on other factors, such as the concentration itself and remains to be verified. The physics of the signal and the geometry of the emitting source dictate the direction of the stimulus $\hat{n}(\vec{r})$. Within a specific infinitesimal element of an organ, the differential growth vector is restricted to the cross-section, i.e., the local (\hat{N}, \hat{B}) plane. Therefore, the relevant directional information of the stimulus lies within its projection perpendicular to the organ surface, as illustrated in **Figure 4**. We define the component of the stimulus perpendicular to this surface, $\vec{I}_\perp(s, t)$, as the effective stimulus sensed by the organ. From geometrical arguments, assuming that the stimulus field changes slowly around the cross-section of the organ, the effective stimulus sensed by a cylindrical surface is given by:

$$\vec{I}_\perp = \hat{T} \times (\vec{I} \times \hat{T}) \equiv I_\perp \hat{n}_\perp, \quad (10)$$

where we have defined $\hat{n}_\perp(s, t)$ as the direction of the perpendicular component of the signal and $I_\perp(s, t)$ as its magnitude given by $I_\perp = I(\vec{r}) \sin(\theta(s, t))$, where $\theta(s, t)$ is the angle between the surface $\hat{T}(s, t)$ and the direction of the stimulus $\hat{n}(s, t)$, as shown in **Figure 4**.

Two central biophysical laws describe sensory responses to input signals, which we term here the sensitivity function $\lambda(I)$. One is a logarithmic relationship $\lambda(I) = a + b \log(I/I_0)$, referred to as the Weber-Fechner law (Norwich and Wong, 1997), and the other is a power law relationship $\lambda(I) = aI^b$, known as Stevens' law (Stevens, 1957). As an example it has been found that

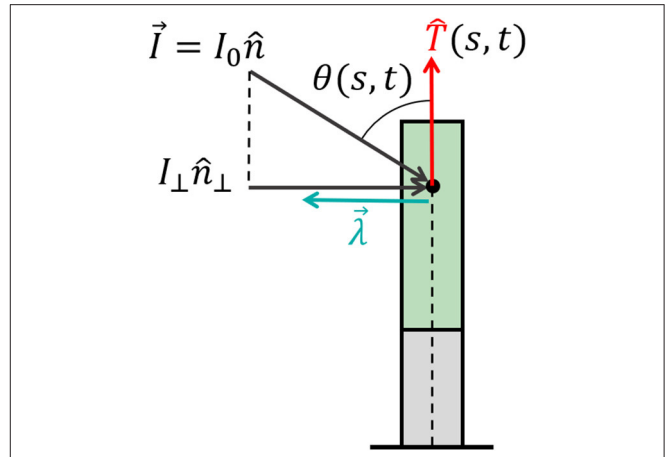


FIGURE 4 | Effective signal and response vector. An example of a signal that can be described by a constant vector field (such as sunlight and gravity) of the form $\vec{I} = I_0\hat{n}$, where I_0 is the magnitude of the stimulus and \hat{n} is its direction. For an element of an organ, the relevant directional information of the stimulus lies within its projection perpendicular to the organ surface, which we define as $\vec{I}_\perp = I_\perp\hat{n}_\perp$ (see Equation 10), where the magnitude is given by $I_\perp = I_0 \sin(\theta(s, t))$ and $\theta(s, t)$ is the angle between the surface \hat{T} and \hat{n} . Biophysical laws generally describe sensory responses to input signals as functions of the signal intensity $\lambda(I)$ (see main text). We define the response vector $\vec{\lambda}(s, t) = -\lambda(I_\perp(s, t))\hat{n}_\perp(s, t)$ where the magnitude of the perceived response is given by the sensitivity function $\lambda(I_\perp(s, t))$, and $\hat{n}_\perp(s, t)$ is the direction of the effective stimulus.

phototropism follows Stevens' Law (Bastien et al., 2015), while in the case of gravitropism, only inclination is sensed, and sensitivity is constant, $\lambda(g) = \text{const}$ (Chauvet et al., 2016). However, very little is known for other plant tropisms. We now define the local response vector:

$$\vec{\lambda}(s, t) = -\lambda(I_\perp(s, t))\hat{n}_\perp(s, t), \quad (11)$$

where the sensitivity function takes the effective stimulus sensed by the organ $\lambda(I_\perp(s, t))$, and $\hat{n}_\perp(s, t)$ is the direction of the effective stimulus. As stated before, the differential growth vector is restricted to the cross-section plane of the organ element, and it is therefore directly related to the perpendicular component of the stimulus field and its response vector, i.e., $\vec{\Delta}(s, t) = \vec{\lambda}(s, t)$.

However, it has been found that a so-called *restoring force* is required for stable posture control, termed *proprioception* (Bastien et al., 2013; Hamant and Moullia, 2016). This is related to an internal process associated with the active tendency of a growing organ to resist being bent (not a mechanical response), and is represented by $-\gamma\kappa(s, t)\hat{N}(s, t)$, where γ is the proprioceptive sensitivity (Bastien et al., 2013). We also note that differential growth may be due to internal processes, such as in the case of circumnutations. Here, an internal oscillator turns the differential growth vector in the (\hat{N}, \hat{B}) plane (Bastien and Meroz, 2016) and can be described as $\vec{\chi}(s, t) = \lambda_0 (\cos(\psi(t))\hat{m}_1(s, t) + \sin(\psi(t))\hat{m}_2(s, t))$, where λ_0 is the intensity of the bending, and $\psi(t)$ is a general function describing the direction of growth at time t relative to fixed vectors (\hat{m}_1, \hat{m}_2) (**Figure 1B**). Here, we chose a circular growth pattern; however, more elaborate forms can be

implemented (Bastien and Meroz, 2016). Assuming that the different mechanisms are additive, and adding the proprioception term and circumnutations, the differential growth vector therefore follows:

$$\vec{\Delta}(s, t) = \vec{\lambda}(s, t) + \vec{\chi}(s, t) - \gamma \kappa \hat{N}(s, t). \quad (12)$$

Together with Equation (9), Equation (12) completes our model for active growth-driven movements of rod-like organs in 3D taking into account external signals, internal cues (circumnutations), and posture control. For multiple stimuli, again assuming additivity, one can replace $\vec{\lambda}$ with the sum of specific response vectors $\sum_m \vec{\lambda}_m$ (Bastien et al., 2015). A number of specific cases, including various types of external and internal cues, are explained in further detail in section 4. A schematic summarizing the governing equations is presented in **Figure 5**.

Lastly, the distribution of sensory systems along the organ also requires attention. Sensory systems in plant organs are generally either distributed along the organ, providing local sensing (Sakamoto and Briggs, 2002; Wan et al., 2008; Hohm et al., 2013), or restricted to the tip, termed apical sensing (Darwin, 1880; Knieb et al., 2004; Holland et al., 2009; Hohm et al., 2013). For example, in the case of shoot phototropism, photoreceptors are localized at the tip alone, such as in wheat, or distributed along the whole growth zone, as in the case of Arabidopsis. In the case of gravitropism, specialized cells called statocytes sense the direction of gravity, and these are generally found throughout the growth zone for aerial organs and restricted to the tip for roots (Morita and Tasaka, 2004; Su et al., 2017). In the case of apical sensing, the local response vector $\vec{\lambda}(s, t)$ will be replaced with that of the apex $\vec{\lambda}(L, t)$ rotated to the local frame, meaning that the whole organ responds to what is sensed at the tip alone.

2.4. Comparison to Previous Models

Different models of growth-driven plant dynamics have been recently developed, encompassing different aspects of tropisms and circumnutations. Bastien et al. (2013, 2014, 2015) have developed a model for tropism in 2D, addressing the influence of growth and identifying the requirement of proprioception. A third model (Bressan et al., 2017) is based on a similar formalism, achieving stable dynamics by controlling the growth-zone and sensitivity rather than proprioception. Another model focuses on circumnutations in 3D (Bastien and Meroz, 2016), disregarding tropic responses. In what follows, we show how our model relates to these previous models while also generalizing them and unifying them.

In order to compare with 2D models, we focus on the case where the dynamics of our model are restricted to a 2D plane, which occurs when the direction of the stimulus \hat{n} is in the plane defined by \hat{T} and \hat{N} . In this case, following Equation (12), only the component in the \hat{N} direction of $\vec{\Delta}$ is not zero. Substituting this into the dynamical equations in Equation (9), since $\vec{\Delta} \cdot \hat{B} = 0$, we get that $D\phi/Dt = 0$, i.e., ϕ is constant. Assuming an initially straight organ, $\phi = 0$ throughout, yielding $\tau = \partial\phi/\partial s = 0$. The geometrical meaning is that when the stimulus and the initial state of the organ are in the same 2D plane, the dynamics of the

organ will remain within that plane and therefore restricted to 2D. In this case, we can compare the dynamics directly to Bastien et al. (2015) by projecting the model to 2D, and assuming a constant signal. We define θ the local angle of \hat{T} along the organ with respect to the direction of the constant signal \hat{n} , as illustrated in **Figure 4**, i.e., $\theta(s, t) = \arccos(\hat{T}(s, t) \cdot \hat{n})$. Taking the derivative over the arc-length s and recalling that $\partial\hat{T}/\partial s = \kappa\hat{N}$ (Equation 4) yields: $\frac{\partial}{\partial s}\theta(s, t) = \pm\kappa(s, t)$, where the sign depends on the direction of \hat{N} . Substituting these expressions into Equations (9) and (12), together with $\hat{n} \cdot \hat{N} = -\sin(\theta)$ and a constant sensitivity function $\lambda(I) = \lambda$, we get:

$$\frac{D}{Dt}\kappa(s, t) = \frac{\dot{E}}{R}(-\lambda \sin \theta(s, t) - \gamma \kappa(s, t)), \quad (13)$$

identical to the ACE model developed in Bastien et al. (2014).

We now consider Bressan et al. (2017). Their main equation of motion appears in Equation (2.8), and translating this into our terminology takes the form:

$$\frac{\partial}{\partial t}\hat{T} = \left(\int_0^s \lambda e^{-\eta(t-\sigma)} (\hat{T} \times \hat{n}) d\sigma \right) \times \hat{T}, \quad (14)$$

where $\lambda > 0$ is a constant measuring the strength of the response, similar to our tropic sensitivity, while $e^{-\eta(t-\sigma)}$ is what they call a stiffness factor. The simplest way to compare with this model is by looking at its 2D projection. Taking $\hat{T} = (\sin \theta(s, t), \cos \theta(s, t))$, where $\theta(s, t)$ is the angle between \hat{T} and \hat{n} , and substituting this in Equation (14) leads to $\frac{\partial}{\partial t}\theta(s, t) = -\int_0^s \lambda e^{-\eta(t-\sigma)} \sin \theta(\sigma, t) d\sigma$. Taking a derivative in s finally yields:

$$\frac{\partial}{\partial t}\kappa(s, t) = -\lambda e^{-\eta(t-s)} \sin \theta(s, t). \quad (15)$$

We note that this model considers accretive growth, where material is added at the tip, and elongation is disregarded. This means that growth is only taken into account implicitly as the driver of the tropic movement, and a material derivative is not required, which is a good approximation of the dynamics in certain cases (Bastien et al., 2013, 2014). In this case, the ACE model in Equation (13) converts to the AC model:

$$\frac{\partial}{\partial t}\kappa(s, t) = -\lambda \sin \theta(s, t) - \gamma \kappa(s, t). \quad (16)$$

Comparing Equations (15) and (16), we see that the equations are similar: the response, appearing on the l.h.s., is identical, and on the r.h.s., the tropic stimulus is represented by $\sin \theta(s, t)$ in both, as well as a sensitivity factor. In Bressan's model the stiffness prefactor $e^{-\eta(t-s)}$ represents a smooth growth zone with a characteristic size of $1/\eta$: in the youngest parts ($s=t$ at the tip) the stiffness factor is 1, while in older parts of the organ (as s goes to zero), the stiffness factor goes to 0. We also notice that Bressan et al. do not use a proprioceptive term, generally required for stable dynamics; however, they were able to circumvent this problem by using small growth zones.

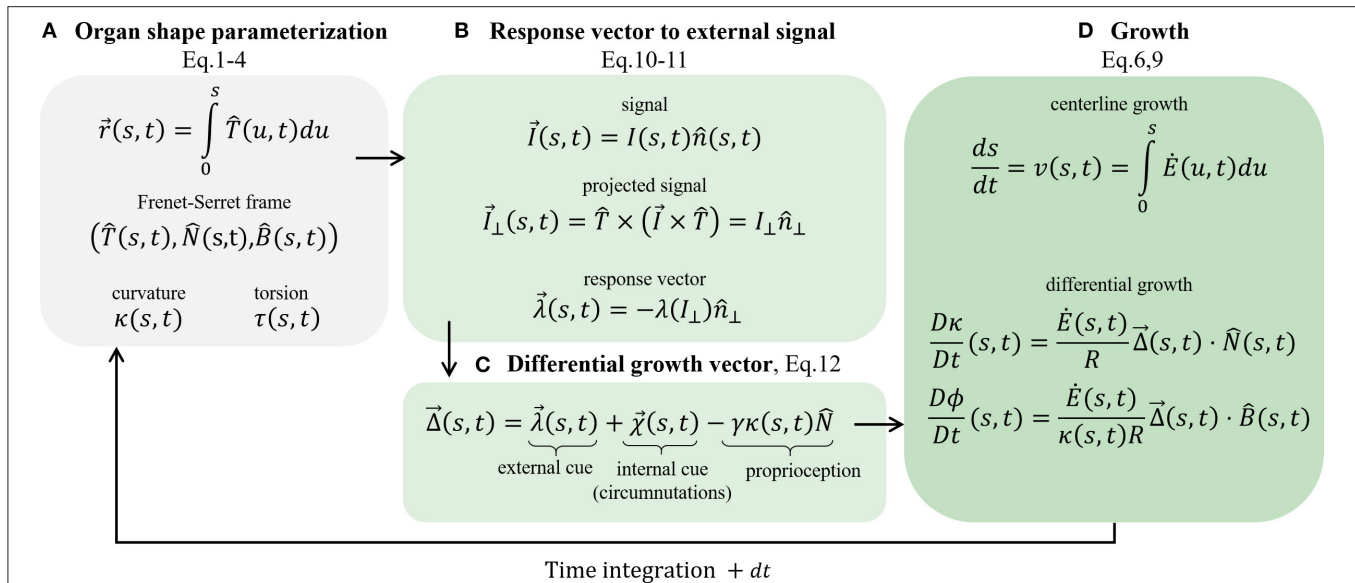


FIGURE 5 | Schematic of the governing equations. We present the main stages involved in the model. **(A)** Organ shape parametrization, section 2.1: the Frenet Serret local frame in Equations (1)–(3), and Frenet-Serret equations that also define κ and τ , introduced in Equation (4). **(B)** Response vector to external signal, section 2.3: assuming a vector field signal, we find the projected signal (Equation 10) and calculate the response vector (Equation 11), which affects the growth response. **(C)** Differential growth vector (Equation 12); includes terms representing external cues (the response vector), internal cues (circumnutations), and proprioception for posture control. **(D)** Implementing growth dynamics, section 2.2. The centerline is updated using Equations (6) and (9), using the constructed differential growth vector.

2.5. Characteristic Length and Time Scales

In section 2.4, we show that in the case where the dynamics of our model are restricted to a 2D plane, our model recovers the ACE model developed by Bastien et al. (2014). Thanks to this relation, we can adopt their dimensional analysis (Bastien et al., 2013), which identifies characteristic length and time scales. Consider the case of a constant stimulus placed perpendicular to a shoot. The length scale is identified by considering the steady state, where the shoot has grown in the direction of the stimulus, achieving a steady-state form, with $\frac{D\kappa(s, t)}{Dt} = 0$ everywhere, including the growth zone. Substituting this into Equation (13) yields the maximal curvature value κ_{\max} , and its inverse, the radius of curvature, corresponds to a characteristic length scale termed the *convergence length* $L_c = 1/\kappa_{\max} = \gamma/\lambda$, where γ and λ are the proprioceptive and tropic sensitivities, respectively. There are two time scales. One is associated with the time it takes for the organ to reach its steady state, termed the *convergence time* and defined as $T_c = R/\dot{E}\gamma$. The other is associated with the time it takes the organ to align in the direction of the stimulus for the first time, termed the *arrival time*, defined as $T_v = R/\dot{E}L_{gz}\lambda$. The ratio between the convergence length L_c and the length of the growth zone L_{gz} , as well as the ratio between the convergence time T_c and arrival time T_v , introduces a dimensionless number B , termed the *balance number* (Bastien et al., 2013; Hamant and Moullia, 2016), which describes the balance between the sensitivity to external stimuli and proprioception and is linearly related to the maximal curvature:

$$B \equiv \frac{L_{gz}}{L_c} = \frac{T_c}{T_v} = \frac{\lambda L_{gz}}{\gamma} = \kappa_{\max} L_{gz}. \quad (17)$$

Low values of B mean that $L_c > L_{gz}$, i.e., the growth zone is not big enough to contain the full arc-length associated with bending toward the stimulus with a given curvature, or alternatively that $T_v > T_c$, i.e., the organ dynamics converge before it is able to arrive to the desired orientation in the direction of the stimulus. High values of B mean that $L_c < L_{gz}$, i.e., the growth zone can contain the full bending, or alternatively that $T_v < T_c$, i.e., the organ arrives at the desired orientation before the dynamics converge, therefore also exhibiting damped oscillations. In other words, we see that the balance number B represents a relation between the final shape of the organ in steady state and the dynamics.

3. NUMERICAL METHOD

3.1. Natural Frame for the Numerical Scheme

As stated in section 2, our model for active growth-driven dynamics, described by Equations (9) and (12) and schematically illustrated in Figure 5, is formulated in the Frenet-Serret frame. The Frenet-Serret frame is a natural choice to describe curves since the second derivative gives the local curvature, $\frac{\partial^2 \vec{r}}{\partial s^2} = \kappa \hat{N}$, a natural geometrical quantity. However, within this framework, \hat{N} is not defined when $\kappa = 0$. In order to avoid related numerical issues, in the numerical scheme, we adopt a related local frame termed the “natural frame” or the “normal development” (Bishop, 1975; Langer and Singer, 1996): assuming $\vec{r}(s, t)$ is a point along the centerline of the organ, the natural frame is described by the orthonormal vectors $(\hat{T}(s, t), \hat{m}_1(s, t), \hat{m}_2(s, t))$, where $\hat{T}(s, t) = \frac{\partial}{\partial s} \vec{r}(s, t)$ is the tangent vector in Equation (1).

The other two orthogonal vectors (\hat{m}_1, \hat{m}_2) span the cross-section plane spanned by (\hat{N}, \hat{B}) in the Frenet Serret frame. The rotations of this local frame with respect to the arc length of the curve are described using the following equations, similar to the Frenet-Serret equations in (Equation 4):

$$\frac{\partial}{\partial s} \hat{T} = \kappa_1 \hat{m}_1 + \kappa_2 \hat{m}_2 \quad (18)$$

$$\frac{\partial}{\partial s} \hat{m}_1 = -\kappa_1 \hat{T} \quad (19)$$

$$\frac{\partial}{\partial s} \hat{m}_2 = -\kappa_2 \hat{T} \quad (20)$$

Here, $\kappa_1(s, t)$ and $\kappa_2(s, t)$ are the curvature components of the local cross-section plane, and the total curvature $\kappa(s, t)$ and torsion $\tau(s, t)$ are given by the relations:

$$\kappa = \sqrt{\kappa_1^2 + \kappa_2^2}, \quad (21)$$

$$\phi = \arctan\left(\frac{\kappa_2}{\kappa_1}\right), \quad (22)$$

$$\tau = \frac{\partial}{\partial s} \phi, \quad (23)$$

where ϕ is the angle between \hat{N} (in the Frenet-Serret frame) and \hat{m}_1 , illustrated in **Figure 1B**, and is used to define τ in Equation (5). This frame is closely related to the Frenet-Serret frame; however, the cross-section directions (\hat{m}_1, \hat{m}_2) are always well-defined, even when $\kappa = 0$. Within this frame, Equation (9) can be rewritten as (see **Appendix A** for a detailed calculation):

$$\frac{D}{Dt} \kappa_1 = \frac{\dot{E}}{R} \vec{\Delta} \cdot \hat{m}_1 \quad (24)$$

$$\frac{D}{Dt} \kappa_2 = \frac{\dot{E}}{R} \vec{\Delta} \cdot \hat{m}_2 \quad (25)$$

In order to solve the dynamics, we integrate Equations (24) and (25).

3.2. Discretization and Integration

The organ is divided into segments of length ds , and we rewrite functions of the centerline in a discrete form, following the general form:

$$X(s, t) \rightarrow X(n \cdot ds, m \cdot dt) \equiv X(n, m). \quad (26)$$

We describe the location of the organ using the local coordinate system:

$$\vec{r}(N, m) = \sum_{n=0}^N \hat{T}(n, m) ds. \quad (27)$$

The dynamics of the organ is described through the evolution of the local coordinate system. We rewrite Equations (18)–(20) in matrix form, which describe the change in the local frame of reference as a function of s :

$$\frac{\partial}{\partial s} D(n, m) = U(n, m) D(n, m), \quad (28)$$

where $D(n, m)$ is the rotation matrix:

$$D(n, m) = \begin{pmatrix} \hat{m}_1(n, m), \hat{m}_2(n, m), \hat{T}(n, m) \end{pmatrix}, \quad (29)$$

and $U(n, m)$ is the skew symmetric Darboux matrix:

$$U(n, m) = \begin{pmatrix} 0 & 0 & -\kappa_1(n, m) \\ 0 & 0 & -\kappa_2(n, m) \\ \kappa_1(n, m) & \kappa_2(n, m) & 0 \end{pmatrix}. \quad (30)$$

In order to integrate Equation (28) while keeping the orthonormality of the local frame, we take inspiration from Gazzola et al. (2018), relating the consecutive discrete matrices $D(n+1, m)$ and $D(n, m)$ via a rotation matrix $R(n, m)$:

$$D(n+1, m) = R(n, m) D(n, m). \quad (31)$$

Since $U(n, m)$ in Equation (28) is skew-symmetric, we use Rodrigues' rotation formula and the exponential map to express matrix $R(n, m)$:

$$R(n, m) = \exp(U(n, m) ds) \quad (32)$$

This can be interpreted as a rotation around the axis $\vec{u} = \frac{\kappa_2}{\kappa} \hat{m}_1 - \frac{\kappa_1}{\kappa} \hat{m}_2$ by an angle $\kappa(n, m) ds$ (or as the identity matrix for $\kappa(n, m) = 0$). It is therefore enough to find the evolution of U or the evolution of κ_1 and κ_2 to describe the organ in time. To integrate κ_1 and κ_2 , we discretize Equations (24) and (25), adopting the following numerical time and arc-length derivatives (where dt is the discretized time step):

$$\dot{X}(n, m) = \frac{X(n, m+1) - X(n, m)}{dt} \quad (33)$$

$$X'(n, m) = \frac{X(n, m) - X(n-1, m)}{ds}, \quad (34)$$

leading to:

$$\dot{\kappa}_1(n, m) + v(n, m) \frac{\kappa_1(n, m) - \kappa_1(n-1, m)}{ds} = \frac{\dot{E}}{R} \vec{\Delta}(n, m) \cdot \hat{m}_1(n, m) \quad (35)$$

$$\dot{\kappa}_2(n, m) + v(n, m) \frac{\kappa_2(n, m) - \kappa_2(n-1, m)}{ds} = \frac{\dot{E}}{R} \vec{\Delta}(n, m) \cdot \hat{m}_2(n, m). \quad (36)$$

The growth speed appearing in the material derivative, $v(n, m)$, is calculated following Equation (6). Assuming a growth-zone of length L_{gz} and uniform growth rate \dot{E} leads to:

$$v(n, m) = (L_{gz} - (N(m) - n) ds) \dot{E} \quad (37)$$

in the case $L_{gz} \geq (N(m) - n) ds$, and $v(n, m) = 0$ otherwise. Extracting $\dot{\kappa}_1$ and $\dot{\kappa}_2$ from Equations (35) and (36), we substitute these into Equation (33). Together with the following straight initial conditions and clamped boundary conditions of the organ, we integrate over time:

$$\begin{aligned} \kappa_1(n, m=0) &= 0, \quad \kappa_2(n, m=0) = 0 \\ \kappa_1(n=0, m) &= 0, \quad \kappa_2(n=0, m) = 0, \end{aligned} \quad (38)$$

finally resulting in $\kappa_1(n, m + 1)$ and $\kappa_2(n, m + 1)$. In order to find the proper relation between spatial and temporal discretization, we consider the equation for the velocity at the tip in Equation (37), in which case $N(m) = n$, and recalling that $\frac{ds}{dt} = v$ yields the relation:

$$ds = L_{gz} \dot{E} dt. \quad (39)$$

3.3. Implementing Growth

As discussed in section 2.2, growth is implemented via a material derivative with a local growth rate described in Equation (6), representing the elongation of cells in the growth zone, creating a one-dimensional growth flow within the organ. When cells reach a certain threshold size, they stop elongating, thus leaving the size of the growth zone L_{gz} constant. Since the total length of the organ increases over time, in the numerical scheme, we add a new segment ds at the tip at each time step:

$$N(m) = N(0) + m, \quad (40)$$

where $N(m)$ is the total number of segments in the organ at time step m , and therefore the total length is $L(m) = N(m) \cdot ds$. This is not to be confused with accretive growth, where material is added at the tip alone. Special care is required in assigning the correct curvature values to the newly added segments. At time $m - 1$, we initialize the next $N(m)$ -th segment so that $\kappa_1(N, m - 1) = 0$, $\kappa_2(N, m - 1) = 0$, $\vec{\Delta}(N, m - 1) = 0$, and $v(N, m - 1) = L_{gz} \dot{E}$ (the velocity at the tip as defined in Equation 6). Substituting these values in Equations (35) and (36) yields $\kappa_1(N, m) = \kappa_1(N - 1, m - 1)$ and $\kappa_2(N, m) = \kappa_2(N - 1, m - 1)$, i.e., the curvature of the new segment is identical to that of its predecessor.

3.4. Simulation Parameters

In the simulations presented in the next section, the initial conditions include a straight vertical organ $\kappa(s, t = 0) = 0$ [i.e., $\kappa_1(s, t = 0) = 0$ and $\kappa_2(s, t = 0) = 0$], with an initial length $L_0 = 1.0$ and a growth zone $L_{gz} = 1.0$. Boundary conditions are defined with a clamped base $\kappa(s = 0, t) = 0$ [$\kappa_1(s = 0, t) = \kappa_2(s = 0, t) = 0$]. The organ radius is $R = 0.1$, the proprioceptive coefficient is $\gamma = 0.01$, and the tropic sensitivity (when applicable) was taken to be either $\lambda_0 = 0.1$ or $\lambda_1 = 0.05$. The ratio of the proprioceptive and tropic sensitivity values substituted in Equation (17) correspond to balance numbers $B = 10$ and $B = 5$ accordingly, both of which are in the range of what has been observed in plants (Bastien et al., 2013). The maximal curvature is $\kappa_{\max} = \lambda_0/\gamma = 10$, yielding $\kappa_{\max}R = 1$. This means that $\kappa R \leq 1$ throughout the simulations, in agreement with the low curvature assumption. The simulation time step is $dt = 0.1$, and the length of the discrete elements is $ds = 0.01$. A constant growth rate was taken all along the growth zone following Equation (39): $\dot{E} = ds/dtL_{gz} = 0.1$. In the next section, we discuss simulations of specific cases. The code is freely available at <https://github.com/poratamir/3D-growth-dynamics>.

4. CASE EXAMPLES AND SIMULATIONS

Here, we discuss various representative cases of internal and external cues. Since the differential growth term is the driver of the dynamics, it is the only term that needs to be defined accordingly. We present the specific form of the differential growth vector for each case, as well as a snapshot of a numerical simulation. Videos of the full simulation dynamics can be found in the **Supplementary Material**, also showing the evolution of κ and ϕ over time. We note that in the following descriptions, the local response vectors do not necessarily reside in the local cross-section plane. However, this does not change the dynamics, in which the differential growth vector is being projected to the local cross-section plane (see Equations 9, 24, and 25).

4.1. Infinitely Distant Constant Stimulus

The simplest type of stimulus is a constant stimulus placed at infinity. In this case, the stimulus is a parallel vector field originating from direction \hat{n} and is constant in space and time, i.e., $\vec{\lambda} = \lambda_0 \hat{n}$:

$$\vec{\Delta}(s, t) = \lambda_0 \hat{n} - \gamma \kappa(s, t) \hat{N}(s, t). \quad (41)$$

The sensitivity λ_0 may depend on the intensity of the stimulus, for example, in the case of phototropism, following either the Weber Fechner or Stevens' Law, as discussed in section 2.3. This is not the case for gravitropism, since plants sense inclination rather than acceleration (Chauvet et al., 2016). A snapshot of the final form of the simulation is shown in **Figure 6A**, and an example of the full dynamics can be found in **Video 1**. Since the projection of this equation in 2D yields the ACE model (Bastien et al., 2013, 2014), we validate our model numerically, showing that our 3D simulations converge to the known analytical solution in 2D with an exponential growth profile (see **Appendix B** for details).

4.2. Point Stimulus

We consider the case of a stimulus whose source is a point located at \vec{r}_p (Bastien et al., 2019), such as a nearby localized light or water source. In this case, the stimulus leads to a radial vector field centered at the point, i.e., $\vec{\lambda} = \lambda_0 \frac{\vec{r}_p - \vec{r}(s, t)}{|\vec{r}_p - \vec{r}(s, t)|}$:

$$\vec{\Delta}(s, t) = \lambda_0 \frac{\vec{r}_p - \vec{r}(s, t)}{|\vec{r}_p - \vec{r}(s, t)|} - \gamma \kappa(s, t) \hat{N}(s, t). \quad (42)$$

Here again, λ_0 is constant in space; however, this can be generalized to depend on space, for example, in the case of a diffusive chemical where $c(|\vec{r}_p - \vec{r}(s, t)|)$. A snapshot of the dynamics is shown in **Figure 6B**, while the full dynamics can be found in **Video 2**.

4.3. General Stimulus Geometry: Twining Around a Line Stimulus

We can generalize the point stimulus to any geometrical form. Here, we show an example of a stimulus in the form of an attracting straight line. Let us assume that the line is parallel to an arbitrary direction \hat{n} whose base position in the x-y plane is

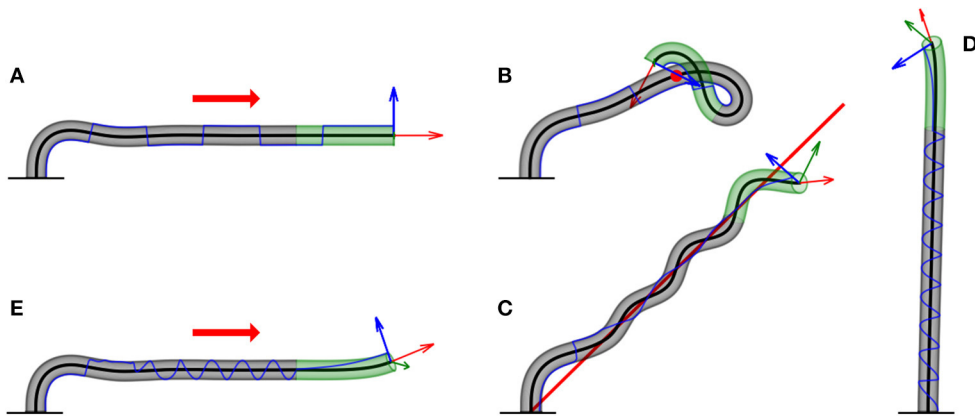


FIGURE 6 | Examples of numerical simulations for various scenarios. Here, we showcase snapshots of simulations for various cases. The subapical active growth zone is in green, while no growth occurs below that in gray. The arrows on the apex are the apical tangent direction \hat{T} (red), normal direction \hat{N} (blue), and bi-normal direction \hat{B} (green). The blue line marks the history of the direction of \hat{N} along the organ. The details of the simulations are given in section 3. We note that elasticity is not implemented here, and therefore the organ grows through itself. **(A)** Infinitely distant constant stimulus (red arrow). The organ reaches a steady state, growing in the direction of the stimulus. \hat{N} switches directions due to damped oscillations in the solution **(Video 1)**. **(B)** Point stimulus (red dot). Illustrates the different dynamics between a distant vs. nearby stimulus **(Video 2)**. **(C)** General geometry: twining around a line stimulus (red line). Any geometry for the source stimulus can be implemented. Here, we chose a line geometry, which, together with a signal in the direction of the line (to prevent self-intersections), yields dynamics similar to the twining of a climbing plant **(Video 3)**. **(D)** Circumnutations. We implement the growth response to an internal cue rather than external cues, yielding inherent periodic movements of plants called circumnutations, generally associated with search processes. The periodic trajectory of \hat{N} visualizes the rotational movement of the growing tip **(Video 4)**. **(E)** Superposition of internal and external stimuli. We combine circumnutations with an infinitely distant external stimulus **(Video 5)**.

$\vec{r}_{\text{line}} = (x_0, y_0, 0)$. The shortest vector between a point on the organ $\vec{r}(s, t)$ and the line is:

$$\vec{\rho}(s, t) = (\vec{r}(s, t) - \vec{r}_{\text{line}}) - \hat{n} ((\vec{r}(s, t) - \vec{r}_{\text{line}}) \cdot \hat{n}). \quad (43)$$

The response vector will then be $\vec{\lambda} = -\lambda_0 \hat{\rho}(s, t)$. As an example of multiple stimuli, we also add a directional stimulus parallel to the line (i.e., gravity or light), $\vec{\lambda} = \lambda_0 \hat{z} - \lambda_1 \hat{\rho}(s, t)$, leading to the following differential growth vector:

$$\vec{\Delta}(s, t) = \lambda_0 \hat{z} - \lambda_1 \hat{\rho}(s, t) - \gamma \kappa(s, t) \hat{N}(s, t), \quad (44)$$

where $\hat{\rho} = \vec{\rho}/|\vec{\rho}|$. The resulting dynamics are reminiscent of the twining motion typical of climbing plants, as shown in **Figure 6C** and **Video 3**. We note that this twining movement is not based on touch, meaning that the organ does not hold the support. Furthermore, no elasticity is involved at this stage, as further discussed in the Discussion section.

4.4. Internal Processes: Circumnutations

Circumnutations are circular periodic movements of the tips of plant organs, generally associated with search processes, for example, climbing plants searching for a support or roots searching for nutrients. Unlike tropisms, these are inherent movements due to internal drivers, not external stimuli, and can be described as $\vec{\chi}(s, t) = \lambda_0 (\cos(\psi(t)) \hat{m}_1(s, t) + \sin(\psi(t)) \hat{m}_2(s, t))$, where λ_0 is the intensity of the bending, $\psi(t)$ is a general function describing the direction of growth at time t , and we described the direction of growth using the natural frame. Here, we chose a circular form; however, more elaborate forms can be

used (Bastien and Meroz, 2016). Following Bastien and Meroz (2016), we substitute $\vec{\chi}(s, t)$ into the differential growth vector:

$$\vec{\Delta}(s, t) = \lambda_0 (\cos(\psi(t)) \hat{m}_1(s, t) + \sin(\psi(t)) \hat{m}_2(s, t)) - \gamma \kappa(s, t) \hat{N}(s, t). \quad (45)$$

In our simulations, we took $\psi(t) = \omega t$ with $\omega = 0.2/dt$. A snapshot is found in **Figure 6**, and the full dynamics can be found in **Video 4**. The trajectory of \hat{N} clearly illustrates the circular movement of the tip over time.

4.5. Superposition of Internal and External Stimuli

As already suggested in the example of a line stimulus, where a directional stimulus is added, we can consider multiple types of stimuli by assuming that they are additive. We present here another example based on plant behavior, where we consider an organ responding to a distant external signal while also exhibiting internally driven circumnutations. In this case, we simply add to Equation (45) the term for the distant stimulus in direction \hat{n} , $\lambda_0 \hat{n}$, yielding:

$$\vec{\Delta}(s, t) = \lambda_0 \hat{n} + \lambda_1 (\cos(\psi(t)) \hat{m}_1(s, t) + \sin(\psi(t)) \hat{m}_2(s, t)) - \gamma \kappa(s, t) \hat{N}(s, t) \quad (46)$$

A snapshot of the resulting dynamics is shown in **Figure 6E**, and the full dynamics are shown in **Video 5**.

5. EXAMPLE OF AN OPTIMAL CONTROL APPROACH

In this last section, we take a step back and consider a simple example illustrating the possible use of control theory to recover tropic dynamics—in a way that may be amenable for robotics use. In what follows, we no longer use the Frenet Serret formalism developed in this paper, relaxing the assumption of a constant arc-length parameterization. Instead, we consider the general case where the curve of the organ is parameterized using the Lagrangian coordinate S_0 , as described in section 2.2, without further reparameterizing the curve as it evolves over time. This general case may be pertinent to some robotics systems. We consider an organ with apical sensing, a fixed length L (neglecting an explicit account for growth, as discussed before), and dynamics restricted to 2D, similar to the case of apical sensing discussed in Bastien et al. (2013). The aim is to find a controlled evolution equation of the tangent $\hat{T}(L, t)$ at the tip, where $\hat{T} = \partial \vec{r} / \partial S_0$. Let $\vec{u}(t) = (u_1(t), u_2(t))$ be a control to orient the tangent at the tip $\hat{T}(L, t)$. The sensing occurring at the tip influences the dynamics at any other point on the organ, and therefore $\hat{T}(s, t)$ will satisfy the following Cauchy problem for any s :

$$\begin{cases} \frac{d}{dt} \hat{T}(s, t) = \int_0^s \vec{u}(t) ds' = s \vec{u}(t), \\ \hat{T}(s, 0) = \hat{T}_0(s). \end{cases} \quad (47)$$

We further limit the family of possible control strategies to those for which:

$$U = \{\vec{u} \in \mathbb{R}^2 \mid \hat{n} \cdot \vec{u} \geq 0\}, \quad (48)$$

where \hat{n} is the direction of the stimulus, since $\hat{n} \cdot \vec{u} \leq 0$ leads to undesired curling dynamics. From these strategies, we wish to choose those that are optimal in some sense. We therefore require that the optimal strategy minimizes some cost function that may manifest some physical element of the robot. Here, we choose the following:

$$W(\hat{T}, \vec{u}) = \int_0^{T_f} \left(\hat{T}(L, t) \cdot \vec{u}(t) \right)^2 dt. \quad (49)$$

In this case, the cost function has a geometric meaning: when the dot product goes to zero, together with Equation (47), we have $\hat{T}(L, t) \perp \hat{T}(L, t)$, i.e., $\|\hat{T}(L, t)\|$ is constant, thus recovering the assumption at the basis of the Frenet-Serret formalism of identical parametrization of the arc length over time. This gives a family of optimal controls:

$$\vec{u}_*(t) = u_N(t) \hat{N}(L, t), \quad (50)$$

where $\hat{N}(L, t)$ is the normal direction of the apex, and $u_N(t) \text{sign}(\hat{N}(L, t) \cdot \hat{n}) \geq 0$ to satisfy Equation (48). These solutions ensure that the tip approaches the stimulus in a strictly decreasing manner. Indeed, if the initial tangent $\hat{T}_0(L)$ is not parallel to \hat{n} , then

$$\begin{aligned} \frac{1}{2} \frac{d}{dt} \|\hat{T}(L, t) - \hat{n}\|^2 &= (\hat{T}(L, t) - \hat{n}) \cdot \frac{d}{dt} \hat{T}(L, t) = -u_N(t) \hat{N}(L, t) \\ &\cdot \hat{n} < 0 \end{aligned} \quad (51)$$

for all t , such that $\hat{T}(L, t)$ is not parallel to \hat{n} . Then, $\hat{T}(L, t)$ remains constantly parallel to \hat{n} . In particular, such a computation implies that the tangent $\hat{T}(L, t)$ does not oscillate around the stimulus direction \hat{n} . We focus our attention to a member of the control family described in Equation (50):

$$\vec{u}_*(t) = \beta \hat{T}_*^\perp(L, t) \left(\hat{n} \cdot \hat{T}_*^\perp(L, t) \right), \quad (52)$$

for all $t \in [0, T_f]$ and $\beta \geq 0$, where $\hat{T}_*^\perp = (-T_{2*}, T_{1*}) = \pm \hat{N}$ is just the vector perpendicular to $\hat{T}_* = (T_{1*}, T_{2*})$. In **Appendix C**, we show the details of the calculation based on Pontryagin's maximum principle (Aronna et al., 2017), showing that this indeed meets the requirements of the optimal control problem described in Equations (47)–(49). Substituting the specific solution described in Equation (52) into the dynamics of Equation (47) while also writing the tangent vector in terms of the angle $\theta(s, t)$ between $\hat{T}(s, t)$ and the stimulus direction \hat{n} , i.e., $\hat{T}(s, t) = (\sin \theta(s, t), \cos \theta(s, t))$, yields the following dynamical equation:

$$\frac{\partial}{\partial t} \frac{\partial}{\partial s} \theta(s, t) = -\sin \theta(L, t), \quad (53)$$

which is identical to the dynamics described in Bastien et al. (2013) in the case of apical sensing, where proprioception is not required for stability.

6. DISCUSSION AND CONCLUSION

In this work, we presented a general and rigorous mathematical framework of a rod-like growing organ whose dynamics are driven by a differential growth vector. We constructed the differential growth vector by taking into account both internal and external cues, as well as posture control, as schematically illustrated in **Figure 5**. The model adopts the 3D Frenet-Serret formalism, which is a natural choice to describe curves and is useful for robotics control purposes. In recent years, there has been an advancement in the mathematical description of plant growth-driven movements, as described in the Introduction. A careful comparison of our model to previous models finds that our model is general, consolidating different aspects in 3D for the first time: growth-driven responses to both external and internal cues, allowing stimuli with different physical and geometrical characteristics while maintaining posture control through proprioception.

We ran numerical simulations of a number of key cases. In the case of the response to external stimuli, we considered a distant stimulus (such as sunlight and gravity), a point stimulus (such as a point light source), and a rod stimulus that emulates *twining* of a climbing plant around a support. We also simulated circumnutations, the response to an internal oscillatory cue associated with search processes. Lastly, we also demonstrated the superposition of the response to an external stimulus and circumnutations. These examples showcase the broad spectrum of cases that this framework can describe and represent interactions with the environment, which are at the basis of the autonomous performance of next-generation self-growing robots in unstructured scenarios,

including movement in uncertain terrains involving obstacles and voids. The model presented here therefore establishes the basis for a control system for robots with a changing and unpredictable morphology.

While building a physical robotic representation that can behave as the model predicts is well out of the realm of current technology, the current model can be simplified so as to be relevant for current technologies, yielding limited behavior. As an example, current additive manufacturing technologies are generally limited to the addition of material at the tip, with no elongation. This accretive growth can be represented in our model by taking the growth zone to an infinitesimal size. In order to account for a robotic structure made of a number of rigid components with hinges, nodes, etc., the infinitesimal segments ds can be taken to be finite. Another example concerns the sensory system of the robot, whose characteristics can be readily represented in the model. In other words, the model is general enough to capture the essence of a variety of different robotic capabilities, which is particularly important in an era of quickly developing technologies.

Following this line of thought, we note that the framework presented here disregards parameters pertinent to robotic structures, such as energy, friction, weight, etc. In this paper, we present a simple example illustrating the possible use of optimal control theory in order to recover tropic dynamics in a way that may be relevant for robotics use. Optimal control theory optimizes processes where some cost function is minimized, and it is therefore useful in engineering problems. The example *per se* does not necessarily present a practical cost function; however, it suggests that future work may include optimizing the current model for tropic movements so as to minimize a cost function associated with a robotic parameter.

This general framework allows a deeper understanding of plant dynamics in response to their environment. Indeed, while current investigations on tropisms are generally restricted to 2D, our model enables the quantitative study of tropisms in 3D, i.e., where single or multiple stimuli are placed outside of the organ plane. Furthermore, careful attention has been paid to relating environmental stimuli to differential growth, discussing stimuli with different physical characteristics categorized by their mathematical description, such as vector fields (light and gravity), and scalar fields (concentration of water or nutrients). Indeed, the latter finally allows a rigorous characterization of plant biosensors in tropisms that are less understood, such as hydrotropism and chemotropism, as well as a currently lacking quantitative analysis of their dynamics.

Understanding plant movements is essential for a rigorous understanding of plant behavior—a field that has only recently become the focus of research. Basic behavioral processes in animals are generally studied through their motor responses to controlled stimuli, and a solid understanding of plant movements (in response to both internal and external cues) paves the way to designing controlled behavioral experiments. For example, simulations incorporating both circumnutations and tropisms will allow quantitative investigation of the role of circumnutations in the successful search for nutrients or light.

Though the framework we develop here successfully describes various scenarios of growth-driven movements of plants, it of course differs from its botanical inspiration. One main difference is that here we do not consider branching. Furthermore, as noted throughout the text, this framework does not currently include mechanics or elasticity, disregarding any elastic responses of the organ to physical forces. However, this can be naturally implemented in the Frenet-Serret frame of reference (Chelakkot and Mahadevan, 2017; Goriely, 2017; Agostinelli et al., 2020), which we plan to pursue, together with branching, in future work. On the other hand, we note that our model is general enough so that it can be customized to represent a specific biological system, e.g., by changing the growth profile of a growth zone or the geometry of the sensory system. Furthermore, note that though this framework is inspired by plant responses, it is not based on biological details and is therefore amenable to any rod-like organisms that respond to signals via growth, such as neurons and fungi.

DATA AVAILABILITY STATEMENT

The numerical code for simulations presented in this work is accessible at: <https://github.com/poratamir/3D-growth-dynamics>.

AUTHOR CONTRIBUTIONS

AP and YM developed the mathematical framework. AP carried out the numerical analysis and simulations and prepared all the figures and videos. FT, MP, and PM developed the optimal control calculation and the comparison with the model by Bressan et al. AP and YM drafted the manuscript. All authors contributed to the authoring of the final manuscript and contributed to the research design.

FUNDING

This project has received funding by the European Union's Horizon 2020 research and innovation program under grant agreement no. 824074 (GrowBot), and is partially supported by the Israel Science Foundation grant (1981/14).

ACKNOWLEDGMENTS

We thank Renaud Bastien for helpful conversations.

SUPPLEMENTARY MATERIAL

The Supplementary Material for this article can be found online at: <https://www.frontiersin.org/articles/10.3389/frobt.2020.00089/full#supplementary-material>

The supplementary material includes one pdf file and 5 videos.

Supplementary Data Sheet 1 | Includes three Appendices:

Appendix A | Derivation of growth dynamics both in the Frenet-Serret frame and the natural frame, relevant to sections 2.2 and 3.

Appendix B | Shows that our 3D simulations converge to the known analytical solution in 2D with an exponential growth profile.

Appendix C | Pontryagin's Maximum Principle, part of the calculation in the optimal control approach in section 5.

The videos show simulations for the different cases presented in section 4, and **Figure 6** shows snapshots of the simulations. The arrows represent the Frenet-Serret Frame (\hat{T} in red, \hat{N} in blue, and \hat{B} in green). The graphs show the values of the curvature $\kappa(s, t)$ and the angle $\phi(s, t)$ as a function of time:

Video 1 | Infinitely distant constant stimulus.

Video 2 | Point stimulus.

Video 3 | General stimulus geometry: twining around a line stimulus.

Video 4 | Internal processes: circumnutations.

Video 5 | Superposition of internal and external stimuli.

REFERENCES

- Agostinelli, D., Lucantonio, A., Noselli, G., and DeSimone, A. (2020). Nutations in growing plant shoots: the role of elastic deformations due to gravity loading. *J. Mech. Phys. Solids* 136:103702. doi: 10.1016/j.jmps.2019.103702
- Aronna, M. S., Tonon, D., Boccia, A., Campos, C. M., Mazzola, M., Van Nguyen, L., et al. (2017). "Optimality conditions (in pontryagin form)," in *Optimal Control: Novel Directions and Applications*, eds D. Tonon, M. Aronna, and D. Kalise (Cham: Springer), 1–125. doi: 10.1007/978-3-319-60771-9_1
- Bastien, R., Bohr, T., Moulia, B., and Douady, S. (2013). Unifying model of shoot gravitropism reveals proprioception as a central feature of posture control in plants. *Proc. Natl. Acad. Sci. U.S.A.* 110, 755–760. doi: 10.1073/pnas.1214301109
- Bastien, R., Douady, S., and Moulia, B. (2014). A unifying modeling of plant shoot gravitropism with an explicit account of the effects of growth. *Front. Plant Sci.* 5:136. doi: 10.3389/fpls.2014.00136
- Bastien, R., Douady, S., and Moulia, B. (2015). A unified model of shoot tropism in plants: photo-, gravi- and proprioception. *PLoS Comput. Biol.* 11:e1004037. doi: 10.1371/journal.pcbi.1004037
- Bastien, R., and Meroz, Y. (2016). The kinematics of plant nutation reveals a simple relation between curvature and the orientation of differential growth. *PLoS Comput. Biol.* 12:e1005238. doi: 10.1371/journal.pcbi.1005238
- Bastien, R., Porat, A., and Meroz, Y. (2019). Towards a framework for collective behavior in growth-driven systems, based on plant-inspired allotropic pairwise interactions. *Bioinspir. Biomim.* 14:055004. doi: 10.1088/1748-3190/ab30d3
- Bishop, R. L. (1975). There is more than one way to frame a curve. *Am. Math. Monthly* 82, 246–251. doi: 10.1080/00029890.1975.11993807
- Bressan, A., Palladino, M., and Shen, W. (2017). Growth models for tree stems and vines. *J. Differ. Equat.* 263, 2280–2316. doi: 10.1016/j.jde.2017.03.047
- Chauvet, H., Pouliquen, O., Forterre, Y., Legué, V., and Moulia, B. (2016). Inclination not force is sensed by plants during shoot gravitropism. *Sci. Rep.* 6:35431. doi: 10.1038/srep35431
- Chelakkot, R., and Mahadevan, L. (2017). On the growth and form of shoots. *J. R. Soc. Interface* 14:20170001. doi: 10.1098/rsif.2017.0001
- Darwin, C. (1880). *The Power of Movement in Plants*. London: John Murray Publishers.
- Del Dottore, E., Mondini, A., Sadeghi, A., Mattoli, V., and Mazzolai, B. (2016). "Circumnutations as a penetration strategy in a plant-root-inspired robot," in *2016 IEEE International Conference on Robotics and Automation (ICRA)* (Stockholm), 4722–4728. doi: 10.1109/ICRA.2016.7487673
- Forterre, Y. (2013). Slow, fast and furious: understanding the physics of plant movements. *J. Exp. Bot.* 64, 4745–4760. doi: 10.1093/jxb/ert230
- Gazzola, M., Dudte, L., McCormick, A. G., and Mahadevan, L. (2018). Forward and inverse problems in the mechanics of soft filaments. *R. Soc. Open Sci.* 5. doi: 10.1098/rsos.171628
- Gilroy, S., and Masson, P. (2007). *Plant Tropisms*. Iowa: Wiley-Blackwell.
- Goriely, A. (2017). *The Mathematics and Mechanics of Biological Growth*. New York, NY: Springer.
- Hamant, O., and Moulia, B. (2016). How do plants read their own shapes? *New Phytol.* 212, 333–337. doi: 10.1111/nph.14143
- Hart, J. W. (1990). *Plant Tropisms and Other Growth Movements*. London: Unwin Hyman.
- Hawkes, E. W., Blumenschein, L. H., Greer, J. D., and Okamura, A. M. (2017). A soft robot that navigates its environment through growth. *Sci. Robot.* 2:eaan3028. doi: 10.1126/scirobotics.aan3028
- Hohm, T., Preuten, T., and Fankhauser, C. (2013). Phototropism: translating light into directional growth. *Am. J. Bot.* 100, 47–59. doi: 10.3732/ajb.1200299
- Holland, J., Roberts, D., and Liscum, E. (2009). Understanding phototropism: from darwin to today. *J. Exp. Bot.* 60, 1969–1978. doi: 10.1093/jxb/erp113
- Jost, L., and Gibson, R. J. H. (1907). *Lectures on Plant Physiology*. Oxford: Clarendon Press.
- Kayser, M., Cai, L., Bader, C., Falcone, S., Inglessis, N., Darweesh, B., et al. (2019). "Fiberbots: design and digital fabrication of tubular structures using robot swarms," in *Robotic Fabrication in Architecture, Art and Design 2018*, eds J. Willmann, P. Block, M. Hutter, K. Byrne, and T. Schork (Cham: Springer International Publishing), 285–296. doi: 10.1007/978-3-319-92294-2_22
- Knieb, E., Salomon, M., and Rdiger, W. (2004). Tissue-specific and subcellular localization of phototropin de- terminated by immuno-blotting. *Planta* 218, 843–851. doi: 10.1007/s00425-003-1164-7
- Langer, J., and Singer, D. A. (1996). Lagrangian aspects of the kirchhoff elastic rod. *SIAM Rev.* 38, 605–618. doi: 10.1137/S0036144593253290
- Laschi, C., and Mazzolai, B. (2016). Lessons from animals and plants: the symbiosis of morphological computation and soft robotics. *IEEE Robot. Autom. Mag.* 23, 107–114. doi: 10.1109/MRA.2016.2582726
- Mazzolai, B., Mattoli, V., and Beccai, L. (2016). *Soft Plant Robotic Solutions: Biological Inspiration and Technological Challenges*, 8th Edn. Vol. 23. Cham: Springer International Publishing.
- Mehling, J. S., Diftler, M. A., Chu, M., and Valvo, M. (2006). "A minimally invasive tendril robot for in-space inspection," in *The First IEEE/RAS-EMBS International Conference on Biomedical Robotics and Biomechanics, 2006. BioRob 2006* (Pisa), 690–695. doi: 10.1109/BIOROB.2006.1639170
- Morita, M. T., and Tasaka, M. (2004). Gravity sensing and signaling. *Curr. Opin. Plant Biol.* 7, 712–718. doi: 10.1016/j.pbi.2004.09.001
- Norwich, K., and Wong, W. (1997). Unification of psychophysical phenomena: the complete form of Fechner's law. *Percept. Psychophys.* 59, 929–940. doi: 10.3758/BF03205509
- Rivière, M., Derr, J., and Douady, S. (2017). Motions of leaves and stems, from growth to potential use. *Phys. Biol.* 14:051001. doi: 10.1088/1478-3975/aa5945
- Ruhland, W. (1959). *Encyclopedia of Plant Physiology*. Vol. 17 *Physiology of Movements*. Berlin: Springer-Verlag.
- Sadeghi, A., Mondini, A., and Mazzolai, B. (2017). Toward self-growing soft robots inspired by plant roots and based on additive manufacturing technologies. *Soft Robot.* 4, 211–223. doi: 10.1089/soro.2016.0080
- Sadeghi, A., Tonazzini, A., Popova, L., and Mazzolai, B. (2014). A novel growing device inspired by plant root soil penetration behaviors. *PLoS ONE* 9:e90139. doi: 10.1371/journal.pone.0090139
- Sakamoto, K., and Briggs, W. (2002). Cellular and subcellular localization of phototropin 1. *Plant Cell* 14, 1723–1735. doi: 10.1105/tpc.003293
- Silk, W. K. (1989). Growth rate patterns which maintain a helical tissue tube. *J. Theor. Biol.* 138, 311–327. doi: 10.1016/S0022-5193(89)80197-3
- Stevens, S. (1957). On the psychophysical law. *Psychol. Rev.* 64, 153–181. doi: 10.1037/h0046162
- Su, S.-H., Gibbs, N. M., Jancewicz, A. L., and Masson, P. H. (2017). Molecular mechanisms of root gravitropism. *Curr. Biol.* 27, R964–R972. doi: 10.1016/j.cub.2017.07.015

Wan, Y., Eisinger, W., Ehrhardt, D., Kubitscheck, U., and Baluska, F. (2008). The subcellular localization and blue-light-induced movement of phototropin 1-gfp in etiolated seedlings of *arabidopsis thaliana*. *Mol. Plant* 1, 103–117. doi: 10.1093/mp/ssm011

Conflict of Interest: The authors declare that the research was conducted in the absence of any commercial or financial relationships that could be construed as a potential conflict of interest.

Copyright © 2020 Porat, Tedone, Palladino, Marcati and Meroz. This is an open-access article distributed under the terms of the Creative Commons Attribution License (CC BY). The use, distribution or reproduction in other forums is permitted, provided the original author(s) and the copyright owner(s) are credited and that the original publication in this journal is cited, in accordance with accepted academic practice. No use, distribution or reproduction is permitted which does not comply with these terms.



Searching and Intertwining: Climbing Plants and GrowBots

James Gallentine¹, Michael B. Wooten¹, Marc Thielen^{2,3,4}, Ian D. Walker^{1*}, Thomas Speck^{2,3,4,5} and Karl Niklas⁶

¹ Department of Electrical and Computer Engineering, Clemson University, Clemson, SC, United States, ² Plant Biomechanics Group and Botanic Garden, University of Freiburg, Freiburg im Breisgau, Germany, ³ FMF, Freiburg Materials Research Center, University of Freiburg, Freiburg im Breisgau, Germany, ⁴ FIT, Freiburg Center for Interactive Materials and Bioinspired Technologies (FIT), Freiburg im Breisgau, Germany, ⁵ Cluster of Excellence livMatS @ FIT – Freiburg Center for Interactive Materials and Bioinspired Technologies, University of Freiburg, Freiburg im Breisgau, Germany, ⁶ School of Integrative Plant Science, Cornell University, Ithaca, NY, United States

OPEN ACCESS

Edited by:

Rebecca Kramer-Bottiglio,
Yale University, United States

Reviewed by:

Barbara Mazzolai,
Italian Institute of Technology (IIT), Italy
Elliot Hawkes,
University of California, Santa Barbara,
United States
Jennifer Case,
National Institute of Standards and
Technology (NIST), United States

*Correspondence:

Ian D. Walker
iwalker@clemson.edu

Specialty section:

This article was submitted to
Soft Robotics,
a section of the journal
Frontiers in Robotics and AI

Received: 09 March 2020

Accepted: 28 July 2020

Published: 25 August 2020

Citation:

Gallentine J, Wooten MB, Thielen M,
Walker ID, Speck T and Niklas K
(2020) Searching and Intertwining:
Climbing Plants and GrowBots.
Front. Robot. AI 7:118.
doi: 10.3389/frobt.2020.00118

Applications in remote inspection and medicine have motivated the recent development of innovative thin, flexible-backboned robots. However, such robots often experience difficulties in maintaining their intended posture under gravitational and other external loadings. Thin-stemmed climbing plants face many of the same problems. One highly effective solution adopted by such plants features the use of tendrils and tendril-like structures, or the intertwining of several individual stems to form braid-like structures. In this paper, we present new plant-inspired robotic tendril-bearing and intertwining stem hardware and corresponding novel attachment strategies for thin continuum robots. These contributions to robotics are motivated by new insights into plant tendril and intertwining mechanics and behavior. The practical applications of the resulting GrowBots is discussed in the context of space exploration and mining operations.

Keywords: lianas, tendrils, intertwining, vines, robot, continuum, stability, grasping

INTRODUCTION

Traditionally, the structures of robotic appendages (arms, legs, fingers) have been based on interconnected rigid links, with the shape of the structures variable at only a small, finite number of locations (joints) (Siciliano and Khatib, 2016). The rigidity of the links and the ability to directly control the joint angles have enabled accuracy and repeatability that has made robots highly successful in numerous applications, notably in assembly operations within highly structured factory environments.

In recent years, however, the need to navigate within narrow, sensitive, and congested environments has motivated the development of a new class of “tongue, trunk, and tentacle” robots, collectively termed continuum robots (Walker, 2013a). Continuum robots feature continuous, compliant backbones that can change shape (bend and often extend/contract) at all locations along the structure. This feature allows them to adapt to and penetrate cluttered and tight spaces. However, regulating the shape of these robots can be challenging, given that only a finite number of actuators can be applied to control the (theoretically infinite) degrees of freedom present in the backbones.

The challenge of shape regulation is magnified in long, thin variants of continuum robots (Walker, 2013b). Although necessary to enable their envisioned applications [for example inspection within and behind equipment racks on the International Space Station (Wooten et al., 2018) and numerous medical procedures (Burgner-Kars et al., 2015)] the thin profile (lengths of a meter or more, with length to diameter ratio of 100 or more) of these structures renders them highly

susceptible to undesired and uncontrollable shape changes as a consequence of external loading (gravity, air currents, environmental contact, etc.).

Many plants experience similar challenges. To meet them, plants have evolved a variety of structures and growth strategies. In particular, numerous climbing plants grow and deploy tendrils or tendril-like structures on their very thin stems, and use these organs to reach out to and stabilize stems via connection with structures in their surrounding environments (Putz and Mooney, 1992; Bohn et al., 2015; Schnitzer et al., 2015), or they intertwine individual stems to form braid-like structures to bridge gaps between supports. This “existence of proof” in the natural world provides many insights into potential innovative robotic solutions to similar problems. Of particular relevancy to robotic applications is the fact that stems bearing tendrils and tendril-like structures and stems with the ability to intertwine have evolved multiple times in phylogenetically unrelated plant lineages, which provides circumstantial evidence for convergent adaptive evolution by means of natural selection. This convergence in the form and function of different plant grasping organs (modified stems, leaves, and even roots) manifests different anatomical and morphological solutions for constructing thin continuum robots.

Vascular plants evolved ~350 million years ago and have been subjected to intense natural selection for this period of time (Niklas, 2016). Consequently, extinct as well as living species can be viewed as evolutionary experiments that have either failed or that have passed the test of selection. Because a primary requirement for survival on land is the ability to cope with internal and external mechanical forces (i.e., self-loading and wind-induced drag forces), the shape, size, internal structure, and behavior of plants provide opportunities to transfer organic mechanical strategies to the construction of engineered artifacts, such as robots.

An important “proof of (evolutionary) concept” is convergence—when different unrelated organisms solve the same problem using similar methods. For example, plant organs such as tendrils, stems, and leaves have evolved independently in many different land plant lineages (e.g., ferns, lycophytes, eudicots, and monocots) (Niklas, 2016). Yet, in each case these organs are made of hierarchically structured composite materials (different cell- and tissue-types) that have strain incompatibilities owing to their different elastic moduli and physical anisotropy. An emergent feature of this mode of construction is the differential storage of strain energy when organs bend or twist, either as a result of self-loading or the application of external loads (wind-induced pressure forces). The stored strain energy can be used to restore the original postures of stems and tendrils when bending forces are removed. One example of this mechanical strategy is seen in hollow stems that are subdivided into smaller cylindrical compartments by transverse diaphragms at nodes, which act as spring-like joints that store strain energy when caused to buckle under bending or twisting forces. Data from resonance frequency tests have been used to calculate spring constants for stem segments and have been shown to agree with those predicted by theory provided that nodes act as spring-like joints. When diaphragms are punctured, nodal spring constants are reduced by as much as 35%.

In this paper we introduce, for the first time, continuum robot hardware (modeled after plants with very thin stems bearing tendrils) specifically equipped with searcher stem hardware designed for environmental contact. The tendril hardware is based on the activation of pre-coiled Shape Memory Alloy (SMA) materials. We demonstrate herein that such structures, when deployed as robotic stems bearing tendrils, can effectively stabilize thin continuum robots via anchoring them to themselves (braiding) and their surroundings (stabilizing). The first development of plant-inspired SMA-based robotic searcher tendril stems, focused toward climbing and grasping robots, was reported in Vidoni et al. (2013, 2015). The work in this paper is the first time, to the best of our knowledge, that continuum robotic stems have been integrated and deployed with attached searcher stems as braiding/stabilizing elements. In this way, this paper offers a completely new approach to physical robot-environment interaction.

Section Thin Continuum Robots and the Need for Environmental Attachment summarizes the state of the art in thin continuum robotics. The discussion is intended to illustrate the critical need for new ways to anchor and stabilize robots. Related structures and strategies evolved and adopted by thin-stemmed plants are discussed in section Tendrils and Intertwining Searchers in Climbing Plants. Motivated in large part by the insight gained from this understanding of plant morphology and behavior, the new robot tendril hardware, and novel strategies for novel robotic operations using it, are presented in section Innovative Attachment with Novel Robot Tendrils. Discussion and conclusions follow.

THIN CONTINUUM ROBOTS AND THE NEED FOR ENVIRONMENTAL ATTACHMENT

Inspired by the success of thin continuum robots in medical procedures (Burgner-Kars et al., 2015), and motivated by the need for remote inspection in, for example, space (Mehling et al., 2006; Wooten and Walker, 2015) and aeronautical applications (Dong et al., 2017), researchers have explored the creation of long (over a meter in length), thin (length to diameter ratios of 100 or larger) continuum robots (Mehling et al., 2006; Mazzolai et al., 2014; Tonapi et al., 2014; Wooten and Walker, 2015; Dong et al., 2017; Greer et al., 2018) that are the mechanical analogs of ultra-thin stems. When viewed as thin stem-like cantilevered beams, these efforts have been further stimulated by recent interest in creating plant-inspired robots (Sadeghi et al., 2013; Mazzolai et al., 2014; Del Dottore et al., 2018; Putzu et al., 2018). For example, when operating thin continuum robots in free space, researchers have been inspired by and therefore adopting models of the circumnutation movements observed in plants, i.e., an oscillatory rotational motion of the growing tips of plant stems that first drew the attention of Charles Darwin (Bastien and Meroz, 2016; Del Dottore et al., 2016; Wooten and Walker, 2018).

However, significant problems arise when external loadings are considered. Continuum robots, by nature of their construction and intended function, are compliant all along

their length. Consequently, long and thin continuum robots typically struggle with bearing external loads, and often even with compensating for their own weight. Such thin continuum robot designs result in an effective exploration device, but as the backbone sections become longer and more numerous, the mass of the structure greatly reduces the load-bearing capacity of the robot overall. Multiple sections, especially when using spring-loaded sections, introduce coupling between these sections, i.e., as a tendon for the tip section is pulled all sections proximal to it are also affected. Additionally, with the actuation being located at the base of the structure (necessary to produce the thin profile), when actuating unconstrained thin continuum structures, the bending energy is distributed throughout the backbone, making it difficult to achieve fine control of the distal end, or tip (the equivalent of the growing apical meristem of a real plant stem).

As an example of these issues, **Figure 1** shows a tendon-actuated thin continuum design that is the mechanical analog of a very thin plant stem (the physical details of which are given in section Novel Robotics Attachment Strategies Exploiting the New Tendril Hardware), mounted vertically pointed downwards. In **Figure 1A**, the robot stem is to the right side, with a fixed, rigid environmental feature (a metal beam) to its right. **Figure 1B** shows bending of the unconstrained robot. Notice that the entire backbone bends, restricting the motion to low curvature bends, so that the robot tip is physically incapable of accessing the marked cross target point in the environment. For applications in inspection, it may be necessary to view behind a feature such as an equipment rack without contacting the rack, risking damage to either it or the robot. **Figure 1C** demonstrates how an attachment point in the environment constrains the motion of the continuum stem, allowing a higher curvature bend closer to the distal end of the robot. This bend allows the tip of the “stem” to view the cross target without contacting an

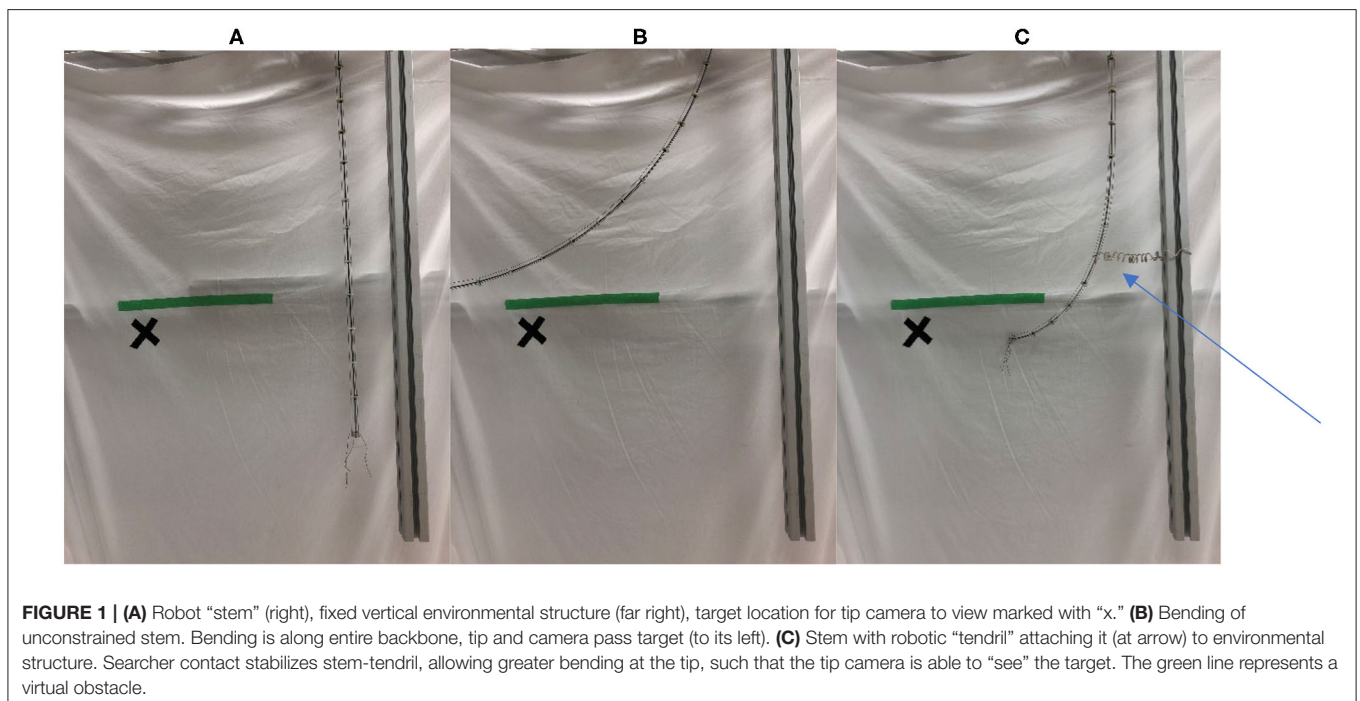
obstacle (green line). Additionally, although an unconstrained robotic continuum “stem” can only bend with fixed curvature, environmental supports allow for more compound curvatures without the addition of more actuated segments.

An initial investigation of the above problems concluded that even a primitive means of environmental attachment (passive hooks inspired by the prickles on rose stems and tendrils on grape stems) could be used to either reduce or, in some cases, negate the above issues (Wooten and Walker, 2015, 2018). However, it proved non-trivial to attach artificial hooks onto environmental features, and a more active means to connect to the environment was sought. **Figure 1C** shows the novel robotic “searcher stem,” introduced in this paper, attached by a tendril, and connecting the entire assembly to its environment, allowing the tip to access (view) the marked environmental point. Note that given the environmental anchoring provided by the tendril, the searcher “stem” is stabilized, with bending distal to the anchor point largely decoupled from the proximal part of the backbone, enabling greater bending of the tip. In creating the enabling robot “searcher” stem (introduced herein in section Innovative Attachment with Novel Robot Tendrils), inspiration has been taken from climbing plants and vines, exploiting similar characteristics in their structures and their adaptive means of active environmental attachment, as discussed in the following section.

TENDRILS AND INTERTWINING SEARCHERS IN CLIMBING PLANTS

Tendrils, Searchers, and Intertwining

Different groups of plants have adaptively converged to produce tendrils and tendril-like organs on their slender stems derived



from different plant organs (i.e., leaves, stems, and even roots) (Putz and Mooney, 1992; Niklas, 2016). Modified leaves and stems are the most frequently used to achieve lateral anchorage. Examples of leaves that have been wholly or in part transformed into tendrils are seen in the common garden pea (*Pisum sativum*), which employs several pairs of leaflets of its compound leaves to develop into cylindrical tapered tendrils (**Figure 2**), the leaves of the Yellow Vetch (*Lathyrus aphaca*), which develop into single tendrils, and the petioles of Potato Vine (*Solanum jasminoides*) and Nasturtium (*Tropaeolum*) which develop into tendrils. In contrast, the tendrils of the common Fox grape (*Vitis*) are stems; there is either a tendril or an inflorescence opposite each leaf (see **Figure 2B**).

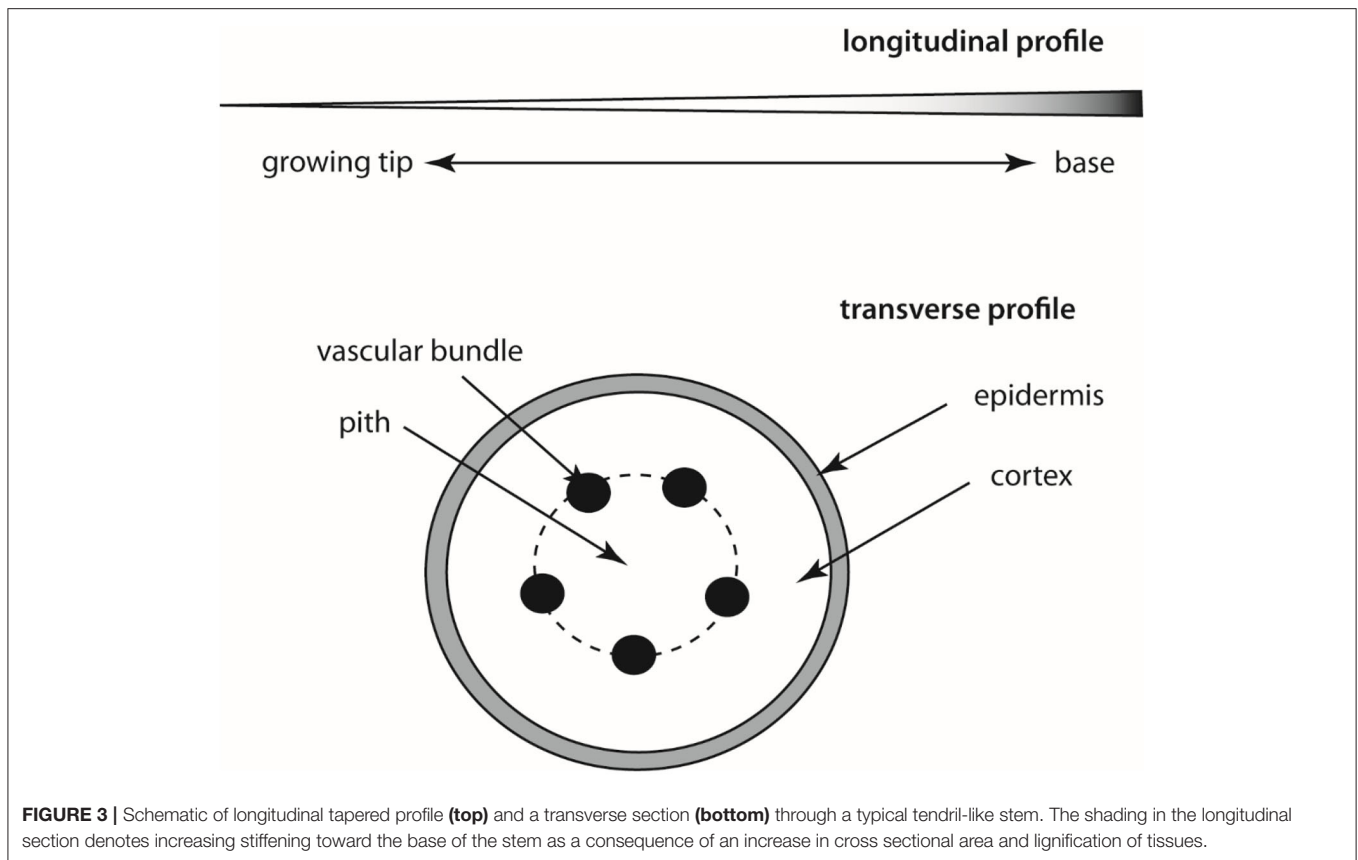
Regardless of the organ-type used to construct a tendril or tendril-like structure, commonalities in form (morphology), anatomy, and behavior are observed across phylogenetically

diverse species that may instruct the engineering and construction of slender robotics. Among these commonalities are (1) tapering in girth along the length of the structure, (2) an increase in stiffness toward the base of the structure, (3) the appearance of an incompressible “core” tissue (called the pith) around which elastic rods (vascular bundles) are distributed symmetrically which are in turn compressed by a sheath of incompressible tissue (called the cortex), that is (4) ensheathed by an elastic tissue (the epidermis) (**Figure 3**). Circumnutation, a phenomenon explored by Charles Darwin, is also typical (i.e., the successive bending in different directions of the growing tip of the stems and tendrils of many plants, especially seen in climbing plants).

Regardless of their organographic origins, tendrils serve to find a support onto which the plant can attach and grow. This requires a mechanism to “search” the local three-dimensional



FIGURE 2 | Examples of clasping plant organs. **(A)** Terminal tendrils of a pea leaf (*Pisum*). **(B)** Axillary tendril-like stems of grape (*Vitis*). **(C)** Adventitious roots of ivy (*Parthenocissus*).



space for a suitable substrate, typically with a lightweight extension sufficiently strong to support its own weight (i.e., the extension being a long antenna-like, stiff yet flexible structure). Observations of numerous climbing plant species reveal that “searcher” shoots often intertwine and provide mutual support within braided structures (Rowe and Speck, 2015). This modular construction offers mechanical advantages, such as enabling conjoined searchers to bridge larger gaps between supports than individual searcher stems could not do, and allowing individual searchers to separate from a braid, change their direction of growth, and locate different support members. Here, we investigate how such intertwined searchers can serve as role models for plant-inspired GrowBots capable of exploring three-dimensional space in which support members are randomly located.

Morphometric Characterization and Efficiency of Intertwining Shoots

Our studies show that the intertwining of searcher stems is a common phenomenon in climbing plants that increases the distance they can bridge for attaching to new host structures. Often, such “braided” structures consist of two to four intertwined searcher stems with a decreasing number of stems from base to growing tip (**Figure 4**). In these intertwined structures, regions with no or only very loose contact alternate with regions where all stems touch each other and form a

dense cluster of stems. These regularly occurring regions of close contact ensure the coherence of the intertwined structure. In order to understand and to quantify the influence the different regions of the intertwined searcher structure (with no, distant, or close contact) have on its bending stiffness, it is helpful to characterize the morphometry of these regions. For this purpose, the axial second moments of area (= moments of inertia) for various arrangements of searcher twigs differing in number and distance from each other were calculated in a simplified approach (**Figure 5**). For a single shoot, a cylindrical shape with radius r_s is assumed (**Figure 5A**). Denoting the cross-sectional area $A = \pi \cdot r_s^2$, the axial second moment of area I_{ax} is given by the equation

$$I_{ax} = I_x = I_y = 0.25 \cdot \pi \cdot r_s^4$$

In order to assess the arrangement of searching shoots in an intertwined braid, the axial second moments of area of the individual searcher stems used to construct a braid can be calculated using the Huygens–Steiner theorem, and summed for the entire system taking advantage of the additivity of axial second moments of area (Rowe and Speck, 2015; Spura, 2019). For each individual searcher stem with the radius r_{si} and cross-sectional area $A_i = \pi \cdot r_{si}^2$ arranged at a distance r_p from the centroid C of the braid structure, the axial second moments of area I_x and I_y are calculated as **Figure 5B**:

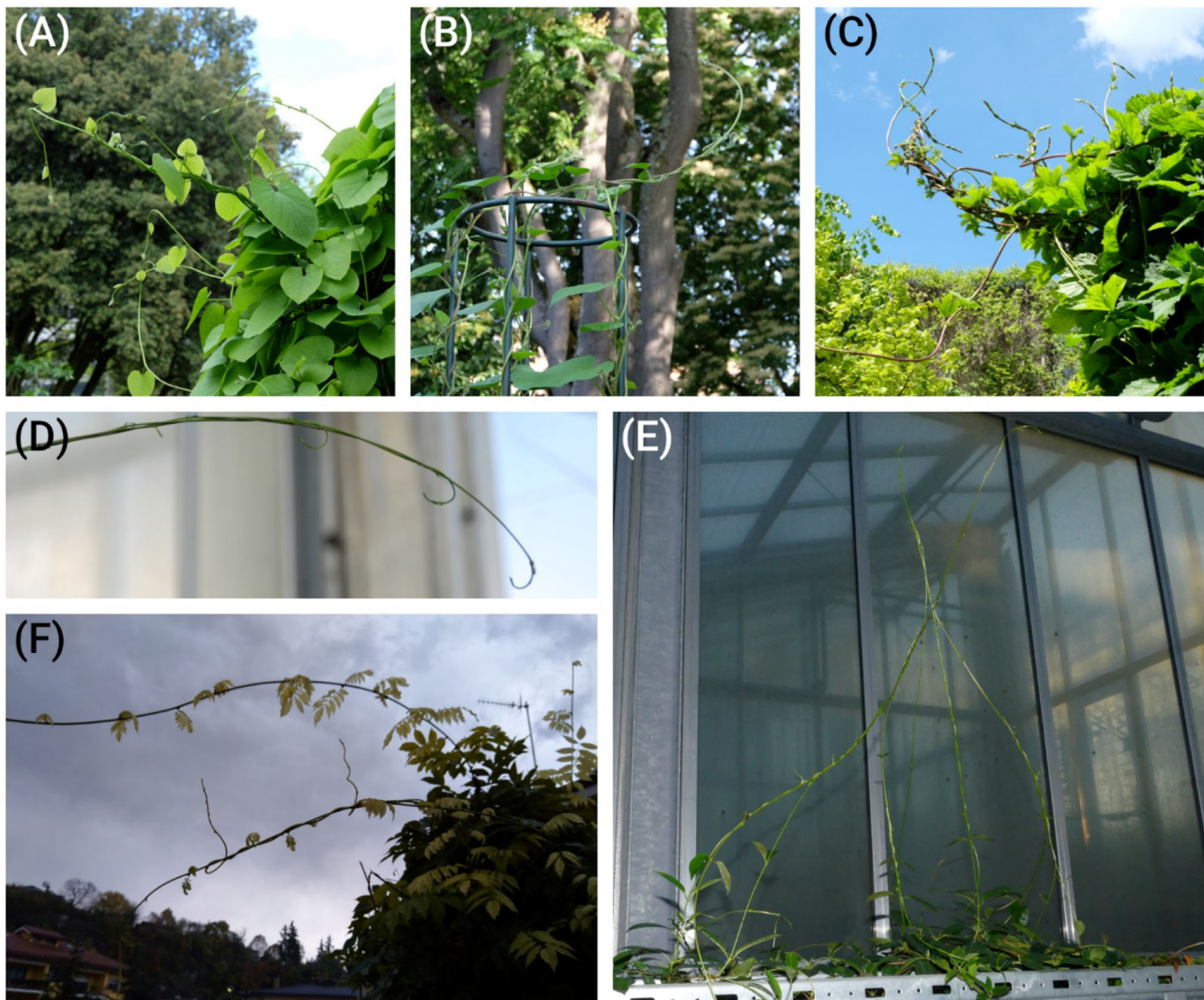


FIGURE 4 | Plants with searcher stems that are intertwining and providing mutual support. *Aristolochia macrophylla* (A), *Ipomoea tricolor* (B), *Humulus lupulus* (C), *Dipladenia* sp. (D–E), and *Wisteria* sp. (F).

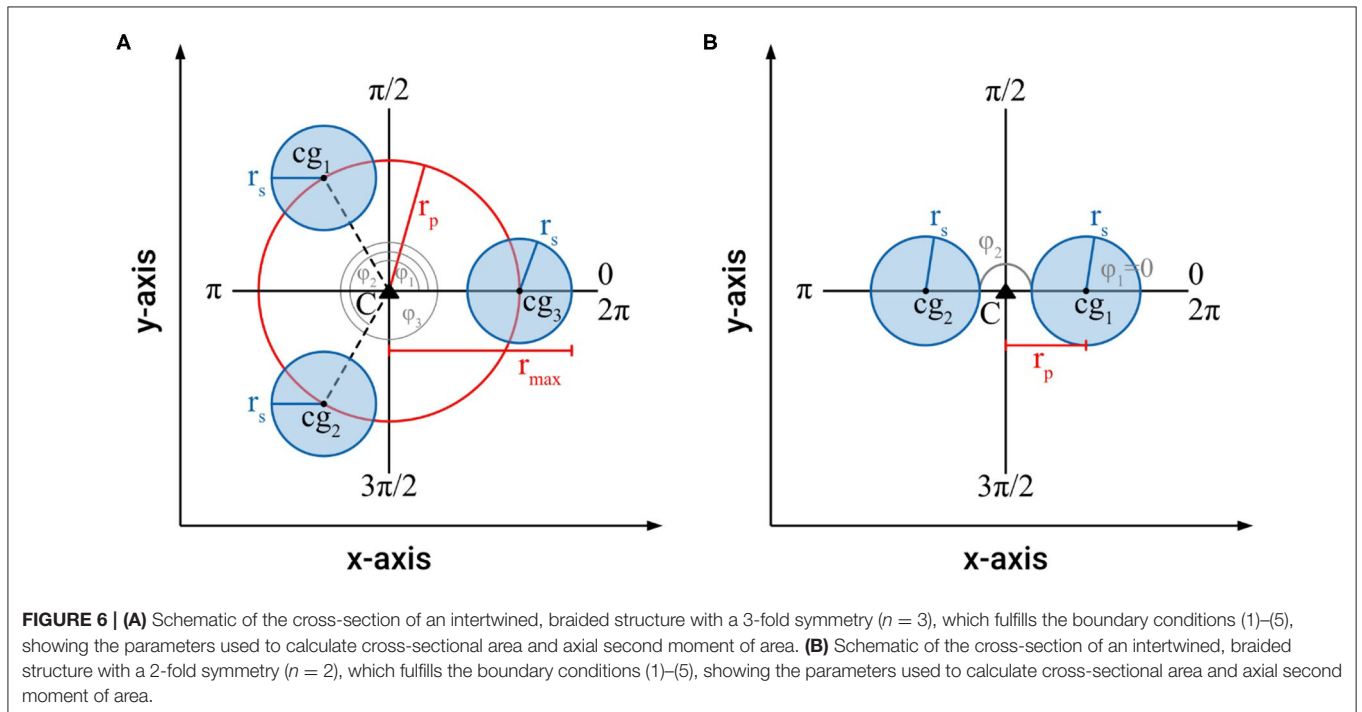
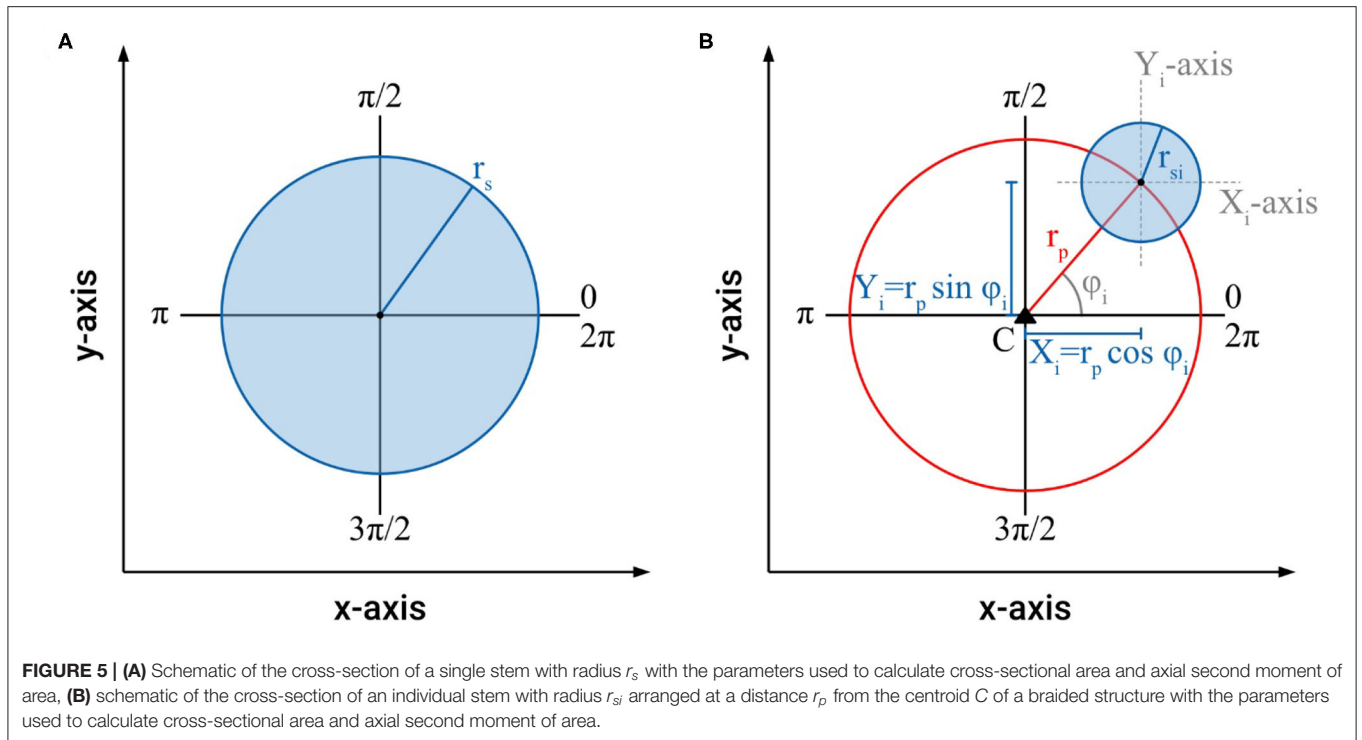
$$I_x = I_{Xi} + Y_i^2 \cdot A_i \text{ with } Y_i = r_p \sin \varphi_i \text{ and } I_{Xi} = 0.25 \cdot \pi \cdot r_{si}^4$$

$$I_y = I_{Yi} + X_i^2 \cdot A_i \text{ with } X_i = r_p \cos \varphi_i \text{ and } I_{Yi} = 0.25 \cdot \pi \cdot r_{si}^4$$

In many aspects, plant searcher braids can be compared to cables or ropes, except that they typically do not have a core around which individual “wires” are wrapped (Evans et al., 2005; Costello, 2012). Based on observations of real intertwined searcher stems, the following boundary conditions were assumed to allow for an approximated calculation of the axial second moments of area of a structure consisting of n intertwined shoots: (1) All searcher stems are cylindrical with circular cross-sections, (2) the cross-sections of individual stems are the same for all stems and remain constant over the length of an intertwined structure, i.e., the stems have no taper, and cross-sectional area is given as $A = n \cdot \pi \cdot r_s^2$ (to simplify comparability, radii are normalized to $r_{si} = r_s = 1$), (3) the centers of gravity of the n intertwined stems (cg_1 ,

cg_2 , cg_3 , cg_4) are at the same constant distance from the centroid of the intertwined structure C, i.e., they are arranged on a circle with radius r_p , and (4) intertwined stems do not overlap and are symmetrically arranged at angles $\varphi_i = 2\pi \cdot i/n$, with $i = 1, 2, 3, 4, \dots, n$, and (5) a searcher braid is treated as a unit in which individual stems are fixed with respect to each other.

For an intertwined braided structure with a 3-fold or higher symmetry, i.e., three or more individual shoots ($n \geq 3$), which fulfills the boundary conditions (1)–(5), it had been proven that, for all reference axes through the centroid of the braided structure, the axial second moments of area are constant (Figure 6A) (Burton, 1979; Speck et al., 1990), i.e., $I_{max} = I_{min} = I_{ax} = 0.5 \cdot \pi \cdot n \cdot (0.5 \cdot r_s^4 + r_s^2 \cdot r_p^2)$. This invariance does not hold for a braided structure with two individual shoots (i.e., 2-fold symmetry with $n = 2$), for which I_{max} and I_{min} differ (Figure 6B) as follows



$$\begin{aligned}
 I_{max} = I_y &= 2 \cdot (I_{Yi} + X_i^2 \cdot A_i) \quad \text{with} \quad X_i = r_p \cos \varphi_i \quad \text{and} \\
 I_{Yi} &= 0.25 \cdot \pi \cdot r_s^4 \\
 I_{min} = I_x &= 2 \cdot (I_{Xi} + Y_i^2 \cdot A_i) \quad \text{with} \quad Y_i = r_p \sin \varphi_i \quad \text{and} \\
 I_{Xi} &= 0.25 \cdot \pi \cdot r_s^4
 \end{aligned}$$

The maximum distance found for real intertwined searcher stems is typically not more than 3 times the radius of an individual stem, i.e., $r_{p,max} = 3 \cdot r_s = 3$ (for normalized $r_s = 1$).

Based on these approximations the cross-sectional areas and axial second moments of area for an individual searcher stem

with $r_s = 1$, and for two, three and four symmetrically arranged searcher stems (each with $r_s = 1$) are calculated for distances of $r_p = r_s, 1.5 r_s, 2 r_s, 2.5 r_s$, and $3 r_s$ (Figure 7). The condition $r_p = r_s$ is only possible for two searcher stems ($n = 2$). In the case of three or four searcher stems $r_p = r_s$ is impossible without violating boundary condition (4). By considering the arrangement of the centers of gravity on an equilateral triangle ($n = 3$) or a square ($n = 4$) it can be shown that in these cases the minimal radius of r_p equals $r_p = 1.155 r_s$ (for $n = 3$) and $r_p = 1.414 r_s$ (for $n = 4$), respectively.

Our results prove that intertwining is a very effective way to increase the axial second moment of area with minimal material investment. For two intertwined searcher stems, the maximal axial second moment of area increases by a factor of 6.34 from $I_{max} = 4.71$ (at $r_p = r_s$) to $I_{max} = 29.85$ (at $r_p = 3 r_s$) at constant cross-sectional area ($A = 6.28$), i.e., constant material investment. The minimal axial second moment of area, however, remains constant ($I_{min} = 1.57 = \text{const.}$) for $r_p = r_s$ to $r_p = 3 r_s$. For three intertwined searcher stems the axial second moment of area increases by a factor of 5.18 from $I_{ax} = 8.64$ (at $r_p = 1.155 r_s$) to $I_{ax} = 44.77$ (at $r_p = 3 r_s$), at constant cross-sectional area ($A = 9.42$), i.e., constant material investment. Finally, for four intertwined searcher stems, the axial second moment of area increases by a factor of 3.80 from $I_{ax} = 15.71$ (at $r_p = 1.414 r_s$) to $I_{ax} = 59.69$ (at $r_p = 3 r_s$), at constant cross-sectional area ($A = 12.57$), i.e., constant material investment. For an individual searcher stem with $r_s = 1$, typically forming the apical region of an intertwined structure, the axial second moment of area is $I_{ax} = 0.785$ with a cross-sectional area of $A = 3.14$.

These idealized calculations show that the axial second moment of area (a parameter that determines the contribution to flexural stiffness made by geometry, shape, and size) can be markedly increased by intertwining. Compared to an individual searcher, for the distance of individual stems to the centroid C of a braided structure of $r_p = 1.5 r_s$, the axial second moment of area increases by a factor of 11.0 for two stems ($n = 2$, here I_{max} is used for comparison), a factor of 16.5 for three stems ($n = 3$), and a factor of 22.0 for four intertwined stems ($n = 4$). For the largest distance to the centroid C of a braided structure with individual stems of $r_p = 3 r_s$, the axial second moment of area increases by a factor of 38.0 for two stems ($n = 2$, here I_{max} is used for comparison), a factor of 57.0 for three stems ($n = 3$), and a factor of 76.0 for four intertwined shoots ($n = 4$).

To compare the efficiency of intertwining, it is convenient to compare the amount of material an individual single stems must invest to gain the same axial second moment of area as that of intertwined stems. If the individual stems are approximated as cylinders with no taper, a comparison of the respective cross-sectional areas of the intertwined structures at different r_p with the ones of an individual stem with the same axial second moments of area can be used for comparison (Figure 8). Our calculations prove that for all considered cases, the cross-sectional area of an individual stem with the same axial second moment of area is markedly higher than the one summed up for intertwined stems. This comparison shows that intertwining represents a very efficient way to increase axial second moment of area with minimized material invest. The assumptions made

for these calculations reflect reality quite well in most cases. However, it should be noted that in boundary condition (2) (i.e., the assumption that all cross-sections are equal) is not always valid. Nevertheless, it represents a good first order approximation. Direct observations of real plants indicate that cross-sectional areas sometimes differ when several braids merge, or when a single searcher-shoot joins an existing braid (see Figure 4E). One aspect that significantly can influence bending stiffness is the way individual shoots interact. If they move against each other, bending stiffness may be considerably lower as compared to a situation in which they do not move against each other (cf. condition 5). In order to fully understand the form-structure-function relationships of the searcher braids it is therefore essential to determine and understand friction between individual shoots, which is subject of current research. It was assumed that fixed searcher-shoots in braids (cf. condition 5) represent an upper estimate of the flexural stiffness and was used here to highlight the maximum potential of intertwining.

To assess the mechanical bending properties of intertwined shoots of real leafy stems, three-point-bending tests were performed on segments of *Dipladenia* sp. braids using a universal testing machine (Instron 4466-10 kN, with a retrofit kit to inspect-DC standard, Hegewald & Peschke Mess- und Prüftechnik GmbH, Nossen, Germany). Stems were prevented from untwining during the handling of braid segments by loosely tying them together with yarn. The results show an increase in flexural stiffness from 8 Nmm² for one stem, to 76 Nmm² for two stems, to 178–533 Nmm² for three intertwined stems up to 1,650 Nmm² for four intertwined stems, corresponding to an increase in bending stiffness from one individual stem by the factors of 10, 22–67, and 206 to two, three, and four stems, respectively. The increases in stiffness observed for two and three intertwined stems agrees well with the calculated increases in the axial second moments of area, whereas the increase in the stiffness of four stems is markedly greater than that predicted by theory. This finding can be explained by the fact that, within the range of one, two and three stems, the elastic modulus does not change markedly, which can be expected for young, still growing searcher stems, whereas, in the case of four intertwining stems, lignification increases proximally (from the growing tip toward the base), resulting in a greater bulk tissue elastic modulus contributing to flexural stiffness. The efficiency gained beyond producing four intertwining stems disproportionately decreases with an increase in the number of stems, which may help to explain why the number of intertwining stems of real plants typically ranges between two and four and very rarely exceeds six.

INNOVATIVE ATTACHMENT WITH NOVEL ROBOT TENDRILS

New Robot Stem-Tendril Hardware

Motivated by the desire to produce capabilities in robots analogous to those seen and described above in plants, we considered several approaches to developing simple robotic “searcher” stems. We ultimately developed prototype hardware

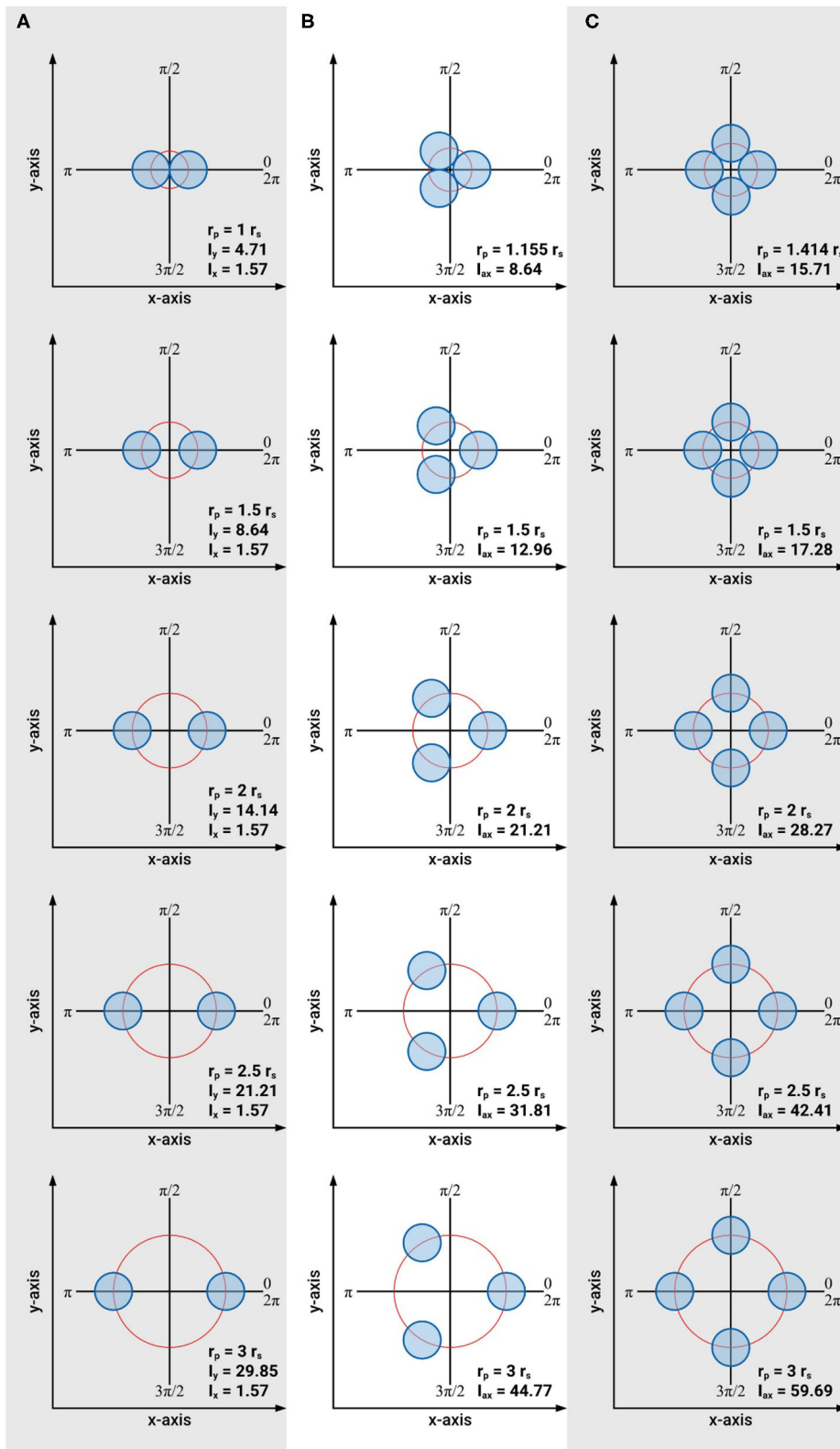
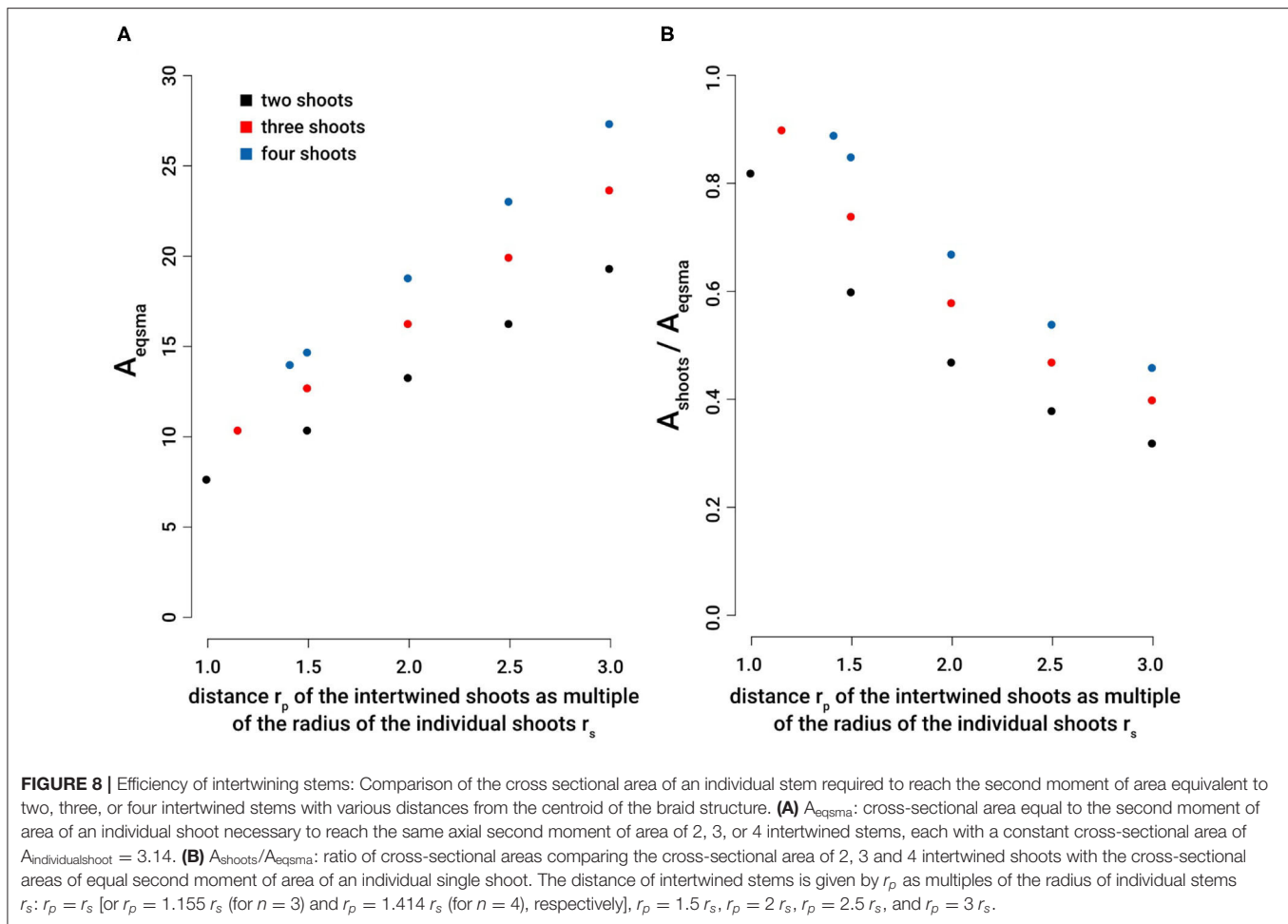


FIGURE 7 | Schematic of the arrangements of intertwined braided stems consisting of one to four individual stems used to calculate axial second moments of area and braiding efficiency. **(A)** Arrangement of two intertwined stems with $r_s = 1 = \text{const.}$ and $A = 6.28 = \text{const.}$, **(B)** arrangement of three intertwined stems with $r_s = 1 = \text{const.}$ and $A = 9.42 = \text{const.}$, **(C)** arrangement of four intertwined stems with $r_s = 1 = \text{const.}$ and $A = 12.57 = \text{const.}$



searchers based on shape-memory alloy (SMA) materials, as detailed in this section.

Numerous approaches to exploiting SMA materials in robotics have been proposed in the literature (Kheirikhari et al., 2011; Coral et al., 2012; Cianchetti, 2013). In particular, the use of SMA materials as actuators and their characterization has been reported (Russell and Gorbett, 1995; Ho and Desai, 2009; She et al., 2016). SMA materials feature the property that, when heated, they return to a pre-deformed shape. Heated SMA wire will pull to its pre-trained form (herein, a spring shape) regardless of plastic deformation at lower temperatures. This physical property offers the potential for designing programmable and repeatable behavior that can mimic behaviors observed in biological searcher stems bearing tendrils or forming intertwined braid-like structures.

Numerous SMA materials have been developed previously, and, in this work, we use nickel-titanium alloy (also referred to as NiTi or Nitinol) wires. As this SMA material is heated to 46°C, it undergoes a martensite phase transformation that causes the alloy to revert into its predetermined (“pre-trained”) shape. Training of the SMA is achieved by passing current through the alloy until it heats to a temperature around 500°C. The wire is held at this temperature briefly, while setting the desired shape.

After this process is completed and the wire cools to the ambient temperature, the wire may be arbitrarily plastically deformed. Upon heating, the wire will revert to the coiled shape in which it was trained.

Robotic searcher stems were constructed from SMA wire, being pre-trained to behave (coil into springs) similarly to the biological searchers that were their inspiration. The robotic searchers are electrically actuated. As the SMA wire conducts electricity, heat is produced which activates the searcher and causes it to move into its trained shape (Figure 9). A brief current from a 16-V, 30-watt doorbell transformer, limited by 2 amp fuses, allowed the tendril to contract fully in ~1 s.

With no current running in the searcher and the SMA at room temperature, each searcher was capable of supporting a 100-g static load hung from the actuator. Once actuated, each searcher was capable of supporting 200 g of static load.

These SMA actuators may be electrically trained into coils which mimic the shapes and behaviors of a variety of biological searchers or tendrils. This can include normal coils and shapes which mimic the reversing pitch of the robots’ biological counterparts.

To mimic behaviors seen in plant searchers and tendrils, the SMA wire was trained in a tight coil. As current is passed through

the searcher after it has been straightened, the SMA coil contracts, and attempts to wrap around any object that it encounters. When mounted on a GrowBot (see section Novel Robotics Attachment Strategies Exploiting the New Tendril Hardware), this coiling may be used to support the GrowBot as shown in **Figure 1C**,

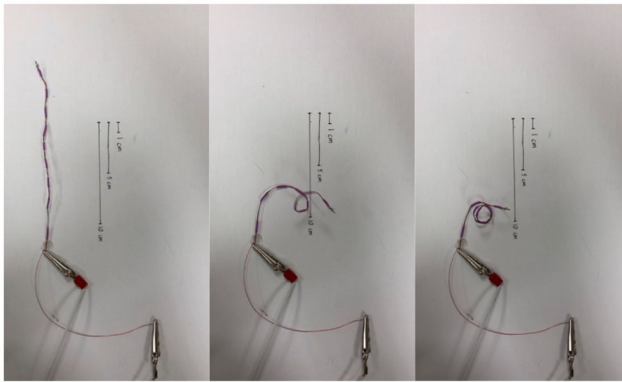


FIGURE 9 | Coiling SMA robotic searcher.

reducing the effects of external forces such as gravity and external loading on robot operation. Additionally, it can be used to form a stiffer braid-like structure on demand by intertwining several SMA wires.

Reversibility may be programmed into the SMA actuators to increase their efficacy in robotics applications, although this option was not explored in the work reported here. Preliminary results show that this could be achieved by combining a straight section of SMA with a pre-coiled elastic backbone. As the searcher is heated, the backbone would be stretched straight. Upon cooling, the elasticity of the backbone would contract the SMA into the backbone's coiled shape. This method would allow for easy construction of a variety of shapes such as the reversing pitch of the searcher's biological counterparts.

Novel Robotics Attachment Strategies Exploiting the New Tendril Hardware

The continuum GrowBot integrated with the robotic searchers of section New Robot Stem-Tendril Hardware is a thin continuum searcher stem (sometimes referred to as a tendril in the robot literature) based on concentric tubes. Its backbone consists of one to three concentric carbon fiber tubes, with the tubes of smaller

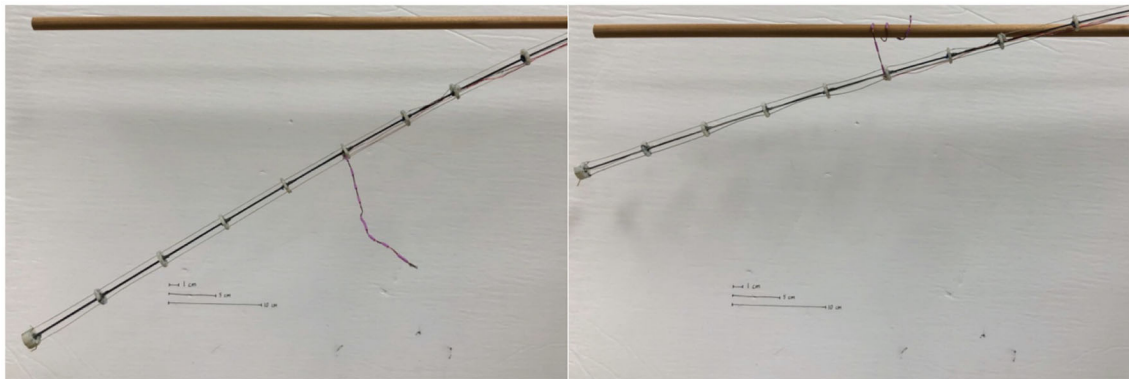


FIGURE 10 | Robot tendril grasping environment with a stabilizing searcher.

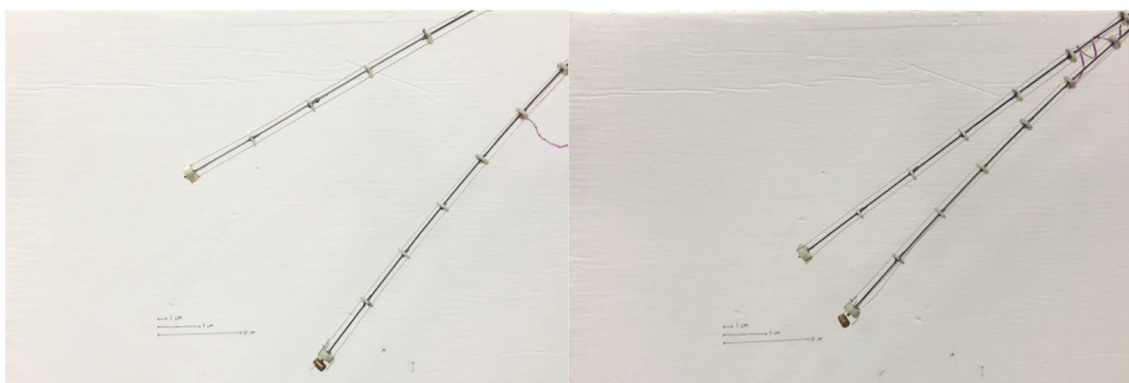


FIGURE 11 | Robot tendril using SMA searcher to braid with a parallel tendril.

radius oriented toward the distal end. Each independently actuated section has three tendons terminating at its tip. Tendons for each section are strung through 3-D printed spacers that run along the backbone. Tendons for distal tubes are strung through proximal spacers to the base.

Robotic searchers of between 7 and 9 mm in (undeformed) length were attached to the spacers of the tendril at various points along the tendril's length and teleoperation was used to anchor the tendril to either fixed supports present in the environment (**Figure 10**) or to other spatially close tendrils (**Figure 11**). Weight at the tip of the tendril caused displacement which allowed for comparison of stiffness when the tendril is braced on its environment using stabilizing searchers.

To quantify the ability of the searchers to improve the load capacity of the system, a series of experiments was conducted, varying the mass of a tip load on the system, for unconstrained and anchored cases with both rigid environmental supports and other collocated tendrils.

Figure 12 provides the displacement of the tip of a stem-tendril robot when subject to a 20-g mass at the tip of a horizontally mounted tendril as a function of the distal displacement of the searcher. The stem-tendril was stabilized using either its environment or via being braided to a second

stem-tendril which was mounted parallel to the first. In these experiments, the stem-tendril experienced displacement from tip to searcher location. The searcher was initially taut, and did not experience displacement. As the searcher was moved away from the distal portion of the stem-tendril, the stem-tendril's structure was closer to that of an unsupported stem-tendril. As the searcher approached the tip, there was an increase in overall stiffness of the stem tendril. These results are consistent with the findings from braiding with plant structures reported in section Morphometric Characterization and Efficiency of Intertwining Shoots.

Figure 13 further illustrates the potential of braiding (intertwining) between two stem-tendril robots using the robot searchers. In **Figure 13A**, the left most searcher stem is actuated, and can reach the leftmost (green) marked target. However, it is too long and cannot bend sufficiently to reach the rightmost (red) marker target. However, when braided with the searcher, and working antagonistically—left stem bending to the left, right stem bending to the right, locally greater curvature is now achievable and the left searcher stem can reach the other target (**Figure 13B**). Note that overall the left most searcher curvature in **Figure 13B** is less than in **Figure 13A**. However, the effect of the braiding allows the creation of sections of different length, and hence different curvatures (straighter and more

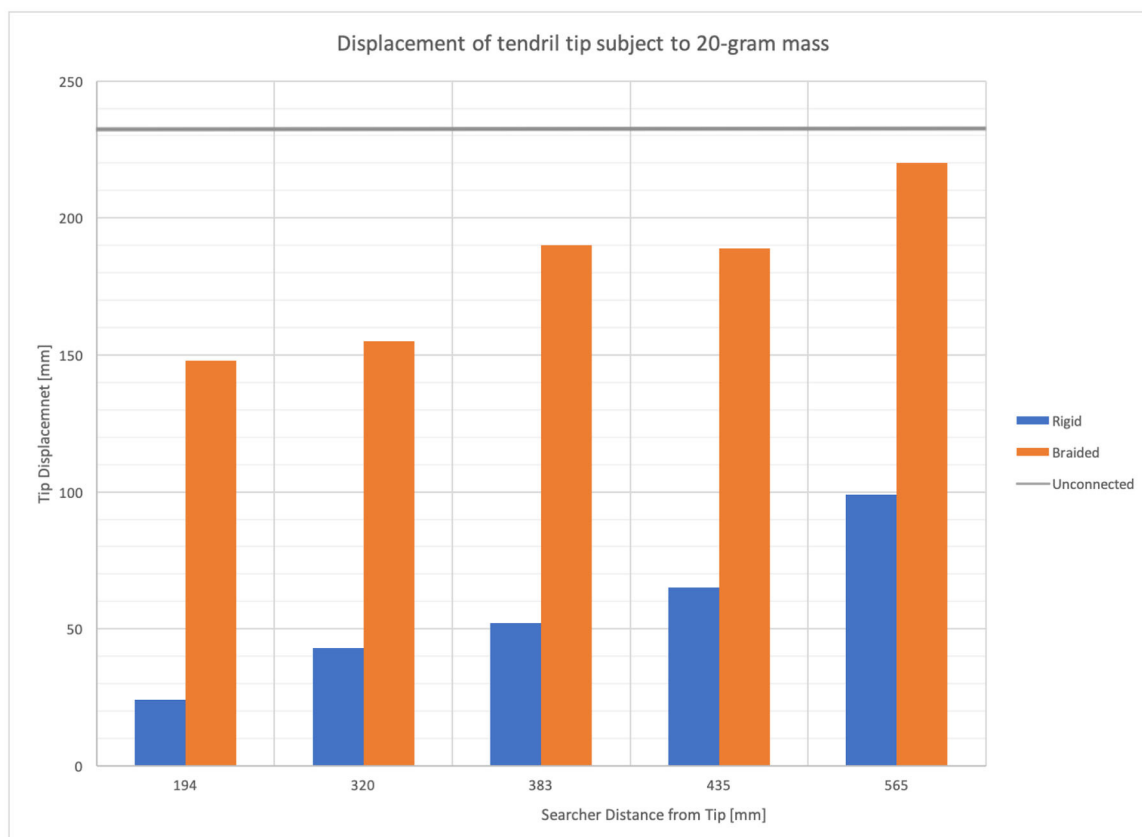


FIGURE 12 | Stem-tendril's tip displacement when subjected to a 20-g mass at the tip. Comparison of displacements in cases where a searcher stem is connected at increasing distances (left to right) from the tip, to a rigid environmental object (blue bars), and when braided to a second stem-tendril (orange bars). Displacement when unconnected shown as gray horizontal line.

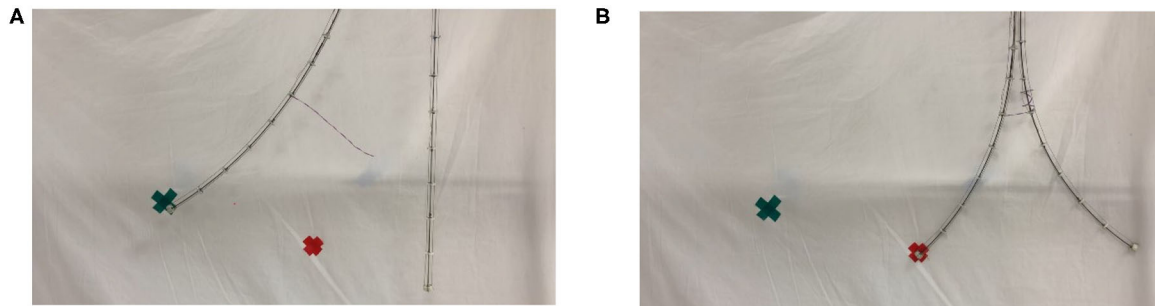


FIGURE 13 | (A) Unconstrained left searcher reached the green (left) cross marker, but not reaching the red (right) cross marker. **(B)** Braided searcher pair, using antagonistic actuation, creates a smaller bending radius, enabling the left searcher to reach the red cross marker.

curved, respectively, in **Figure 13B**), allowing the robot to reach configurations not otherwise available.

The simple experiment illustrated in **Figure 13** demonstrates the potential for searchers to provide self-stabilization in multiple intertwining structures via twining/braiding. This offers a completely new robot/robot interaction mode, in addition to the novel robot/environment interaction illustrated in **Figure 9**.

DISCUSSION AND CONCLUSIONS

This paper introduced novel plant-inspired “searcher” stem-tendrils robots, based on Shape Memory Alloy (SMA) materials. The robotic searchers were attached to and employed to stabilize robotic tendrils. This allows the proximal section of the robot (between the searcher and base) to be effectively isolated from the effects of outside forces. The remaining distal portion of the searcher is then able to act as a smaller unit, achieving tighter bending radii, finer positional control, and greater stability under load. Calculations based on intertwined plant searchers show that the interaction of individual and essentially independent subunits leads to an increase in efficiency in terms of weight, which in turn allows a higher reach of the “braided” structure. The independent appearance of vines and tendril-like organs among many different plant lineages (e.g., lycophytes, ferns, gymnosperms, and flowering plants) provides evidence for the adaptive nature of these structures and it provides inspiration for adopting these organic structures as models for future robotics.

DATA AVAILABILITY STATEMENT

The datasets generated for this study are available on request to the corresponding author.

REFERENCES

- Bastien, R., and Meroz, Y. (2016). The kinematics of plant nutation reveals a simple relation between curvature and the orientation of differential growth. *PLoS Comput. Biol.* 12:e1005238. doi: 10.1371/journal.pcbi.1005238
- Bohn, H. F., Günther, F., Fink, S., and Speck, T. (2015). A passionate free climber: structural development and functional morphology of the adhesive

AUTHOR CONTRIBUTIONS

JG: robot tendril design and hardware and experimental results with robots. MW: robot stem-searcher hardware and experimental results with robots. IW: development of robotic twining concept and robot design. TS and MT: theoretical and experimental studies on intertwining of searcher stems in climbing plants and contribution to ideas for transferring these structural features to novel plant-inspired GrowBots. KN: insight and understanding of structures and adaptations of plant tendrils and searchers. All authors: contributed to the first draft of the manuscript, improved further versions, and gave final approval for publication.

FUNDING

This work has been supported in part by the U.S. National Science Foundation under grants IIS-1527165 and IIS-1718075 and in part by NASA under contract NNX12AM01G. This project has also received funding from the European Union’s Horizon 2020 Research and Innovation Programme under Grant Agreement No. 824074. TS acknowledges additional funding by the Deutsche Forschungsgemeinschaft (DFG, German Research Foundation) under Germany’s Excellence Strategy—EXC-2193/1–390951807.

ACKNOWLEDGMENTS

The authors acknowledge Phanideep Gonthina for the origination of the concept of braiding stem-searcher robots.

tendrils in *Passiflora discophora*. *Int. J. Plant Sci.* 176, 294–305. doi: 10.1086/680231

- Burgner-Kars, J., Rucker, D. C., and Choset, H. (2015). Continuum robots for medical applications: a survey. *IEEE Trans. Robot.* 31, 1261–1280. doi: 10.1109/TRO.2015.2489500
- Burton, P. (1979). *Kinematics and Dynamics of Planar Machinery*. Upper Saddle River, NJ: Prentice Hall.

- Cianchetti, M. (2013). "Chapter 10: Fundamentals on the use of shape memory alloys in soft robotics," in *Interdisciplinary Mechatronics*, eds M. K. Habib and J. P. Davim (Wiley).
- Coral, W., Rossi, C., Colorado, J., Lemus, D., and Barrientos, A. (2012). "SMA-based muscle-like actuation in biologically inspired robots: a state of the art review," in *Smart Actuation and Sensing Systems – Recent Advances and Future Challenges* (Intech), 53–82.
- Costello, G. A. (2012). *Theory of Wire Rope*. New York, NY: Springer Science & Business Media.
- Del Dottore, E., Mondini, A., Sadeghi, A., Mattoli, V., and Mazzolai, B. (2016). "Circumnutations as a penetration strategy in a plant-root-inspired robot," in *Proceedings IEEE International Conference on Robotics and Automation* (Stockholm), 4722–4728. doi: 10.1109/ICRA.2016.7487673
- Del Dottore, E., Sadeghi, A., Mondini, A., and Mazzolai, B. (2018). "Continuous growth in plant-inspired robots through 3D additive manufacturing," in *Proceedings IEEE International Conference on Robotics and Automation* (Brisbane, QLD), 54–60. doi: 10.1109/ICRA.2018.8460616
- Dong, X., Axinte, D., Palmer, D., Cobos, S., Raffles, M., Rabani, A., et al. (2017). "Development of a slender robotic system for on-wing inspection/repair of gas turbine engines," in *Robotics and Computer-Integrated Manufacturing*.
- Evans, J. J., and Ridge I. M. L. (2005). "Rope and rope-like structures," in *Compliant Structures in Nature and Engineering*, ed C. J. M. Jenkins (Southampton: WIT Press), 133–169.
- Greer, J. D., Blumenschein, L. H., Okamura, A. M., and Hawkes, E. W. (2018). "Obstacle-aided navigation of a soft growing robot," in *Proceedings IEEE International Conference on Robotics and Automation* (Brisbane, QLD), 4165–4172. doi: 10.1109/ICRA.2018.8460777
- Ho, M., and Desai, J. P. (2009). "Characterization of SMA actuator for applications in robotic neurosurgery," in *Proceedings IEEE EMBS Conference* (Minneapolis, MN), 6856–6859.
- Khairikhar, M. M., Rabiee, S., and Edalat, M. E. (2011). "A review of shape memory alloy actuators in robotics," in *Proceedings Robot Soccer World Cup* (Berlin; Heidelberg: Springer), 206–217.
- Mazzolai, B., Beccai, L., and Mattoli, V. (2014). Plants as model in biomimetics and biorobotics: new perspectives. *Front. Bioeng. Biotechnol.* 2:2. doi: 10.3389/fbioe.2014.00002
- Mehling, J. S., Diftler, M. A., Chu, M., and Valvo, M. (2006). "A minimally invasive tendril robot for in-space inspection," in *Proceedings BioRobotics 2006 Conference* (Pisa), 690–695. doi: 10.1109/BIOROB.2006.1639170
- Niklas, K. J. (2016). *Plant Evolution: A Short Introduction to the History of Life*. Chicago: University of Chicago Press.
- Putz, F. E., and Mooney, H. A. (eds.). (1992). *The Biology of Vines*. Cambridge: Cambridge University Press.
- Putzu, F., Abrar, T., and Althoefer, K. (2018). "Plant-inspired soft pneumatic eversion robot," in *Proceedings IEEE International Conference on Biomedical Robotics and Biomechatronics* (Enschede), 1327–1332. doi: 10.1109/BIOROB.2018.8487848
- Rowe, N. P., and Speck, T. (2015). "Stem biomechanics, strength of attachment, and developmental plasticity of vines and lianas," in *The Ecology of Lianas*, eds S. Schnitzer, F. Bongers, R. Burnham, and F. E. Putz (Chichester: Wiley-Blackwell), 323–341.
- Russell, R. A., and Gorbett, R. B. (1995). "Improving the response of SMA actuators," in *Proceedings IEEE International Conference on Robotics and Automation* (Nagoya), 2299–2304. doi: 10.1109/ROBOT.1995.525604
- Sadeghi, A., Tonazzini, A., Popova, I., and Mazzolai, B. (2013). "Robotic mechanism for soil penetration inspired by plant root," in *Proceedings IEEE International Conference on Robotics and Automation* (Karlsruhe), 3457–3462. doi: 10.1109/ICRA.2013.6631060
- Schnitzer, S., Bongers, F., Burnham, R., and Putz, F. (eds.). (2015). *The Ecology of Lianas*. Chichester: Wiley-Blackwell.
- She, Y., Chen, J., Shi, H., and Su, H.-J. (2016). Modeling and validation of a novel bending actuator for soft robotics applications. *Soft Robot.* 3, 71–81. doi: 10.1089/soro.2015.0022
- Siciliano, B., and Khatib, O. (2016). *Springer Handbook of Robotics*, 2nd Edn. Berlin: Springer-Verlag.
- Speck, T., Spatz, H.-Ch., and Vogelhehner, D. (1990). Contributions to the biomechanics of plants. I. Stabilities of plant stems with strengthening elements of different cross-sections against weight and ind forces. *Botanica Acta* 103, 111–122. doi: 10.1111/j.1438-8677.1990.tb00136.x
- Spura, C. (2019). *Technische Mechanik 2. Elastostatik*. Wiesbaden: Springer Vieweg.
- Tonapi, M. M., Godage, I. S., and Walker, I. D. (2014). "Design, modeling and performance evaluation of a long and slim continuum robotic cable," in *Proceedings IEEE/RSJ International Conference on Intelligent Robots and Systems (IROS)* (Chicago, IL), 2852–2859. doi: 10.1109/IROS.2014.6942954
- Vidoni, R., Mimmo, T., and Pandolfi, C. (2015). Tendril-based climbing plants to model, simulate and create bio-inspired robotic systems. *J. Bionic Eng.* 12, 250–262. doi: 10.1016/S1672-6529(14)60117-7
- Vidoni, R., Mimmo, T., Pandolfi, C., Valentinuzzi, F., and Cesco, S. (2013). SMA bio-robotic mimesis of tendril-based climbing plants: first results," in *16th International Conference on Advanced Robotics (ICAR)* (Montevideo: IEEE), 1–6.
- Walker, I. D. (2013a). Continuous backbone "continuum" robot manipulators: a review. *ISRN Robot.* 2013, 1–19. doi: 10.5402/2013/726506
- Walker, I. D. (2013b). "Robot strings: long, thin continuum robots," in *Proceedings IEEE Aerospace Conference* (Big Sky, MT), 1–12.
- Wooten, M., and Walker, I. (2015). "A novel vine-like robot for in-orbit inspection," in *Proceedings 45th International Conference on Environmental Systems* (Bellevue, WA), 1–11.
- Wooten, M., and Walker, I. D. (2018). Vine-inspired continuum tendril robots and circumnutations. *Robotics* 7, 1–16. doi: 10.3390/robotics7030058
- Wooten, M. B., Frazelle, C. G., Walker, I. D., Kapadia, A. D., and Lee, J. H. (2018). "Exploration and inspection with vine-inspired continuum robots," in *Proceedings IEEE International Conference on Robotics and Automation (ICRA)* (Brisbane, QLD), 5526–5533.

Conflict of Interest: The authors declare that the research was conducted in the absence of any commercial or financial relationships that could be construed as a potential conflict of interest.

The reviewer BM declared a past co-authorship with the authors IW and TS to the handling Editor.

Copyright © 2020 Gallentine, Wooten, Thielen, Walker, Speck and Niklas. This is an open-access article distributed under the terms of the Creative Commons Attribution License (CC BY). The use, distribution or reproduction in other forums is permitted, provided the original author(s) and the copyright owner(s) are credited and that the original publication in this journal is cited, in accordance with accepted academic practice. No use, distribution or reproduction is permitted which does not comply with these terms.



The Bio-Engineering Approach for Plant Investigations and Growing Robots. A Mini-Review

Barbara Mazzolai^{1*}, Francesca Tramacere¹, Isabella Fiorello^{1,2} and Laura Margheri¹

¹ Center for Micro-BioRobotics, Istituto Italiano di Tecnologia, Pontedera, Italy, ² The BioRobotics Institute, Scuola Superiore Sant'Anna, Pisa, Italy

OPEN ACCESS

Edited by:

Antonio DeSimone,
Sant'Anna School of Advanced
Studies, Italy

Reviewed by:

Heiko Hamann,
University of Lübeck, Germany
Donato Romano,
Institute of BioRobotics, Italy

*Correspondence:

Barbara Mazzolai
barbara.mazzolai@iit.it

Specialty section:

This article was submitted to
Soft Robotics,
a section of the journal
Frontiers in Robotics and AI

Received: 15 June 2020

Accepted: 18 August 2020

Published: 24 September 2020

Citation:

Mazzolai B, Tramacere F, Fiorello I and
Margheri L (2020) The Bio-Engineering
Approach for Plant Investigations and
Growing Robots. A Mini-Review.
Front. Robot. AI 7:573014.
doi: 10.3389/frobt.2020.573014

It has been 10 years since the publication of the first article looking at plants as a biomechatronic system and as model for robotics. Now, roboticists have started to look at plants differently and consider them as a model in the field of bioinspired robotics. Despite plants have been seen traditionally as passive entities, in reality they are able to grow, move, sense, and communicate. These features make plants an exceptional example of morphological computation - with probably the highest level of adaptability among all living beings. They are a unique model to design robots that can act in- and adapt to- unstructured, extreme, and dynamically changing environments exposed to sudden or long-term events. Although plant-inspired robotics is still a relatively new field, it has triggered the concept of growing robotics: an emerging area in which systems are designed to create their own body, adapt their morphology, and explore different environments. There is a reciprocal interest between biology and robotics: plants represent an excellent source of inspiration for achieving new robotic abilities, and engineering tools can be used to reveal new biological information. This way, a bidirectional biology-robotics strategy provides mutual benefits for both disciplines. This mini-review offers a brief overview of the fundamental aspects related to a *bioengineering approach in plant-inspired robotics*. It analyses the works in which both biological and engineering aspects have been investigated, and highlights the key elements of plants that have been milestones in the pioneering field of growing robots.

Keywords: bioinspired robotics, soft robotics, growing robots, plants biology, smart materials, bioengineering

1. INTRODUCTION

How we see plants has changed significantly, as has the importance of protecting them for the benefit of the entire terrestrial ecosystem (Baluška and Mancuso, 2020). From an ecological role and evolutionary path, plants are producers in the food net of an ecosystem. They are photoautotroph organisms, so able to self-produce organic compounds by using mineral substances through photosynthesis. By exploiting substances directly from air and soil, they “do not need traditional locomotion,” but they evolved a number of singular strategies to interact with the environment, including complex movements, sensing, growing and propagation. New technologies, such as time-lapse recording, have demonstrated such abilities both above and below ground (Vincent et al., 2011; Silverberg et al., 2012; Vlad et al., 2014; Poppinga et al., 2015; Guerra et al., 2019; Rambaud-Lavigne and Hay, 2020).

Also robotics has contributed to this change in perspective by starting to mimic plants at both components and system level (Mazzolai et al., 2010, 2011; Sadeghi et al., 2014, 2020; Hawkes et al., 2017; Nahar et al., 2017; Wooten and Walker, 2018; Must et al., 2019; Bolt et al., 2020; Geer et al., 2020).

This mini-review focuses on the vision of “science for robotics and robotics for science,” to highlight the results of a bioengineering approach in simultaneously driving innovative technological design and obtaining new biological insights.

2. FROM PLANTS TO ROBOTS

Plants are sessile organisms, and this means that they spend their entire lives at the site of seed germination. They have thus evolved a high level of plasticity enabling them to thrive, adapt and respond to changing conditions and survive under stress (Karban, 2008). Due to their exceptional adaptability, plants are the first living beings to colonize hostile environments, and have the unique capability to live contemporary in two different environments (e.g., soil and air, or water and air; Niklas and Spatz, 2012). These behaviors are linked to a complex and dynamic interaction between their morphology, distributed sensory-motor control, and the environment, which in turn represent the basic principles of what is called “morphological computation” (Laschi and Mazzolai, 2016): a modern perspective on intelligence in which the physical body has a primary role (Paul, 2006; Pfeifer and Bongard, 2007) and the behavior depends strongly on the mechanical properties, the form/morphology, and the arrangement of the perceptual, motor and “processing units” (Zambrano et al., 2014).

Plants are thus the perfect candidates to be a model to deal with a key challenge in robotics: the capacity to function in unstructured environments. This skill requires heightened abilities of perception, efficient use of energy resources, and high adaptability to dynamic environments and changing situations. Plants offer several ideas for designing innovative technologies, such as: (1) indeterminate growing capabilities; (2) movements without muscles; (3) structural materials with morphological adaptability and variable stiffness; (4) distributed intelligence and sensory systems; (5) anchoring/attachment strategies; (6) intra-system and inter-system communication; and (7) energy-saving mechanisms. Belowground, plants represent the best example among living beings for efficient soil non-destructive and capillary exploration. They have a network of growing and branching roots, whose tips are highly sensorized and efficiently move the soil volume and search for nutrients. Aboveground, plants are a unique model for the design of low-mass low-volume robots capable of anchoring themselves, negotiating voids, and climb where current climbing robots based on wheels, legs, or rails would get stuck or fall.

Table 1 reports the biological features, measurements and characterization methods, biological specifications, and plant-inspired robotic solutions discussed throughout the following sections.

3. MOVEMENTS IN PLANTS WITHOUT MUSCLES

From the growing of shoots and roots, to the opening and closing of stomata at the leaf surface, to the rapid snapping of carnivorous plants and the explosive launch of seed pods, plants have evolved a remarkable range of mechanisms to generate motions without the need for a muscular structure (Darwin, 1880; Gilroy and Masson, 2008; Forterre, 2013; Jung et al., 2014; Geitmann, 2016; Echevin et al., 2019; Morris and Blyth, 2019).

3.1. Water Transport

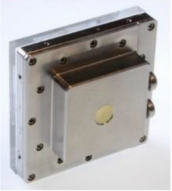

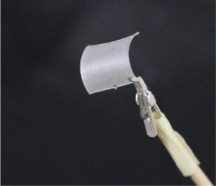


Plants turn out in a perfect hydraulic engine. At the macro level, plants exploit a sophisticated strategy, relying on water potential gradient, for moving water from the soil (i.e., at soil level ≈ -0.3 MPa) to the leaves (i.e., at the leaf level ≈ -7.0 MPa; McElrone et al., 2013). At the cell level, plants draw the water in and out of their cells using the osmotic gradient across semipermeable membranes. The turgor pressure thus changes creating a local change in the cellular volume and tissue stiffness, and by exploiting the thin and stiff cell-wall features, enables the large-scale tissue deformations required for motion (Dumais and Forterre, 2012). The characteristics of the water flow induced by gradients of water potential, the level of turgor pressure, and the mechanical properties of cell-wall deformation, are the key elements of water-driven movements in plants.

In roots, the movement of primary growth is characterized by the expansion of the cells facilitated by water uptake generating turgor pressure to inflate the cell and stretch the walls (Taiz and Zeiger, 2002). Plants are thus able to penetrate and explore soil in a non-destructive way. Such mechanism was first investigated from a robotics point of view in Mazzolai et al. (2011), with an osmotic actuation module implementing electro-osmosis by three cells separated by pairs of semipermeable osmotic membranes and ion-selective membranes, individually coupled with a piston mechanism. To aid the robotic design, Sinibaldi et al. (2013) followed a bioengineering approach to model the dynamics of osmotic actuation and represent a formal expression of scaling laws for the physical parameters necessary for the actuation strategy: characteristic time, maximum force, peak power, power density, cumulative work and energy density, role of volume-surface aspect ratio. This model was then exploited to design a forward osmosis-based actuator (Sinibaldi et al., 2014), fabricated on the basis of an analysis of plant movements, plant cell characteristics, and osmotic actuation modeling. The system has a typical size of 10 mm, produces forces above 20 N, with a power consumption in the order of 1 mW, and a characteristic time of 2–5 min.

3.2. Elastic Energy


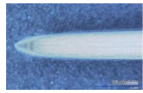




To obtain faster movements, plants exploit instability and fluid-solid coupling together with hydraulic mechanisms: elastic energy is first stored in the cell walls by means of a water flow, and released suddenly when a critical threshold of energy barrier is surpassed (Forterre et al., 2005; Dumais and Forterre, 2012). The rapid movement of leaf closure in the carnivorous plant *Dionaea*

TABLE 1 | Summary of plants' biological features, measurements and characterization methods, biological specifications, plant-inspired robotic solutions.

Biological features		Measurements and characterization methods	Biological specifications and guidelines		Robotic solutions	
Osmosis-based unit: water, turgor pressure, cell-wall properties (section 3)		Mathematical modeling defining scaling laws (characteristic time, maximum force, peak power, power density, cumulative work and energy density, role of volume-surface ratio)	Plant cell: <ul style="list-style-type: none"> • Typical size: 10^{-5}-10^{-4} m; • Timescale for water transport e.g., in stomata: 10^2-10^3 s • Membrane permeability: 10^{-13}-10^{-11} m/sPa; • Volumetric stiffness: 1–50 MPa 		Osmotic actuator: <ul style="list-style-type: none"> • Typical size: 10^{-2} m • Time: 2–5 min; • Membrane permeability: 10^{-13}-10^{-11} m/sPa • Volumetric stiffness: 25 MPa (with AT31F elastomer) – 35 MPa (with Viton elastomer) • $F > 20$N; $P \sim 1$mW 	
			References - Dumais and Forterre, 2012 - Forterre, 2013		References - Mazzolai et al., 2011 - Sinibaldi et al., 2013, 2014	References - Sinibaldi et al., 2014
		High speed video imaging, mathematical modeling and microscopy techniques (i.e., polarized light microscopy for microfibrils visualization)	<ul style="list-style-type: none"> • Bistable structure with orthogonal curvature shapes • Timescale from open to close state: 100 ms • Directional reinforcement fibers 		<ul style="list-style-type: none"> • Bistable actuator structure: low/high stiffness layers (i.e., epoxy resin/carbon fiber) or passive/active layers (i.e., PDMS/hydroscopic nanofibers) • Combined actuation: SMA or pneumatic plus SMA spring • Timescale for movements: 100 ms 	
			References - Forterre et al., 2005 - Poppinga et al., 2015 - Lunni et al., 2020	References - Lunni et al., 2020	References - Kim et al., 2014 - Lunni et al., 2020 - Esser et al., 2019, 2020	References - Lunni et al., 2020
Roots growth and soil exploration (section 4)	Kinematics	Analyzer for Root Tip Tracks – for tip displacement kinematics in both primary and secondary roots	Kinematics of tip displacement due to growth and circumnutations, free and with obstacles. Growth patterns (<i>Zea mays</i> primary roots): T 64° A 0.7 mm D 0–1 mm; T 60–100° A 0.25 mm D 1–3 mm Obstacle avoidance (<i>Zea mays</i>): approaching phase orientation angle < 20°; crossing phase orientation angle ~ 70°; recovery phase orientation angle ~ 30°		Data for: trajectory, displacement, velocity, direction and orientation, circumnutations amplitudes and period, variation of orientation during root obstacle avoidance	
			Reference - Russino et al., 2013		Reference: - Russino et al., 2013	
	Growing	Digital microscope analysis and mechanical tests via robotic mock-ups	Growing from the tip strategy <ul style="list-style-type: none"> • Meristematic region behind the root cap • Turgor in cells in the elongation zone to push the apex forward • Mucilage exudation and external sloughing of root cap cells for low-friction lining • Anchoring via root hairs and secondary roots in mature zone 		<ul style="list-style-type: none"> • Growing robot based on monotonic filament deposition and growing from the tip strategy • 3D printing-based growing robot with thermoplastic material for growing from the tip, bending and morphological adaptation • Other growing mechanism: via pressurization of an inverted thin-walled vessel 	
			References - Ishikawa and Evans, 1995 - Bengough et al., 1997; Sadeghi et al., 2014		References - Sadeghi et al., 2014, 2017 - Hawkes et al., 2017	Reference - Sadeghi et al., 2020

(Continued)

TABLE 1 | Continued

Biological features		Measurements and characterization methods	Biological specifications and guidelines		Robotic solutions	
	Circumnutations	Mathematical modeling, circumnutation tracking system, and robotic mock-ups mechanical tests	<ul style="list-style-type: none"> Trade-off among penetration velocity, circumnutation period, and amplitude to optimize energy consumption, expressed by helical path angle between 46 and 65° 33% of energy efficiency improvement in penetration with circumnutations <p><i>References</i></p> <ul style="list-style-type: none"> - Popova et al., 2012 - Del Dottore et al., 2018b 		Robotic root with bending abilities via spring-based soft actuation and implementing a stimulus oriented behavior combined with circumnutations	
	Tip morphology	Optical microscope morphometric analysis and robotic mock-ups mechanical tests	<p><i>Reference</i></p> <ul style="list-style-type: none"> - Mishra et al., 2018 		3D-printed root-like morphology	
Climbing and coiling (section 5)	Circumnutations	Kinematics models and control algorithms implemented and validated with robotic tendril-like systems	<ul style="list-style-type: none"> Contact coiling: curling around a support via asymmetric G fibers contraction (for water loss) initiated in response to a local mechanical stimulus Secondary coiling ("free-coiling"): pulling movement created via elastic spring-like connection between the stem and the grasped support, increase of rigidity and lignification Reversible coiling: variable stiffness regulated via turgor pressure variation <p><i>References</i></p> <ul style="list-style-type: none"> - Darwin, 1865 - Bowling and Vaughn, 2009 - Niklas and Spatz, 2012 		<ul style="list-style-type: none"> Grasping-by-coiling implemented by contact coiling plus secondary coiling kinematic model and robotic prototype with SMA springs tendril-like actuator Circumnutation-based algorithms and multi-tendon based actuation in tendril-like continuum robot Reversible coiling and uncoiling of tendril-like robot with variable stiffness regulated via artificial osmotic actuator <p><i>References</i></p> <ul style="list-style-type: none"> - Vidoni et al., 2015 - Wooten and Walker, 2016 - Must et al., 2019 	
	Leaves	Kelvin force microscopy to measure charge accumulation in leaves, and specialized phytochamber equipped with an active climate control system and wind source	<ul style="list-style-type: none"> The cuticle-cellular tissue bilayer of plant leaves functions as an integrated triboelectric generator conductor couple capable of converting mechanical stimuli into electricity Natural mechanical stimuli by wind or touching of leaves are converted into electrical signals by a triboelectric mechanism  <p><i>References</i></p> <ul style="list-style-type: none"> - Jie et al., 2018 - Meder et al., 2018 - Pic: Meder et al., 2018 		Plant-hybrid generator system to convert wind-induced vibrations between natural leaf and silicone-rubber leaf from multiple directions into electric power (e.g., with 4 hybrid leaves, and wind speed of ~ 3 m/s, the capacitor charges to 1.5 V in ~ 15 min)	
Energy harvesting (section 6)			<p><i>References</i></p> <ul style="list-style-type: none"> - Meder et al., 2018 - Meder et al., 2020 			<i>Reference</i> - Meder et al., 2020
Morphological computation (section 7)	Seeds (e.g., maple)	Mathematical model, measurements of 3D flow around dynamically scaled seed models, flight dynamic analysis	Auto-rotating seeds attain high lift by generating leading-edge vortex		Auto-rotative robotic seed able to hover, climb and translate	
			<p><i>References</i></p> <ul style="list-style-type: none"> - Lentink et al., 2009 - Ulrich et al., 2010 		<p><i>References</i></p> <ul style="list-style-type: none"> - Lentink et al., 2009 - Ulrich et al., 2010 	

muscipula (Venus flytrap) derives from the accumulation of elastic energy in the leaves, driven by swelling and shrinkage coupled with a double curvature geometry of lobes. This allows a snap-buckling mechanism of 100 ms after the initial trigger stimulus. These features inspired a flytrap-like robot described in Kim et al. (2014) which can reach rapid speed motion (~ 100 ms) and large deformations (18 m^{-1}). The system consists of an asymmetrically laminated carbon fiber prepreg (CFRP), which acts as a bistable artificial leaf, and a shape memory alloy (SMA), which acts as triggering actuator to induce the snap motion. Differently, Esser et al. (2019) combined different actuation systems (pneumatic, plus SMA spring) to translate the principles of movements of Venus flytrap and waterwheel plant in systems able to respond to different environmental triggers (heat, moisture or magnetic stimuli). More recently, polarized light microscopy revealed the presence of microfibrils reinforcing the leaf, running perpendicular to its midrib in the upper and lower epidermis. This additional feature, integrated with bistability, inspired the design of an artificial hygroscopic bistable system, obtained by bonding prestretched poly(dimethylsiloxane) – PDMS layers prior to depositing electrospun polyethylene oxide (PEO) nanofibers (Lunni et al., 2020). The Venus flytrap is an interesting model for robotic components and artificial materials, which have been recently deeply reviewed by Esser et al. (2020).

4. BELOW-GROUND MOBILITY: STRATEGIES AND MORPHOLOGICAL FEATURES OF ROOTS FOR SOIL EXPLORATION

4.1. Moving-By-Growing

The movement of roots inside the soil occurs by adding new cells to the apex. This strategy allows minimizing the resistance forces during penetration, and is helped by lateral hairs and diameter expansions that keep the whole system anchored. The roots' strategy of *growing from the tip* is a key specification for the development of robotic systems for soil exploration. To quantify the influence of this mechanism during penetration, Tonazzini et al. (2013) used a physical robotic demonstrator and showed that the growth from the tip reduces penetration energy from 20 to up 50%, depending on the initial depth. Following these quantitative analyses, Sadeghi et al. (2014) designed the first root-like system implementing a growing mechanism by means of a monotonic process that continuously adds new material to the base of the tip, in the form of a layer, and pushes forward the tip itself layer-by-layer.

This concept triggered the idea of *moving-by-growing*, paving the way for growing robots: by integrating a miniaturized 3D printer into the tip of a root-like device and using a thermoplastic filament, the body of the root-like system can be created layer-by-layer thus replicating the natural mechanism of cell deposition and consolidation that occurs in plants growth (Sadeghi et al., 2017). The concept of growing system has been approached also using other technologies. For example, the robot described in Hawkes et al. (2017) grows via pressurization of an inverted thin-walled vessel.

4.2. Circumnutations

To further enhance exploration abilities, circular movements (known as “circumnutations”) are performed by the root tip due to a combination of internal factors and external factors (i.e., gravitropism, Brown, 1993; Stolarz, 2009; Migliaccio et al., 2013). Circumnutations are a class of movements that are found in all plants organs, but in particular in those that are involved in growth (roots, shoots, branches, flower stalks) and generate elliptical or circular trajectories (Mugnai et al., 2015).

To quantify the characteristics of root circumnutations in soil for robotic design purposes, Popova et al. (2012), Del Dottore et al. (2018b), and Tedone et al. (2020) have proposed a methodology for the analysis of the movement, including a time-lapse videos observation (in air and in soil) and the study of tip kinematics using the “Analyser for Root Tip Tracks” (ARTT, Russino et al., 2013), which combines a segmentation algorithm with additional software imaging filters in order to realize a 2D tip detection. Measurements of the growing speed and circumnutation amplitude were extracted to implement the circumnutation behavior in a soft robotic root that bends using soft spring-based actuators (Sadeghi et al., 2016). Experiments in the air with the robotic root were performed to demonstrate that the system can follow an external stimulus while performing a circumnutation movement, similarly to a natural root. Additional experiments have been performed in a soil-like testbed showing that the use of plant root-like circumnutations improves the efficiency of penetration (33%) compared to moving directly forwards with no circular movement. In line with these results, additional investigations using “robophysical” modeling have revealed the benefits of tip nutation movements for navigating obstacles and exploring heterogeneous terrains (McCaskey et al., 2019; Taylor et al., 2020).

4.3. Roots Morphology

To better understand the role of morphology of roots in soil, high-resolution imaging methods, such as micro-CT (Kaestner et al., 2006; Tracy et al., 2010) can be used to investigate natural roots and thus obtain a 3D reconstruction for bioinspired design insights. Mishra et al. (2018) used imaging capture of *Zea mays* roots via an optical microscope. The aim was to extract the morphological features of the tip profile and implement a 3D CAD model to guide the design and fabrication of 3D printed root-like probes. These devices, with different diameters and shapes, were compared in terms of energy consumption and penetration force via experimental tests in real soil and discrete element simulations, demonstrating the higher penetration performance of the bioinspired tip profile with respect to the other ones.

5. ABOVE-GROUND MOVEMENTS: REMARKABLE ABILITIES IN CLIMBING PLANTS

Climbing plants show interesting abilities to grow search for a support, and then attach, anchor or coil themselves onto it. They use several types of movements, including circumnutations,

and exploit their tactile perception, adhesive properties, and ability to change their mechanical and morphological properties (Rowe and Speck, 2005, 2015). From a biomimetic perspective, recent reviews have focused on the attachment mechanisms (Burris et al., 2018) or those features that ensure highly flexible, soft and continuum robotic appendages (Fiorello et al., 2020). Tendrils and vines are particularly interesting in this framework, and specifically for the development of “searcher-like” robots (Wooten and Walker, 2016, 2018; Visentin et al., 2020).

5.1. Searching

Early stem growth, where young shoots extend into spaces and search for support, are known as “searchers.” An outstanding example of a light-mass searcher can be found in the climbing cactus *Selenicereus setaceus* (Soffiatti and Rowe, 2020). Searchers often have a light but stiff structure, and are capable to extend across voids and perform circumnutations to improve the probability of touching a support (Gallenmüller et al., 2004). Circumnutations offer a valuable solution for adaptation algorithms in motion planning (Wooten and Walker, 2016, 2018). By analyzing the behavior of vines, circumnutation-based algorithm improves the performance of a tendril-like continuum robots, enabling efficient environmental contact and helping to guide and stabilize the system. Such strategy could be used, for example, in space for positioning sensors or exploring the surrounding environment (Mehling et al., 2006; Tonapi et al., 2014; Wooten and Walker, 2015; Nahar et al., 2017).

5.2. Coiling

In climbing plants, contact coiling starts when a local mechanical stimulus occurs in a tendril, which then start to curl around the support and grip to it. This coiling is associated with the presence of gelatinous fibers (“G fibers,” Bowling and Vaughn, 2009). A differential decrease in the water content of a G fibers-bilayer ribbon generates an asymmetric contractile force, which drives the coiling (Gerbode et al., 2012). Then, a secondary coiling (“free-coiling”) pulls the plant closer to the support, creating an elastic spring-like anchorage resistant to external loads or wind. The loss of water during the free-coiling phase leads to an increase in structural rigidity, or lignification, which prevents it from uncoiling. Contact and secondary coiling were investigated from a kinematic viewpoint in Vidoni et al. (2015) to design and develop a tendril-like system able to grasp-by-coiling.

In some cases, the natural mechanism of coiling is reversible, so if the support is not suitable, the tendril uncoils. This feature was implemented in a small-scale system by Must et al. (2019). The actuation strategy derives from a plant’s capacity to actively control osmolyte gradients, and is based on the electrosorption of ions on flexible electrodes (in porous carbon), driven at low input voltages (1.3 V). A 1 cm electroactive unit reversibly controls the concentration of ions (acting as osmolyte) obtained through the dissolution of an electrolyte. This tendril-like soft robot, coupled to the control unit, performs coiling and uncoiling with reversible stiffening and actuation.

6. ENERGY HARVESTING FROM PLANT LEAVES

In addition to their photosynthetic apparatus, leaves can also work as an integrated triboelectric generator and convert mechanical stimuli into electrical signals (Jie et al., 2018; Meder et al., 2018). Meder et al. (2018) used Kelvin force microscopy to investigate how the charge is generated at the leaving plant leaf and reported that the electric signal due to cuticle triboelectrification can be generated by natural mechanical stimuli, such as wind or contact with other leaves. This discovery inspired the first living plant-hybrid system that can convert wind energy into electricity. Tested under outdoor conditions in a controlled environment, these plant-hybrid generators convert wind from multiple directions to directly power light-emitting diodes or a digital thermometer (Meder et al., 2020).

7. MORPHOLOGICAL COMPUTATION: PLANT SEEDS

Seeds are one of the most significant examples of morphological computation in the natural world. They provide a rich library of morphological and mechanical features optimized for passive take-off, flying, landing, and drilling (Fratzl and Barth, 2009). Although seeds lack active metabolism, hence no internal energy is produced, they are highly responsive to environmental conditions (e.g., temperature and humidity) and have anisotropic and reversible movements.

Environmental responsiveness is due to materials (Chambers and MacMahon, 1994; Burgert and Fratzl, 2009; Sadlo et al., 2018) and structural features (Abraham and Elbaum, 2013) of the seed tissues. As example, autorotating seeds of maples generate a surprisingly high lift by creating a stable leading-edge vortex as they descend (Lentink et al., 2009). Taking into account their geometries and flight trajectories, such capabilities can be used for the design of auto-rotative robotic samara air vehicles (Ulrich et al., 2010).

New fabrication technologies, like 4D printing, are allowing to advance multi-functional materials capabilities, such as in the case of biomimetic hygro-responsive composite polymer inspired by the reversible shape-changes of Bhutan pine (*Pinus wallichiana*) cone seed scales (Correa et al., 2020).

8. CONCLUSIONS

Plants as a model has been officially accepted within the robotics community, inspiring also new sensors (Sareh et al., 2014; Lucarotti et al., 2015; Su et al., 2015; Blandin et al., 2017; Cheng et al., 2018) and swarm communication strategies (Ciszak et al., 2012; Del Dottore et al., 2018a).

Besides, plant-inspired robots (Sadeghi et al., 2014), robophysical models (McCaskey et al., 2019), and behavior models (Agostinelli et al., 2020), have been crucial to

validate hypothesis on plants' mechanisms, closing the circle of bio-robotics.

There is a new vision for bioinspired robots, in which robots are seen as environmentally responsible machines that can grow, adapt, and are built with recyclable, or biodegradable, or biohybrid materials (Yang et al., 2018; Mazzolai and Laschi, 2020).

To achieve this, we need to look at a more global level, investigating the strategies and synergies of natural organisms (Aartsma et al., 2017; Paudel Timilsena et al., 2020), and at how they are integrated harmoniously within the natural ecosystem. All these aspects need to be further studied with a multi-disciplinary approach to develop a new wave of environmentally responsible robots.

Plants are not only a source of inspiration for current and future technological progress in an environmentally responsible integrated vision. Equally importantly, they are key to our future welfare. In order for us to better understand and protect the biodiversity of species and the whole global environment, it is imperative that we learn more about their features, as well as how they deal with the natural ecosystem.

REFERENCES

- Aartsma, Y., Bianchi, F. J., van der Werf, W., Poelman, E. H., and Dicke, M. (2017). Herbivore-induced plant volatiles and tritrophic interactions across spatial scales. *New Phytol.* 216, 1054–1063. doi: 10.1111/nph.14475
- Abraham, Y., and Elbaum, R. (2013). Hygroscopic movements in geraniaceae: the structural variations that are responsible for coiling or bending. *New Phytol.* 199, 584–594. doi: 10.1111/nph.12254
- Agostinelli, D., Lucantonio, A., Noselli, G., and DeSimone, A. (2020). Nutations in growing plant shoots: the role of elastic deformations due to gravity loading. *J. Mech. Phys. Solids* 136:103702. doi: 10.1016/j.jmps.2019.103702
- Baluška, F., and Mancuso, S. (2020). Plants, climate and humans: plant intelligence changes everything. *EMBO Rep.* 21:e50109. doi: 10.15252/embr.202050109
- Bengough, A. G., Croser, C., and Pritchard, J. (1997). A biophysical analysis of root growth under mechanical stress. *Plant Soil* 189, 155–164. doi: 10.1023/A:1004240706284
- Blandin, A. A., Totaro, M., Bernardeschi, I., and Beccai, L. (2017). "Tunable normal and shear force discrimination by a plant-inspired tactile sensor for soft robotics," in *Conference on Biomimetic and Biohybrid Systems*, (Springer: Cham), 25–34. doi: 10.1007/978-3-319-63537-8_3
- Bolt, M., Prather, J. C., Horton, T., and Adams, M. (2020). Massively deployable, low-cost airborne sensor motes for atmospheric characterization. *Wireless Sens. Netw.* 12:1. doi: 10.4236/wsn.2020.121001
- Bowling, A. J., and Vaughn, K. C. (2009). Gelatinous fibers are widespread in coiling tendrils and twining vines. *Am. J. Bot.* 96, 719–727. doi: 10.3732/ajb.0800373
- Brown, A. H. (1993). Circumnutations: from darwin to space flights. *Plant Physiol.* 101:345. doi: 10.1104/pp.101.2.345
- Burgert, I., and Fratzl, P. (2009). Plants control the properties and actuation of their organs through the orientation of cellulose fibrils in their cell walls. *Integr. Comp. Biol.* 49, 69–79. doi: 10.1093/icb/icp026
- Burris, J. N., Lenaghan, S. C., and Stewart, C. N. (2018). Climbing plants: attachment adaptations and bioinspired innovations. *Plant Cell Rep.* 37, 565–574. doi: 10.1007/s00299-017-2240-y
- Chambers, J. C., and MacMahon, J. A. (1994). A day in the life of a seed: movements and fates of seeds and their implications for natural and managed systems. *Annu. Rev. Ecol. Syst.* 25, 263–292. doi: 10.1146/annurev.es.25.110194.001403

AUTHOR CONTRIBUTIONS

BM and LM conceived the focus and the format of the mini-review. BM, LM, FT, and IF curated the existing bibliography, contributed to the table contents, and to the writing of the manuscript. All authors contributed to the article and approved the submitted version.

FUNDING

This work was funded by GrowBot, the European Union's Horizon 2020 Research and Innovation Programme under Grant Agreement No. 824074, by SMASH-Smart Machines for Agricultural Solutions Hightech (Tuscany-Italy POR FESR 2014–2020), and by RoboCom ++, the European Commission under the FLAG-ERA Joint Transnational Call (JTC) 2016.

ACKNOWLEDGMENTS

The authors acknowledge Dr. Emanuela Del Dottore and Dr. Dario Lunni for their kind contribution with some of the pictures.

- Cheng, Y., Wang, R., Chan, K. H., Lu, X., Sun, J., and Ho, G. W. (2018). A biomimetic conductive tendril for ultrastretchable and integratable electronics, muscles, and sensors. *ACS Nano* 12, 3898–3907. doi: 10.1021/acsnano.8b01372
- Ciszak, M., Comparini, D., Mazzolai, B., Baluska, F., Arechchi, F. T., Vicsek, T., et al. (2012). Swarming behavior in plant roots. *PLoS ONE* 7:e29759. doi: 10.1371/annotation/8e6864fc-c4b7-46e7-92b3-80767f4a5d3a
- Correa, D., Poppinga, S., Mylo, M. D., Westermeier, A. S., Bruchmann, B., Menges, A., et al. (2020). 4D pine scale: biomimetic 4D printed autonomous scale and flap structures capable of multi-phase movement. *Philos. Trans. R. Soc. A* 378:20190445. doi: 10.1098/rsta.2019.0445
- Darwin, C. (1865). *On The Movements and Habits of Climbing Plants*. London: John Murray. doi: 10.1111/j.1095-8339.1865.tb00011.x
- Darwin, C. (1880). *The Power of Movements in Plants*. London: Ed. Murray. doi: 10.5962/bhl.title.102319
- Del Dottore, E., Mondini, A., Sadeghi, A., Mattoli, V., and Mazzolai, B. (2018b). An efficient soil penetration strategy for explorative robots inspired by plant root circumnutation movements. *Bioinspir. Biomimet.* 13:015003. doi: 10.1088/1748-3190/aa9998
- Del Dottore, E., Mondini, A., Sadeghi, A., and Mazzolai, B. (2018a). Swarming behavior emerging from the uptake–kinetics feedback control in a plant-root-inspired robot. *Appl. Sci.* 8:47. doi: 10.3390/app8010047
- Dumais, J., and Forterre, Y. (2012). "Vegetable dynamics": the role of water in plant movements. *Annu. Rev. Fluid Mech.* 44, 453–478. doi: 10.1146/annurev-fluid-120710-101200
- Echevin, E., Le Gloanec, C., Skowronska, N., Routier-Kierzkowska, A. L., Burian, A., and Kierzkowski, D. (2019). Growth and biomechanics of shoot organs. *J. Exp. Bot.* 70, 3573–3585. doi: 10.1093/jxb/erz205
- Esser, F., Scherag, F. D., Poppinga, S., Westermeier, A., Mylo, M. D., Kampowski, T., et al. (2019). "Adaptive biomimetic actuator systems reacting to various stimuli by and combining two biological snap-trap mechanics," in *Conference on Biomimetic and Biohybrid Systems*, (Springer: Cham), 114–121. doi: 10.1007/978-3-030-24741-6_10
- Esser, F. J., Auth, P., and Speck, T. (2020). Artificial venus flytraps: a research review and outlook on their importance for novel bioinspired materials systems. *Front. Robot. AI* 7:75. doi: 10.3389/frobt.2020.00075
- Fiorello, I., Del Dottore, E., Tramaccere, F., and Mazzolai, B. (2020). Taking inspiration from climbing plants: methodologies and benchmarks—a review. *Bioinspir. Biomimet.* 15:031001. doi: 10.1088/1748-3190/ab7416

- Forterre, Y. (2013). Slow, fast and furious: understanding the physics of plant movements. *J. Exp. Bot.* 64, 4745–4760. doi: 10.1093/jxb/ert230
- Forterre, Y., Skotheim, J. M., Dumais, J., and Mahadevan, L. (2005). How the venus flytrap snaps. *Nature* 433, 421–425. doi: 10.1038/nature03185
- Fratzl, P., and Barth, F. G. (2009). Biomaterial systems for mechanosensing and actuation. *Nature* 462, 442–448. doi: 10.1038/nature08603
- Gallenmüller, F., Rowe, N., and Speck, T. (2004). Development and growth form of the neotropical liana croton nuntians: the effect of light and mode of attachment on the biomechanics of the stem. *J. Plant Growth Regul.* 23, 83–97. doi: 10.1007/s00344-004-0045-z
- Geer, R., Iannucci, S., and Li, S. (2020). Pneumatic coiling actuator inspired by the awns of erodium cicutarium. *Front. Robot. AI* 7:17. doi: 10.3389/frobt.2020.00017
- Geitmann, A. (2016). Actuators acting without actin. *Cell* 166, 15–17. doi: 10.1016/j.cell.2016.06.030
- Gerbode, S. J., Puzey, J. R., McCormick, A. G., and Mahadevan, L. (2012). How the cucumber tendril coils and overwinds. *Science* 337, 1087–1091. doi: 10.1126/science.1223304
- Gilroy, S., and Masson, P. H. (2008). *Plant Tropisms*. Oxford: Ed. Blackwell. doi: 10.1002/9780470388297
- Guerra, S., Peressotti, A., Peressotti, F., Bulgheroni, M., Baccinelli, W., D'Amico, E., et al. (2019). Flexible control of movement in plants. *Sci. Rep.* 9:16570. doi: 10.1038/s41598-019-53118-0
- Hawkes, E. W., Blumenschein, L. H., Greer, J. D., and Okamura, A. M. (2017). A soft robot that navigates its environment through growth. *Sci. Robot.* 2:eaan3028. doi: 10.1126/scirobotics.aan3028
- Ishikawa, H., and Evans, M. L. (1995). Specialized zones of development in roots. *Plant Physiol.* 109:725. doi: 10.1104/pp.109.3.725
- Jie, Y., Jia, X., Zou, J., Chen, Y., Wang, N., Wang, Z. L., et al. (2018). Natural leaf made triboelectric nanogenerator for harvesting environmental mechanical energy. *Adv. Energy Mater.* 8:1703133. doi: 10.1002/aenm.201703133
- Jung, W., Kim, W., and Kim, H. Y. (2014). Self-burial mechanics of hygroscopically responsive awns. *Integr. Comp. Biol.* 54, 1034–42. doi: 10.1093/icb/icu026
- Kaestner, A., Schneebeli, M., and Graf, F. (2006). Visualizing three-dimensional root networks using computed tomography. *Geoderma* 136, 459–469. doi: 10.1016/j.geoderma.2006.04.009
- Karban, R. (2008). Plant behaviour and communication. *Ecol. Lett.* 11, 727–739. doi: 10.1111/j.1461-0248.2008.01183.x
- Kim, S. W., Koh, J. S., Lee, J. G., Ryu, J., Cho, M., and Cho, K. J. (2014). Flytrap-inspired robot using structurally integrated actuation based on bistability and a developable surface. *Bioinspir. Biomimet.* 9:036004. doi: 10.1088/1748-3182/9/3/036004
- Laschi, C., and Mazzolai, B. (2016). Lessons from animals and plants: the symbiosis of morphological computation and soft robotics. *IEEE Robot. Autom. Mag.* 23, 107–114. doi: 10.1109/MRA.2016.2582726
- Lentink, D., Dickson, W. B., Van Leeuwen, J. L., and Dickinson, M. H. (2009). Leading-edge vortices elevate lift of autorotating plant seeds. *Science* 324, 1438–1440. doi: 10.1126/science.1174196
- Lucarotti, C., Totaro, M., Sadeghi, A., Mazzolai, B., and Beccai, L. (2015). Revealing bending and force in a soft body through a plant root inspired approach. *Sci. Rep.* 5:8788. doi: 10.1038/srep08788
- Lunni, D., Cianchetti, M., Filippeschi, C., Sinibaldi, E., and Mazzolai, B. (2020). Plant-inspired soft bistable structures based on hygroscopic electrospun nanofibers. *Adv. Mater. Interfaces* 7:1901310. doi: 10.1002/admi.2019.01310
- Mazzolai, B., and Laschi, C. (2020). A vision for future bioinspired and biohybrid robots. *Sci. Robot.* 5:eba6893. doi: 10.1126/scirobotics.aba6893
- Mazzolai, B., Laschi, C., Dario, P., Mugnai, S., and Mancuso, S. (2010). The plant as a biomechatronic system. *Plant Signal. Behav.* 5, 90–93. doi: 10.4161/psb.5.2.10457
- Mazzolai, B., Mondini, A., Corradi, P., Laschi, C., Mattoli, V., Sinibaldi, E., et al. (2011). A miniaturized mechatronic system inspired by plant roots for soil exploration. *IEEE/ASME Trans. Mechatron.* 16, 201–212. doi: 10.1109/TMECH.2009.2038997
- McCaskey, E. N., Lehner, K., Murray-Cooper, M., Ozkan-Aydin, Y., Hawkes, E. W., Benfey, P. N., et al. (2019). “Circumnutation facilitates effective root-surface exploration of rice roots,” in *Integrative and Comparative Biology*. eds R. D. Evans and N. C. Cary (Oxford Univ Press Inc).
- McElrone, A. J., Choat, B., and Gambetta, G. A. Brodersen, C. R. (2013). Water uptake and transport in vascular plants. *Nat. Educ. Knowledge* 4:6. Available online at: <https://www.nature.com/scitable/knowledge/library/water-uptake-and-transport-in-vascular-plants-103016037/#>
- Meder, F., Must, I., Sadeghi, A., Mondini, A., Filippeschi, C., Beccai, L., et al. (2018). Energy conversion at the cuticle of living plants. *Adv. Func. Mater.* 28:1806689. doi: 10.1002/adfm.201806689
- Meder, F., Thielen, M., Mondini, A., Speck, T., and Mazzolai, B. (2020). Living plant-hybrid generators for multidirectional wind energy conversion. *Energy Technol.* 8:2000236. doi: 10.1002/ente.202000236
- Mehling, J. S., Diftler, M. A., Chu, M., and Valvo, M. (2006). “A minimally invasive tendril robot for in-space inspection,” in *The First IEEE/RAS-EMBS International Conference on Biomedical Robotics and Biomechanics*, (IEEE). doi: 10.1109/BIOROB.2006.1639170
- Migliaccio, F., Tassone, P., and Fortunati, A. (2013). Circumnutation as an autonomous root movement in plants. *Am. J. Bot.* 100, 4–13. doi: 10.3732/ajb.1200314
- Mishra, A. K., Tramacere, F., Guarino, R., Pugno, N. M., and Mazzolai, B. (2018). A study on plant root apex morphology as a model for soft robots moving in soil. *PLoS ONE* 13:e0197411. doi: 10.1371/journal.pone.0197411
- Morris, R. J., and Blyth, M. (2019). How water flow, geometry, and material properties drive plant movements. *J. Exp. Bot.* 70, 3549–3560. doi: 10.1093/jxb/erz167
- Mugnai, S., Azzarello, E., Masi, E., Pandolfi, C., and Mancuso, S. (2015). “Nutation in plants,” in *Rhythms in Plants*, eds S. Mancuso and S. Shabala (Springer: Cham), 19–34. doi: 10.1007/978-3-319-20517-5_2
- Must, I., Sinibaldi, E., and Mazzolai, B. (2019). A variable-stiffness tendril-like soft robot based on reversible osmotic actuation. *Nat. Commun.* 10:344. doi: 10.1038/s41467-018-08173-y
- Nahar, D., Yanik, P. M., and Walker, I. D. (2017). “Robot tendrils: long, thin continuum robots for inspection in space operations,” in *IEEE Aerospace Conference*, (IEEE: Big Sky, MT). doi: 10.1109/AERO.2017.7943940
- Niklas, K. J., and Spatz, H. C. (2012). *Plant Physics*. Chicago, IL: University of Chicago Press. doi: 10.7208/chicago/9780226586342.001.0001
- Paudel Timilsena, B., Seidl-Adams, I., and Tumlinson, J. H. (2020). Herbivore-specific plant volatiles prime neighboring plants for nonspecific defense responses. *Plant Cell Environ.* 43, 787–800. doi: 10.1111/pce.13688
- Paul, C. (2006). Morphological computation: a basis for the analysis of morphology and control requirements. *Robot. Auton. Syst.* 54, 619–630. doi: 10.1016/j.robot.2006.03.003
- Pfeifer, R., and Bongard, J. (2007). *How the Body Shapes the Way We Think: a New View of Intelligence*. MIT press. doi: 10.7551/mitpress/3585.001.0001
- Popova, L., Russino, A., Ascrizzi, A., and Mazzolai, B. (2012). Analysis of movement in primary maize roots. *Biologia* 67, 517–524. doi: 10.2478/s11756-012-0023-z
- Poppinga, S., Haushahn, T., Warnke, M., Masselter, T., and Speck, T. (2015). Sporangium exposure and spore release in the peruvian maidenhair fern (*Adiantum peruvianum*, pteridaceae). *PLoS ONE* 10:e0138495. doi: 10.1371/journal.pone.0138495
- Ramnaud-Lavigne, L., and Hay, A. (2020). Floral organ development goes live. *J. Exp. Bot.* 71, 2472–2478. doi: 10.1093/jxb/era038
- Rowe, N., and Speck, T. (2005). Plant growth forms: an ecological and evolutionary perspective. *New Phytol.* 166, 61–72. doi: 10.1111/j.1469-8137.2004.01309.x
- Rowe, N. P., and Speck, T. (2015). “Stem biomechanics, strength of attachment, and developmental plasticity of vines and lianas,” in *The Ecology of Lianas*, eds S. Schnitzer, F. Bongers, R. Burnham, and F. E. Putz (Chichester: Wiley-Blackwell), 323–341.
- Russino, A., Ascrizzi, A., Popova, L., Tonazzini, A., Mancuso, S., and Mazzolai, B. (2013). A novel tracking tool for the analysis of plant-root tip movements. *Bioinspir. Biomimet.* 8:025004. doi: 10.1088/1748-3182/8/2/025004
- Sadeghi, A., Del Dottore, E., Mondini, A., and Mazzolai, B. (2020). Passive morphological adaptation for obstacle avoidance in a self-growing robot produced by additive manufacturing. *Soft Robot.* 7, 85–94. doi: 10.1089/soro.2019.0025

- Sadeghi, A., Mondini, A., Del Dottore, E., Mattoli, V., Beccai, L., Taccola, S., et al. (2016). A plant-inspired robot with soft differential bending capabilities. *Bioinspir. Biomimet.* 12:015001. doi: 10.1088/1748-3190/12/1/015001
- Sadeghi, A., Mondini, A., and Mazzolai, B. (2017). Toward self-growing soft robots inspired by plant roots and based on additive manufacturing technologies. *Soft Robot.* 4, 211–223. doi: 10.1089/soro.2016.0080
- Sadeghi, A., Tonazzini, A., Popova, L., and Mazzolai, B. (2014). A novel growing device inspired by plant root soil penetration behaviors. *PLoS ONE* 9:e90139. doi: 10.1371/journal.pone.0090139
- Sadlo, J., Chytrý, M., Pergl, J., and Pyšek, P. (2018). Plant dispersal strategies: a new classification based on the multiple dispersal modes of individual species. *Preslia* 90, 1–22. doi: 10.23855/preslia.2018.001
- Sareh, S., Jiang, A., Faragasso, A., Noh, Y., Nanayakkara, T., Dasgupta, P., et al. (2014). “Bio-inspired tactile sensor sleeve for surgical soft manipulators,” in *2014 IEEE International Conference on Robotics and Automation (ICRA)*, (IEEE), 1454–1459. doi: 10.1109/ICRA.2014.6907043
- Silverberg, J. L., Noar, R. D., Packer, M. S., Harrison, M. J., Henley, C. L., Cohen, I., et al. (2012). 3D imaging and mechanical modeling of helical buckling in *Medicago truncatula* plant roots. *Proc. Natl. Acad. Sci. U.S.A.* 109, 16794–16799. doi: 10.1073/pnas.1209287109
- Sinibaldi, E., Argiolas, A., Puleo, G. L., and Mazzolai, B. (2014). Another lesson from plants: the forward osmosis-based actuator. *PLoS ONE* 9:e102461. doi: 10.1371/journal.pone.0102461
- Sinibaldi, E., Puleo, G. L., Mattioli, F., Mattoli, V., Di Michele, F., Beccai, L., et al. (2013). Osmotic actuation modelling for innovative biorobotic solutions inspired by the plant kingdom. *Bioinspir. Biomimet.* 8:025002. doi: 10.1088/1748-3182/8/2/025002
- Soffiatti, P., and Rowe, N. P. (2020). Mechanical innovations of a climbing cactus: functional insights for a new generation of growing robots. *Front. Robot. AI* 7:64. doi: 10.3389/frobt.2020.00064
- Stolarz, M. (2009). Circumnutation as a visible plant action and reaction: physiological, cellular and molecular basis for circumnutations. *Plant Signal. Behav.* 4, 380–387. doi: 10.4161/psb.4.5.8293
- Su, B., Gong, S., Ma, Z., Yap, L. W., and Cheng, W. (2015). Mimosa-inspired design of a flexible pressure sensor with touch sensitivity. *Small* 11, 1886–1891. doi: 10.1002/sml.201403036
- Taiz, L., and Zeiger, E. (2002). *Plant Physiology*, 3rd Edn. (Sunderland, MA: Sinauer).
- Taylor, I. W., Lehner, K. R., McCaskey, E. N., Nirmal, N. A., Ozkan-Aydin, Y., Murray-Cooper, M., et al. (2020). Mechanism and function of root circumnutation. *bioRxiv [Preprint]*. doi: 10.1101/2020.05.04.075127
- Tedone, F., Del Dottore, E., Palladino, M., Mazzolai, B., and Marcati, P. (2020). Optimal control of plant root tip dynamics in soil. *Bioinspir. Biomimet.* 15:056006. doi: 10.1088/1748-3190/ab9a15
- Tonapi, M. M., Godage, I. S., and Walker, I. D. (2014). “Next generation rope-like robot for in-space inspection,” in *2014 IEEE Aerospace Conference*, (IEEE), 1–13. doi: 10.1109/AERO.2014.6836183
- Tonazzini, A., Sadeghi, A., Popova, L., and Mazzolai, B. (2013). “Plant root strategies for robotic soil penetration,” in *Conference on Biomimetic and Biohybrid Systems*, (Springer, Berlin, Heidelberg), 447–449. doi: 10.1007/978-3-642-39802-5_62
- Tracy, S. R., Roberts, J. A., Black, C. R., McNeill, A., Davidson, R., and Mooney, S. J. (2010). The X-factor: visualizing undisturbed root architecture in soils using X-ray computed tomography. *J. Exp. Bot.* 61, 311–313. doi: 10.1093/jxb/erp386
- Ulrich, E. R., Pines, D. J., and Humbert, J. S. (2010). From falling to flying: the path to powered flight of a robotic samara nano air vehicle. *Bioinspir. Biomimet.* 5:045009. doi: 10.1088/1748-3182/5/4/045009
- Vidoni, R., Mimmo, T., and Pandolfi, C. (2015). Tendril-based climbing plants to model, simulate and create bio-inspired robotic systems. *J. Bionic Eng.* 12, 250–262. doi: 10.1016/S1672-6529(14)60117-7
- Vincent, O., Weißkopf, C., Poppinga, S., Masselter, T., Speck, T., Joyeux, M., et al. (2011). Ultra-fast underwater suction traps. *Proc. R. Soc. B Biol. Sci.* 278, 2909–2914. doi: 10.1098/rspb.2010.2292
- Visentin, F., Naselli, G., and Mazzolai, B. (2020). “A new exploration strategy for soft robots based on proprioception,” in *2020 3rd IEEE International Conference on Soft Robotics*, (RoboSoft) doi: 10.1109/RoboSoft48309.2020.9115976
- Vlad, D., Kierzkowski, D., Rast, M. I., Vuolo, F., Ioio, R. D., Galinha, C., et al. (2014). Leaf shape evolution through duplication, regulatory diversification, and loss of a homeobox gene. *Science* 343, 780–783. doi: 10.1126/science.1248384
- Wooten, M. B., and Walker, I. D. (2015). “A novel vine-like robot for in-orbit inspection,” in *45th International Conference on Environmental Systems*.
- Wooten, M. B., and Walker, I. D. (2016). “Circumnutation: from plants to robots,” in *International Conference on Simulation of Adaptive Behavior*, (Cham: Springer), 1–11. doi: 10.1007/978-3-319-43488-9_1
- Wooten, M. B., and Walker, I. D. (2018). Vine-inspired continuum tendril robots and circumnutations. *Robotics* 7:58. doi: 10.3390/robotics7030058
- Yang, G. Z., Bellingham, J., Dupont, P. E., Fischer, P., Floridi, L., Full, R., et al. (2018). The grand challenges of science robotics. *Sci. Robot.* 3:eaar7650. doi: 10.1126/scirobotics.aar7650
- Zambrano, D., Cianchetti, M., Laschi, C., Hauser, H., Fuchslin, R., and Pfeifer, R. (2014). “The morphological computation principles as a new paradigm for robotic design,” in *Opinions and Outlooks on Morphological Computation*, eds. H. Hauser, R. M. Fuchslin, and R. Pfeifer (Zurich: University of Zurich), 214–225.

Conflict of Interest: The authors declare that the research was conducted in the absence of any commercial or financial relationships that could be construed as a potential conflict of interest.

Copyright © 2020 Mazzolai, Tramacere, Fiorello and Margheri. This is an open-access article distributed under the terms of the Creative Commons Attribution License (CC BY). The use, distribution or reproduction in other forums is permitted, provided the original author(s) and the copyright owner(s) are credited and that the original publication in this journal is cited, in accordance with accepted academic practice. No use, distribution or reproduction is permitted which does not comply with these terms.



Design, Modeling, Control, and Application of Everting Vine Robots

Laura H. Blumenschein^{1*}, Margaret M. Coad², David A. Haggerty³, Allison M. Okamura² and Elliot W. Hawkes³

¹ Mechanical Engineering, Purdue University, West Lafayette, IN, United States, ² Mechanical Engineering, Stanford University, Stanford, CA, United States, ³ Mechanical Engineering, University of California, Santa Barbara, Santa Barbara, CA, United States

OPEN ACCESS

Edited by:

Barbara Mazzolai,
Italian Institute of Technology (IIT), Italy

Reviewed by:

Nabil Derbel,
University of Sfax, Tunisia
Mattia Gazzola,
University of Illinois at
Urbana-Champaign, United States

*Correspondence:

Laura H. Blumenschein
lhblumen@purdue.edu

Specialty section:

This article was submitted to
Soft Robotics,
a section of the journal
Frontiers in Robotics and AI

Received: 02 April 2020

Accepted: 29 October 2020

Published: 10 November 2020

Citation:

Blumenschein LH, Coad MM,
Haggerty DA, Okamura AM and
Hawkes EW (2020) Design, Modeling,
Control, and Application of Everting
Vine Robots.
Front. Robot. AI 7:548266.
doi: 10.3389/frobt.2020.548266

In nature, tip-localized growth allows navigation in tightly confined environments and creation of structures. Recently, this form of movement has been artificially realized through pressure-driven eversion of flexible, thin-walled tubes. Here we review recent work on robots that “grow” via pressure-driven eversion, referred to as “everting vine robots,” due to a movement pattern that is similar to that of natural vines. We break this work into four categories. First, we examine the design of everting vine robots, highlighting tradeoffs in material selection, actuation methods, and placement of sensors and tools. These tradeoffs have led to application-specific implementations. Second, we describe the state of and need for modeling everting vine robots. Quasi-static models of growth and retraction and kinematic and force-balance models of steering and environment interaction have been developed that use simplifying assumptions and limit the involved degrees of freedom. Third, we report on everting vine robot control and planning techniques that have been developed to move the robot tip to a target, using a variety of modalities to provide reference inputs to the robot. Fourth, we highlight the benefits and challenges of using this paradigm of movement for various applications. Everting vine robot applications to date include deploying and reconfiguring structures, navigating confined spaces, and applying forces on the environment. We conclude by identifying gaps in the state of the art and discussing opportunities for future research to advance everting vine robots and their usefulness in the field.

Keywords: tip-extending robot, soft robot, soft actuator, mechanism design, continuum robot, everting robot, vine robot

1. INTRODUCTION

Growth via tip extension is a form of movement seen in nature across scales and kingdoms, from single-cell pollen tubes (Steer and Steer, 1989) and micro-scale hyphae (Lew, 2011) to creeping vines (Weigel and Jürgens, 2002) and the proboscises of certain worms (Zuckerkindl, 1950; Gibson, 1977). Tip growth has recently been replicated in a variety of robotic systems, referred to as “growing robots” or “vine robots,” using a range of techniques. In addition to tip extension, vine robots are characterized by length change of many thousands of percent and control of their growth direction. We have worked extensively with one method for creating tip extension: pressure-driven “eversion” (i.e., turning inside out) of flexible, thin-walled material. We refer to robots that move in this way as “everting vine robots.”

In this paper, we review much of the existing work on everting vine robots. We discuss the tradeoffs in everting vine robot designs, including materials, actuation, and payloads. We describe the existing quasi-static, kinematic, and force-balance models of growth and steering, and the range of control strategies, from autonomous to teleoperated, that have been implemented. We also describe the important functions and wide range of application of everting vine robots. We conclude by identifying gaps in existing everting vine robot research and highlighting important opportunities for future research. While this paper focuses primarily on our research groups' work on everting vine robots, other groups have contributed to the everting vine robot literature, and their work is referenced throughout the paper where appropriate. Our website, www.vinerobots.org, shares everting vine robot designs and maintains a repository of relevant research.

2. GROWTH AND EVERSION

Vine robots move via tip extension, which is similar to some forms of biological growth and distinct from locomotion or other animal-like whole body movements. Whereas, movement strategies like locomotion are defined by translation of the body from one location to another (Alexander, 2003), movement by tip extension functions by lengthening the body (Goriely, 2017), reducing or completely eliminating the need to translate relative to the environment.

2.1. Bioinspiration

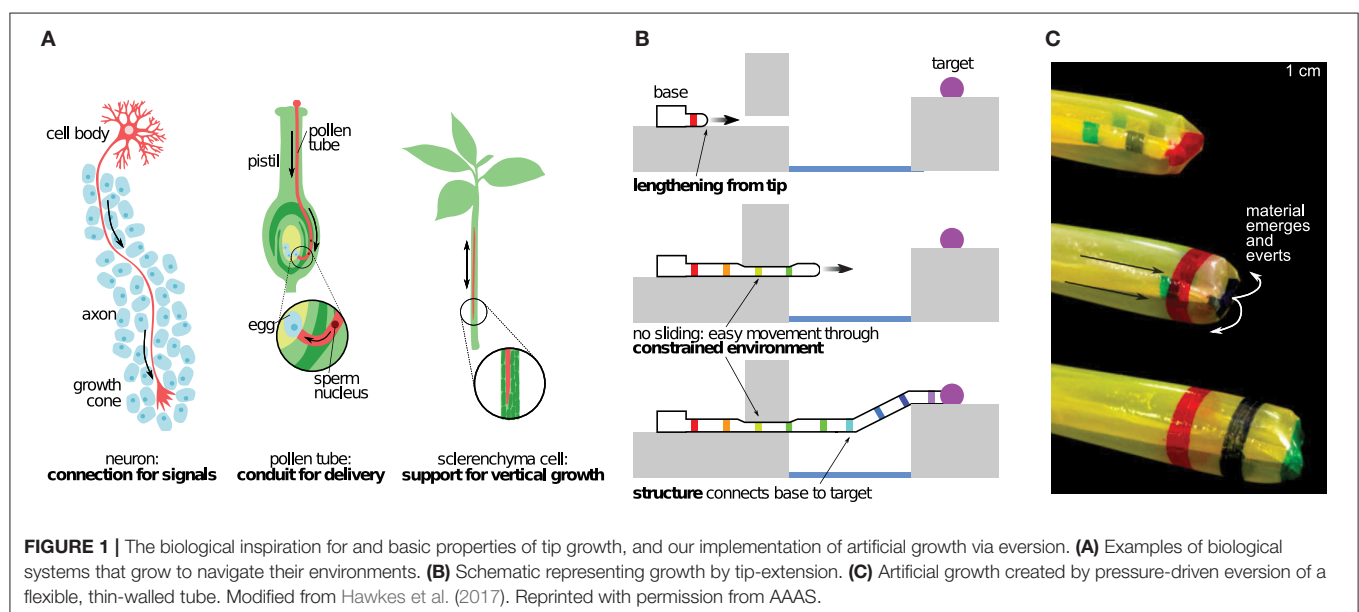
The term “growth” refers to a variety of phenomena found in nature, where organisms add mass to their forms. Depending on the exact function, this growth can be an increase in volume (bulk growth), in surface area (accretive growth), or in length (tip growth) (Goriely, 2017). Tip growth (Figure 1A) is often used

by systems with non-deterministic body forms to explore their environments and react to changing stimuli. This form of growth is used in nature by a wide variety of plants, animals, and cells to connect locations, deliver payloads, support construction, and more (Sanati Nezhad and Geitmann, 2013). During tip growth, new material is added only in a small region at the tip of a filament (Goriely, 2017). Neurons grow through constrained tissue to create structures that act as signal pathways (Dent and Gertler, 2003). Pollen tubes grow through pistil tissue to build conduits to deliver sperm to the ovary (Palanivelu and Preuss, 2000). Sclerenchyma cells grow within the xylem and phloem to create supporting structures (Sanati Nezhad and Geitmann, 2013). Tip growth is utilized across scales, ranging from the micron scale of fungal hyphae (Lew, 2011), to the millimeter scale of invertebrates that deploy invaginated appendages (Zuckerandl, 1950), to the centimeter scale of vines and plant roots (Weigel and Jürgens, 2002; Vaughn et al., 2011; Gerbode et al., 2012; Manca, 2018). Through tip growth, these organisms rely minimally on their past states, and instead can pursue evolving nutrient gradients without reconfiguring their bodies.

Such a mechanism for movement is a potentially rich source of bioinspiration in the field of robotics, due to its inherent ability to adapt to complex situations. While traditional robots are effective in controlled settings, and soft end-effectors enhance their ability to interact with a variety of objects, leveraging embodied intelligence for exploration and interaction with dynamic environments remains an open challenge.

2.2. Growth in Robots

Replicating elements of biological tip growth, henceforward referred to as “growth,” in robotic systems, i.e., vine robots, has two main benefits (Figure 1B). First, because only the tip moves, there is no relative movement of the body with respect to the environment. This means growth allows for easy movement



through constrained environments. Second, as the tip moves, the body forms into a structure in the shape of the tip's path, which can be used for payload delivery, force transfer or self-support, and physical construction. Unlike locomotion, which depends on the reaction forces and mechanical properties of the environment, growth allows vine robots to transfer forces through their bodies, back to their fixed base. Therefore, forces can be generated independent of the contact conditions between the robot tip and the local environment.

Several methods of creating vine robots have been explored thus far. Nested flexible continuum arms have been extended to resemble growth of thin filament structures without concentrating the growth to the tip (Wooten and Walker, 2015). Tip-localized 3D printing has been demonstrated to irreversibly build a robot structure much like in a plant root (Sadeghi et al., 2017). Stored material can be reversibly extended in a variety of ways to replicate the natural behavior of growth, including pulling a chain of rigid links from base to tip (Yan et al., 2019), pulling flexible material from base to tip (Tsukagoshi et al., 2011; Talas et al., 2020), and unreeling flexible material stored at the tip (Dehghani et al., 2017; Satake et al., 2020). Eversion is a particularly elegant method of imitating growth, and it is inspired by mechanisms found in some animals, like the extendable proboscises of certain worms (Zuckerandl, 1950; Gibson, 1977).

2.3. Eversion Growth

Eversion, the opposite of inversion, is the process by which the material internal to a structure turns inside out and becomes part of the outside of the structure. Eversion has been used in toroidal robots to create whole skin locomotion (Hong et al., 2009), imitating cytoplasmic streaming in amoebas, as well as to create a grasping behavior during inversion (Zhu et al., 2016; Li et al., 2020). Everting vine robots achieve growth through pressure-driven eversion of flexible, thin-walled material (Figure 1C). Unlike toroidal robots, which continuously recycle material, an everting vine robot holds one end of its body fixed, while internal pressure effectively pulls the material through the body to the other end. This material everts at the robot tip, resulting in an increase in length. By using pressure-driven eversion of pre-manufactured material, everting vine robots are able to achieve movement by growth to arbitrary lengths, at speeds equivalent to animal locomotion. Additionally, everting vine robots can continue moving even when encountering gaps smaller than their body diameter.

3. DESIGN

While the underlying principle of growth through pressure-driven eversion is shared by all everting vine robot designs, the implementation varies. These differences in design, produced by the choice of materials, growth and steering actuation methods, and payload deployment systems, result in different behaviors that must be carefully considered given a desired application.

3.1. Materials and Manufacturing

The materials available to manufacture the main body tube of an everting vine robot are confined to those that are inextensible

enough to produce eversion as opposed to radial expansion upon pressurization and that are both fluid impermeable and sealable, such that a closed pressure vessel can be developed. Everting vine robot manufacturing techniques are largely material and configuration dependent. While specific designs can necessitate complex and labor intensive manufacturing processes, most everting vine robots are constructed in few steps. In the simplest of cases, an everting vine robot can be constructed by sealing one end of a tube and inverting this sealed end inside the rest of the body (detailed instructions can be found at www.vinerobots.org). This section describes a variety of materials often employed in everting vine robot research and presents the manufacturing methods for each. A summary of these considerations is presented in Table 1.

3.1.1. Materials Overview

3.1.1.1. Thermoplastics

Thermoplastics are the easiest materials with which to prototype everting vine robots. These off-the-shelf films come manufactured in sheets or tubes, and the two main films used in everting vine robot construction have been low density polyethylene (LDPE) (Hawkes et al., 2017) and thermoplastic polyurethane (TPU). LDPE has an elastic strain limit on the order of 5% (Xu et al., 2016), while the elastic strain limit of TPU is on the order of 50% (Lee et al., 2009). These materials are lightweight, airtight, and inert with respect to most liquids. However, LDPE fatigues easily, often failing after a moderate number of repeated eversions (on the order of 10–50). LDPE is generally purchased in rolls of preshaped tube, and devices are constructed by simply cutting this tube to length and heat sealing the distal end. TPU, however, is often available only as a

TABLE 1 | Various materials used in everting vine robot designs, with their key behaviors and manufacturing methods.

Material	Key behaviors	Manufacturing method
Thermoplastics (LDPE, TPU)	Fastest prototyping Material uniformity Low burst pressure	Heat sealing/preformed
Thermosets (latex, silicone)	Slow prototyping Variable burst pressure Low hysteresis	Casting/preformed
Thermoplastic-coated fabrics (TPU-coated nylon)	Fast prototyping Moderate burst pressure Good structural characteristics	Heat sealing
Thermoset-coated fabrics (silicone-infused nylon)	Slow prototyping High burst pressure Lowest eversion friction Extensible/inextensible	Adhesives
Uncoated fabrics (ballistic nylon)	Slow prototyping High structural strength High eversion friction	Sewing with internal bladder Ultrasonic welding

Material choice presents tradeoffs in ease of manufacture, strength, stiffness properties, and actuation pressure.

film, so the film needs to be formed into a tube first, generally through heat sealing. Depending on the application, TPU may also need to be sheathed in a strain-limiting fabric to control radial expansion.

3.1.1.2. Thermosets

Some thermosets, like latex and silicone, can be used, though whether they primarily grow or strain depends on their modulus of elasticity and thickness. These materials are difficult to prototype with, often requiring a strain-limiting layer to evert properly. However, they do have very low hysteresis, and the burst pressure can be controlled by choosing the material stiffness. Thermoset everting vine robots can be manufactured from sheets of thermoset using latex or silicone adhesives or they can be directly cast from liquid silicone into the needed shape.

3.1.1.3. Coated fabrics (thermoplastic and thermoset)

More robust everting vine robots can be built from a variety of fabrics, the most common of which are fabrics coated to be airtight. Everting vine robots constructed from these fabrics can often withstand higher pressures and therefore loads, and they do not fatigue as easily as their plastic counterparts. The woven structure of fabrics also prevents the propagation of holes, thereby reducing the potential for catastrophic failure and allowing for continued operation, assuming the pressure source can provide sufficient airflow to overcome leaks. Thermoplastic-coated fabrics, like TPU-coated ripstop nylon (Coad et al., 2020a), improve the durability of everting vine robots over thermoplastics alone. However, they can suffer from delamination of the thermoplastic layer from the fabric at stress concentrations, resulting in leaks. Other coated fabrics used in everting vine robots include thermoset-coated fabrics, like the silicone-infused ripstop nylon used by Haggerty et al. (2019) and Naclerio and Hawkes (2020). These fabrics do not suffer from delamination but do require different manufacturing techniques than thermoplastics. Silicone-infused ripstop nylon additionally has a low self-friction and, therefore, a much lower required pressure to evert (section 4.1) compared to TPU-coated ripstop nylon, making it desirable for long or very small robots.

Everting vine robots made from coated fabrics are generally manufactured using adhesion methods specific to the coating. For thermoplastic-coated fabrics (e.g., TPU-coated ripstop nylon), the coating is generally on a single side, so the fabric is joined into a tube using an “abutted” joint, i.e., a joint where the single coated side of the material contacts itself. This joint can then be heat-sealed as described above for thermoplastics. For thermoset-coated fabrics (e.g., silicone-infused ripstop nylon), the fabric coating is double-sided, so a tube can be formed using the stronger “lap” joint, i.e., a joint where the opposite sides of the material touch, as described in Naclerio and Hawkes (2020). This joint can be sealed using silicone-based adhesives with light pressure application to ensure a continuous bead of adhesive between the two layers of fabric. The end of the tube can be sealed using a similar method or knotted closed.

3.1.1.4. Uncoated fabrics

Uncoated fabrics, like ballistic nylon, are not airtight, but they have many of the desirable properties of coated fabrics and

can be used as a shell for thermoplastic everting vine robots to greatly increase their structural strength. Ballistic nylon was demonstrated in this form-factor for a soft robot without growth in Usevitch et al. (2020). To manufacture an everting vine robot with an uncoated fabric layer, matching tubes of fabric and an airtight layer like thermoplastic (TPU or LDPE) are manufactured. The fabric does not need to be airtight, so it can be sewn together with an abutted seam. An additional seam sewn at the distal end of the robot, passing through the fabric and through the airtight bladder beyond the end seal, can be used to join the two layers. While not necessary, spray adhesive can also be used to form a bond between the two layers along the full length.

3.1.2. Material Extensibility

In addition to the specific class of material, an important design consideration across material type is material extensibility. Soft robotics generally is concerned with using selective strain to produce a specified behavior; soft grippers and crawlers are prime examples of this (Rus and Tolley, 2015; Lee et al., 2017). While early work on everting vine robots exclusively used nearly inextensible materials (Hawkes et al., 2017), later work has investigated the novel behaviors and challenges that come with varying the strain properties of everting vine robot material.

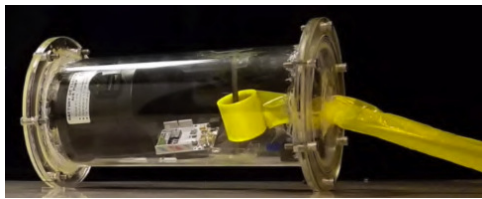
Inextensible materials produce relatively high axial stiffness in everting vine robots, enabling everting vine robots to create self-supporting structures and carry payloads. Everting vine robots made with inextensible materials have been used for reconfigurable antennas (Blumenschein et al., 2018a), haptic wearables (Agharese et al., 2018), and manipulators (Stroppa et al., 2020). As shown in Hammond et al. (2017) and Haggerty et al. (2019), assuming inextensibility can simplify modeling (section 4.1). However, high axial stiffness also means that relatively high forces must be applied to bend or buckle the robot body. This can limit the applicability of these everting vine robots in navigation tasks where environmental contact aids in steering but applied forces must be minimized.

Using body materials with directional extensibility allows everting vine robot stiffness to be varied along different axes. Directional extensibility can be created in thermosets using strain limiting layers, and woven fabrics naturally have a “bias,” i.e., unequal strain along different axes relative to the fabric weave or “grain.” Ripstop nylon in particular has nearly no strain in the direction of the fibers but can strain up to 20% along the 45°-axis (Naclerio and Hawkes, 2020). Everting vine robots made out of silicone-infused ripstop nylon exchange high axial stiffness, when the fabric grain is along the robot body’s axis (the “unbiased” orientation), for high torsional stiffness, when the fabric bias is along the robot body’s axis (the “biased” orientation). However, the fact that extensible materials reduce everting vine robot stiffness along at least one axis limits the ability of such robots to create self-supporting structures and apply force in certain directions.

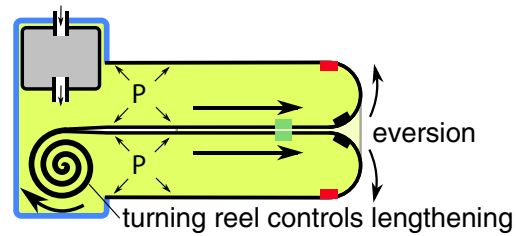
3.2. Actuating Length Change

Actuation of length change can be considered in two parts: growth, or increasing in length, and retraction, or decreasing in

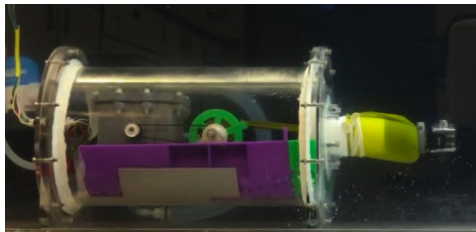
A Growth to Arbitrary Lengths



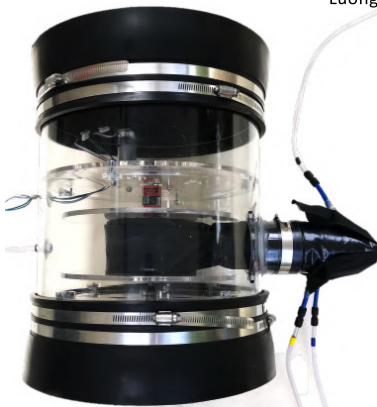
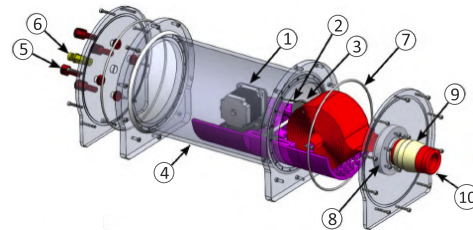
Hawkes et al. (2017)



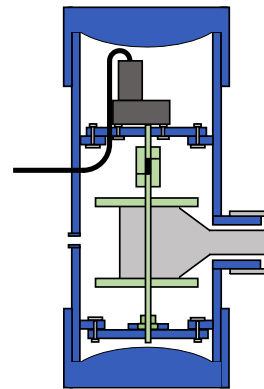
B Retraction



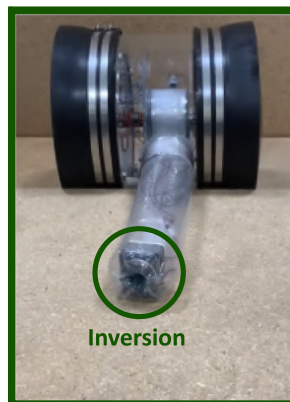
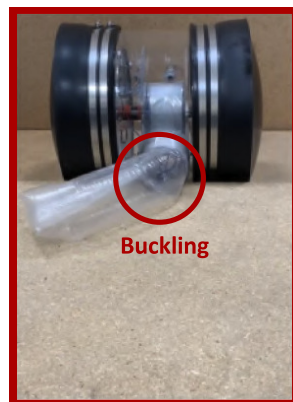
Luong et al. (2019)



Coad et al. (2020a)



c Retraction without Bending/Buckling



Coad et al. (2020b)

Soft Robot Body with Device

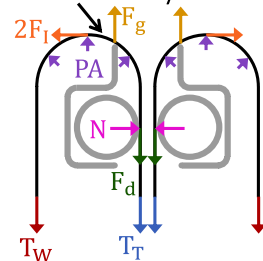


FIGURE 2 | Designs for actuating length change of everting vine robots. **(A)** Storing robot body material on a spool in the base allows growth to arbitrary lengths. **(B)** Reversing the spool direction with a motor allows retraction after growth. **(C)** Adding a retraction device at the robot tip allows retraction without undesired bending or buckling of the robot body. Modified from Hawkes et al. (2017). Reprinted with permission from AAAS. Modified from Luong et al. (2019) © IEEE 2019, Coad et al. (2020a) © IEEE 2020, and Coad et al. (2020b) © IEEE 2020.

length, both from the tip. Designs for actuating length change are shown in **Figure 2**.

3.2.1. Growth

Everting vine robot growth is driven by a higher fluid pressure inside the robot body relative to the outside. As growth occurs, the “tail” material travels within the robot body, everts at the robot tip, and becomes part of the robot body wall, i.e., the outer part that moves neither away from nor toward the base.

Depending on the amount of length change that is desired in an everting vine robot, there are two common methods of storing the robot body material before it is everted at the tip. An everting vine robot that doubles in length can be achieved by creating a closed tube of robot body material with a pressure inlet at one end. The tube can be inverted on itself and shortened to half its original length while storing the tail straight inside.

When length change of more than 100% is desired, the robot tail must either be stored in a more compact form or outside the pressurized area of the robot body. Thus far, everting vine robots that store their tail material outside the pressurized area have not been demonstrated in the literature, due to the difficulty of developing an airtight seal through which the tail material can slide during growth, but several everting vine robots have been demonstrated that store the robot tail rolled up on a reel, allowing growth to arbitrary lengths, only limited by the amount of material stored. Hawkes et al. (2017) demonstrated one implementation of this reeled everting vine robot design, where a pressure chamber, the base, was used as a rigid grounding point to attach the robot body wall and a reel of tail material (**Figure 2A**). Using this design, the robot was demonstrated to grow from a package the size of the base (28 cm) to 72 m long. Provided the base is able to hold pressure needed to grow, the robot length can be scaled arbitrarily.

3.2.2. Retraction

In contrast to growth, in most cases retracting an everting vine robot cannot be accomplished by simply decreasing the relative pressure between the inside and the outside of the robot body. To achieve retraction of the robot body, a force must be exerted on the tail to pull it toward the base while a moderate level of pressure is maintained in the body. Luong et al. (2019) and Coad et al. (2020a) implemented everting vine robot versions where a motor drives the reel in the base, allowing not only control of the material release for growth but also reeling in the material for retraction (**Figure 2B**).

While this method of retraction works well in a highly constrained environment, everting vine robots retracted in free space tend to bend or buckle into an uncontrollable shape before shortening in length. This uncontrolled behavior, studied in Coad et al. (2020b), is due to the discrepancy between the critical loads for bending or buckling, which are dependent on length, and the force required to invert the material, which is independent of length (see section 4.1 for more discussion of these forces). Thus, above a certain length, an everting vine robot will always bend or buckle rather than retract in a controlled manner. To avoid this problem, Coad et al. (2020b) developed a retraction device (**Figure 2C**), which sits inside the robot tip and applies the force required to retract the robot body directly to the robot

tip, thus making bending or buckling during retraction effectively impossible. When using a retraction device, a motorized reel in the base is still useful to keep slack from building up in the tail and to store the robot body, but the amount of tension on the robot tail can be kept to a minimum (see section 5.1.1).

3.3. Actuating Growth Direction

Achieving a desired task with an everting vine robot is often dependent on the ability to dictate the growth direction and the robot shape as it grows and retracts. Here we summarize the different designs investigated to achieve this, while control aspects of everting vine robot steering are discussed in section 5.1.2.

Steering the everting vine robot body presents a design challenge, since the robot body can grow arbitrarily long. For some applications, the grown length may be less than a meter, while for others, the everting vine robot will be over 10 m in length when in use. Specific design considerations include: the number of actuation inputs needed to sufficiently control the robot shape, the acceptability of uncontrolled robot movements, the scaling of actuator magnitude and speed with the length of the system, and the use of the environment to decrease the required actuation inputs. These design considerations do not have universal answers and often result in application-specific solutions. Generally, actuating growth direction functions by changing the relative length of material on opposite sides of the flexible, thin-walled tube, i.e., shortening or lengthening a side of the tube. **Figure 3** shows four different methods of steering everting vine robots, all of which locally shorten or lengthen the robot body material on one side compared to its original length.

3.3.1. Distributed Strain Actuation

One actuation method for steering everting vine robots uses actuators that contract uniformly along their length, so that a single input can uniformly curve the entire robot body. Soft pneumatic actuators are the primary examples of this type of actuation, since the actuator can be long enough to match the full robot length and its compliance allows them to evert with the robot (**Figure 3A**). All the distributed strain actuators used thus far have been limited in their maximum strain. We quantify this strain using the metric of contraction ratio, defined as the ratio of the difference between shortened and fully extended length to the fully extended length.

Inverse pneumatic artificial muscles (IPAMs), first demonstrated in Hawkes et al. (2016) and used in Zhu et al. (2020) to create fabric muscle sheets, are constructed using a cylindrical rubber bladder enclosed by a strain limiting layer. This layer forces the bladder to expand lengthwise, not radially, when pressurized. IPAMs have been attached to everting vine robots by sewing them into the fabric of the body. Because IPAMs extend at high pressure and contract at low pressure, the robot body needs to be shortened when attaching the IPAMs. Blumenschein et al. (2018a,b) used IPAMs to create helical actuation. Even though these actuators have relatively high maximum contraction ratio (75% was reported in Hawkes et al., 2016), it is difficult to attach IPAMs to an everting vine robot in a way that distributes the strain equally, leading to unpredictable robot shapes.

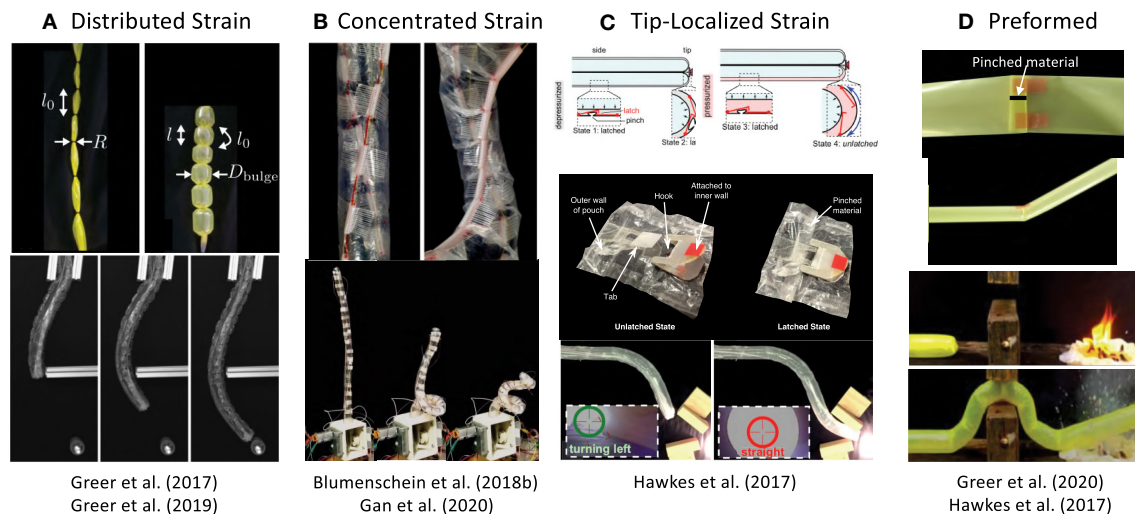


FIGURE 3 | Methods of actuating everting vine robot growth direction and shape, including (top) actuation principles and (bottom) examples of implementation. **(A)** Distributed strain uses pneumatic artificial muscles to create strain along the length where they are attached. **(B)** Concentrated strain uses tendons actuated from the base to change the robot shape. **(C)** Tip-localized strain couples steering and growth to create responsive steering at the tip only. **(D)** Preformed steering shapes the robot for known tasks before deployment. Modified from Greer et al. (2019). The publisher for this copyrighted material is Mary Ann Liebert, Inc. publishers. Modified from Greer et al. (2017) © IEEE 2017, Blumenschein et al. (2018b) © IEEE 2018, and Gan et al. (2020) © IEEE 2020. Modified from Hawkes et al. (2017). Reprinted with permission from AAAS. Modified from Greer et al. (2020).

Unlike IPAMs, both series pneumatic artificial muscles (sPAMs) and series pouch motors (SPMs) shorten when pressurized, making them easy to attach uniformly to an everting vine robot in their unactuated state. These actuators are constructed by creating either radial (sPAMs) or flat (SPMs) constrictions at regular intervals along the length of a tube of airtight, inextensible material. A small space for airflow is allowed through the constriction, yielding a series of small interconnected bubbles or pouches (Niiyama et al., 2015), which shorten lengthwise as they balloon out radially during pressurization. SPMs have a lower maximum contraction ratio than sPAMs [20 vs. 40%, respectively (Greer et al., 2017)], but they are easier to construct and attach to everting vine robots, making them more practical for very long systems. Greer et al. (2017, 2019) demonstrate an everting vine robot steering with 1–2 m long sPAMs, while Coad et al. (2020a) shows steering with 7–10 m long SPMs in a system deployed in the field. The constrictions inherent in these actuator designs can cause drawbacks. They result in high internal fluidic resistance, leading to noticeable time delays in actuation of the more distal segments of a long robot, and they lead to stress concentrations, making the actuators fatigue upon repeated pressurization and depressurization.

Fabric pneumatic artificial muscles (fPAMs) are similar to sPAMs and SPMs but remove the high fluidic resistance. fPAMs are constructed using the bias stretching fabric described in section 3.1.2 formed into a tube with the bias direction oriented along the length of the actuator. When pressurized, fPAMs expand radially and shorten in length, similar to a McKibben actuator (Gaylord, 1958; Geddes et al., 1959). fPAMs were demonstrated in Naclerio and Hawkes (2020) and Selvaggio et al.

(2020) to steer everting vine robots. They have a slightly lower maximum contraction ratio (30% was reported in Naclerio and Hawkes, 2020) than sPAMs, but also show very little hysteresis.

3.3.2. Concentrated Strain Actuation

An alternative to distributed strain actuation is concentrated strain actuation. In this category, the actuation comes entirely from the base of the robot instead of distributed along the length, and the actuators are attached only at discrete points on the robot. Generally, concentrated strain actuation has been achieved through tendons routed along the surface of the pressurized tube and pulled by DC motors.

Unlike the pneumatic artificial muscles described in the previous section, actuation using tendons is not inherently strain limited, so tendons can achieve much more dramatic steering. However, the decrease in local stiffness that comes after the onset of local wrinkling of the robot body material (He and Chen, 2014), in addition to the friction that exists in the tendons, means bending due to tendon actuation will concentrate in a single location. This type of actuation was used in Stroppa et al. (2020) to create an approximation of a spherical joint at the base of a growing robot manipulator.

Having all the bending concentrated at a single point can limit the usable actuation scenarios, so other tendon actuation designs include a limit on the local bending. In Blumenschein et al. (2018a,b), Gan et al. (2020), and Wang et al. (2020) this was accomplished through physical hard stops placed along the tendon's routed path on the surface of the tube (**Figure 3B**). This feature creates a “traveling wave” of bending, with the point most proximal to the base bending first, followed by more distal points as the hard stops connect. While actuating from the base

in this way is not generally a better method for steering the tip compared to distributed curvatures from pneumatic artificial muscles, tendon actuation with hard-stops has been used to create complex, well-defined shapes like helices (Blumenschein et al., 2018b) and self-knotting paths (Blumenschein et al., 2020).

3.3.3. Tip-Localized Strain Actuation

The previous two actuation methods show the ability to steer the everting vine robot body independent of growth, so the robot shape can be changed either while at a set length or while growing. However, in these previous methods, more distal portions of the robot body can only be actuated if more proximal sections of the body are as well, limiting the shapes that can be produced. Adding more independently actuated segments along the length of the robot body is possible, but this increases control and design complexity and does not scale well with length. If independent steering control along the full length of the robot as it grows is desired, the robot can instead be actuated by coupling the steering to the growth through tip-localized strain actuation. This has been previously accomplished using preloaded strain that can be released only at the tip, as demonstrated in Hawkes et al. (2017). Mechanical latches hold preloaded strain and can be unlatched when they reach the tip by pressurizing pockets that run along the entire length of the robot (**Figure 3C**). This couples the steering to the growth, and, as a result, minimizes the actuation signals needed to achieve complex shapes. In 2D, two pressure signals are sufficient to fully shape the robot. A more recent implementation of this actuation method used tensioned strings to pre-load the actuation and servos mounted at the tip to cut the strings as the everting vine robot grew (Cinquemani et al., 2020).

3.3.4. Preformed Actuation

While all the previous actuation strategies created actively controlled robot shapes, active shape change is not needed for some applications. In these cases, the robot body can be preformed into the desired final shape before it grows. Two methods have been developed for preforming everting vine robots. In Slade et al. (2017) and Agharese et al. (2018), the robot was shaped by heating the thermoplastic body material (LDPE) while it was stretched over molds of the desired shape. This allowed the material to be heat-set and maintain the shape of the mold once removed, creating smoothly varying shapes. Pinching the body material at discrete points and holding the pinches with pieces of tape creates a similar effect but with discrete turns (Hawkes et al., 2017), which can be seen in **Figure 3D**.

3.3.5. Passive Environment Steering

In addition to creating steering actuation, there are various methods to modify existing actuation, one of which is using the environment to help steer the robot. Everting vine robots can passively adapt to their environment, reaching different final shapes than they would have without environment constraint. Early results of this effect are shown in Hawkes et al. (2017). The compliance and growth behavior of everting vine robots allow them to easily deform around obstacles and follow natural pathways in their environment. Passive steering using the

environment was further demonstrated, with heuristic modeling, in Greer et al. (2018). This model was used to design for intentional passive deformations of preformed everting vine robots in Greer et al. (2020) (**Figure 4A**). The modeling and planning associated with using passive deformation for steering, including using passive deformation with active distributed steering (Selvaggio et al., 2020), will be discussed in sections 4.2 and 5.3.

3.3.6. Stiffness Change

Stiffness change gives a second method of modifying actuation of growth direction and robot shape. As discussed for concentrated strain actuation (section 3.3.2), the local stiffness of inflated tubes rapidly decreases where local wrinkling occurs. Actively increasing the stiffness of the pneumatic tube has recently been investigated to modify this behavior. These designs follow the same considerations as steering actuation: design that minimize the number of control signals and while being scalable with length and remaining flexible enough to allow growth.

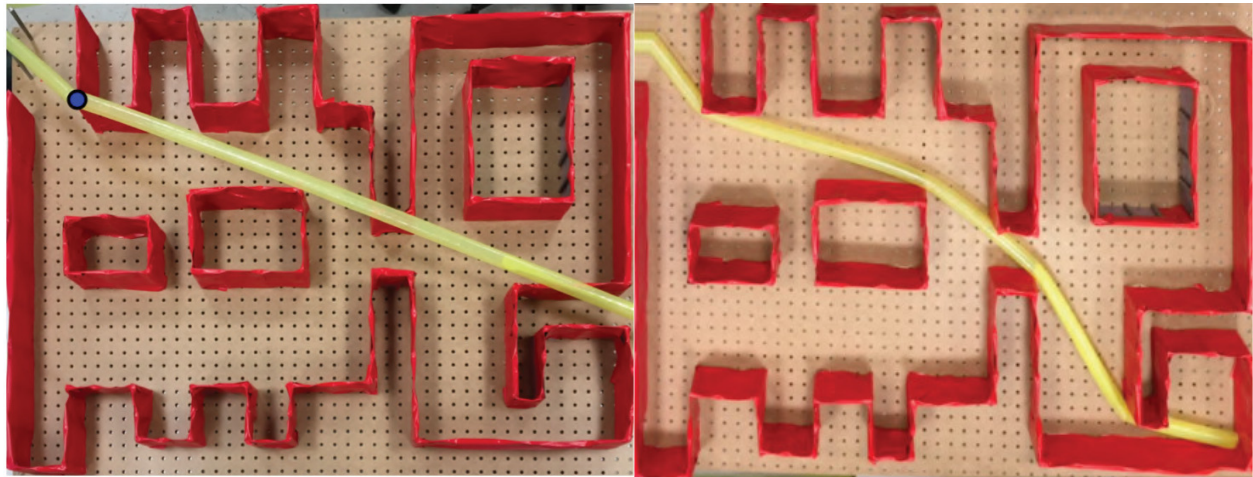
Vacuum jamming, i.e., using the frictional forces between particles, lines, or sheets of material to increase the apparent stiffness (Kim et al., 2013), is one method to change stiffness in soft robotic systems. For everting vine robots, Do et al. (2020) showed an implementation of layer jamming that can be used to modify the bending and buckling behavior under concentrated-strain actuation (**Figure 4Bi**). The passive valves maintain the pressure state of the layer jamming sections and a device traveling inside the everting vine robot body switches the states of those valves (see section 3.4.3 for more discussion of devices inside the robot body).

Stiffness change can also be used to lock previous actuation as the everting vine robot grows, allowing complex robot body shapes to be actuated with only a few actuators. This behavior was achieved in 2D in Wang et al. (2020) using channels on either side of the everting vine robot. Smaller everting vine robots were grown and retracted within these side channels, locking the actuation state of the proximal section of the robot body due to the added friction between the channels and smaller everting vine robots. The distal section of the robot remained steerable via concentrated-strain actuation (**Figure 4Bii**). This stiffness change design produces behavior similar to that of tip-localized strain actuation, but with the additional ability to reversibly actuate the movement of the distal portion of the robot body.

3.4. Mounting Sensors and Tools

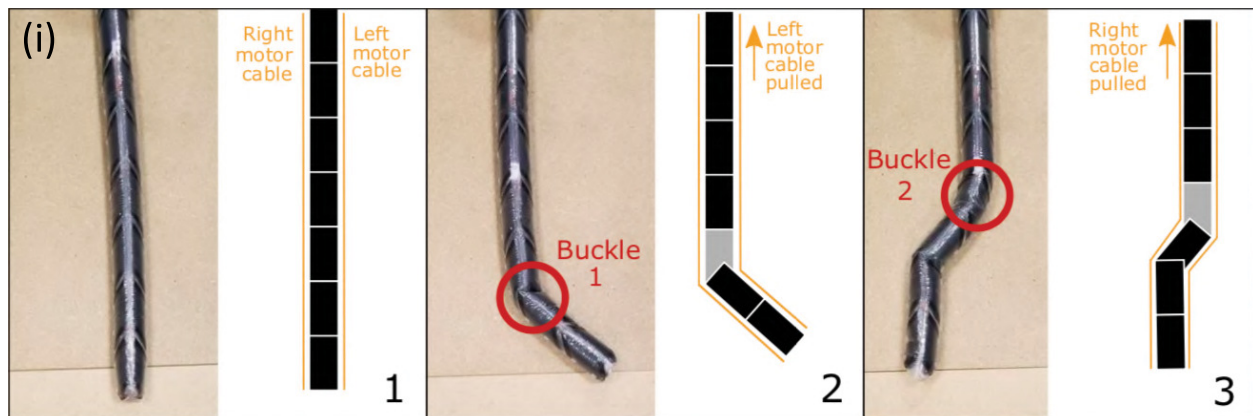
Many applications of everting vine robots are made possible by mounting sensors and tools on the robot body and using the robot's movement to transport them through the environment or to reconfigure their shape. Five locations for mounting sensors and tools have been explored thus far and are shown in **Figure 5**. For some mounting locations, the sensors and tools are fixed to the material of the robot body, and for others, they move in a way that is linked to the robot's movement, but they are not fixed to its material. Key considerations

A Modifying steering through obstacle interaction



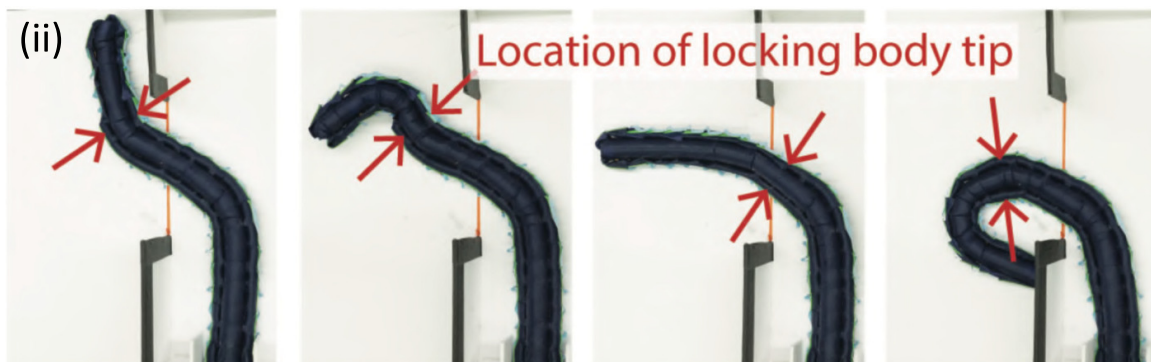
Greer et al. (2020)

B Modifying steering through stiffness change



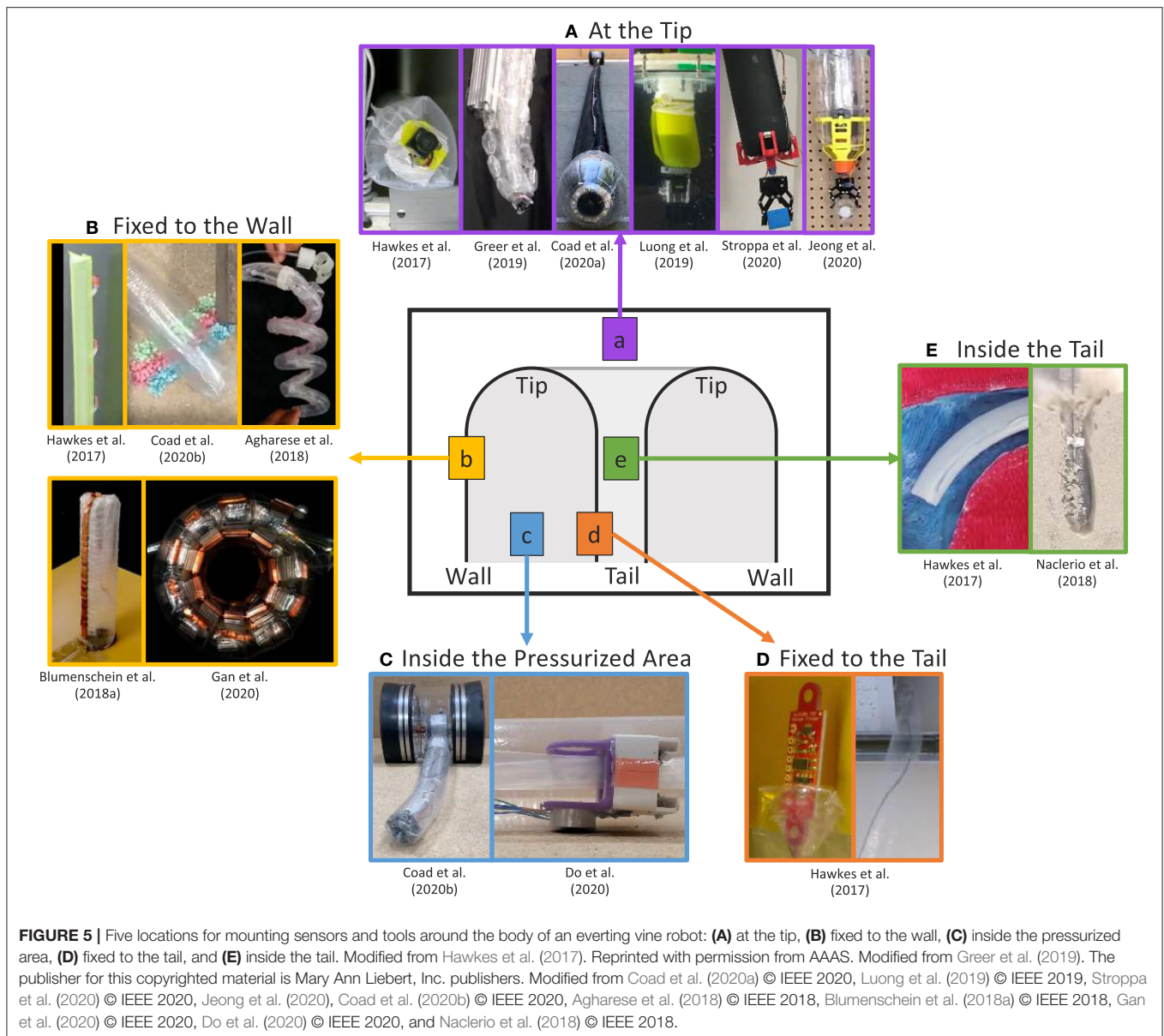
■ Stiffened sections ■ Compliant sections

Do et al. (2020)



Wang et al. (2020)

FIGURE 4 | Methods for modifying steering and shape of everting vine robots apart from actuation. **(A)** Steering can be modified by obstacle interaction, where the robot passively conforms to its environment as it grows. **(B)** Steering can also be modified by changing the body stiffness. **(B,i)** Increasing the stiffness of sections through layer jamming allows control of the wrinkling point under tendon actuation. **(B,ii)** Side tubes can be used to shape-lock previous actuation, allowing steering of the tip only and formation of compound curves. Modified from Greer et al. (2020), Do et al. (2020) © IEEE 2020, and Wang et al. (2020) © IEEE 2020.



when choosing a mounting location include: how and where sensors and tools need to interact with the environment and how placement will encumber the movement of the everting vine robot.

3.4.1. At the Tip

Because the tip of an everting vine robot is often the first point to enter a new space, this is an important area to mount sensors and tools that interact with the environment (**Figure 5A**). Sensors mounted at the robot tip, such as a camera (Hawkes et al., 2017; Greer et al., 2019; Luong et al., 2019; Coad et al., 2020a), can be used to sense properties of the environment and to provide feedback of the robot state during navigation and exploration. Meanwhile, tip-mounted tools, such as a gripper (Jeong et al.,

2020; Stroppa et al., 2020), enable environment interactions, such as picking up objects and pulling on the environment.

Mounting to the robot tip is challenging, since the specific section of robot body material at the tip continually changes during eversion and inversion. Thus, a tip mount must move relative to the robot body material, not merely be adhered to the material. Jeong et al. (2020) analyzed the various tip mount designs that have been developed and defined design principles for successful tip mounts. The methods by which sensors and tools have been attached to the tip include: cables inside the tail (Mishima et al., 2006; Hawkes et al., 2017; Greer et al., 2019), friction with the wall (Coad et al., 2020a), magnets (Luong et al., 2019; Stroppa et al., 2020), and rolling interlocks (Jeong et al., 2020). Many of these tip mount designs use parts both outside the robot body and inside the pressurized area at the robot tip

to stay attached. Wire management is also a challenge because wires must move relative to the robot's body. Luong et al. (2019) showed a wireless tip mount, but previous solutions to manage wired connections have consisted of wires inside the robot tail (Hawkes et al., 2017; Greer et al., 2019) and external wires with a self-sealing zipper pocket to avoid snagging on the environment (Coad et al., 2020a). Mounting at the tip involves a tradeoff between reliable attachment and encumbrance of the everting vine robot's natural ability move through confined spaces. The sensors, tools, and mounting methods can also add large or heavy elements at the robot tip, limiting the everting vine robot's ability to support its own weight, pass through small apertures, and move relative to the environment without friction.

3.4.2. Fixed to the Wall

Another method to directly place sensors and tools in contact with the environment is fixing them to the robot body wall (Figure 5B). This location is well-suited for mounting items that are deployed during growth or that need to interact with the environment along the entire length of the robot body, although anything mounted must be flexible enough or small enough to be everted and inverted along with the robot body material. While this location can be useful for some sensing applications, many of the demonstrated designs have mounted non-traditional robot payloads to the robot body wall. Adhesive patches attached to the outside of the body can be used to grip the environment, in one case to provide additional support when climbing vertically (Hawkes et al., 2017) and in another to takes samples of the environment (Coad et al., 2020b). Items attached to the body can also be deployed and shaped by the robot. Agharese et al. (2018) shows deployment of soft haptic actuators, and Blumenschein et al. (2018a) and Gan et al. (2020) show deploying and shaping segmented antenna pieces in order to form functional devices.

3.4.3. Inside the Pressurized Area

Items that do not need to interact physically with the environment can be mounted inside the pressurized area of the robot body (Figure 5C). The structure of the robot body acts as a pathway which can be traveled independent of the growth of the robot and without contacting the environment. The physical separation from the environment means mounting inside the pressurized area is best suited for sensors and tools used to interact with the robot body itself, or those that can interact with the environment in a non-contact fashion. This mounting location was used in Coad et al. (2020b) to attach the retraction device (section 3.2.2), which applies force to the robot tail to retract the robot body after growth. Similarly, Do et al. (2020) demonstrated a motorized carriage device moving internal to the robot to carry an electromagnet. Wired transmission of power from the base helps reduce device weight. As with wires passed to tip mounts, these wires must span a changing length as the device moves along the robot, so the wires should be managed to keep them taut while reeling them in or out as needed. Mounting inside the pressurized area does not require an active carriage device, as friction with the tail can passively keep devices at the tip during growth. Watson and Morimoto (2020) used this method

to keep a ring magnet at the tip of a millimeter-scale everting vine robot for tip-localization.

3.4.4. Fixed to the Tail

Due to eversion, the robot tail moves at twice the speed that the robot tip moves relative to the base. Mounting sensors and tools to the robot's tail is therefore a useful way to transport items between the robot base and the tip, using the growth and retraction of the robot itself (Figure 5D). Items fixed to the inside of the tail can contact the environment once that portion of the tail reaches the robot tip; rather than becoming part of the wall, the items may be deployed into the environment or reach the tip at the fully grown robot length. Hawkes et al. (2017) used this mounting location to demonstrate delivery of items from the robot base to the robot tip during growth through difficult environments. A sensor packaged safely inside the tail was protected from environmental hazards until the very end of growth when it was deployed out into the environment, and a wire was tied to the robot tail and pulled through the inside of the robot body, easily routing the wire through a confined space. The main disadvantage of this mounting location is that the robot length when the payloads will reach the tip is fixed at the time of manufacture. Either the desired final robot length must be known before launching the robot or it must be determined through trial and error.

3.4.5. Inside the Tail

To overcome the disadvantages of fixing payloads to the tail, sensors and tools can be mounted inside, but not fixed to, the robot tail (Figure 5E). Using this mounting location, items can be passed from the base to the tip such that some part of them stays continually at the tip during growth and retraction. As mentioned in the previous subsection, the robot tail and the robot tip move at different speeds relative to the base, so the payload must slide within the robot tail to remain at a desired location. If the everting vine robot material is not stored on a reel, this can be achieved by leaving the end of the tail partially unsealed so that items can pass from outside the base through the tail. However, the internal pressure used to grow the robot will cause the tail to naturally squeeze anything inside it, so some way to balance the pressure, like sending a steady stream of air through the tail, is needed to allow sliding of items inside the tail. Hawkes et al. (2017) used this mounting location to pass a tool through the robot body from base to tip in a demonstration of a medical procedure, while, Naclerio et al. (2018) passed a tube through the tail to the robot tip to send compressed air to fluidize a granular environment and allow the robot to grow through it with ease. While mounting inside the tail is good for passing items through the robot body to the outside of the robot tip, also storing the robot body material on a reel in the base is impossible, because of the need for relative movement between the tail material and the items inside the tail. This provides incentive to find other methods of storing the robot body material compactly when not in use. Additionally, maintaining the appropriate relative speed of movement between the tail material and the items inside such that part of the items remains at the tip is challenging. The items inside the tail need to be pulled toward the base during

growth and pushed away from the base during retraction (not yet demonstrated in the literature).

4. MODELING

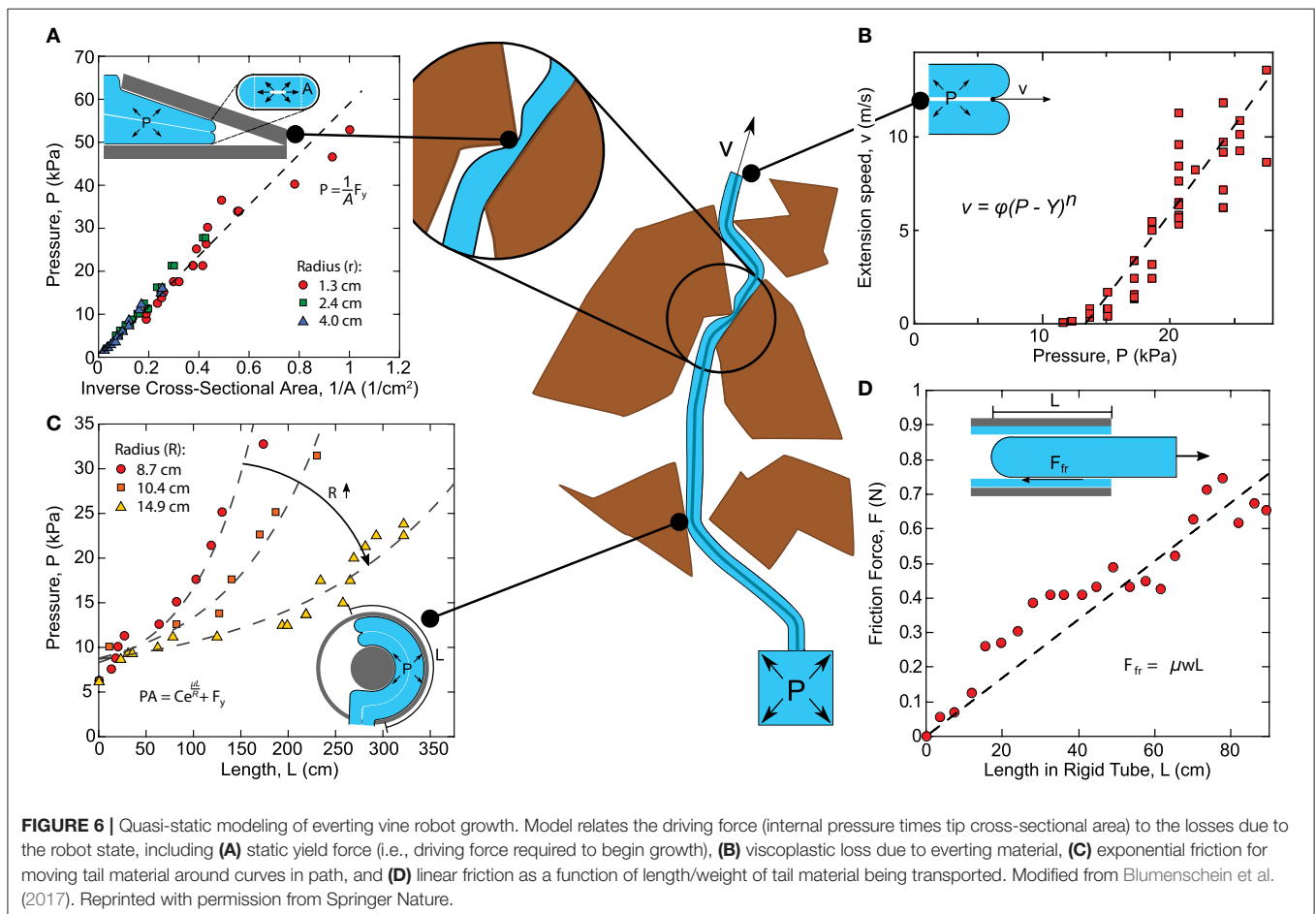
As with many soft robots, everting vine robots present specific challenges for modeling, and even more so because growth is such a unique form of movement. As a result, models for growth and steering of everting vine robots draw inspiration from a variety of sources, including models of other soft robotic systems and models of naturally occurring growth and steering. Even though the method of growth through eversion is unlike many natural systems, the mathematics of biological growth as seen in the literature (Goriely, 2017) has a close link to the models of growth that describe everting vine robots, and the principles that describe how a plant shapes itself, for example, how a cucumber tendril forms a helix (Gerbode et al., 2012), closely relate to the understanding of how differential shortening allows everting vine robots to form similar shapes (Blumenschein et al., 2018b). Section 4.1 outlines the quasi-static analyses conducted to generate models of growth (Figure 6), as well as bending and buckling due to growth into obstacles and due to retraction (Figure 7). Section 4.2 describes the kinematic and force-balance

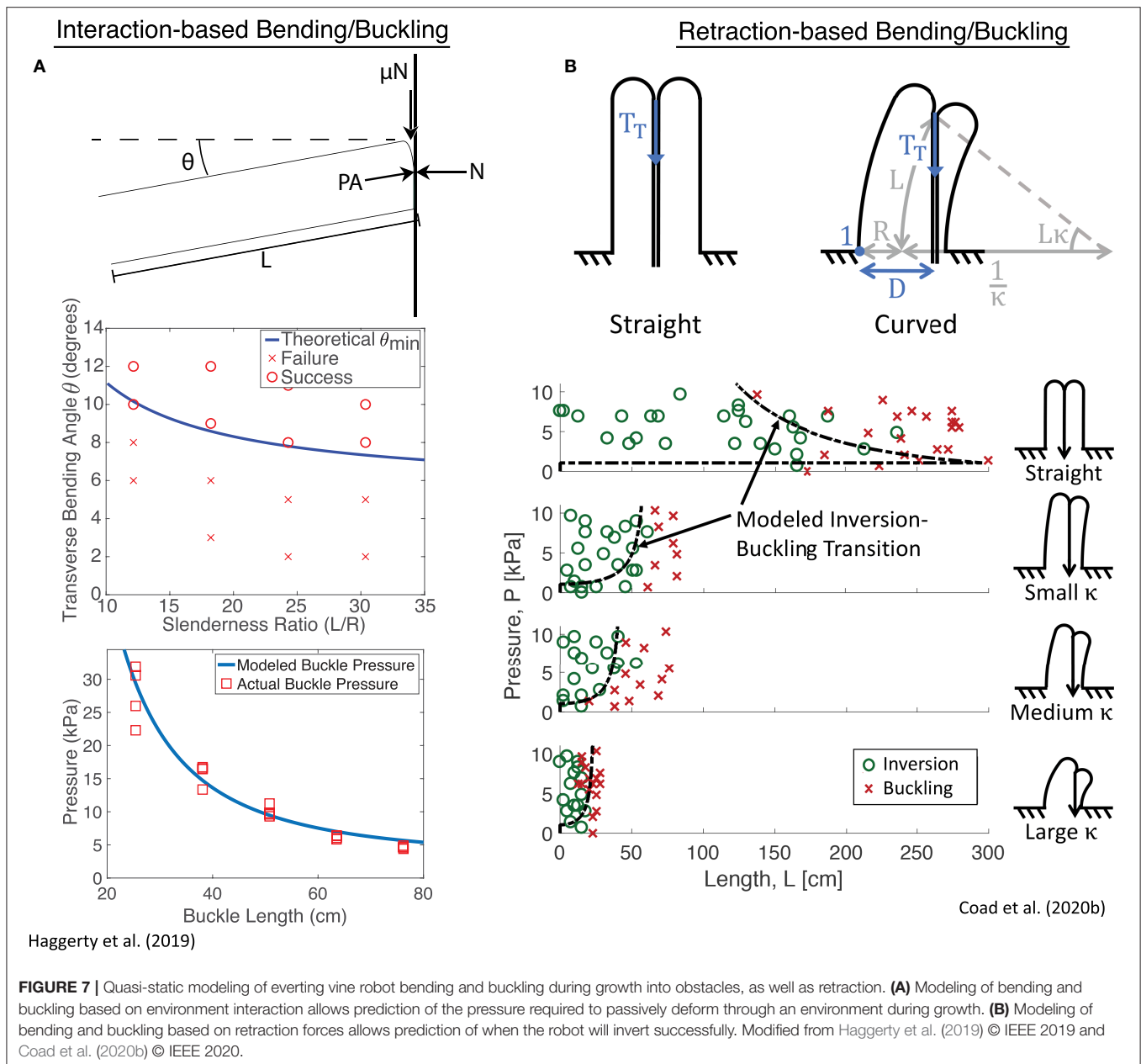
modeling employed to predict robot shape due to both active and passive steering (Figure 8).

4.1. Modeling of Growth

An important portion of everting vine robot modeling has focused on understanding everting vine robot growth and retraction, including the forces at play due to interaction with the environment. Thus far, these models have all been limited to quasi-static analyses, i.e., those that neglect dynamics. Many of the analyzed movements were slow enough that dynamics could be discounted, but faster growth movements have also shown negligible inertial effects.

Blumenschein et al. (2017) showed a quasi-static model for growth via pressure-driven tip eversion based on an equilibrium force balance (Figure 6). The model equates the driving force, i.e., the internal pressure multiplied by the tip area, to internal losses. The losses break down into two categories: losses associated with transporting material from the base to the tip, and losses associated with everting new material at the tip. Material transport is dominated by the frictional interaction of the everting vine robot material with itself, due to the weight of the tail material (Figure 6D), and the tension of the inner material being pulled around curves (i.e., the capstan equation,





see Lubarda, 2014) (Figure 6C). At the tip, Hawkes et al. (2017) show experimentally that eversion losses closely match the viscoplastic behavior of other pressure-driven growing systems (Figures 6A,B), like the expansion of plant cells (Green et al., 1971) or deployment of invertebrate proboscises (Zuckerandl, 1950), with a yield force (i.e., a minimum driving force to begin growth) and a viscous damping as a function of growth speed, with negligible inertial effects. This model allows the user to predict whether growth will occur, and at what speed, given the pressure and robot geometry.

Naclerio et al. (2018) and Haggerty et al. (2019) expand on this model by adding the effects of external forces from the environment. In Naclerio et al. (2018), the model was specifically

adjusted to account for the resistive forces of the sand on growth during burrowing. Haggerty et al. (2019) focused more broadly on the environmental interaction forces that passively steer an everting vine robot while navigating a cluttered environment through self-buckling or self-bending (section 3.3.5). Simple geometric and pressure dependent models predict bending and buckling for everting vine robots (Figure 7A), largely informed by existing bending and buckling models for inflated beams (Comer and Levy, 1963; Fichter, 1966; Le-van and Wielgosz, 2005). Godaba et al. (2019) further considered the buckling and bending loads to determine payload capabilities, and Putzu et al. (2018) looked into the relationship between force applied to the robot tip in compression and the robot's growth speed.

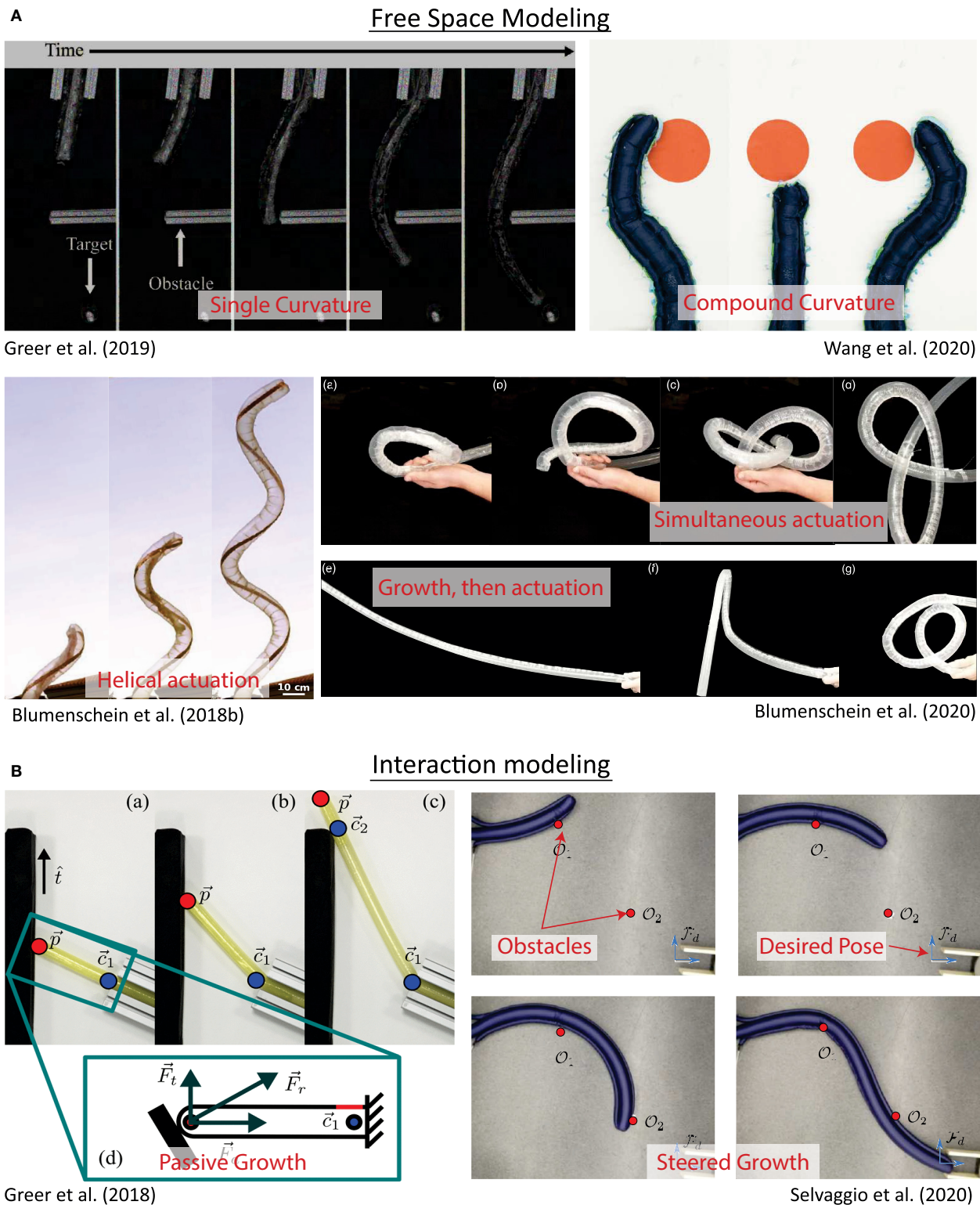


FIGURE 8 | Kinematic and force-balance modeling of everting vine robot shape/steering. **(A)** Modeling of robot shape in free space has included kinematic models based on constant curvature and piecewise constant curvature sections, some of which also consider forces, as well as kinematic models based on helical and piecewise helical actuator routings. **(B)** Modeling of robot shape during environment interaction has developed heuristics for both passively and actively steered growth based on kinematics and force-balance models. Modified from Greer et al. (2019). The publisher for this copyrighted material is Mary Ann Liebert, Inc. publishers. Modified from Wang et al. (2020) © IEEE 2020, Blumenschein et al. (2018b) © IEEE 2018, Greer et al. (2018), Blumenschein et al. (2020) © IEEE 2018, and Selvaggio et al. (2020) © IEEE 2020.

These bending and buckling behaviors can also occur due to forces applied during retraction (section 3.2.2). Coad et al. (2020b) described the critical points for inversion-based buckling as a function of curvature, length, and internal pressure (**Figure 7B**). The same length-independent yield force that must be overcome to begin eversion is also required to begin inversion, while the forces required to bend and buckle the robot body decrease with increasing length. This means that regardless of robot curvature and internal pressure, above a certain length, the robot body will always bend or buckle instead of inverting.

4.2. Modeling of Steering

Kinematic and force-balance models have been employed to calculate the robot shape both due to actuators and due to obstacle interaction. These models are highlighted in **Figure 8**.

Early models for everting vine robot steering were inspired by constant curvature models used for flexible-backbone continuum robots (Webster and Jones, 2010). In Greer et al. (2017), constant curvature kinematics are used to define the 3D shape of a flexible, thin-walled inflated backbone, without eversion, steered by distributed strain actuators (**Figure 8A**). This model incorporates a force balance, taking into account the backbone and actuator stiffnesses due to pressure. Greer et al. (2019) then incorporates the effects of the changing body length when growing. While these effects are mainly accounted for using control strategies (section 5.1.2), it is noted that the change in body length also causes a reduction in the frequency response of the actuators as they increase in length, due to the fluidic resistance of sPAMs (section 3.3.1). Greer et al. (2019) also showed that the mapping between internal actuator pressures and instantaneous tip displacements is fairly consistent throughout the robot's workspace. This allowed Coad et al. (2020a) to develop a simplified kinematic model assuming a linear relationship between change in actuator pressure and instantaneous tip displacement. This model commands instantaneous tip displacements, instead of absolute tip positions.

Adding shape-locking (section 3.3.6) to a robot with constant curvature actuation allows for the creation of complex compound curvatures, but this requires a modification of the constant curvature models as a result. Wang et al. (2020) developed a steering model to determine the tip position of a shape-locking everting vine robot (**Figure 8B**). This method of shape-locking causes the more proximal sections to be held in place while the most distal section, past the end of the locking bodies, can actuate into a constant curvature shape. The full robot shape is a compound curve made of constant curvature segments. As the locking bodies grow or retract along the robot, new static segments are added or removed from the curve, and the tip position can be reconstructed by taking the kinematics of each curved segment in order.

These constant curvature models only apply to actuators mounted parallel to the backbone, i.e., parallel to the growing direction of the everting vine robot. Blumenschein et al. (2018b) expanded these steering models to actuators attached to the everting vine robot body in a helix (**Figure 8A**). The developed closed-form kinematics for helical actuators relate the 3D actuator shape to the 3D deformed robot shape based only on

geometry. To model the kinematics of general actuator shapes on everting vine robots, Blumenschein et al. (2020) took this helical kinematics model and approximated general paths as piecewise helical. This approximation accurately predicts the actuated shapes resulting from generally shaped actuators. The kinematic modeling was also used to design the actuation to achieve a desired path, like a self-knotting everting vine robot (**Figure 8A**).

Steering can also result from obstacle interactions. A model presented in Greer et al. (2018) developed a simple kinematic heuristic for a straight (unactuated) everting vine robot as it grows into an obstacle in 2D: the tip will slide along the obstacle in a direction determined by the initial contact angle, and the robot will bend at the previous contact with the environment (**Figure 8B**). Given an environment including some set of obstacles, this model predicts the robot's path based entirely on the obstacle locations and initial robot state, keeping track of obstacle contact points on the everting vine robot. In Greer et al. (2020), a slight modification of the obstacle interaction model was used to account for preformed turns as well, and this model was used to plan 2D paths through environments with known obstacles (section 5.3).

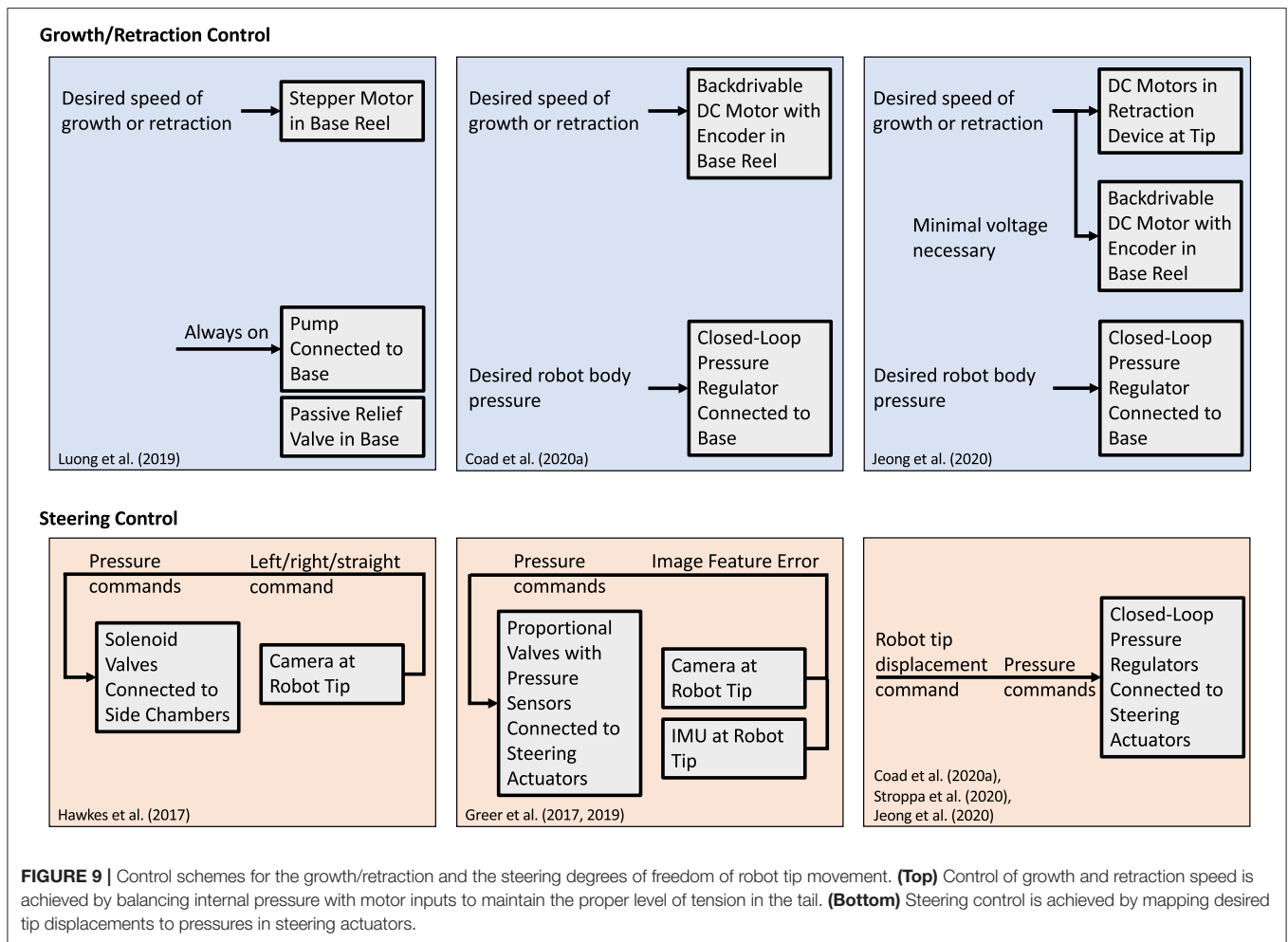
Active steering and obstacle interaction models can be combined to model controlled everting vine robots moving through obstacle-filled environments. Selvaggio et al. (2020) shows a piecewise formulation to calculate the robot shape during environment contact in 2D. The free length of the robot body (i.e., the section not constrained by the environment) takes on a constant curvature shape determined by the pressures in the actuators, while the constrained length of the robot body is shaped based on the obstacle contact locations (**Figure 8B**). A point-loaded cantilever inflated beam model determines the deflection and moment of the constrained section of the body. This model can similarly be used for planning (section 5.3).

5. CONTROL AND PLANNING

The unique properties and mechanisms of everting vine robot movement provide new opportunities and challenges for robot control and planning, both teleoperated and autonomous. Considerations include what behaviors can be planned and how to bring a human operator into the control loop. The main everting vine robot control and planning topics studied thus far have been (1) robot-level control of growth, retraction, and steering, (2) interface design to allow human operators to teleoperate everting vine robots, and (3) planning methods that consider obstacle interaction models of everting vine robots.

5.1. Robot-Level Control

Robot-level control strategies are concerned with controlling the fundamental movements of the everting vine robot. Since growth and steering are generally actuated independently, the control strategies are handled separately as well. Even when steering is coupled to growth, the control of steering is separate and reactive to growth. Control schemes that have been demonstrated in the literature are diagrammed in **Figure 9**.



5.1.1. Growth and Retraction Control

Due to the variability of length scales of everting vine robots, growth and retraction have been speed controlled. Accurate control of the robot's length relies on being able to apply forces that both lengthen and shorten the robot. Since internal pressure can only drive growth, an antagonistic actuator, like a motor attached to the tail, is needed to have full control. Using the antagonistic combination of pressure to drive growth and motor to resist growth, speed control has been achieved for limited length change (Greer et al., 2019) and arbitrary length change (Luong et al., 2019; Coad et al., 2020a) robots.

The exact implementation of growth control differs between these systems. Luong et al. (2019) used a continuously-running pump with a relief valve to maintain a constant pressure (20 kPa), while growth and retraction speed were controlled via commands sent to a stepper motor. Care was needed to ensure that the stepper motor did not introduce slack if obstacles or steering slowed the robot. Coad et al. (2020a) used a backdrivable DC motor with an encoder and a closed-loop pressure regulator to make growth speed control robust to these disturbances without sensing the true growth speed. By setting the motor to only resist growth and allowing the pressure to backdrive the motor up to the desired speed,

the speed could be controlled without allowing slack in the tail.

While retraction can be accomplished with the architecture described above, controlled retraction has been implemented with the addition of a retraction device (Coad et al., 2020b) as discussed in section 3.2. With this device, the motor inputs of the base motor and the retraction device motor(s) must be synchronized and their combination must balance the internal pressure. Jeong et al. (2020) presented an implementation of growth and retraction control using a retraction device without an encoder. The retraction device motors determined the speed of growth or retraction, while the base motor applied the forces necessary to maintain material tension and reel material slack as it developed.

5.1.2. Steering Control

Unlike growth and retraction control, steering control methods are dependent on the actuation method used. This section only discusses steering control when in free space; the steering behavior of everting vine robots under environmental contact is treated as a planning problem instead.

Control for tip-localized strain actuation (section 3.3.3) was demonstrated in Hawkes et al. (2017). Since steering could only

occur at discrete points when the robot grew, bang-bang control was used, where the next command—left, right, or straight—was queued according to the target location relative to the tip. This method could stably control the everting vine robot heading as long as the growth speed was sufficiently slow, since actuation inputs occurred at discrete intervals and resulted in irreversible shape change of the body.

Control of reversible steering was first demonstrated in Greer et al. (2017, 2019) with an everting vine robot using distributed strain actuation. Since steering is completely decoupled from growth and retraction, instantaneous movement of the robot tip in any direction is possible. For autonomous control, tip motion from steering was commanded with a visual servo control law to keep tracked features centered in the field of view. Even though an image-space Jacobian could be derived based on constant curvature models (section 4.2), the control instead used model-free approaches and calibrated an image-space Jacobian approximation during startup. The Jacobian translated actuator pressures to image-space displacements. The camera could spin relative to the robot, so an IMU attached to the camera was used to estimate the relative rotation of the tip camera and update the Jacobian.

Coad et al. (2020a) also demonstrated steering control for distributed strain actuators, using a simplified kinematic model of the robot instead of a model-free image-space Jacobian, and for the purposes of teleoperation. This method controlled the robot body at relatively long lengths (7.5–10 m) for the first time,

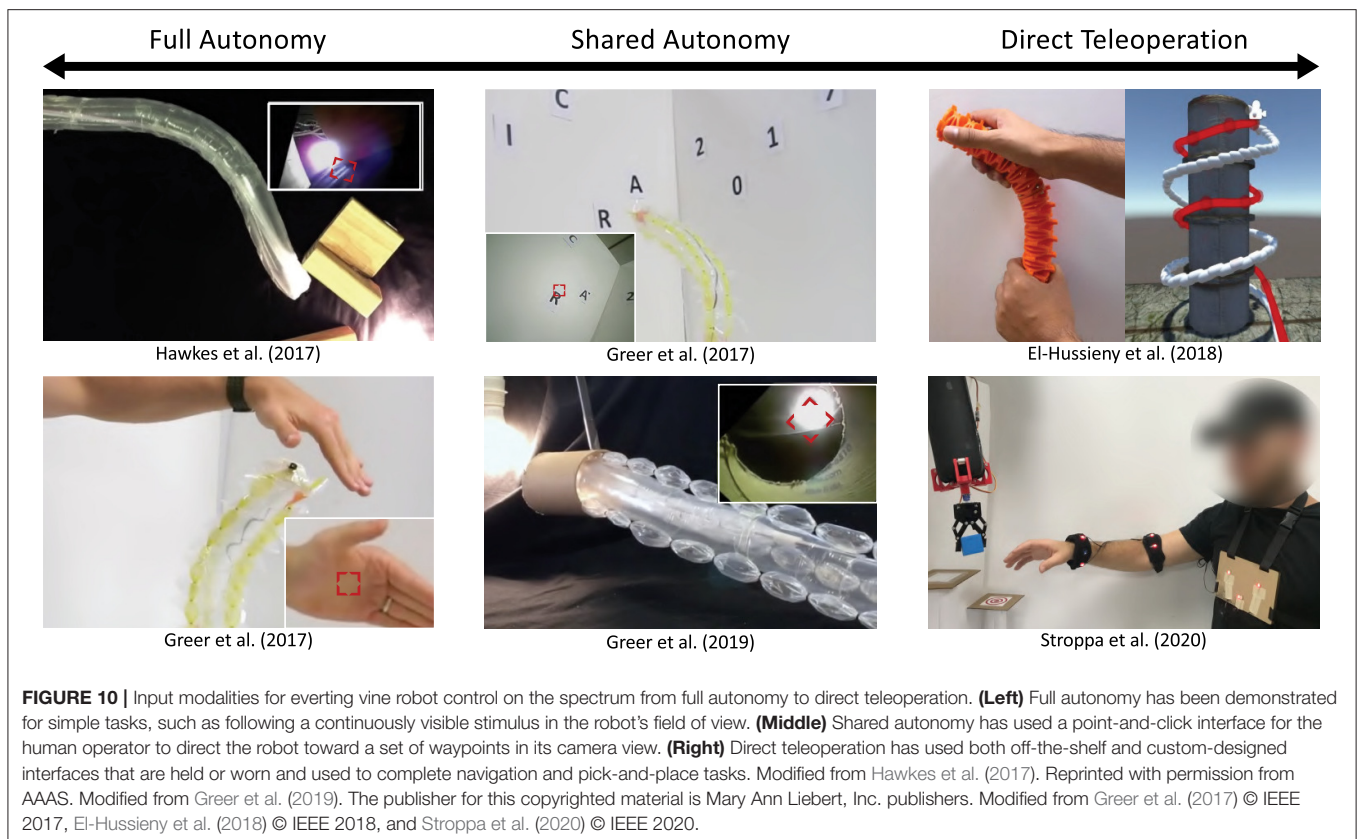
demonstrating that constant curvature assumptions break down at long length. Only the most distal meter long section of the robot body achieves a consistent curvature, so past that length, the kinematics can be considered approximately independent of length. Since human-in-the-loop teleoperation was used to provide reference inputs instead of feedback from a tip camera, the steering control was open-loop and based on the inverse kinematics. This steering control method was also modified to be used with concentrated strain actuation in Stroppa et al. (2020) and was demonstrated with retraction in Jeong et al. (2020), and model-based control using beam bending models was shown in Ataka et al. (2020).

5.2. Input Modalities

Input modalities refer to the methods used to provide reference commands to the robot (**Figure 10**). Everting vine robots can be fully or semi-autonomous, relying only on high-level commands from operators and feedback from sensing within their control loop, or they can be directly teleoperated, taking low-level commands from a human operator.

5.2.1. Full and Shared Autonomy

Full and shared autonomy was demonstrated in Greer et al. (2017, 2019) and Hawkes et al. (2017), using a camera and video processing to track image features that are selected by the operator (**Figure 10**). Full autonomy is possible in cases where the tracked image feature is constant and always in view, allowing the everting vine robot to navigate toward a light in Hawkes et al.



(2017) or to follow a person's hand in Greer et al. (2017). When different features need to be tracked over time, either due to changing goals or because the end goal is not in sight, humans can provide updates to the target object in a shared autonomy setup. Shared autonomy was shown in Greer et al. (2017) to switch targets in a sequence, and in Greer et al. (2019) to navigate toward a target hidden behind an obstacle in the workspace.

5.2.2. Direct Teleoperation

A variety of devices have been used to provide inputs for direct teleoperation, including off-the-shelf input devices and custom-designed interfaces. Since growth is a degree of control not found in many robots, a key early consideration for interface design was the intuitiveness of the control. El-Husseyeny et al. (2018) conducted a user study of teleoperation using a simulated everting vine robot with first-person view as though from a camera at the robot tip (**Figure 10**). Three off-the-shelf input devices (keyboard, joystick, and Phantom Omni) were compared to a novel flexible joystick. Overall, the novel flexible joystick outperformed the other input devices on all measured metrics and was found to have the lowest self-rated mental workload. A similar flexible joystick was used in Coad et al. (2020a) for teleoperation of an everting vine robot within a previously unexplored rocky tunnel in an archaeological site. Joystick displacements were mapped to robot tip displacements and the growth speed of the robot was input using a sliding potentiometer embedded in the joystick. The human operator received feedback of the robot tip position by viewing images from a camera at the robot tip. A different interface for direct teleoperation of everting vine robots was demonstrated in Stroppa et al. (2020) for a pick-and-place task (**Figure 10**). This interface used a motion capture system with markers placed on the human operator's chest and arm, tracking the operator's gestures to control the growth, retraction, and steering of the robot, while the human operator viewed the entire robot body and its environment via direct line of sight. In a user study, participants teleoperated the everting vine robot to successfully transfer a cube from one platform to another in 95% of trials.

5.3. Planning

Everting vine robots interact with their environment in ways desirable for navigation, creating opportunities for planning methods that are unique to these types of robots. Thus far, the literature has focused on defining and using heuristics for everting vine robot interaction with a known, rigid environment. These planning methods demonstrate that designs that use environmental contact have a higher probability of reaching a target in the face of actuation uncertainty, and that the dexterous range of everting vine robots can be increased by contacting the environment. The planning methods that have been demonstrated in the literature for everting vine robots are shown in **Figure 11**.

Greer et al. (2020) used the obstacle interaction heuristics for an everting vine robot with preformed steering to develop a planning method for choosing the initial robot shape, i.e., the pinch locations and pinch angles (section 3.3.4). The planning method maximized the probability of reaching a desired target

given noise in the design parameters. This planning method uses the certainty of the robot tip position when contacting obstacles to counteract the uncertainty in manufacturing the preformed everting vine robot, as well as offloading some of the manipulation of the robot shape to the environment, reducing the required actuation. To find a plan, a sequence of waypoints overlaid on the known map and linking the start and end while requiring the minimal amount of preformed actuation were identified. Then, from the possible designs, the one that maximizes the probability of reaching each waypoint was selected.

Selvaggio et al. (2020) presents a similar planning method with the addition of active steering. A slightly different model (detailed in section 4.2) is used to describe the obstacle interaction of these robots. This model can calculate the reachable workspace of the robot tip as a function of a sequence of obstacle interactions; the more obstacles that can be used to manipulate the robot's path, the greater the possible range of approach angles of a target location. For a desired approach angle, the planning problem iterates through all possible permutations of obstacle contact states to find the sequence of obstacle contacts that minimize the orientation error at the target.

6. APPLICATIONS

While the work discussed in previous sections has investigated methods to understand and expand the capabilities of everting vine robots, here we discuss the previously explored applications for these systems, including the benefits and challenges of using everting vine robots for a given application. **Figure 12** shows three main application areas of everting vine robots: deploying and reconfiguring structures, navigating constrained environments, and applying forces on the environment.

6.1. Deploying and Reconfiguring Structures

Because everting vine robots create structures as they grow, one area of application has been to create deployable and reconfigurable structures. As discussed in section 3.4.2, sensors and tools can be fixed to the wall of an everting vine robot, allowing controlled deployment and reconfiguration during the growth and steering of the body. In these applications, the shape change of the robot body allows the deployed item to achieve its desired function.

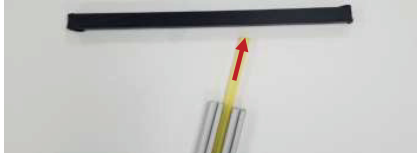
Agharese et al. (2018) designed an everting vine robot to create a deployable wearable haptic device. Haptic devices that modify their surface area are easier to don and doff and can create variable contact depending on the situation. This system begins in a wrist form factor and grows to cover the lower arm, deploying soft pneumatic haptic actuators (Raitor et al., 2017) that provide direction and intensity cues to the wearer. Structure "programmability" also allowed for the development of deployable and reconfigurable antennas. In Blumenschein et al. (2018a), copper strips were attached

Preformed Actuation, Inextensible Material

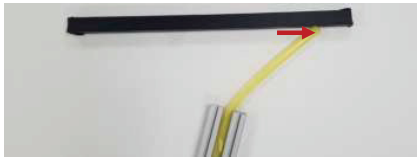
Heuristics:

Greer et al. (2018, 2020)

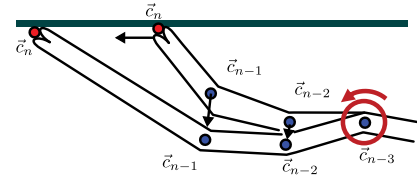
1. In free growth, robot tip moves straight or turns at a pinch



2. In obstacle contact, robot tip moves along obstacle

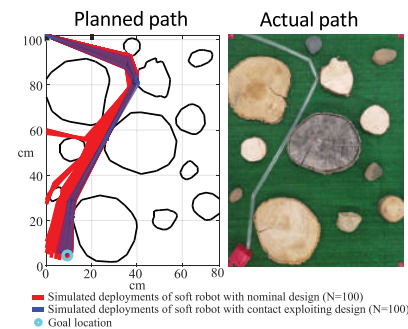


3. Robot body bends about base or a previous pinch



Results:

Planning algorithm minimizes actuation input, and thus uncertainty, to reach a target position



Distributed Strain Actuation, Extensible Material

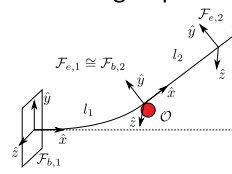
Heuristics:

Selvaggio et al. (2020)

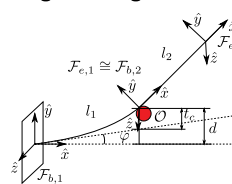
1. In free growth and steering, robot body follows a constant-curvature arc



2. In obstacle contact, robot body deforms according to point-loaded beam deflection



3. Robot body bends about base if moment is high enough



Results:

Planning algorithm minimizes orientation error to reach a target position

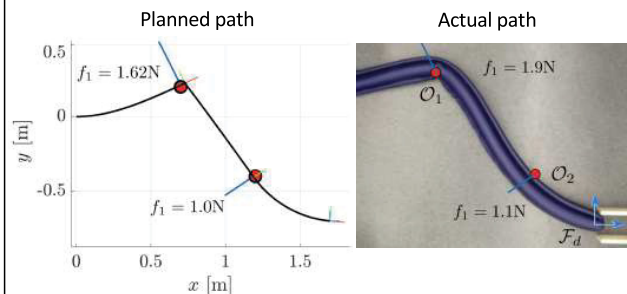
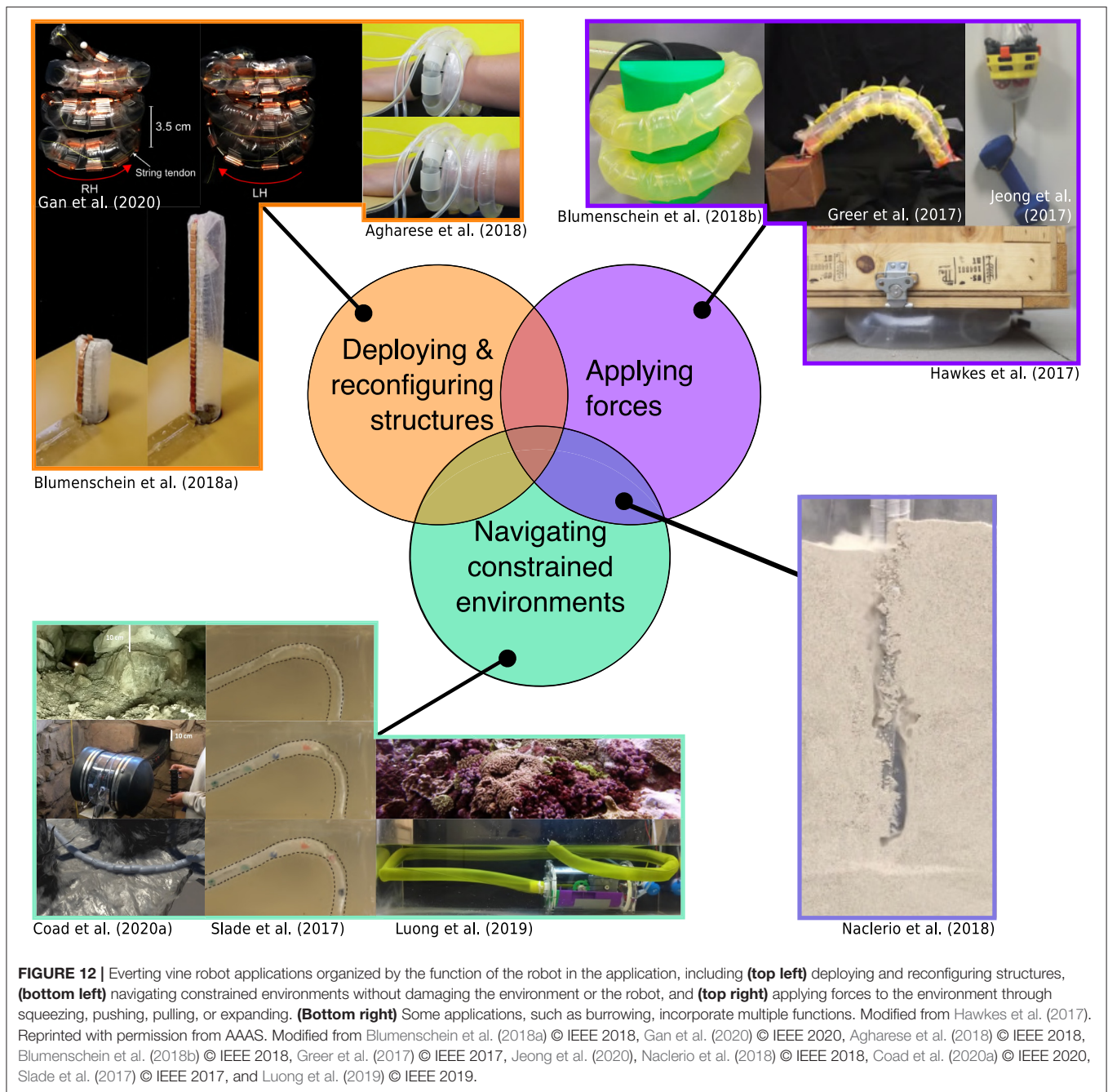


FIGURE 11 | Planning methods for (left) a preformed everting vine robot made of inextensible plastic and (right) an everting vine robot steered with distributed strain actuators and made of extensible fabric. The planning methods leverage heuristics about robot shape and environment interaction to minimize actuation input or orientation error while reaching a target position. Modified from Greer et al. (2020) and Selvaggio et al. (2020) © IEEE 2020.

to the robot body wall in an overlapping fashion to form a monopole antenna. As the robot grew and retracted it changed the length of the deployed monopole antenna. Deployment of more complex antenna shapes was shown in Gan et al. (2020), where a handedness-reconfiguring helical antenna was deployed. Other applications that rely on creation of deployable and reconfigurable structures could include deployment of structures in space and the formation of structural metamaterials.

6.2. Navigating Constrained Environments

Everting vine robots are well-suited for navigation of constrained environments, especially in situations where non-destructive sensing of the environment and/or delivery of items is needed. The requirements of these applications vary; the goal may be to reach and inspect a particular target with the robot tip, or the robot body itself may be used as a conduit to transport items from its proximal to distal ends, though there is often the additional goal of minimizing the force applied to the environment.



Coad et al. (2020a) reported on the first field deployment of an everting vine robot system in an archaeology application. A portable everting vine robot system was developed that could deliver a camera to collect video inside spaces in an archaeological site that are too small for a human to enter. Due to its ability to navigate tortuous paths, traverse rock blockages, and support its own body through vertical shafts, the everting vine robot was able to collect video in areas previously unobserved by the archaeology team. A similar application area was proposed in Luong et al. (2019), using a water-filled everting vine robot to non-destructively monitor underwater ecosystems. In the field of

medicine, preliminary demonstrations have shown the ability of everting vine robots to navigate tortuous paths similar to those encountered inside the human body, with minimal force applied to the environment compared to standard catheters and other medical tools pushed from the base (Slade et al., 2017). Continued work on mounting items at the robot tip without encumbering the robot's navigation ability will enable new capabilities for these types of applications.

In addition to navigating constrained environments through existing paths, everting vine robots can be grown to create a path where no natural pathway already exists. Naclerio et al. (2018)

investigated this problem via the development of an everting vine robot capable of burrowing through sand. To adapt the everting vine robot for burrowing, an air line internal to the tail was added to allow for granular fluidization, after which the everting vine robot grew into the sand, using its internal pressure to apply outward forces on the sand to keep its body from being crushed. This combines the navigation and force application abilities of everting vine robots, and it could allow for soil monitoring, non-invasive underground installation, and root-like foundation structures. Another related work (Ozkan-Aydin et al., 2019) showed the benefits of oscillating the everting vine robot tip during navigation of an environment containing both free space and rigid obstacles, similar to how plant roots oscillate their tips when burrowing through soil. This result has also been seen in other growing robot mechanisms (Del Dottore et al., 2017). These designs demonstrate an interesting application of everting vine robots and plant inspired robots in general: as model systems for understanding bio-physical behaviors of plants, similar to how animal inspired robots have been used to better understand animal biophysics (Libby et al., 2012; Li et al., 2013).

6.3. Applying Forces

Several potential everting vine robot applications center around applying force on the environment. For example, the natural compliance of an everting vine robot body makes it potentially safe for manipulation around humans. Everting vine robots may be especially useful in environments where a combination of the ability to navigate confined spaces and the ability to apply forces to the environment is needed, such as turning a valve in a disaster scenario (Hawkes et al., 2017).

Moving payloads attached to the robot tip often relies on having sufficient stiffness to resist bending and buckling loads on the everting vine robot body, which depends on the internal pressure and the length of the robot. Because everting vine robots are hollow and filled with fluid, their critical bending and buckling loads tend to be lower than those of traditional robots (section 4.1). Greer et al. (2017) and Stroppa et al. (2020) demonstrated that forces applied using transverse and compressive loading on the everting vine robot body are sufficient to move lightweight objects (200 g) around the robot's 3D workspace, and there is ongoing work on methods to control stiffness (section 3.3.6), which will increase the weight-bearing capacity of everting vine robots to allow the extension to more manipulation tasks.

The use of inextensible materials in many everting vine robots means that, while they tend to be much weaker than traditional robots in compression, they can be strong in tension, and this strength is not dependent on the robot length. Jeong et al. (2020) demonstrated that, with the addition of a tip mount to pull on the environment, everting vine robots can support up to 7 kg of weight and lift up to 2.5 kg in tension, only limited by the strength of the tip mount materials and the tip-mount motors. In a similar application, everting vine robots were used as tensile linear actuators (Abrar et al., 2019).

Finally, everting vine robots can apply forces through the everted body more efficiently than through the everting tip. Pressure has an impressive ability to produce high forces when

multiplied by a large area, so, by directly using the internal pressure to apply forces, Hawkes et al. (2017) demonstrated a pneumatic jack capable of growing into a small gap and then lifting over 75 kg, with increasing force capability as the robot grew. Nakamura and Tsukagoshi (2018) applied this lifting capability to design a tool that gently lifts and turns people in bed. Wrapping around objects to grasp them is another common continuum robot behavior that everting vine robots can achieve. Preliminary work on this concept was presented in Blumenschein et al. (2018b), which demonstrates helical grasping.

7. CONCLUSION

Everting vine robots are characterized by their ability to achieve growth through pressure-driven eversion. Within this category are a variety of designs, modeling techniques, control and planning strategies, and application areas. In this review, we summarized and organized much of the recent work on everting vine robots. We highlighted the relative benefits and deficits of everting vine robot design components, from material choice to actuation strategy to sensor and tool delivery method. We also showed the uses for and limitations of existing modeling and control strategies, and we explained application areas by the features of everting vine robots that facilitate them.

With the previous work in everting vine robots in mind, there are a number of open questions in each of the areas discussed. Everting vine robot functionality could be increased through design methods. The majority of everting vine robot materials have been tested at the same scale, so investigation of how these materials function within everting vine robots at much smaller and larger scales is needed. Because the materials are relatively cheap, future exploration of manufacturing methods for mass production of everting vine robots could support the development of vine robot swarms and multi-robot coordination. Within actuation design, future work should include expanding methods for creating complex curves and 3D shapes and investigating actuation strategies to facilitate force control in addition to position control. However, the most pressing area of future research in design is the need to develop methods for attachment of sensors and tools that do not encumber everting vine robots' ability to move through constrained environments and squeeze through gaps smaller than their body cross-section, since these beneficial behaviors are currently difficult to achieve with many of the existing tip mounts described in section 3.4.1.

The biggest gap in modeling for everting vine robots is understanding their dynamic responses and behaviors. A dynamic model could expand the capabilities of everting vine robots, allowing for faster movement and greater force application. Initial work in modeling dynamics for everting vine robots has been completed in simulation (El-Hussieny et al., 2019). Part of developing dynamic models that account for environment interaction involves incorporating more accurate kinematic models for the robots. Continuum models like Kirchhoff and Cosserat rod models have been applied successfully to many systems with similar thin flexible form factors in robotics and in graphics (Bergou et al., 2008; Gazzola et al., 2018; Zhang

et al., 2019), so adapting these models for everting vine robots is an interesting area of future research. As we continue to use everting vine robots in constrained environments, another area of research in modeling is expanding obstacle interaction models to include compliant obstacles, especially since compliant environments are often the type that require delicate interaction.

Future steps within control and planning should focus on two goals: increasing the ease and functionality of teleoperating everting vine robots, and investigating shared or full autonomy for behaviors that are difficult to achieve under teleoperation. For teleoperation, better robot-level control should be investigated by integrating accurate model-based control methods. In autonomous control, everting vine robot behaviors could be greatly expanded by creating control and planning methods of the body shape and the applied forces. These autonomous behaviors could take inspiration from the tropisms and control strategies seen in natural growth. In all these cases, new sensors that can be incorporated in everting vine robots are needed to sense shape, orientation, or interaction force of the robot, or to measure additional properties of the environment. These sensors may be located at the tip, distributed along the length, or actively re-positioned along the robot. For incorporating these sensors for teleoperation, future studies should look at what sensing modalities and displays give users the best sense of situational awareness. New human interfaces will be needed to allow operators to easily and quickly command more complex, high-level everting vine robot behaviors in teleoperated or shared control.

Lastly, there are many exciting application to explore in the future, many of which can be built based on existing ones. In navigating constrained environments, animal burrows are a well-suited environment to explore using everting vine robots. These burrows are difficult to navigate with existing technology, and everting vine robots could provide a tool to conduct minimally-intrusive population surveying of various species, as well as to gather information on the structures and climates of these underground environments. Everting vine robots have also shown promise in creating or augmenting medical devices (Saxena et al., 2020). Many medical procedures, like colonoscopy and endoscopy, require moving medical devices along existing pathways in the human body, and using everting vine robots could cause reductions in procedure time and reductions in unintended forces applied to the body. Everting vine robots also show great potential in creating tools to aid in search and rescue, due to their ability to move through constrained environments and carry sensors and other payloads.

REFERENCES

- Abrar, T., Putzu, F., Konstantinova, J., and Althoefer, K. (2019). "Epam: eversive pneumatic artificial muscle," in *IEEE International Conference on Soft Robotics* (Seoul), 19–24. doi: 10.1109/ROBOSOFT.2019.8722787
- Agharese, N., Cloyd, T., Blumenschein, L. H., Raitor, M., Hawkes, E. W., Culbertson, H., et al. (2018). "Hapwrap: soft growing wearable haptic device," in *IEEE International Conference on Robotics and Automation* (Brisbane, QLD), 5466–5472. doi: 10.1109/ICRA.2018.8460891
- Alexander, R. M. (2003). *Principles of Animal Locomotion*. Princeton, NJ: Princeton University Press.
- Ataka, A., Abrar, T., Putzu, F., Godaba, H., and Althoefer, K. (2020). Model-based pose control of inflatable eversion robot with variable stiffness. *IEEE Robot. Autom. Lett.* 5, 3398–3405. doi: 10.1109/LRA.2020.2976326
- Bergou, M., Wardetzky, M., Robinson, S., Audoly, B., and Grinspun, E. (2008). "Discrete elastic rods," in *ACM SIGGRAPH* (New York, NY: Association for Computing Machinery), 1–12.
- Many other potential applications build into new areas. A growing manipulator, for example, would be able to navigate cluttered human environments while keeping a minimal form factor and then apply forces to pick up or move objects in the environment. Future work for application of everting vine robots will also look at incorporating more actuation and control technologies to yield new behaviors. For example, robot applications that combine navigation of constrained environments and force application through manipulation may require on-demand change of everting vine robot properties to allow low-force application during navigation and high force application during manipulation.
- Everting vine robots are a technology still in their infancy. Yet, despite the relatively short time, diverse and interesting applications have been unlocked by their unique abilities. There remain many more questions to understand about their governing physics and how their behaviors can be leveraged and controlled to produce useful technologies, but the work to date has shown that everting vine robots provide a compelling framework through which new soft robotic opportunities can arise.

AUTHOR CONTRIBUTIONS

LB defined the scope of this review. LB, MC, and DH wrote the first draft of the manuscript. All authors contributed to manuscript revision and read and approved the submitted version.

FUNDING

This work was supported in part by the Air Force Office of Scientific Research under award FA2386-17-1-4658, the National Science Foundation under Award 1637446, Award 1944816, and Award 2024247, and Toyota Research Institute (TRI). TRI provided funds to assist the authors with their research, but this article solely reflects the opinions and conclusions of its authors and not TRI or any other Toyota entity.

ACKNOWLEDGMENTS

We thank our many collaborators on everting vine robot research for discussions related to the topics presented here. We especially thank Jee-Hwan Ryu, Sean Follmer, Sang-Goo Jeong, Nicholas Naclerio, Nathan Usevitch, Nathaniel Agharese, Brian Do, and Rachel Thomasson.

- Blumenschein, L. H., Gan, L., Fan, J., Okamura, A. M., and Hawkes, E. W. (2018a). A tip-extending soft robot enables reconfigurable and deployable antennas. *IEEE Robot. Autom. Lett.* 3, 949–956. doi: 10.1109/LRA.2018.2793303
- Blumenschein, L. H., Koehler, M., Usevitch, N. S., Hawkes, E. W., Rucker, D. C., and Okamura, A. M. (2020). Geometric solutions for general actuator routing on inflated beam soft growing robots. *arXiv*. Available online at: <https://arxiv.org/abs/2006.06117> (accessed August 30, 2020).
- Blumenschein, L. H., Okamura, A. M., and Hawkes, E. W. (2017). “Modeling of bioinspired apical extension in a soft robot,” in *Biomimetic and Biohybrid Systems*, eds M. Mangan, M. Cutkosky, A. Mura, P. F. Verschure, T. Prescott, and N. Lepora (Cham: Springer International Publishing), 522–531. doi: 10.1007/978-3-319-63537-8_45
- Blumenschein, L. H., Usevitch, N. S., Do, B., Hawkes, E. W., and Okamura, A. M. (2018b). “Helical actuation on a soft inflated robot body,” in *2018 IEEE International Conference on Soft Robotics* (Livorno: IEEE), 245–252. doi: 10.1109/ROBOSOFT.2018.8404927
- Cinquemani, S., Bianchi, G., Antonacci, N., and Resta, F. (2020). “Design of a soft pneumatic robot inspired to plant roots’ growth,” in *Bioinspiration, Biomimetics, and Bioreplication X*, Vol. 11374, eds M. Knez, A. Lakhtakia, and R. J. Martín-Palma (International Society for Optics and Photonics, SPIE), 100–109. doi: 10.1117/12.2558554
- Coad, M. M., Blumenschein, L. H., Cutler, S., Zepeda, J. A. R., Naclerio, N. D., El-Hussieny, H., et al. (2020a). Vine robots: design, teleoperation, and deployment for navigation and exploration. *IEEE Robot. Autom. Mag.* 27, 120–132. doi: 10.1109/MRA.2019.2947538
- Coad, M. M., Thomasson, R. P., Blumenschein, L. H., Usevitch, N. S., Hawkes, E. W., and Okamura, A. M. (2020b). Retraction of soft growing robots without buckling. *IEEE Robot. Autom. Lett.* 5, 2115–2122. doi: 10.1109/LRA.2020.2970629
- Comer, R., and Levy, S. (1963). Deflections of an inflated circular-cylindrical cantilever beam. *AIAA J.* 1, 1652–1655. doi: 10.2514/3.1873
- Dehghani, H., Welch, C. R., Pourghodrat, A., Nelson, C. A., Oleynikov, D., Dasgupta, P., et al. (2017). Design and preliminary evaluation of a self-steering, pneumatically driven colonoscopy robot. *J. Med. Eng. Technol.* 41, 223–236. doi: 10.1080/03091902.2016.1275853
- Del Dottore, E., Mondini, A., Sadeghi, A., Mattoli, V., and Mazzolai, B. (2017). An efficient soil penetration strategy for explorative robots inspired by plant root circumnutation movements. *Bioinspir. Biomimet.* 13:015003. doi: 10.1088/1748-3190/aa9998
- Dent, E. W., and Gertler, F. B. (2003). Cytoskeletal dynamics and transport in growth cone motility and axon guidance. *Neuron* 40, 209–227. doi: 10.1016/S0896-6273(03)00633-0
- Do, B. H., Banashek, V., and Okamura, A. M. (2020). “Dynamically reconfigurable discrete distributed stiffness for inflated beam robots,” in *IEEE International Conference on Robotics and Automation* (Paris), 9050–9056. doi: 10.1109/ICRA40945.2020.9197237
- El-Hussieny, H., Jeong, S.-G., and Ryu, J.-H. (2019). “Dynamic modeling of a class of soft growing robots using euler-lagrange formalism,” in *Society of Instrument and Control Engineers 2019* (Hiroshima).
- El-Hussieny, H., Mehmood, U., Mehdi, Z., Jeong, S.-G., Usman, M., Hawkes, E. W., et al. (2018). “Development and evaluation of an intuitive flexible interface for teleoperating soft growing robots,” in *IEEE/RSJ International Conference on Intelligent Robots and Systems* (Madrid), 4995–5002. doi: 10.1109/IROS.2018.8593896
- Fichter, W. (1966). A theory for inflated thin-wall cylindrical beams. *Natl. Air Space Admin. Tech. Note* 3466, 1–19.
- Gan, L. T., Blumenschein, L. H., Huang, Z., Okamura, A. M., Hawkes, E. W., and Fan, J. A. (2020). 3D electromagnetic reconfiguration enabled by soft continuum robots. *IEEE Robot. Autom. Lett.* 5, 1704–1711. doi: 10.1109/LRA.2020.2969922
- Gaylord, R. H. (1958). *Fluid Actuated Motor System and Stroking Device*. United States patent US 2,844,126, USPTO, Alexandria, VA.
- Gazzola, M., Dudte, L., McCormick, A., and Mahadevan, L. (2018). Forward and inverse problems in the mechanics of soft filaments. *R. Soc. Open Sci.* 5:171628. doi: 10.1098/rsos.171628
- Geddes, L., Moore, A., Spencer, W., and Hoff, H. (1959). Electropneumatic control of the mckibben synthetic muscle. *Orthoped. Prosthet. Appl. J.* 13, 33–36.
- Gerbode, S. J., Puzey, J. R., McCormick, A. G., and Mahadevan, L. (2012). How the cucumber tendril coils and overwinds. *Science* 337, 1087–1091. doi: 10.1126/science.1223304
- Gibson, R. (1977). A new genus and species of lineid heteronemertean from South Africa, polybrachiorhynchus dayi (nemertea: Anopla), possessing a multibranching proboscis. *Bull. Mar. Sci.* 27, 552–571.
- Godaba, H., Putzu, F., Abrar, T., Konstantinova, J., and Althoefer, K. (2019). “Payload capabilities and operational limits of eversion robots,” in *Annual Conference Towards Autonomous Robotic Systems* (London), 383–394. doi: 10.1007/978-3-030-25332-5_33
- Goriely, A. (2017). *The Mathematics and Mechanics of Biological Growth*, Vol. 45. New York, NY: Springer.
- Green, P., Erickson, R., and Buggy, J. (1971). Metabolic and physical control of cell elongation rate: *in vivo* studies in nitella. *Plant Physiol.* 47, 423–430. doi: 10.1104/pp.47.3.423
- Greer, J. D., Blumenschein, L. H., Alterovitz, R., Hawkes, E. W., and Okamura, A. M. (2020). Robust navigation of a soft growing robot by exploiting contact with the environment. *Int. J. Robot. Res.* doi: 10.1177/0278364920903774. [Epub ahead of print].
- Greer, J. D., Blumenschein, L. H., Okamura, A. M., and Hawkes, E. W. (2018). “Obstacle-aided navigation of a soft growing robot,” in *IEEE International Conference on Robotics and Automation* (Brisbane, QLD), 4165–4172. doi: 10.1109/ICRA.2018.8460777
- Greer, J. D., Morimoto, T. K., Okamura, A. M., and Hawkes, E. W. (2017). “Series pneumatic artificial muscles (sPAMs) and application to a soft continuum robot,” in *IEEE International Conference on Robotics and Automation* (Singapore), 5503–5510. doi: 10.1109/ICRA.2017.7989648
- Greer, J. D., Morimoto, T. K., Okamura, A. M., and Hawkes, E. W. (2019). A soft, steerable continuum robot that grows via tip extension. *Soft Robot.* 6, 95–108. doi: 10.1089/soro.2018.0034
- Haggerty, D. A., Naclerio, N. D., and Hawkes, E. W. (2019). “Characterizing environmental interactions for soft growing robots,” in *IEEE/RSJ International Conference on Intelligent Robots and Systems* (Macau), 3335–3342. doi: 10.1109/IROS40897.2019.8968137
- Hammond, Z. M., Usevitch, N. S., Hawkes, E. W., and Follmer, S. (2017). “Pneumatic reel actuator: design, modeling, and implementation,” in *IEEE International Conference on Robotics and Automation* (Singapore), 626–633. doi: 10.1109/ICRA.2017.7989078
- Hawkes, E. W., Blumenschein, L. H., Greer, J. D., and Okamura, A. M. (2017). A soft robot that navigates its environment through growth. *Sci. Robot.* 2:eaan3028. doi: 10.1126/scirobotics.aan3028
- Hawkes, E. W., Christensen, D. L., and Okamura, A. M. (2016). “Design and implementation of a 300% strain soft artificial muscle,” in *IEEE International Conference on Robotics and Automation* (Stockholm), 4022–4029. doi: 10.1109/ICRA.2016.7487592
- He, Y., and Chen, W. (2014). Experiment and theoretical analysis study of ETFE inflatable tubes. *Int. J. Aerospace Eng.* 2014, 1–10. doi: 10.1155/2014/925428
- Hong, D. W., Ingram, M., and Lahr, D. (2009). Whole skin locomotion inspired by amoeboid motility mechanisms. *J. Mech. Robot.* 1, 1–7. doi: 10.1115/1.2976368
- Jeong, S., Coad, M. M., Blumenschein, L. H., Luo, M., Mehmood, U., Kim, J., et al. (2020). “A tip mount for transporting sensors and tools using soft growing robots,” in *IEEE/RSJ International Conference on Intelligent Robots and Systems*. Available online at: <https://arxiv.org/abs/1912.08297> (accessed August 30, 2020).
- Kim, Y.-J., Cheng, S., Kim, S., and Iagnemma, K. (2013). A novel layer jamming mechanism with tunable stiffness capability for minimally invasive surgery. *IEEE Trans. Robot.* 29, 1031–1042. doi: 10.1109/TRO.2013.2256313
- Lee, C., Kim, M., Kim, Y. J., Hong, N., Ryu, S., Kim, H. J., et al. (2017). Soft robot review. *Int. J. Control Autom. Syst.* 15, 3–15. doi: 10.1007/s12555-016-0462-3
- Lee, Y.-H., Kang, B.-K., Kim, H.-D., Yoo, H.-J., Kim, J.-S., Huh, J.-H., et al. (2009). Effect of hot pressing/melt mixing on the properties of thermoplastic polyurethane. *Macromol. Res.* 17, 616–622. doi: 10.1007/BF03218918
- Le-van, A., and Wielgosz, C. (2005). Bending and buckling of inflatable beams: some new theoretical results. *Thin Wall. Struct.* 43, 1166–1187. doi: 10.1016/j.tws.2005.03.005
- Lew, R. R. (2011). How does a hypha grow? The biophysics of pressurized growth in fungi. *Nat. Rev. Microbiol.* 9, 509–518. doi: 10.1038/nrmicro2591
- Li, C., Zhang, T., and Goldman, D. I. (2013). A terradynamics of legged locomotion on granular media. *Science* 339, 1408–1412. doi: 10.1126/science.1229163

- Li, H., Yao, J., Liu, C., Zhou, P., Xu, Y., and Zhao, Y. (2020). A bioinspired soft swallowing robot based on compliant guiding structure. *Soft Robot.* 7, 491–499. doi: 10.1089/soro.2018.0154
- Libby, T., Moore, T. Y., Chang-Siu, E., Li, D., Cohen, D. J., Jusufi, A., et al. (2012). Tail-assisted pitch control in lizards, robots and dinosaurs. *Nature* 481, 181–184. doi: 10.1038/nature10710
- Lubarda, V. A. (2014). The mechanics of belt friction revisited. *Int. J. Mech. Eng. Educ.* 42, 97–112. doi: 10.7227/IJME.0002
- Luong, J., Glick, P., Ong, A., deVries, M. S., Sandin, S., Hawkes, E. W., et al. (2019). “Eversion and retraction of a soft robot towards the exploration of coral reefs,” in *IEEE International Conference on Soft Robotics* (Seoul), 801–807. doi: 10.1109/ROBOSOFT.2019.8722730
- Manca, J. (2018). *Hampton Court Palace, Gardens, Great Vine, Detail*. Hampton Court Palace.
- Mishima, D., Aoki, T., and Hirose, S. (2006). Development of a pneumatically controlled expandable arm for rescue searches in tight spaces. *Int. J. Robot. Res.* 25, 103–110. doi: 10.1177/0278364906061159
- Naclerio, N., and Hawkes, E. W. (2020). Simple, low-hysteresis, foldable, fabric pneumatic artificial muscle. *IEEE Robot. Autom. Lett.* 5, 3406–3413. doi: 10.1109/LRA.2020.2976309
- Naclerio, N., Hubicki, C., Aydin, Y., Goldman, D., and Hawkes, E. W. (2018). “Soft robotic burrowing device with tip-extension and granular fluidization,” in *IEEE/RSJ International Conference on Intelligent Robots and Systems* (Brisbane, QLD), 5918–5923. doi: 10.1109/IROS.2018.8593530
- Nakamura, T., and Tsukagoshi, H. (2018). “Soft pneumatic manipulator capable of sliding under the human body and its application to preventing bedsores,” in *IEEE/ASME International Conference on Advanced Intelligent Mechatronics* (Auckland), 956–961. doi: 10.1109/AIM.2018.8452429
- Niiyama, R., Sun, X., Sung, C., An, B., Rus, D., and Kim, S. (2015). Pouch motors: printable soft actuators integrated with computational design. *Soft Robot.* 2, 59–70. doi: 10.1089/soro.2014.0023
- Ozkan-Aydin, Y., Murray-Cooper, M., Aydin, E., McCaskey, E. N., Naclerio, N., Hawkes, E. W., et al. (2019). “Nutation aids heterogeneous substrate exploration in a robophysical root,” in *IEEE International Conference on Soft Robotics* (Seoul), 172–177. doi: 10.1109/ROBOSOFT.2019.8722717
- Palanivelu, R., and Preuss, D. (2000). Pollen tube targeting and axon guidance: parallels in tip growth mechanisms. *Trends Cell Biol.* 10, 517–524. doi: 10.1016/S0962-8924(00)01849-3
- Putzu, F., Abrar, T., and Althoefer, K. (2018). “Plant-inspired soft pneumatic eversion robot,” in *IEEE International Conference on Biomedical Robotics and Biomechanics* (Enschede), 1327–1332. doi: 10.1109/BIOROB.2018.8487848
- Raitor, M., Walker, J. M., Okamura, A. M., and Culbertson, H. (2017). “WRAP: wearable, restricted-aperture pneumatics for haptic guidance,” in *IEEE International Conference on Robotics and Automation* (Singapore), 427–432. doi: 10.1109/ICRA.2017.7989055
- Rus, D., and Tolley, M. T. (2015). Design, fabrication and control of soft robots. *Nature* 521, 467–475. doi: 10.1038/nature14543
- Sadeghi, A., Mondini, A., and Mazzolai, B. (2017). Toward self-growing soft robots inspired by plant roots and based on additive manufacturing technologies. *Soft Robot.* 4, 211–223. doi: 10.1089/soro.2016.0080
- Sanati Nezhad, A., and Geitmann, A. (2013). The cellular mechanics of an invasive lifestyle. *J. Exp. Bot.* 64, 4709–4728. doi: 10.1093/jxb/ert254
- Satake, Y., Takanishi, A., and Ishii, H. (2020). Novel growing robot with inflatable structure and heat-welding rotation mechanism. *IEEE/ASME Trans. Mechatron.* 25, 1869–1877. doi: 10.1109/TMECH.2020.2999467
- Saxena, A., Pauli, E. M., Haluck, R. S., Fell, B., and Moore, J. (2020). Tubular locomotion and positioning using tip eversion for endoscopy. *J. Med. Dev.* 14:021004. doi: 10.1115/1.4046433
- Selvaggio, M., Ramirez, L., Siciliano, B., and Hawkes, E. (2020). “An obstacle interaction planning method for navigation of actuated vine robots,” in *International Conference on Robotics and Automation* (Paris), 3227–3233. doi: 10.1109/ICRA40945.2020.9196587
- Slade, P., Gruebele, A., Hammond, Z., Raitor, M., Okamura, A. M., and Hawkes, E. W. (2017). “Design of a soft catheter for low-force and constrained surgery,” in *IEEE/RSJ International Conference on Intelligent Robots and Systems* (Vancouver, BC), 174–180. doi: 10.1109/IROS.2017.8202154
- Steer, M. W., and Steer, J. M. (1989). Pollen tube tip growth. *New Phytol.* 111, 323–358. doi: 10.1111/j.1469-8137.1989.tb00697.x
- Stroppa, F., Luo, M., Yoshida, K., Coad, M. M., Blumenschein, L. H., and Okamura, A. M. (2020). “Human Interface for Teleoperated Object Manipulation with a Soft Growing Robot,” in *IEEE International Conference on Robotics and Automation* (Paris), 726–732. doi: 10.1109/ICRA40945.2020.9197094
- Talas, S. K., Baydere, B. A., Altinsoy, T., Tutcu, C., and Samur, E. (2020). Design and development of a growing pneumatic soft robot. *Soft Robot.* 7, 521–533. doi: 10.1089/soro.2019.0083
- Tsukagoshi, H., Arai, N., Kiryu, I., and Kitagawa, A. (2011). Tip growing actuator with the hose-like structure aiming for inspection on narrow terrain. *Int. J. Autom. Technol.* 5, 516–522. doi: 10.20965/ijat.2011.p0516
- Usevitch, N. S., Hammond, Z. M., Schwager, M., Okamura, A. M., Hawkes, E. W., and Follmer, S. (2020). An untethered isoperimetric soft robot. *Sci. Robot.* 5:eaa0492. doi: 10.1126/scirobotics.aa0492
- Vaughn, K. C., Bowling, A. J., et al. (2011). 1 biology and physiology of vines. *Hortic. Rev.* 38:1. doi: 10.1002/9780470872376.ch1
- Wang, S., Zhang, R., Haggerty, D., Naclerio, N., and Hawkes, E. (2020). “A dexterous tip-extending robot with variable-length shape-locking,” in *IEEE International Conference on Robotics and Automation* (Paris), 9035–9041. doi: 10.1109/ICRA40945.2020.9197311
- Watson, C., and Morimoto, T. K. (2020). Permanent magnet-based localization for growing robots in medical applications. *IEEE Robot. Autom. Lett.* 5, 2666–2673. doi: 10.1109/LRA.2020.2972890
- Webster, R. J. III, and Jones, B. A. (2010). Design and kinematic modeling of constant curvature continuum robots: a review. *Int. J. Robot. Res.* 29, 1661–1683. doi: 10.1177/0278364910368147
- Weigel, D., and Jürgens, G. (2002). Stem cells that make stems. *Nature* 415, 751–754. doi: 10.1038/415751a
- Wooten, M. B., and Walker, I. D. (2015). “A novel vine-like robot for in-orbit inspection,” in *International Conference on Environmental Systems* (Bellevue, WA), 1–11.
- Xu, M.-M., Huang, G.-Y., Feng, S.-S., McShane, G. J., and Stronge, W. J. (2016). Static and dynamic properties of semi-crystalline polyethylene. *Polymers* 8:77. doi: 10.3390/polym8040077
- Yan, T., Teshigawara, S., and Asada, H. H. (2019). “Design of a growing robot inspired by plant growth,” in *IEEE/RSJ International Conference on Intelligent Robots and Systems* (Macau), 8006–8011. doi: 10.1109/IROS40897.2019.8968200
- Zhang, X., Chan, F. K., Parthasarathy, T., and Gazzola, M. (2019). Modeling and simulation of complex dynamic musculoskeletal architectures. *Nat. Commun.* 10, 1–12. doi: 10.1038/s41467-019-12759-5
- Zhu, M., Do, T. N., Hawkes, E., and Visell, Y. (2020). Fluidic fabric muscle sheets for wearable and soft robotics. *Soft Robot.* 7, 179–197. doi: 10.1089/soro.2019.0033
- Zhu, T., Yang, H., and Zhang, W. (2016). “A spherical self-adaptive gripper with shrinking of an elastic membrane,” in *International Conference on Advanced Robotics and Mechatronics* (Macau), 512–517. doi: 10.1109/ICARM.2016.7606973
- Zuckerklund, E. (1950). Coelomic pressures in sipunculus nudus. *Biol. Bull.* 98, 161–173. doi: 10.2307/1538578

Conflict of Interest: LB, AO, and EH have a pending patent on the combination of growth and steering. LB, MC, and AO have a pending patent on the device for retracting growing robots.

The remaining author declares that the research was conducted in the absence of any commercial or financial relationships that could be construed as a potential conflict of interest.

Copyright © 2020 Blumenschein, Coad, Haggerty, Okamura and Hawkes. This is an open-access article distributed under the terms of the Creative Commons Attribution License (CC BY). The use, distribution or reproduction in other forums is permitted, provided the original author(s) and the copyright owner(s) are credited and that the original publication in this journal is cited, in accordance with accepted academic practice. No use, distribution or reproduction is permitted which does not comply with these terms.



Root Systems Research for Bioinspired Resilient Design: A Concept Framework for Foundation and Coastal Engineering

Elena Stachew¹, Thibaut Houette¹ and Petra Gruber^{2*}

¹Biomimicry Research and Innovation Center BRIC, Department of Biology, The University of Akron, Akron, OH, United States,

²Biomimicry Research and Innovation Center BRIC, Myers School of Art and Department of Biology, The University of Akron, Akron, OH, United States

OPEN ACCESS

Edited by:

Barbara Mazzolai,
Italian Institute of Technology (IIT), Italy

Reviewed by:

Matthew Aaron Robertson,
Queen's University, Canada
Olusegun Oguntona,
University of Johannesburg,
South Africa

*Correspondence:

Petra Gruber
pgruber@uakron.edu

Specialty section:

This article was submitted to
Soft Robotics,
a section of the journal
Frontiers in Robotics and AI

Received: 09 April 2020

Accepted: 08 April 2021

Published: 26 April 2021

Citation:

Stachew E, Houette T and Gruber P
(2021) Root Systems Research for
Bioinspired Resilient Design: A
Concept Framework for Foundation
and Coastal Engineering.
Front. Robot. AI 8:548444.
doi: 10.3389/frobt.2021.548444

The continuous increase in population and human migration to urban and coastal areas leads to the expansion of built environments over natural habitats. Current infrastructure suffers from environmental changes and their impact on ecosystem services. Foundations are static anchoring structures dependent on soil compaction, which reduces water infiltration and increases flooding. Coastal infrastructure reduces wave action and landward erosion but alters natural habitat and sediment transport. On the other hand, root systems are multifunctional, resilient, biological structures that offer promising strategies for the design of civil and coastal infrastructure, such as adaptivity, multifunctionality, self-healing, mechanical and chemical soil attachment. Therefore, the biomimetic methodology is employed to abstract root strategies of interest for the design of building foundations and coastal infrastructures that prevent soil erosion, anchor structures, penetrate soils, and provide natural habitat. The strategies are described in a literature review on root biology, then these principles are abstracted from their biological context to show their potential for engineering transfer. After a review of current and developing technologies in both application fields, the abstracted strategies are translated into conceptual designs for foundation and coastal engineering. In addition to presenting the potential of root-inspired designs for both fields, this paper also showcases the main steps of the biomimetic methodology from the study of a biological system to the development of conceptual technical designs. In this way the paper also contributes to the development of a more strategic intersection between biology and engineering and provides a framework for further research and development projects.

Keywords: root architecture, root research, biomimicry, bioinspired design, building foundations, coastal engineering

INTRODUCTION

Currently, 40% of the global population lives in cities and by 2050, this number will increase to 66% (Li, 2018). 40% of the global population and 75% of the world's megacities are within 100 km of a coastline and this percentage is also expected to increase (Mayer-Pinto et al., 2019). These population migration trends highlight the need for built infrastructure, competing for space with natural habitats that provide essential protective and regulating ecosystem services (Duraiappah et al., 2005; Lotze

et al., 2006; Grimm et al., 2008). Compounded by climate change, damage to the built environment from natural disasters incurs massive economic losses (Tamura and Cao, 2010; Dinan, 2017).

Continued urban migration results in growth of infrastructure and of impermeable surface cover. The overuse of material with respect to foundation construction specifically, also increases soil compaction. Soil compaction and impermeability compromise water storage and infiltration and so contribute to increasing risks of flooding and erosion (Yang and Zhang, 2011; Alaoui et al., 2018). Soil erosion becomes a problem for foundations as their anchorage depends on soil stability. Increasing frequency and intensity of storm events will also impose more severe loading scenarios (Dinan, 2017). Reducing soil compaction, preventing erosion, and adapting to extreme loading scenarios are crucial needs, questioning the current design of building foundations. A multifunctional adaptive approach to foundation engineering should aim at alleviating flooding and erosion potential, while also lowering material usage in construction required to support a structure under various loading scenarios. As seen in the evolution of biological systems, multifunctionality typically increases design complexity. The difficulty of inserting complex structures in the soil without significant excavation in current civil engineering methods limits foundation design to simple morphologies.

Coastal infrastructure protects populations and the built environment against wave action and landward erosion (Bulleri and Chapman, 2010; McLachlan and Defeo, 2018). Continued coastal migration and the effects of climate change require more protective infrastructure that is also substantially larger in size and scale (Ferrario et al., 2014). This trend eliminates, displaces, or fragments natural coastal habitats which provide multiple significant ecosystem functions (Barbier et al., 2008; Strain et al., 2018), not to mention substantially decreasing biodiversity for some of the most diverse global ecosystems (Duarte, 2009). Additionally, traditional coastal engineering practices often cause downstream erosion, wave reflection, bottom scour and subsequent increased nearshore wave heights, and disruption of natural nearshore littoral transport (Silvester, 1972; McLachlan and Defeo, 2018). A multifunctional adaptive approach to coastal engineering should aim at wave attenuation, dissipation, and dispersion to reduce wave action and erosion potential, while also creating physical conditions, such as quiescent flow regimes and habitat refuge spaces, to increase and maintain biodiversity across multiple taxa (e.g., plants, macroinvertebrates, and fish).

We propose that the overarching design framework of biologically inspired design (BID), hereinafter referred to as bioinspired design, can inform the development of sustainable, multifunctional, and adaptive innovations to built infrastructure. Bioinspired design utilizes inspiration from nature to develop technical outcomes (Lenau et al., 2018). In our case, understanding how living organisms embed and stabilize themselves with minimal disruption and degradation to their surroundings, dynamic environment is crucial to our application areas of building foundations and coastal infrastructure. Natural ecosystems contain herbaceous vegetation, woody plants, and trees, in which roots contribute significantly to anchorage of an aboveground structure and subsequent substrate stability. In the case of mangroves and other coastal forests, their root systems

must significantly contribute to wave attenuation and substrate stability along coasts for survival (Koch et al., 2009). Roots also perform multiple functions other than anchorage and substrate stability and adapt to changes detected in the surrounding soil environment through a variety of mechanisms (Malamy, 2005). Therefore, we hypothesize that the study of root systems informs multiple engineering design applications in the areas of foundation and coastal engineering.

Within the framework of bioinspired design lies both biomimetics and biomimicry (Lenau et al., 2018). For the scope of this work we utilize the terms synonymously and employ primarily the problem-driven process of biologically inspired design as our research methodology to present design proposals for our specific application areas. Problem driven biologically inspired design takes on a technical question that is answered by a strategic search for analogous solution in biology. The first step in the problem-driven bioinspired design process and in our research investigation is an assessment of common practices, uses, and applications to identify the technical shortcomings of current building foundation and coastal infrastructure designs. Next, these shortcomings are abstracted, so that the problem, its context, constraints, and necessary functions can be transposed to biology and connected to biological analogs. Principles are extracted from biological models (in our case, root systems) out of their natural context, so that they may be emulated in technological solutions (Vincent et al., 2006; Fayemi et al., 2017). While biomimicry primarily follows the same design steps as biomimetics, its unique attribute is on an ecological philosophy and ethos to meet the challenges of sustainable development (Benyus, 2011; Lenau et al., 2018).

To demonstrate the hypothesis that the study of root systems informs multiple engineering design applications through the overarching design lens of bioinspired design, we present an overview of relevant root biology in “**Roots as Biological Model**” section, with a special focus on adaptation and biomechanics. Through the biomimetics process, specific biological information is then related to infrastructure problems and vulnerabilities through a functional translation in a comprehensive analogy table in “**Abstraction and Analogy**” section (Table 1). “**Application of Root Biology to Technical Designs**” section presents a range of current and future innovative bioinspired design concepts for the fields of building foundation and coastal engineering, followed by Discussion and Conclusion in sections “**Discussion**” and “**Conclusion**”.

ROOTS AS BIOLOGICAL MODEL

Rather than a comprehensive encyclopedia this section provides a general overview of root biology and an understanding of strategies and mechanisms found in root systems for mechanical anchorage, soil stability, and other dynamic external loading conditions relevant for biomimetic translation to the two application spaces of building foundation and coastal infrastructure design. Additionally, there is a general introduction to the use of root systems (and other woody components) in natural constructions by humans, whose

strategies and mechanisms of construction are also relevant to biomimetic translation.

Root Basics

Root Structure Components

Root structure is generally described by four regions or zones (Bidlack et al., 2011). These regions, starting from the end of the root, are the root cap, region of cell division, region of elongation, and region of maturation. The root cap and apical meristem located in the region of cell division are the only regions that push through the soil. The other regions remain stationary. Root diameter gradually increases through addition of secondary tissues in the region of elongation (i.e., radial growth). Lastly, the region of maturation is where root hairs are produced. These are short-lived extensions that adhere tightly to soil particles and increase the total water and mineral nutrient absorptive surface of the root.

Root Classification: Different Types of Roots

There are three main types of roots: primary (i.e., seminal), adventitious (i.e., nodal), and lateral roots (Malamy, 2005). Primary roots stem from seed, while nodal roots initiate from non-root tissue and are coordinated with aboveground shoot development. Many mature plants have a combination of taproot (a thick, vertical, centrally located primary root) and diffuse fibrous (i.e., nodal) root systems (Malamy, 2005; Bidlack et al., 2011). Lateral roots develop by branching, which is coordinated with root elongation (Lecompte and Pagès, 2007), with an equilibrium maintained between root number and length (Malamy, 2005). From a spatial perspective, structural “coarse” roots (sometimes referred to as basal roots) are often near the base of the stem. Their primary function is anchorage, and they may develop considerable secondary thickening. Fine “thin” roots are often much further away from the stem (sometimes referred to as distal roots). Their primary functions are soil exploration to source water and nutrients.

Root Growth Processes

Axial growth and radial growth are the two main types of root growth processes (Hodge et al., 2009). Axial growth is defined as the root extending in length and the tip pushing forward into the soil, with the root parts behind the elongation zone anchored in the soil. The direction of root elongation is triggered by different tropisms, such as gravitropism and hydrotropism (Lynch and Brown, 2001). Axial growth is significantly limited when zones with high soil mechanical resistance is present (Hoad et al., 2001).

Radial growth is defined as additional layers of growth on individual roots, root thickening, or secondary thickening (Hodge et al., 2009). This growth process is important in expanding the range of root functions, including axial transport properties, mechanical strength and anchorage, storage capacity, and protection against predation, drought, or pathogens.

Root System Architecture and Morphology

Root System Architecture, or spatial configuration of the root system, varies greatly depending on plant species, soil composition, water, nutrient, and mineral availability (Malamy, 2005; Hodge et al., 2009). The shape of a root

system is characterized by how the roots occupy the soil and is defined specifically by the traits of root depth, lateral root expansion, and root length densities. The shape of the root system can also be described by abstract synthetic descriptors like fractal dimensions (Tatsumi et al., 1989). The structure is characterized by root system components and their relationships, defined by the traits of root gradients, cross section, topology, and connection between roots (i.e., branching angle) (Malamy, 2005). Root topology describes the abstracted pattern of root branching. Topological order is an important parameter of root trait analysis as it can be a stronger predictor of mechanical properties than root diameter (Mao et al., 2018).

There are three main categories of root system morphology (Ennos, 2000). The plate morphology, often found in mature trees, is characterized by thick lateral roots radiating horizontally or slightly obliquely from the main stem, followed by tapering and branching, in addition to sinker roots originating from lateral roots close to the stem. The taproot morphology, characterized by the single, centrally located taproot, is often found in dicotyledon species (Ennos and Fitter, 1992) and some rainforest pioneer species (Crook et al., 1997). Coronal and prop root morphology is often found in monocotyledon species, as they cannot undergo radial growth and therefore cannot produce a taproot. This type is characterized by thick lignified nodal roots growing obliquely from the stem (Ennos, 1991; Ennos et al., 1993). Many species possess intermediate morphologies (Crook and Ennos, 1998). Intraspecific root grafting seen in forests is believed to contribute to mechanical support and nutrient exchange (Graham and Bormann, 1966; Kumar et al., 1985; Keeley, 1988). Additionally, root system morphology can be affected by symbiotic root—microorganism relationships in the rhizosphere, such as mycorrhizal fungi and actinomycete bacteria (Steeves and Sussex, 1989; Hodge et al., 2009).

Root Function, Development, and Adaptation

Root Adaptation to Soil Patches

To effectively deploy in transient soil patches rich in moisture or nutrients, roots exhibit significant morphological plasticity through modular root structure and tissue differentiation along the root axis (Hodge et al., 2009). Drew and Saker (1975) reported an increase in lateral root initiation in soil patches, while Linkohr et al. (2002) found a repression of lateral root elongation outside the patches. Root systems also shed roots when resource uptake becomes insufficient (Hodge et al., 2009).

Root Adaptation to Soil Density, Compaction, Resistance, and Moisture

Roots must overcome soil resistance to displace soil particles as the root grows. As a result, root diameter increases and root elongation decreases with increasing soil strength (Correa et al., 2019). Soil zones of variable resistance impact root growth rate, morphology, orientation, and the local soil-root environment (Hodge et al., 2009 and associated references therein). Roots generally follow the path of least resistance, leading to distinct environments compared to the bulk soil (Pierret et al., 1999; Hodge et al., 2009).

To grow through soils, root tips need to generate enough force to expand a hole in the soil, exceed frictional resistance of the root tip with the soil particles, and exceed the internal tension in the root cell walls (Bengough et al., 2011). It is suggested that up to 80% of total penetration resistance results from friction (Greacen et al., 1968; Bengough et al., 1997). The friction between soil particles and roots, presence of root hairs, and potential root trajectory also assist in anchoring the root, so that tissues in the elongation zone can push the root tip forward (Bengough et al., 2011).

Circumnutations (i.e., revolving nutation), present in all plant organs (Hart, 1990; Kiss, 2006; Mugnai et al., 2007), are the result of differential growth, resulting in active growth movement following an elliptical path in a left-handed or right-handed rotation (Johnsson, 1997). The role of root circumnutations is still debated, but Dottore et al. (2018) found that this movement reduces the pressure and energy required to penetrate soil.

Roots passively secrete low molecular weight organic compounds in the rhizosphere, called root exudates. These exudates promote microbial activity and soil stabilization through mucus like adhesion, known as mucilage (Tisdall et al., 1978; Cheshire, 1979; Amellal et al., 1998). Rapid wetting/drying cycles induce shrinkage and cracks in the soil, which reduces hydraulic conductivity due to the presence of large pores in the soil matrix (Grant and Dexter, 1989). Czarnes et al. (2000) found that a root mucilage analog (e.g., polygalacturonic acid) stabilized the soil structure against the disruptive effects of wetting/drying cycles.

Root Adaptation to Continual Water Inundation and High Salinity

Flooding induces ethylene production in the root, which signals increased nodal and lateral root formation posited for increased stability (Hodge et al., 2009). Mangroves, exhibiting a complex stilted root network, only exist in tropical climates in cyclically submerged environments, with muddy, waterlogged anoxic soils and high salinity. Mangrove roots can generally be classified into four types: stilt root, knee root, snorkel root, and buttress root (Tomlinson, 2016). To obtain adequate oxygen supply from the air to belowground roots, mangroves increase adventitious root production specifically with spongy, erenchymous tissue near the sediment surface (Hodge et al., 2009). Pneumatophores, vertical erect roots that emerge from shallow adventitious roots (Bidlack et al., 2011), are known to slow water currents, attenuate waves, and increase sedimentation (Mazda et al., 1997; Hogarth, 2015).

Contractile Roots Adapted to Environments With Low Water Availability

Contractile roots are found across multiple plant groups, which mostly inhabit environments with harsh seasons such as drought or cold temperatures (Pütz, 2002). This behavior, which protects plant organs and young shoots from harsh conditions by pulling them down into the soil, is also known to improve plant anchorage and water uptake (Jernstedt, 1984; Pütz, 2002; North et al., 2008; Bidlack et al., 2011).

Root Biomechanics

The Root-Soil Plate: Effects of Behavior as One Mechanical Entity

In Coutts (1983) and associated references therein, various studies on the behavior of rooted soil under stress found that tree roots increased soil shear strength by 1–17 kPa. When resistance of the root-soil interface is higher than the surrounding soil strength, the root-soil mass behaves as a single unit under applied load, known as the root-soil plate. This plate is especially visible in uprooted trees. Root-soil resistance is affected by branching and distribution in number and size of roots. Roots stiffen the soil similarly to how rebar rods stiffen a beam, as they mostly resist tensile loads. Depending on soil conditions, root breakage and slippage through soil are the main failure mechanisms. In clay soils where the soil resistance is greater, roots slip instead of break, meaning that root-soil resistance is more a function of soil resistance than root morphology and strength (Waldron, 1977). Root morphology and strength play a greater role when the soil moisture content is a little below its saturation point.

Effect of Root Hairs on Anchorage and Growth

Ennos (1989) suggests in a study on sunflowers that root hairs play a major role for the anchorage of young plants against uprooting by increasing the effective root surface area in contact with the soil. Additionally, Stolzy and Barley (1968) saw an increase in tension resistance of individual roots of *Pisum sativum* seedlings with root hairs compared to ones without root hairs. According to Ennos (2000), it is far less likely that root hairs are useful in the anchorage of mature plants, since root hairs are only produced near the tip of elongating roots in the maturation zone where mechanical stresses are relatively low for large mature plants. In this case, the major mechanical role of root hairs is in root tip growth, as root hairs anchor the root while the tip is pushed forward through the soil (Stolzy and Barley, 1968; Ennos, 2000; Bengough et al., 2011).

Effect of Roots on Slope Stability

Trees reduce soil erosion and prevent shallow landslides through a network of coarse and fine roots just below the surface that increase the shear strength of the soil medium, and sinker roots that anchor the surface layers to a deeper, more stable soil mass (Nicoll et al., 2005). Structural root mass has been found to be greater on the upslope side of exposed trees on slopes, explaining the increase in resistance to upslope overturning (Nicoll and Ray, 1996). Liang et al. (2017) demonstrated in a slope stability simulation using a 3D printed root structure that root strengthening pushes the soil shear plane deeper in the soil. Root strengthening depends on species-specific root mechanical properties, surrounding confining stress, depth of the initial soil slip plane, and root morphology. The maximum reinforcing effect from root strengthening may require increased root depth of sinker roots and lateral extension to enhance soil shear strength. In a Fiber Bundle Model (FBM) framework to estimate root cohesion, Arnone et al. (2016) found that the effects of root water uptake may be more significant than mechanical reinforcement for slope stability, especially in fine soils.

Effect of Roots on Wave Attenuation

In a mature mangrove forest, Mazda et al. (1997) observed that wave attenuation does not decrease with increasing water depth, which is very beneficial in cases of storm surge and sea level rise. Mangrove swamps of *Rhizophora spp.* or *Bruguiera spp.* have intricate and large pneumatophores and therefore provide resistance to flow due to increased projection area. Wave energy loss is caused by both bottom friction and flow resistance (i.e., drag force) by mangrove vegetation (trees, trunks, and roots) through the entire water column. The submerged tree volume and projection area of aboveground mangrove root morphology play a significant role in attenuating tsunami inundation flow (Ohira et al., 2013).

Effect of Roots to Lateral Aboveground Stresses

The components and relevant parameters of anchorage under lateral forces (e.g., wind) include root-soil plate dimension, root and soil tensile strength beneath the plate, root-soil resistance specifically on the windward side, and stiffness at the pivot point at the base of the tree (Coutts, 1983). A root system of a tree subjected to wind loads responds through increased growth of the roots aligned with the plane of stimulation (Nicoll and Dunn, 2000). On the leeward side, bending and compressive forces push the root-soil interface against the soil below. On the windward side, tensile and/or shear forces are present due to uplifting.

A study conducted by Tamasi et al. (2005) showed that wind loading on young *Quercus robur* L. trees resulted in increased total lateral root number and length in wind stressed trees compared to control trees. Wind loading appears to result in increased growth of more lateral roots and higher structural root mass on the leeward side. Root systems of adult *Picea sitchensis* trees exposed to a natural prevailing wind had higher structural root mass on the leeward side instead of the windward side (Nicoll and Ray, 1996). A study conducted by Stokes et al. (1995, 1997) on young *Picea sitchensis*, showed greater numbers of both windward and leeward roots, more elongated and branched morphology, and increased root diameter.

Although tap roots play a role in initial tree anchorage (Crook et al., 1997), evidence suggests that lateral roots are the major component of anchorage in response to dynamic loading conditions (Ennos et al., 1993; Stokes et al., 1995; Ennos, 2000; Stokes, 2002; Dupuy et al., 2003; Cucchi et al., 2004). If there are too many roots in the soil however, the soil will likely fail in shear and tension at the edge of the soil-root plate (Ennos et al., 1993). Ennos (2000) also notes that plants minimize the total energy cost of anchorage when exposed to uprooting potential by only strengthening (i.e., thickening) the basal parts of the root system.

The location of roots defines their cross-sectional shape. Bending resistance seems to occur through changes in structural roots cross-sections, producing I-beam, T-beam, and oval cross-sections (Rigg and Harrar, 1931). Ennos (2000) describes the components of root system morphology that resist lateral stresses. The plate morphology has three components of anchorage: resistance of leeward hinge to bending, resistance of the windward roots to uprooting, and

weight of the root-soil plate. The taproot morphology has two components of anchorage: soil compressive resistance and taproot bending resistance. The morphology of coronal and prop roots also have two components: soil compressive resistance and buckling resistance of the windward roots.

Effect of Buttress Roots to Lateral Aboveground Stresses

Uneven secondary thickening between root and stem results in the development of supporting buttresses (Bidlack et al., 2011). Crook et al. (1997) studied the anchorage of taproot systems: buttressed trees of *Aglaia* and *Nephelium* possessing sinker roots, and non-buttressed *Mallotus wrayi* trees with thin lateral roots. Buttresses provided six times more anchorage than the thin lateral roots of non-buttressed trees and approximately 60% of the anchorage acting in tension and compression. Buttresses of tropical trees are also more often found on the less dense side of an asymmetric crown, suggesting that buttresses partly serve as tension elements to equalize mechanical stresses (Young and Perkocha, 1994; Crook and Ennos, 1998). In addition, buttresses are believed to reduce the risk of buckling failure (Young and Perkocha, 1994), and reduce bending and concentration of stress at the base of the tree (Mattheck et al., 1993).

Root Utilization in Human Constructions

Tree root systems have been directly utilized in several natural constructions by humans. These constructions are an example of bio-utilization or biotechnology, and in combination with traditional engineered or technical components, can take on the form of bio-hybrid approaches. In the case of streambank stabilization and restoration ecology practices using large woody debris (LWD—e.g., fallen trees, stumps, rootwads, and branches) (Svoboda and Russell, 2011), their biological analogs are in beaver dams and complexes (Wright et al., 2002), natural woody debris (WD), and natural log jams (Larson et al., 2001). Naturally occurring LWD jams were removed from many rivers for flood control and navigation during the 20th century (Montgomery et al., 2003), but these structures are currently being re-introduced due to benefits such as habitat complexity and restoration, debris retention, in addition to erosion protection, stabilization, and grading control (USBR and ERDC, 2016).

Abbe et al. (1993) studied the distinctive patterns exhibited by natural LWD jams, identifying categories and types of accumulations and jams by size, position, orientation, frequency, and type of WD. Continued in the study by Abbe and Montgomery (2003), this categorization provides a framework and typological basis for which to describe the ways these jams influence stream geomorphology, floodplain formation, and riparian habitat. Different LWD configurations and jams produce erosional and depositional zones at varying lengths downstream of the structure and/or within the structure depending on hydraulic and geomorphic project objectives. These jams can also be designed to freely move during higher velocity flows or persist for centuries as stable structures (Svoboda and Russell, 2011). The position of logs within a stream channel, wood density, and decay rates as a function of tree species and

TABLE 1 | Analogy table ("Abstraction and Analogy" section).

		Biological role models	Functions/Working principles	Problems/vulnerabilities
Soil erosion	1	Root/soil plate network behaving as one entity due to adhesion between soil particles and presence of root hairs Coutts (1983); Bailey et al. (2002)	Network of thread-like elements in contact with granular media to distribute load prevents movement of this media in response to tensile and shear forces	Soil erosion around building foundations; for example, during heavy precipitation events, or exposed location on a steep slope/cliff (with or without precipitation)
	2	Single root fan facing upstream deflects flow, additionally disrupts, partitions and slows the flow that passes through fan via drag, resulting in less scour within the structure Svoboda and Russell (2011)	Single flow deflection structure oriented in direction of predominant flow, composed of cylindrical elements with variable length, cross section, diameter/width, orientation and curvature arranged in a non-uniform porous branching pattern that disrupts flow through structure	High water velocity leading to erosion and poor habitat conditions
	3	Position and orientation of several tightly placed rootwads in naturally occurring, stable log jams, including those constructed by beaver for habitat Abbe et al. (1997); Abbe and Montgomery (2003); Svoboda and Russell (2011)	Large cylindrical elements with complex fractal-like endings facing the flow act as key anchoring and stabilizing elements of a single assembled porous yet stable structure of multiple elements	Coastal erosion and scour, specifically caused by wave action and reflection
	4	Irregular distribution, configuration and porosity of roots and tree trunks in mangrove swamps resulting in flow obstruction/wave attenuation Mazda et al. (1997); Kazemi et al. (2017)	Semi-rigid elements in a varied distribution of spacing and orientation in a continuous and connected system causing wave attenuation with reduced reflection; also increasing drag, which reduces downstream flow velocity and shear stress	High velocities and wave action in nearshore area leading to coastal erosion, turbidity, poor habitat conditions due to high water flow and poor water quality, and inland flooding risk
Structural support	5	Root system architecture recruiting large volume of soil and surface area to support tree and respond to variable loading conditions	Structural support through a wider distributed network of elements	Low resilience of foundation piles to changing loading conditions due to limited volume of soil used for support due to simple shape
	6	Interweaving of roots and root grafting between trees of same species contributing to mechanical support Graham and Bormann (1966); Kumar et al. (1985); Keeley (1988)	Continuous weaving of thread and stem like elements into a connected network in granular media	New engineering structures not connected to or benefiting from existing artificial structures already in place
	7	Asymmetric root morphology resisting asymmetric loading conditions due to wind and weight of tree canopy Young and Perkocha (1994); Nicoll and Ray (1996); Nicoll and Dunn (2000); Tamasi et al. (2005)	Structural adaptation under asymmetrical load by increasing number of rigid elements on the compression side and thread-like elements on the tension side	Engineering structures not designed to support and adapt to specific directional loading conditions
	8	Differentiated root morphology for sloped terrain Reubens et al. (2007); Danjon et al. (2008); Stokes et al. (2009); Liang et al. (2017)	Main deep sinker element providing anchorage with shallow thread-like elements retaining soil particles in a sloped terrain to stabilize structure and media	Engineering structures—such as foundations and coastal infrastructure—lacking specialized adaptation or design for sloped terrain
	9	Adapted root distribution to chemical and mechanical soil conditions Ennos (2000)	Adaptation of structural morphology to changing environment	Fixed engineering structures unable to change/adapt to changing environment
	10	Mangrove root morphology supporting and erating the tree in both low-tide (roots surrounded by air) and high tide (roots surrounded by water) environments Ohira et al. (2013); Hogarth (2015)	Flexible branching/network able to transfer varying loads to granular media when surrounded by fluid of different densities	Structures built for one water level not effective outside of their designed range (e.g., seawall height unable to counter sea level rise)
	11	Buttresses transferring loads from the trunk to the soil/root plate Young and Perkocha (1994); Crook et al. (1997)	Element connection shape optimized for stress reduction based on the tension triangles rule Mattheck et al. (2006)	Stress concentrations in connections
	12	Development of a "T" or "I" cross section in structural roots Nicoll and Ray (1996); Nicoll (2006)	Adaptation of the element's cross-sectional profile in response to specific loading conditions	Fixed cross section of elements, overdesigned to resist diverse loading conditions
	13	Design of lateral roots and root hairs that physically attach to soil particles at the micro scale Bailey et al. (2002)	Increase loading capacity of macro structures through skin frictional contact between granular media and network of thread-like elements by integrating highly textured micro surfaces	Foundations designed at macro scale not utilizing micro interactions between foundation and soil particles to increase loading capacity
	14	Root mucilage enhancing bond strength between soil particles and roots to counteract soil shrinkage/expansion caused by rapid wetting/drying cycles Czarnes et al. (2000); Galloway et al. (2020)	Increase loading capacity of macro structures by attaching thread-like elements to granular media with chemical adhesion	Foundations not chemically connected to the soil particles at the micro scale for increased loading capacity

(Continued on following page)

TABLE 1 | (Continued) Analogy table (“Abstraction and Analogy” section).

		Biological role models	Functions/Working principles	Problems/vulnerabilities
Soil penetration	15	Cone shaped root morphology due to growth resulting in diameter gradient along root axis from thin root tip (earliest growth) to thick root flair (mature growth)	Tapered element to facilitate penetration of granular media	Mechanical resistance of soil overcome with higher forces to penetrate soil
	16	Contractile root behavior pulling the plant into the soil to protect plant organs from extreme temperature, low moisture and increase anchorage North et al. (2008)	Creating a shortening of the attachment to lower attached element to reduce exposure to extreme conditions, also increases tensile force and improves anchoring	Engineering structures degrading over time under weathering and tensile structures yielding under constant loading
	17	Root turning in the soil by differential growth response, triggered by auxin distribution in the elongation zone Chen et al. (1999); Blancaflor and Masson (2003)	Turning in a granular media by differential expansion of a thread-like element	Inability to change direction of soil penetration in granular media when driving foundation piles into soil, mostly vertical or near-vertical orientation
	18	Root hairs and root curvature anchoring the root allowing the root tip to move forward in the soil due to cell elongation Bengough et al. (2011)	Combination of functions: Anchorage and size expansion from anchoring point, therefore resulting in forward movement	Construction equipment limited to pushing and expanding a structure just from the surface through the soil
	19	Circumnutations of root tip to find path of least resistance in the soil to facilitate growth Minorsky (2003); Migliaccio et al. (2013)	Moving the tip of the digging element in a circular or spiral path to find least resistance regions in granular media	Difficulty of finding path of least resistance when digging or pushing through granular media
Conditions for living organisms	20	Space between mangrove roots differing with respect to height Twilley and Day (2013)	Distribution and geometry of voids with respect to organism body size supporting habitats for organisms, diverse predator-prey interactions and prey refuge	Lack of habitat complexity along hardened shorelines reducing diverse food web interactions
	21	Snag/root roughness preferred substrate for invertebrate colonization, increasing foraging habitat for prey fish Angermeier and Karr (1984); Wallace and Benke (1984); Benke et al. (1985)	Heterogeneous surface textures and structures	Hard, flat and smooth surfaces of coastal infrastructure reducing habitat availability for sessile or habitat-forming organisms
Multifunctionality	22	Thermal energy absorption from the soil by roots and distribution to the tree Ballard et al. (2009)	Utilizing stable temperature of soil to heat/cool a system	Current building foundations not designed to actively contribute to geothermal exchange in buildings
	23	Mangrove root adaptation in anaerobic, high salinity, waterlogged soils Robertson and Alongi (1992); Hogarth (2015)	System able to develop in harsh environment due to adaptive survival strategies that creates favorable environment for other systems to function and exchange resources	Static, heavy and bulky structures required to provide stability of waterlogged muddy soils eliminating space for natural habitat
	24	Root system and soil exchange of nutrients, carbon and water, also between mycorrhizal fungi when present	Constant exchange of resources with the environment to enhance growth and adaptation to stimuli	Engineering structures unable to facilitate exchange of water and resources with the soil (e.g., water uptake, water discharge, carbon sequestration)
	25	Self-healing properties of trees by accretional growth around wounds Bloch (1952); Cremaldi and Bhushan (2018)	Adaptive gap closure through material accretion	Engineering structures—such as foundations - often inaccessible for active repair

moisture content, all affect the structure’s stability and life expectancy, but will commonly exceed the design life of most engineering projects (Abbe et al., 1997).

LWD drag depends on the cross-sectional area of a flow obstruction, incident flow velocity, an “obstruction form descriptor” coefficient, and a blockage coefficient equal to the ratio of the structure’s total cross-sectional area to the channel cross-sectional area perpendicular to flow (Gippel et al., 1992; Abbe and Montgomery, 1996; Abbe et al., 1997). Similar geometrical parameters governing drag are also seen in a study conducted to examine the flow-structure interactions of modeled mangrove circular patches (Kazemi et al., 2017). Porosity, defined in the study as the ratio of submerged root volume to total defined volume, spacing ratio between cylindrical models of mangrove roots, and flexibility are influencing parameters for drag and mean downstream velocity.

ABSTRACTION AND ANALOGY

Based on the review of root biology and current problem areas, an analogy table (Table 1) was created to link relevant biological principles with technical problems or vulnerabilities in the civil and coastal engineering fields via an identified abstracted function and working principle. The table can be read from both sides: starting with root biology, it allows for linking the working principle to an engineering field and starting with the technical problem area, it allows for linking to a working principle also present in biology. The main themes (i.e., soil erosion, structural support, soil penetration, conditions for living organisms, and multifunctionality), point to broader problem areas. This table provides an overview of the translation opportunities that were found from investigating both biology and engineering through the lens of biomimetics.

APPLICATION OF ROOT BIOLOGY TO TECHNICAL DESIGNS

In this section, we present the two main application areas for the problem-driven biomimetic approach, building foundations and coastal infrastructure. We discuss current practices, limitations and shortcomings, followed by a broad listing of current experimental and innovative solutions. We end by exploring a range of speculative, bioinspired design concepts informed by root biology to illustrate the biomimetic approach.

Building Foundations

Current Foundation Design and Problem Review

Building foundations transfer aboveground structural stresses to the underlying soil by transmitting gravitational loads, stabilizing the structure against overturning and lateral movement, and providing resistance to uplift. Current foundations function by creating a contact surface area with the soil bearing the loads, pre-consolidating the underlying soil, utilizing the foundation weight under gravity, and/or anchoring it to a rock layer (Hobst and Zajíc, 1983).

Depending on soil conditions and loading scenario, foundation design follows two main types: shallow and deep foundations. Shallow foundations, such as strip footing, spread footing, or raft, transfer loads to the soil close to the soil surface and are used for low loading capacities. Deep foundations, such as piles, drilled shafts, and caissons, are used for high intensity heavy building types and resist lateral and uplifting forces. They are also used when the upper layers of soil are weak, collapsible, expansive, or subject to soil erosion (Das, 2007). They can reach depths of hundreds of meters into the ground (Frost et al., 2017).

The structural capacity of foundation piles depends on the bearing capacity of the pile tip and lateral friction of the pile (Das, 2007). Foundation pile design is determined by loading type, subsoil conditions, and location of the water table. In weak soils, point bearing piles are built up to the rock surface or into a strong soil layer if within reasonable depth. Otherwise, piles relying on friction with the soil particles or increased soil compaction are placed. In clayey soils, adhesion also helps to hold the pile in place (Das, 2007). Vibro-compaction and vibro-replacement methods are economical and well-established techniques to improve weak or loose soils through compaction (Baumann and Bauer, 1974). Depending on pile design and material, different techniques are used to insert them in the ground. Piles are driven in the soil with various types of hammers or vibratory drivers, but other techniques may be employed for specific scenarios such as jetting and partial augering (Das, 2007).

Typical foundation piles are made of wood (e.g., timber piles), concrete (e.g., precast or cast-in-situ piles), and steel (e.g., pipes or rolled H-section piles) (Das, 2007). Steel piles are easily managed, supporting high driving stresses, penetrating hard soil layers, and carrying relatively high loads. They are expensive, subject to corrosion, and may be damaged during soil insertion. Precast concrete piles also support high driving stresses while resisting corrosion, but they are more difficult

to maneuver and properly cut. Cast-in-situ piles are cheaper, and the steel cast can be inspected before pouring the concrete, but the casing may be damaged during soil insertion and the resulting pile can be difficult to connect after pouring. Timber piles are limited in terms of driving force and loading conditions (i.e., capacity and direction). Composite piles are composed of different materials which are difficult to join, so they are not widely used (Das, 2007).

There are several limitations and shortcomings to current foundation design, engineering, and construction practices. First, deep foundations are limited to simple vertical or near vertical (i.e., 0° with respect to the pile axis) cylindrical piles, due to the inability of current drill and dig construction techniques to actively change direction in the soil (Frost et al., 2017). It has been demonstrated that increasing the angle of foundation piles from 0° to 15° and 30° increases the loading capacity of the foundation due to a larger bearing area (i.e., surface area of the soil in contact with the pile and supporting pile weight) (Frost et al., 2017). Compared to a traditional smooth vertical pile, the introduction of a branching angle of 15° doubled the downward bearing capacity, and a branching angle of 30° tripled this capacity (Frost et al., 2017). Additionally, orchard tree root systems showed an increase of vertical pullout resistance by 8–13 times compared to traditional micropile foundations of comparable volume and mass (Burrall et al., 2020). Second, foundations are monofunctional as they are only designed to support a structure, while we use other artificial subsurface technical structures for other functions (e.g., energy conversion). Third, the capacity of foundations to resist loads and forces is not dynamic and adaptable (some exceptional technologies exist for earthquake prone applications). Foundations are usually built as static structures and are expected to maintain morphology and materiality over time. They cannot adapt to changing environmental conditions, such as varying loads applied to the structure and soil movement, therefore operating on a single timescale. Lastly, foundations are located underground, therefore inaccessible for maintenance. The use of materials that lack self-healing properties requires an over-design to counter this potential drift in performance over time.

Root systems can serve as inspiration as they share similar functionality and design requirements with foundations such as anchorage and soil penetration, but also provide adaptability and multifunctionality. Root systems possess a large bearing area compared to their volume, due to their branched morphology and the presence of microstructures. Complex root morphology is also a result of the multiple functions provided for the tree such as soil exploration, nutrient/water exchange and transport, anchorage, and thermal regulation, which in turn provides additional ecosystem services such as erosion prevention. Additionally, root systems adapt and respond to stimuli over multiple timescales (e.g., daily fluctuations and constant long-term loads) through transient (e.g., damping) and permanent responses (e.g., reaction wood growth, self-healing). Since root systems are part of a living multicellular organism, they can heal and regenerate tissues of their anatomy. The foundation designs of the future could mimic these root system strategies.

With this biomimetic approach to foundation design, multiple research questions arise: Which design parameters informed by root systems would increase the loading capacity of foundations without adding weight? How can complex branched structures be inserted in soil with minimal disturbance? How can a foundation actively or passively adapt to changing external internal loads as informed by root adaptation mechanisms? Which additional functions could be fulfilled by foundations other than anchoring a building in place? How could biological organisms be integrated into bio-hybrid foundation designs and to what benefit?

Current Innovative Solutions for Foundation Design

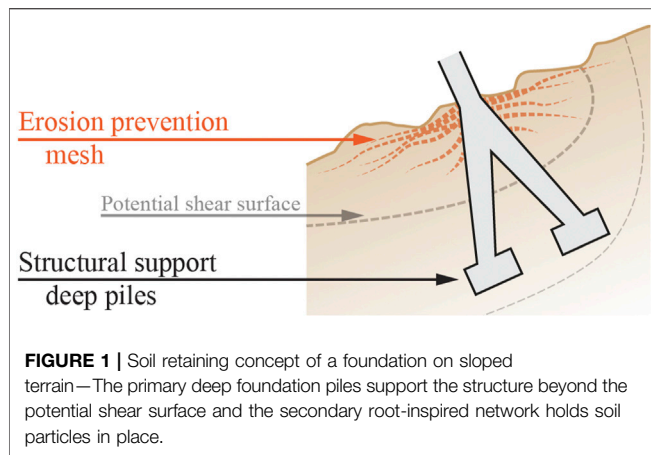
In the following list, we summarize current innovative strategies for future foundation designs, from morphological variation to integration of biological organisms. They are organized under four main topics of interest referring to the analogy table in “**Abstraction and Analogy**” section (Table 1): soil erosion, structural support, soil penetration, and self-healing, as an aspect of multifunctionality.

- Preventing soil erosion—Various geosynthetic products are available on the market. The stabilizing effect of a thread-like element in granular media has been investigated by the placement of a textile filament layer by layer around loose rocks and exposed at the Chicago Architecture Biennial 2015.¹ Additionally, bacteria that bind to soil particles, have been used to strengthen the mechanical properties of soil through Microbial Induced Calcium Carbonate Precipitation (MICP) (DeJong et al., 2006; Whiffin et al., 2007; Van Wijngaarden et al., 2011). The use of genetically modified bacteria to precipitate calcium carbonate when soil pressure is detected to react to changing loading conditions is tested with computational models (Dade-Robertson et al., 2018).
- Geometric alternatives to support structures—Foundation geometry is a defining factor for total loading capacity and pile displacement (Frost et al., 2017). Conical piles provide an increased bearing capacity compared to straight-sided cylindrical piles (Manandhar and Yasufuku, 2012). The lateral surface texture of foundation piles is another parameter to increase loading capacity by increasing shear strength of its interface with soil (Martinez and Frost, 2017). Research in this field stressed the need to design foundation surface roughness, in opposition to current smooth or only randomly structured construction materials, such as randomly textured high-density polyethylene geomembranes and roughly finished concrete (Frost et al., 2002). Biological textures, such as snakeskin, were studied to produce bioinspired surfaces designed for foundation piles and yielded promising results for increasing directional friction (Martinez et al., 2018; Martinez et al., 2019).
- Robots for soil penetration—Due to the difficulty of inserting non-linear structures in soils, burrowing robots inspired by animal (Calderón et al., 2016; Khosravi et al., 2018; Calderón et al., 2019) and plant strategies (Sadeghi et al., 2014; Hawkes et al., 2017; Sadeghi et al., 2017; Dottore et al., 2018; Greer et al., 2019; Ozkan-Aydin et al., 2019) have been explored in the past decade. For example, an earthworm inspired robot mimicking peristaltic waves by activating axial and radial contraction, was built with three silicone body segments and able to crawl through straight and curved pipes (Calderón et al., 2016; 2019). While current soil monitoring techniques use probes that are pushed in the ground, self-burrowing probes, based on radial expansion of sections of the probe, have been studied and simulated in sandy soils (Khosravi et al., 2018). Animals use their musculature to move and dig in soils whereas the root tip of plants grows through the substrate (Sadeghi et al., 2014). Root systems, and especially root tip growth, have served as inspiration for growing robots (Del Dottore et al., 2018). For example, root tip growth has been translated into a robot that can sense its environment and grow in diverse directions through additive manufacturing (Sadeghi et al., 2014; Sadeghi et al., 2017). Directional growth by extension of the body tip has also been translated in soft robotics to conform to constrained environments (Hawkes et al., 2017). In addition, the influence of circumnutation to facilitate soil penetration has been tested with artificial probe tips (Dottore et al., 2018). These movements have also been implemented in a soft robot growing in a 2D environment (Ozkan-Aydin et al., 2019).
- Self-healing—Self-healing in biology has been explored and is being translated into bioinspired healing materials with the following mechanisms: protective coating, autogenous healing, shape memory, chemical activity, vascular systems, and bio-healing (Cremaldi and Bhushan, 2018). Bio-healing refers to the use of biological organisms to perform self-healing, such as spore-forming bacteria in self-healing concrete (Jonkers, 2007). Concrete also can self-heal cracks with water and carbon dioxide through chemical activity (Li and Yang, 2007). The crack closure of two different systems of self-healing concretes, based on polyurethane and superabsorbent polymers, has been successfully tested on large-scale prototypes (e.g., concrete beams of 150 mm × 250 mm × 3000 mm) (Van Tittelboom et al., 2016). Self-healing concrete has yet to be tested at the scale and environmental conditions of building foundations.

Root-Inspired Design Proposals for Building Foundations

Studying, abstracting, and transferring biological root system strategies to the field of foundation engineering can yield innovative designs, addressing the shortcomings of current foundation designs. In the following section, various bioinspired design strategies are presented at an abstract conceptual level, disregarding scaling and materiality at this point, which should be explored in further research projects.

¹<https://selfassemblylab.mit.edu/rock-printing/>



Root-Inspired Erosion Prevention

The following soil retention concept for a foundation is inspired by the erosion prevention of root systems in sloped terrains. Root systems have the capacity to prevent soil erosion by soil particle retention through entanglement and chemical bondage, but foundations are only designed to structurally support a structure (row 1 of **Table 1**). Foundations located in environments subject to soil erosion such as riverbanks, cliffs, or steep slopes would benefit from erosion prevention measures. The root system of a tree growing in sloped terrain develops vertical roots along with horizontal thin lateral roots retaining soil particles downslope of the tree (row 8 of **Table 1**). A technical building foundation could mimic this strategy and combine a main vertical structure to anchor the building with a secondary structure to retain soil particles (**Figure 1**). A mesh, similar to existing geosynthetic fabrics or a network of laterally branched elements near the surface, can be integrated in the design of foundations to reduce erosion. Soil particle retention could be achieved through chemical or mechanical attachment.

Root-Inspired Structural Support

The first concept of root-inspired structural support is inspired by the root grafting strategy found in forests to achieve cooperative building foundations (row 6 of **Table 1**). A newly constructed foundation can be connected to existing infrastructures to increase the load bearing area and the volume of soil recruited to support the structure, while making the foundation more resilient under extreme loading scenarios. Additionally, the connection to existing structures can provide an interface to exchange resources, such as water and thermal energy. The multifunctional aspect of this network of foundations is further described in section “**Multifunctional Root-Inspired Foundations**”.

The second concept is on structural optimization based on both root adaptation to specific loading conditions as well as machine learning (row 7 and 12 of **Table 1**). Studying the adaptation of root systems to changing loads and environments can inform the design of root-inspired structural support systems subjected to similar loads. Computer simulations and machine learning can be used to process root adaptation data

and apply the algorithms to foundation design. The following steps are required. First, root trait data about adaptation to various loading scenarios needs to be collected. A database will be populated with relevant traits in relation to the type of loads applied to the tree. A machine learning algorithm can then simulate how a root system would react to specific loading conditions. Finally, the morphology of this simulated root system could be used to inform the design of a new foundation (**Figure 2**).

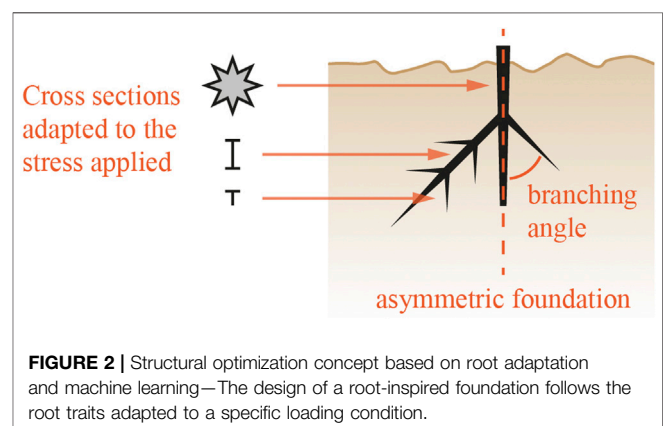
The third concept of root-inspired structural support aims at translating the hierarchical structure of root systems for the transfer of structural loads to soil particles down to the microscale (row 13 of **Table 1**) through highly textured foundation surfaces. As this is interconnected with the soil insertion techniques, those concepts are explored in section “**Root-Inspired Soil Penetration Devices**”. Biological adhesives could also be secreted by the foundation to strengthen the bond between the foundation and soil particles as an analogy for mucilage (row 14 of **Table 1**).

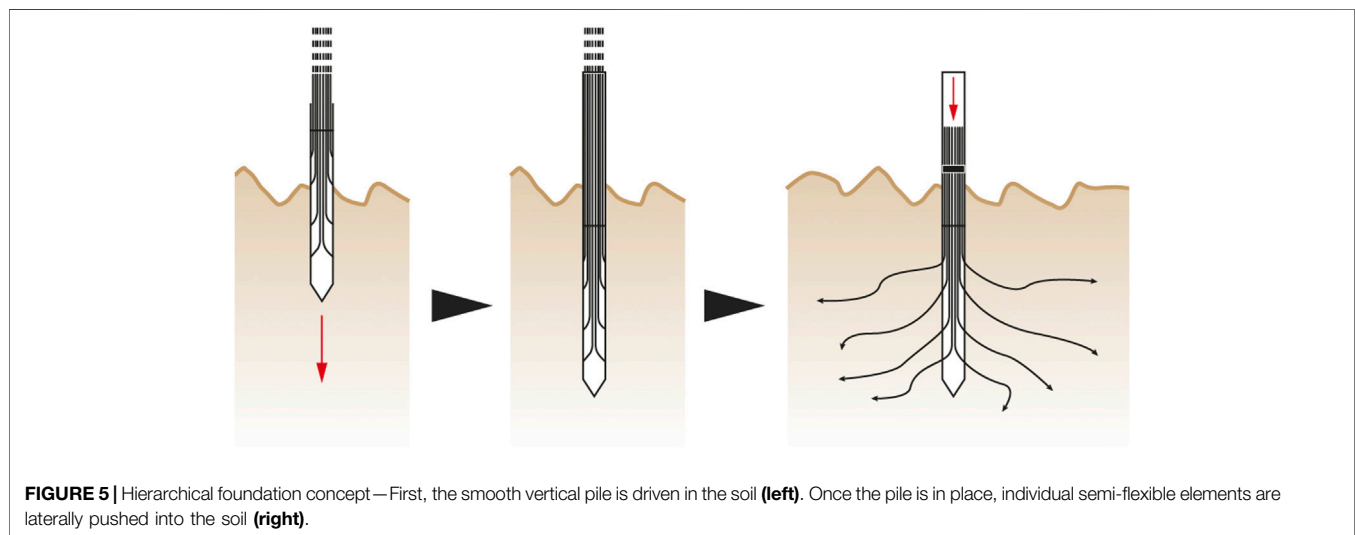
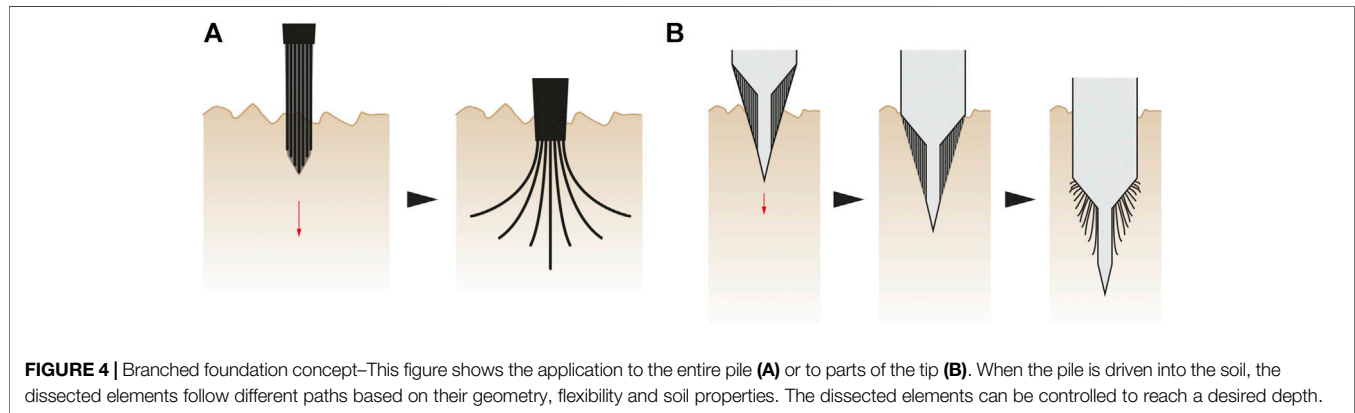
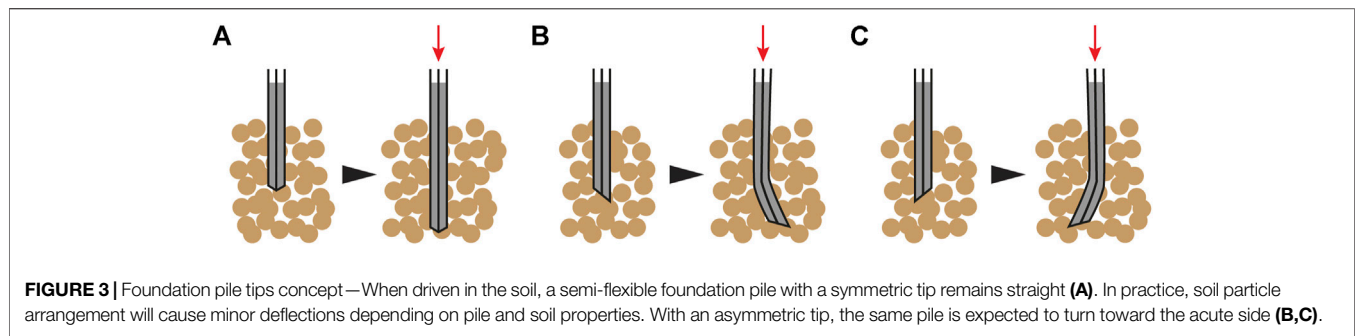
Root-Inspired Soil Penetration Devices

In biology, multiple mechanisms allow organisms from animals to plants to move through granular media. The main question addressed in the following concepts is how to transfer biological strategies of root systems to an artificial soil penetrating system.

The first concept of root-inspired soil penetration is on foundation pile tips inspired by the tapered root tip geometry that facilitates soil penetration (row 15 of **Table 1**). The tip geometry of a semi-flexible linear element affects its interaction with soil particles and the resulting path through soils during soil insertion. Therefore, controlling tip geometry could serve to guide a semi-flexible pile to follow a specific path (**Figure 3**).

The second concept of root-inspired soil penetration is on branched foundations, emerging from the previous concept on tip geometry. First, the cross section of a pile made of semi-flexible material is extended into multiple thinner elements. Driving this dissected pile in the soil will produce a branched geometry that increases the load bearing area (row 5 of **Table 1**). The branched geometry is expected to be a result of the pile material properties, geometry of the dissected elements and their

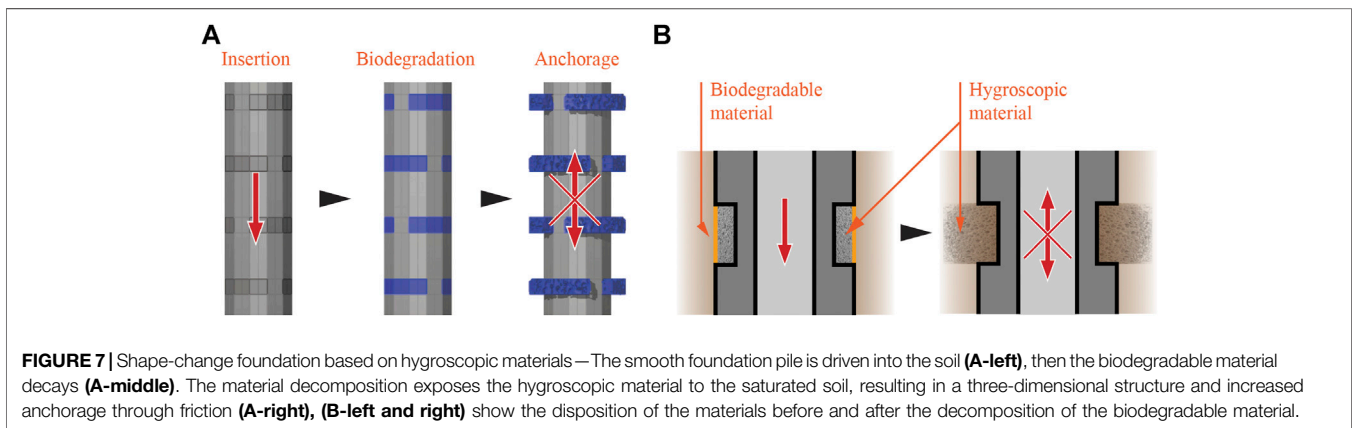
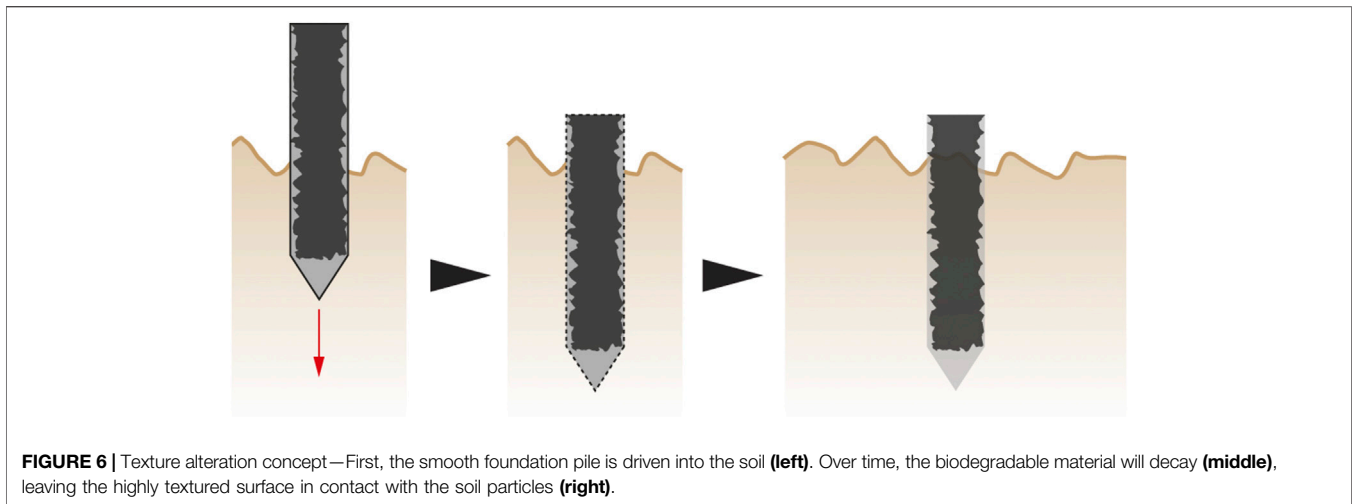




tips, and soil properties (**Figure 4A**). The tip geometry can also be actively controlled to distribute the branched structure throughout the soil in a specific arrangement. This concept of branched foundations can be applied to an entire pile tip (**Figure 4A**) or tip parts (**Figure 4B**).

The third concept of root-inspired soil penetration is on hierarchical foundations, based on the ability of roots to produce a complex branched structure in the soil through initial insertion of linear elements only. This strategy

facilitates soil penetration while providing structural support at a later stage. Following this analogy, foundations can be designed for multi-phase implementation. A smooth linear vertical foundation pile can first be inserted in the ground. Thinner linear elements can then be pushed from this vertical pile into the soil laterally to improve anchorage (**Figure 5**). These lateral elements can also serve as anchors to push against while the foundation tip is driven deeper into the soil through axial expansion (row 18 of **Table 1**).



The fourth concept of root-inspired soil penetration devices is on texture alteration through material decay. Biodegradable material is placed around a highly textured foundation pile to create a smooth surface which facilitates soil penetration. Once inserted in the soil, this material will biodegrade and expose the highly textured surface, from the third concept of root-inspired structural support (“**Root-Inspired Structural Support**” section, row 13 of **Table 1** and **Figure 6**). For this concept, additional bioinspiration of directional friction is interesting, especially if the directionality of the surface structure could change over time and by this, control the movement of the element through the soil. Bacteria known to precipitate calcium carbonate can be introduced under the biodegradable layer to further strengthen the bond between the foundation and soil particles.

Multiphase design was further conceptualized through the investigation of shape-change materials and structures for increased friction of foundation piles with weak soils, for example in wetlands (refer to the third concept of root-inspired structural support in “**Root-Inspired Structural Support**” section and row 13 of **Table 1**). Shape-change behaviors are used in three different concepts to counter the

trade-off between the ease of pile insertion in soils and the surface friction of the pile.

The first concept of shape-change foundations is based on the swelling properties of hygroscopic materials when they absorb water. A hygroscopic material is located behind a biodegradable layer along the surface of a pile (**Figure 7B**). After placement in the soil and decomposition of the biodegradable layer, the hygroscopic material becomes exposed to water in wetland soil. The water triggers material expansion, creating a three-dimensional structure to increase the surface contact with soil (**Figure 7**).

The second concept of shape-change foundations is based on bi-layer materials, which change curvature under humidity gradients. Bi-layer plywood materials, inspired by pinecones, have been researched for their ability to bend under humidity gradients and applied to architectural prototypes (Menges and Reichert, 2015). Such composite material is located at the surface of the foundation pile. Once inserted in the soil, water absorption induces curvature change of the bilayer elements (**Figure 8**). The success of such shape-change concepts also depends on the resistance of the soil particles.

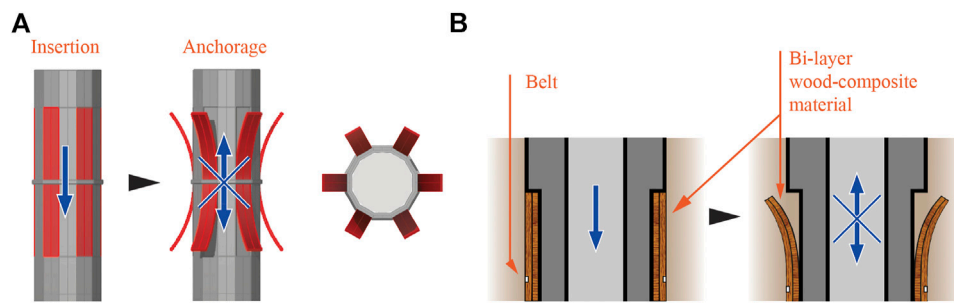


FIGURE 8 | Shape-change foundation based on bi-layer materials—The smooth foundation pile is driven into the soil (**A-left**). Over time, the bi-layer composite material, exposed to humidity, curves outwards resulting in increased anchorage through friction (**A-middle**), (**A-right**) presents a top view of this deployed pile system. (**B-left and right**) show the disposition of the bi-layer composite material and the belt holding it in place, before and after the curvature change.

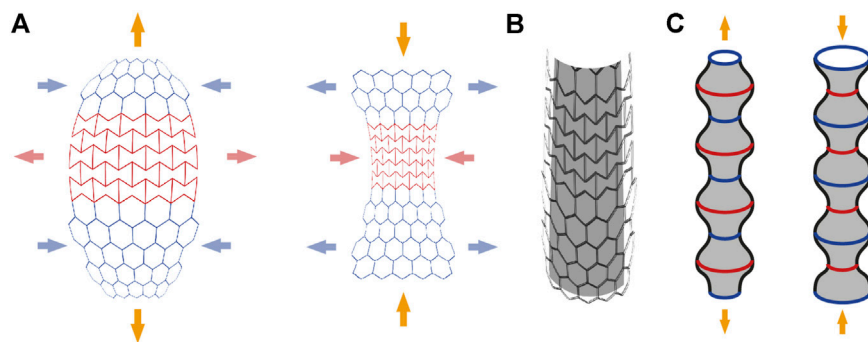


FIGURE 9 | Shape-change foundation based on auxetic behavior—The combination of auxetic and non-auxetic structures in a plane produces edge curvature when compressed or stretched as simplified in (**A**). When this combined structure is longitudinally stretched (i.e., yellow arrows), the auxetic section (i.e., in red) stretches while the non-auxetic one (i.e., in blue) shortens (**A-left**). The reverse behavior happens when the combined structure is compressed longitudinally (**A-right**). When rolled into a cylinder (**B**), the longitudinal compression or stretching produces horizontal wrinkles (**C**). This cylinder can serve as a vertical foundation pile to resist compression and tensile loads.

The third concept of shape-change foundations is based on the behavior of auxetic structures with a negative Poisson's ratio. When stretched or compressed in one direction, they also respectively expand or compress in the perpendicular direction. By assembling auxetic and non-auxetic structures together in a plane, stretching of the assembly in one direction (see yellow arrows on **Figure 9**) induces a geometrical change of the structure (see red and blue arrows on **Figure 9A**) (Mirzaali et al., 2018). The assembly needs to be made of a semi-flexible material to allow material deformation. The flat assembly can be rolled to produce a cylindrical structure for a foundation pile (**Figure 9B**). During soil insertion, the structure can be locked and, once in place, released. Compressive or tensile loads on the auxetic foundation pile will create wrinkles leading to a higher bearing surface area (**Figure 9C**).

Multifunctional Root-Inspired Foundations

The multifunctional foundation concept is inspired by the added functionality in biological root systems and targets preventing erosion and exchanging energy and resources

with the soil and other artificial structures (row 1 and 22 of **Table 1**). With the development of self-burrowing technologies and smart materials, multifunctional foundations can be envisioned. The benefits of erosion prevention have already been stated in “**Root-Inspired Erosion Prevention**” section. Foundations and geothermal systems abide by the same constraints of soil penetration and anchorage. Their combination into a multifunctional system could economize resources. Another further strategy to exchange thermal energy is to connect buildings through their foundations (refer to the cooperative concept in “**Root-Inspired Structural Support**” section). Appliances producing massive amounts of heat, such as data centers, can serve as a heat source for buildings (Woodruff et al., 2014). In addition to thermal energy, other resources such as water can be exchanged between buildings (row 6 of **Table 1**). By increasing load transfer through friction with the soil medium, the surface area of the foundations needs to be increased, but their weight can be decreased. As a result, hollow foundations can be a route for additional functionality, such as geothermal energy, water storage and transport.

The concepts presented in this section provide examples of how strategies found in root systems can inform the design of future foundations. These concepts do not take materiality, scaling, and rigorous technical feasibility into consideration however, but they should be the basis for future research and development projects.

Coastal Infrastructure

Current Coastal Infrastructure Design and Problem Review

Typical built coastal infrastructure serves two main objectives: protection from wave action and landward erosion (USACE and Army Engineer Waterways Experiment Station Coastal Engineering Research Center, 1984). While generally effective at these objectives, coastal structures are static, often anchored, and therefore cannot adapt to rapid, dynamic conditions. In light of climate change, current static structures do not hold up to raising water levels, storm surges, and flooding. For example, a post Hurricane Katrina rebuild of the New Orleans, LA, USA seawall was almost overtopped by waves from storm surge in 2018.² Additionally, hard infrastructure alters and displaces the structure and function of natural habitats that existed before, eliminating both significant biodiversity, and habitat complexity that supports trophic structure development for a rich, interconnected food web, refuge for mobile organisms and fish, and attachment surfaces for sessile and habitat-forming organisms (Strain et al., 2018).

Common typologies of hardened infrastructure include: shore-parallel attached smooth vertical or concave surfaces (e.g., seawalls, such as bulkheads), shore-parallel attached sloped variable surfaces (e.g., revetments, such as riprap), shore-perpendicular attachments (e.g., groins and jetties), detached shore-parallel sloped above-water structures (e.g., breakwaters), and detached shore-parallel submerged structures (e.g., breakwaters and artificial reefs). Shore-parallel attached structures prevent erosion of land from wave action but fragment the land-water interface and contribute to the loss of natural habitats (Goodsell et al., 2007). Seawalls and some revetments reflect waves, which increases nearshore turbulence (Silvester, 1972). Often this turbulence is too rough for native plants to establish and maintain, attracting invasive species establishment. Increased turbulence also increases sediment resuspension and reduces water clarity.³ Depending on wave action and nearshore particle size, sediment may be carried through wave reflection out into the open shore, reducing the available sediment budget for natural littoral deposition processes. Riprap revetments can fail due to toe scour, outflanking, wave overtopping and subsequent erosion of material behind the revetment, and settlement. Wave reflection also causes scour, deepening the water level adjacent to a seawall, allowing for larger wave heights to approach the shore (Griggs

and Fulton-Bennett, 1988). Shore-perpendicular attached structures redirect littoral transport to prevent erosion or allow river mouths to remain deep enough for navigation in the case of harbor infrastructure, but often cause downdrift erosion due to a reduced available sediment budget for continued nearshore transport. This disruption of natural littoral processes induces a negative feedback loop, requiring more downstream infrastructure to protect against this erosion (Hanson and Lindh, 1993). Both detached above-water and submerged structures attenuate waves (through surface wave breaking and bottom roughness, respectively) and provide fish habitat, but above-water structures restrict coastlines from migrating landward or seaward in response to varying water levels (McLachlan and Defeo, 2018; Scape/Landscape Architecture PLLC, 2014).

Mangrove forests show a pathway to remediate these shortcomings. Mangrove roots stabilize soils, while their ecosystem provides habitat and a gradual land-water transition. On a long time scale, mangrove forests migrate landward or seaward in response to varying water levels (Robertson and Alongi, 1992). Wave dissipation through these complex flow obstruction configurations significantly reduces wave reflection and subsequent turbulence in the nearshore environment. Even if mangroves are overtopped by waves during storm surge, the roots and trees still provide adequate bottom roughness and flow obstruction to effectively attenuate wave energies (Mazda et al., 1997). Manmade constructions using wood, such as rootwad revetments, engineered log jams, cribwalls, deflectors, weirs and pile dikes, also stabilize soils, reduce flows, while also providing habitat and maintaining a more gradual land-water transition. Interestingly, while these structures are cheaper, exceed project design life, and often match or exceed performance objectives compared to rock structures, these LWD human constructions are rarely used (Abbe et al., 1997). Additionally, mangrove roots, naturally occurring log jams, and woody overhang along riverbanks or shorelines, provide habitat for a variety of organisms. Complex morphologies, such as root systems, protect from wave action and stabilize sediment to primarily provide anchorage for an aboveground structure, as well as provide habitat. Complex morphologies would similarly allow for multifunctional coastal infrastructure design.

To undertake a redesign of coastal infrastructure that expands beyond its primary objectives of protection from wave action and landward erosion, a biomimetic approach via the study and abstraction of root systems can be employed. Investigating specific themes of erosion prevention, multifunctionality, spatial variability, and adaptation to dynamic external loads involves answering the following research questions: What is the minimum level of complexity required from a root-inspired structure (e.g., topology, orientation of elements, density, distribution of individual cross-sections across topological orders, distribution of orientation across topological orders, texture) and at what scale(s) is it most effective for the following functions of (a) wave dissipation and dispersion (vs. wave reflection), (b) downstream development of reduced flow velocities through the depth of the water column that match

²<https://www.nytimes.com/interactive/2018/02/24/us/new-orleans-flood-walls-hurricanes.html>

³<https://www.mishorelinepartnership.org/erosion-at-the-shoreline.html>

preferential velocity ranges of native taxa, (c) flow speeds for sediment deposition, and (d) refuge/pore space habitat creation? What minimum combination of effective length scales as informed by root systems are needed to discourage localized erosion and scour development by dissipating the formation of vortices? Furthermore, can topographically complex infrastructure be produced that more closely resembles the structure and function of the natural habitat (such as woody overhang, exposed root systems) that has been displaced? With regards to adaptation and multifunctionality, coastal infrastructure of the future should adapt to changing external loads such as wave height, storm surge, sediment movement, or landslides in sloped banks or shorelines. Coastal infrastructure should also participate in additional ecosystem services such as provision of habitats, nutrient cycling, and carbon sequestration.

Current Innovative Solutions for Coastal Infrastructure Design

In the following list, we summarize current alternative approaches to traditional engineered coastal infrastructure design, spanning complex forms, coastal ecosystem restoration, to living infrastructure. They are organized under four main topics of interest referring to the analogy table in “**Abstraction and Analogy**” section (Table 1): soil erosion, structural support, conditions for living organisms, and multifunctionality.

- Geo- and bio-textile fabrics to prevent soil erosion—As mentioned in “**Current Innovative Solutions for Foundation Design**” section, geosynthetic products are currently used to stabilize soils through placement of a polymeric textile filament layer by layer around loose rocks, gravel, or sediment. This practice is also seen in coastal engineering. Geotextile tubes or bags, a synthetic fabric filled with sediment, are used to line riverbanks, shorelines, or protect young plant seedlings as part of a nearshore ecological restoration initiative. Biodegradable coconut coir pith logs packed in tubular netting, known as coir logs, are an example of soil bioengineering that reduce water velocities at the edge of slopes, shorelines, and riverbanks (Rella and Miller, 2012).
- Complex concrete forms for increased structural support—Concrete forms for revetments, breakwaters, or additional reinforcement of seawalls have become more complex since the 1950s with inventions such as Tetrapods, Akmons, Seabees, Accropodes, Xbloccs, dolos, and KOLOS. Their complex shapes, pack density, and porosity allow for wave dissipation that reduces wave run-up, overtopping and reflection, but also facilitates interlocking of individual units and increased stability of the overall structure (Dupray and Roberts, 2009).
- Establishing conditions for living organisms through ecosystem conservation and restoration—Wetlands, mangroves, coral reefs, oyster reefs, and salt marshes are proving cheaper and more effective in reducing wave energy than building hard artificial structures. Meta-analysis of the literature indicates that coral reefs reduce wave heights by 70%, salt marshes by 72%, mangroves by 31%, and seagrass/kelp beds by 36% (Ferrario et al., 2014; Narayan et al., 2016).
- Establishing conditions for living organisms through eco-engineering—Locations such as harbors, nearshore navigation routes, and dense urban areas are not suitable for restoration. In this case, ecological engineering or “eco-engineering” is an approach that considers recovery of prior ecosystem services in the design of hard infrastructure (Mayer-Pinto et al., 2017). Habitat features to increase fish productivity or biodiversity of key functional groups of organisms can be integrated via textures, crevices, pits, intertidal water retaining features, raises, ledges, ridges, and soft, flexible protruding elements such as rope, ribbon, or twine (Strain et al., 2018). Grooves, dimples, and grooved shelf features were incorporated into the submerged toe blocks of offshore breakwaters in Lake Erie, part of the Great Lakes freshwater system, to increase habitat for fish and invertebrates with limited success (Suedel et al., 2016).
- Multifunctional, living infrastructure—ECONcrete uses a special concrete mix to lower the pH closer to that of seawater, a common criticism of traditional marine grade concrete, to facilitate organism attachment and growth (Finkel and Ido, 2017). The concrete blocks are formed with molds to create the surface texture and roughness to promote attachment by oysters, bryozoans, coralline algae, and several other habitat-forming species (Perkol-Finkel and Sella, 2015). Uses include offshore breakwaters, revetments, seawall panels, or attachments to existing seawall panels.⁴ Reef Design Lab 3D prints unique surface features on seawall panels using marine grade concrete to improve recreational fishing opportunities and increase biodiversity, specifically to maximize colonization of native species.⁵ Mangrove Reef Wall was first studied to understand flow-structure development behind modeled mangrove roots, as well as wave attenuation and sediment deposition characteristics to create bioinspired infrastructure (Kazemi et al., 2017). The current application of this research is a living seawall application for wave attenuation, colonization, and increased biodiversity.
- Multifunctionality of hard infrastructure to assist with coastal restoration and rehabilitation—A wide range of coastal restoration and rehabilitation projects use hard modular structures from concrete mixtures. TetraPOT, by designer Sheng-Hung Lee at National Cheng Kung University, creates an interlocking system of concrete pods that use mangrove trees and roots to keep the pods in place as a line of coastal defense along shorelines.⁶ Reef Design Lab takes a similar approach with a reusable planter to promote mass planting of a native mangrove species for coastal defense.⁷ CEMEX

⁴<https://econcretetech.com/>

⁵<https://www.reefdesignlab.com/>

⁶<https://www.jamesdysonaward.org/en-GB/2016/project/tetrapot/>

⁷<https://www.reefdesignlab.com/mangroveplanters>

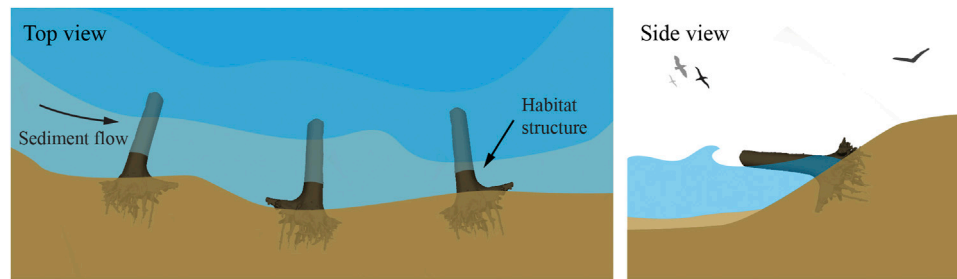


FIGURE 10 | Erosion prevention concept along a shoreline—The top view (left) shows modeled rootwads embedded along a shoreline with root fan facing landward and truncated trunk (note transparency in open water) facing seaward. The side view (right) shows one rootwad with root fan embedded along a sloped shoreline face.

created the Rhizolith Island (“Isla Rhizolith”) prototype, consisting of a mosaic of floating concrete structures with a “head” and a “fin” that functions as a seed carrier for mangroves, to restore mangrove forests while also providing coastal protection. The fin is also designed to serve as marine habitat, offering shelter for fish and surfaces for barnacles.⁸ Reef Ball also uses a specialized concrete mixture to lower the pH and a textured outer surface to promote growth of transplanted corals. Reef Ball uses similar principles to develop concrete domes to serve as oyster beds for oyster reef restoration. Used in more than 70 countries, on more than 4,000 projects, there are more than 700,000 Reef Balls in the oceans around the world.⁹

- Complex scaffolding to establish conditions for living organisms—Grow Oyster Reefs LLC has created complex concrete scaffolds mimicking the oyster shape, in addition to mimicking the oyster shell’s material formula through a calcium-enriched, patent-pending mixture that also aims to reduce nitrogen levels in water.¹⁰ Additionally, Reef Design Lab 3D prints ceramic scaffolds using D-shape technology to assist with coral reef rehabilitation.⁵ These two examples show the possibility of production of complex coastal structures.

Root-Inspired Design Proposals for Coastal Infrastructure

In this section, several bioinspired design strategies from the biology of root systems are presented for coastal engineering. Since these strategies do not depend on the availability of real mangrove trees, riparian tree species, or rootwads, the properties of these root-inspired structures can be fine-tuned according to the learnings from biomechanics investigations. Parameters like the distribution of cross-sections, lengths, spacing, branching angles, and orientations, can be adjusted to a specific shoreline

reach with its predominant wave and storm surge conditions. Additionally, the arrangement, stacking, and orientation of several root-inspired structures can be adjusted for different shoreline configurations and wave energy conditions, as well as intended ecosystem service restoration goals and outcomes, and/or maintenance strategies.

Root-Inspired Erosion Prevention

The first erosion prevention concept builds upon the concept of engineered log jams and complexes discussed in “**Root Utilization in Human Constructions**” section (row 3 in **Table 1**), a windthrown tree overhang along a river or stream still embedded in the bank by its root system, and mangrove roots encouraging sediment deposition (row 4 in **Table 1**). If erosion is of highest concern, a root-inspired structure (or several structures) can be inserted perpendicular to a beach or shoreline face with the root fan embedded in the shoreline (**Figure 10**). The multi-scale elements of the root-inspired structure, such as overall shape, topological orders, and branching angle/orientation, will need to be tested to determine their effects on vortex development, localized erosion, and scour, so as not to be a further detriment to the shoreline. These multi-scale elements could be engineered such that vortices do not form (or are quickly dissipated) behind or downstream from the structure, further enhancing sediment deposition potential. Additionally, since groins and jetties cause downstream erosion issues due to a perpendicular element facing seaward into the nearshore, the seaward end of a root-inspired structure can be truncated so as not to cause similar issues. This truncation is shown in **Figure 10** (left) as the transparent ends of the trunk of a 3D modeled rootwad. This seaward end could then be formed to provide heterogeneous substrate for habitat. Sediment penetration of the complex root fan like end of this structure into the shoreline face may be difficult. Concepts to increase contact area with the sediment previously described in “**Root-Inspired Soil Penetration Devices**” section on building foundations could be employed.

This erosion prevention concept could also be utilized particularly during high water years to protect shoreline property. Depending on sediment type (silt, clay, sand, mud), particle size distribution, and wave energy exposure, this concept could unintentionally cause localized scour around the large

⁸<https://www.cemex.com/-/cemex-develops-floating-concrete-island-to-revitalize-mangrove-shorelines>

⁹<https://www.eternalreefs.com/the-eternal-reefs-story/about-reef-balls/>

¹⁰<http://www.growoysterreefs.com/>



FIGURE 11 | Erosion prevention concept for engineering structures—A typical exposed root system along a riverbank catching plastic debris (**left**) can be one of several functions of an abstracted root structure (**right**) that could replace the ends of bridge abutments or the edges of culverts to reduce erosion and scour.

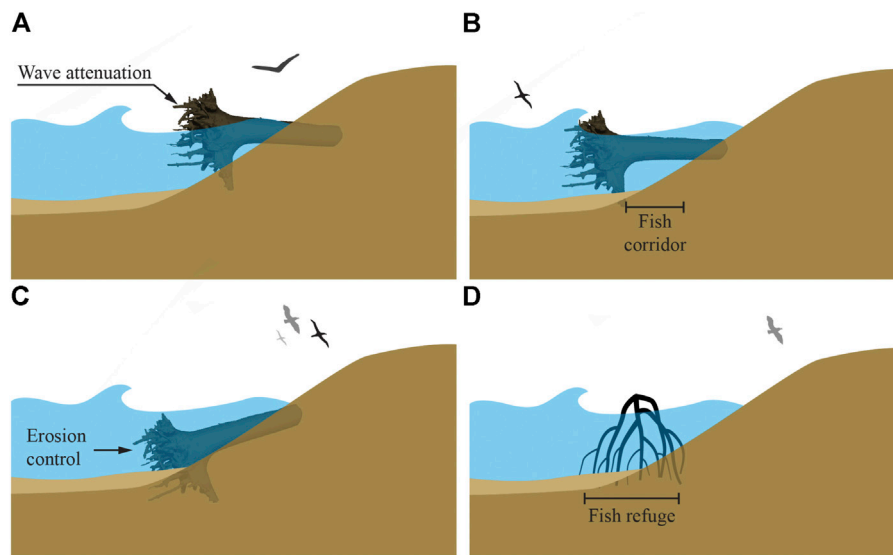


FIGURE 12 | Multifunctional revetment concept designs—(A)—A modeled rootwad illustrating wave attenuation with the root fan facing seaward, and the trunk end embedded along the sloped shoreline face. (B)—Spacing between the root fan and sloped shoreline face shows possible passage for a fish corridor. (C)—A root fan embedded more in the sediment bottom may provide greater toe protection of a steeper shoreline face. (D)—A mangrove like structure can attenuate waves in addition to providing habitat (fish refuge) through spacing control.

anchoring elements (Svoboda and Russell, 2011) and would need to be tested to confirm its effects. Additionally, several engineered log jams or complexes, such as bar apex jams (“**Root Utilization in Human Constructions**” section), could potentially be embedded in beach sediment at different distances from the water line to provide erosion protection of the entire beach front. The complexes can be designed more as a fixed structure, but may still more closely mimic the process of both large driftwood and windthrown trees near a historically forested shoreline forming natural protective “structures” along a beach (Abbe et al., 1997).

The second erosion prevention concept specifically addresses additional engineered structures in or near waterways that can cause significant erosion issues. This includes structures such as bridge abutments and culverts, not primarily used for erosion prevention of coasts, streams, or riverbanks, that cause localized scour or erosion at the edge or slightly downstream of the

structure. These engineered structures could be redesigned based on the geometry of root systems (Figure 11—right), in order to reduce localized scour and erosion and additionally deposit sediments further downstream that are a result of scour or erosion. When implemented, rootwad-inspired structures will also catch plastic waste (Figure 11—left) that could be collected at regular intervals, to reduce overall transport of waste to lakes and oceans. The same structure placed strategically at the bottom of a river could reduce bedload movement and scour.

Root-Inspired Multifunctional Revetments

Multifunctional revetment design concepts are additional iterations of the concept described in Figure 10, but with the root fan facing seaward. This design concept (Figure 12) is different from current wooden revetments in that there is a complex flow obstructing end, but similar to riverbank stabilization practices used in restoration ecology (row 2 in

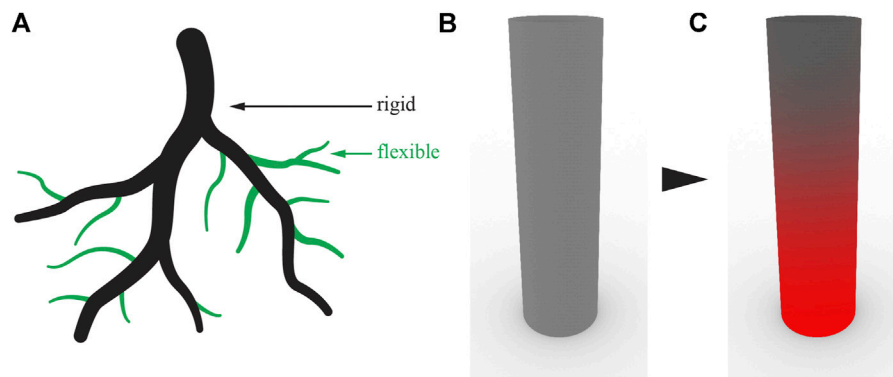


FIGURE 13 | Multifunctional composites—(A)—A root-like structure with the black elements comprising a rigid material and the green elements comprising a flexible material. A standard construction pile made of one material is shown in **(B)** while an innovative composite pile is shown in **(C)**, composed of a material gradient from more rigid (red) at the base of the pile to more flexible (grey) at the top of the pile.

Table 1 and “**Root Utilization in Human Constructions**” section). One purpose of the root fan like end is wave attenuation, breaking up and dissipating the waves due to the density, orientation, and cross-section of the individual elements in the structure (**Figure 12A**). Wave attenuation also in turn reduces erosion potential. The spacing between the root fan and shoreline face can be manipulated, creating space for a protected fish corridor or passage behind the root fan, a slower moving wake region for aquatic plants to establish and maintain, and/or the ability for the shoreline to migrate landward or seaward (**Figure 12B**). This sub-strategy tackles the larger theme of creating conditions for living organisms (rows 20–21 in **Table 1**.) Shipping and navigational activities, recreational activities, and predominant wave conditions may restrict available space. The root fan can also be angled down and embedded into the sediment bottom, offering more traditional toe protection for a sloped shoreline face in addition to habitat, dependent on wave conditions (**Figure 12C**). Mangrove like revetment structures could be adapted to provide habitats (rows 20–21 in **Table 1**), by controlling spacing between individual elements of a single structure (**Figure 12D**).

Root-Inspired Multifunctional Composite Structure

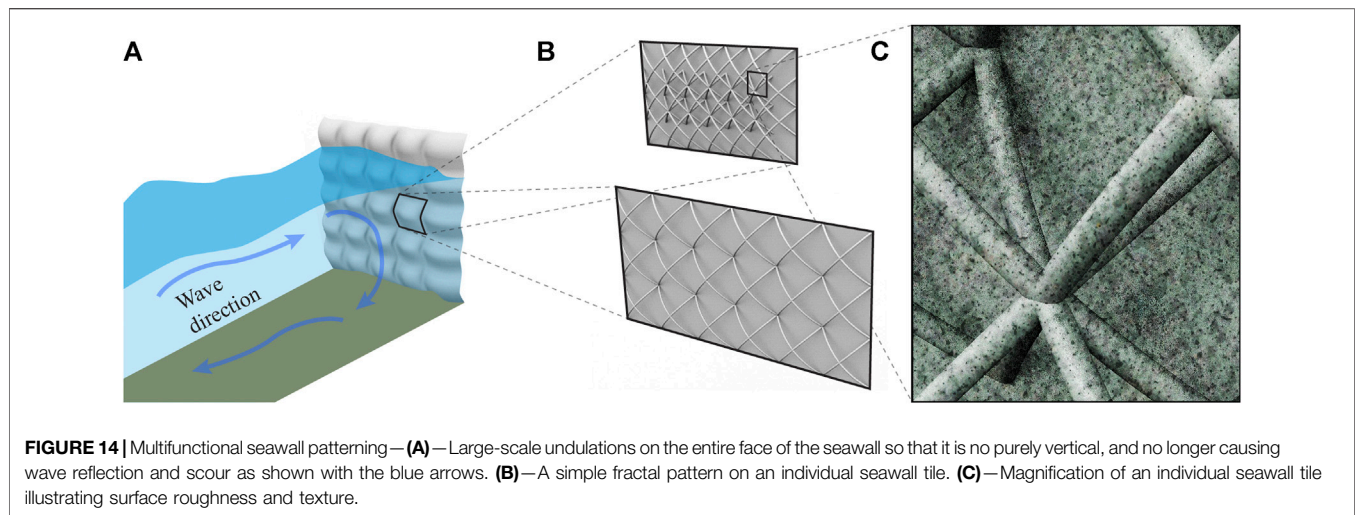
Two design concepts shown in **Figure 13** illustrate the same principle idea: use of multifunctional material composites. With the advent of additive manufacturing, even in using traditional coastal construction materials such as marine grade concrete and ceramic (“**Current Innovative Solutions for Coastal Infrastructure Design**” section), material composites reveal new possibilities in multifunctional infrastructure. Building on the fact that roots have different functions and respective morphology, in addition to the morphological adaptation principles illustrated in rows 7–9 of **Table 1**, material properties could be varied. A composite structure may employ more rigid, thicker material allocation in places exposed to wave energy and erosion potential (i.e., higher stress), while softer, more flexible material could be allocated in sheltered orientations for habitat or refuge. **Figure 13A** shows this division in material rigidity and flexibility in a root-inspired structure, while

Figure 13B shows a gradient in material rigidity in a standard pile. As previously mentioned in Kazemi et al. (2017), flexibility of a modeled mangrove root resulted in higher drag in shallow waters; therefore, flexibility along the axis of a standard structural pile may offer greater flow reduction in some lower flow scenarios than a standard rigid pile. A structure modeled after an engineered log jam could also have both rigid and flexible elements assembled in one continuous, porous, yet stable structure (row 3 and 4 in **Table 1**).

Root-Inspired Patterning for Multifunctional Seawall

This concept suggests a large-scale redesign of a seawall, including micro and macro approaches. Building on the existing living seawall innovations described in “**Current Innovative Solutions for Coastal Infrastructure Design**” section, a seawall could have large-scale undulations on the entire face rather than just at the top and bottom like a recurved seawall. The hypothesis is that this large-scale undulation (**Figure 14A**) would significantly reduce wave reflection and subsequent toe scour compared to a recurved seawall. **Figure 14B** shows a seawall concept with a hierarchical surface design. The designs of Reef Design Lab and Mangrove Reef Wall (“**Current Innovative Solutions for Coastal Infrastructure Design**” section) could also be utilized at this scale. These existing designs offer spatial variability, referring to horizontally heterogeneous and topographically complex structures and surfaces typically observed in natural habitats. **Figures 14–C** magnifies the surface roughness and texture, building on the habitat utility of snag/root roughness as described in row 21 of **Table 1**. While a seawall does not mimic a root system in any tangible abstract way, the concept of irregularity (row 4 of **Table 1**), root curvature, spacing, and morphology can be integrated by the application of two-dimensional patterns or three-dimensional surface structures.

The concepts presented in this section provide an overview of how strategies found in root systems can inform the design of technical coastal infrastructure. These concepts do not take into consideration however, materiality, scaling, and rigorous



technical feasibility, which could be further researched in future projects.

DISCUSSION

This paper demonstrates utility of the bioinspired design approach through the study of the biology of root systems to inform multiple engineering design applications. Through design of a comprehensive analogy table that relates specific biological information about roots to engineering infrastructure problems and vulnerabilities, functional principles were established to link the two fields as outlined specifically through the biomimetic process. These principles informed design proposals for foundation and coastal engineering that can fulfill various functions, such as erosion prevention, structural support, soil penetration, and habitat creation. Many questions emerging from this work are not addressed in this paper however, specifically in the areas of materiality, technology, sustainability, and implementation.

Considering materiality, typical foundation and coastal engineering constructions use wood, concrete, rock, and steel. The resources required to shape these traditional materials and their desired material properties result in simple morphologies. New techniques such as 3D/4D printing, dual-extrusion, D-shape technology, and CNC machining, allow for customizable and complex organic forms, such as root-inspired structures. Field scanning techniques, parametric design, and advanced manufacturing techniques could be combined into a unified design process to customize structures to specific site conditions and desired functions. Traditional engineering materials can be shaped with these new technologies, but in parallel, such technologies foster the exploration of a wide range of material composites. Engineered material composites can be highly tuned with specific properties and performance characteristics to potentially respond and adapt to dynamic loading conditions. A material's engineered response at smaller scales (i.e., micro- and nano-level) is akin to biomass

accumulation in locations of higher stress in trees. Added functionality, complexity, and feedback loops through the developing fields of biotechnology and synthetic biology can also be considered in subsequent design iterations. The use of living organisms (e.g., mycelium, coral polyps, oyster spat) and modified living organisms can lead to emerging techniques like MICP (Dade-Robertson et al., 2018). To abstract root systems principles for foundation and coastal engineering, the transfer of different timescales needs to be addressed in further research. Damping systems, responsive MICP, and self-healing materials could respond to everyday fluctuations. Digging/growing agents, programmable structural growth, and design flexibility to repurpose infrastructure meanwhile, could serve as an adaptation to long-term loads.

Advanced technologies and materials could lead the way to adaptable engineered systems. In foundation design, we can envision adaptation through material or shape change response to changing soil conditions, changing structural loads throughout the lifetime or utility of the structure, or to strengthen the foundation over time (similar to secondary thickening in root systems). In coastal infrastructure design, we can envision adaptation to the changing energetics of nearshore systems, water levels, nutrient or pollutant concentrations (e.g., material surface properties facilitating in removal or sequestration), and/or dissolved oxygen provisioning for aquatic life. For achieving sustainability, the design of a product should be evaluated for its entire life cycle, which cannot be performed at this early design stage. Therefore, concepts presented in this paper focus on the primary functions required and opportunities for improving existing practices toward greater sustainability, a key aspect of biomimicry. Assessing the sustainability of these concepts would need to question and include the longevity, adaptation, decay, degradation, and/or reusability of such systems. Should elements of foundation and coastal systems naturally decompose or degrade in the ground or water, or should they be reusable or recyclable? Does the design for adaptation to changing conditions over time increase design complexity to the point where it may lead to reduced sustainability? For material selection, biological-

based fillers originating from agricultural or construction waste streams can be utilized in material composites. Especially in coastal engineering, degradation of these inert biological-based fillers in an engineered material composite is an additional component to consider, whether by saltwater intrusion, ice, or UV light. Degradation could be seen as beneficial, considering if the by-products offer a food source for native organisms, do not disrupt organismal primary productivity and reproductive cycles, and if habitat-forming organisms may take the place of the degrading structure over time. Must the coastal structure be permanent, or once the desired physical conditions are established (i.e., sediment deposition, coastal vegetation fully established to reduce wave heights), the structure becomes indistinguishable from its surroundings? Similarly, the life cycle of a building foundation could be designed such that it decomposes or “dies” (similar to lateral roots or root hairs no longer needed for water and nutrient acquisition) when the building is no longer occupied. The foundation could also connect to the soil matrix at the individual soil particle scale to continue preventing erosion, even though aboveground structural support may no longer be needed.

Lastly, in the case of implementation, where do bioinspired design concepts of built infrastructure fit in the existing array of technical options? The possibility to reuse, retrofit, or recycle existing foundations should be a priority to reduce waste production and urban decay. Instead of following the ‘take-make-dispose’ linear process in building construction, technological advancements allow for analysis and adaptation of existing structures to current needs, instead of building new structures to fit new needs. Future designs must follow a more integrated approach, “managing engineered landscapes as ecological systems,” that evolve, adapt, and respond through time (DeJong et al., 2015). Additionally, root-inspired structures should not replace necessary hard coastal infrastructure in high energy nearshore systems where it is required nor restoration of ecosystems in low energy systems where it is possible. Their inclusion may offer additional functionality or allow for conditions for successful ecosystem restoration to take place in systems where these projects typically cannot succeed.

CONCLUSION

The design of built infrastructure often regards soil properties as stable through time. By default, building foundations to seawalls are both bulky and heavy to respond to predominant loads and to ensure stability and durability over a long lifetime. Dynamic changes to soil properties and environmental conditions, in addition to inefficient use of material and poorly optimized construction by viewing soil as stable, compromises built infrastructure performance.

While foundation designs are limited to simple vertical geometries by current building techniques, diverse strategies from root systems give insights to develop multifunctional foundations able to anchor structures, prevent erosion, and adapt to various stresses. Several conceptual designs were

made by abstracting and combining multiple root strategies relating to adaptive soil penetration, surface texture, complex topology, hierarchical morphology, self-healing materials, and growth principles. Similarly, coastal infrastructure is often limited to two technical objectives, simplifying form, material, construction, and implementation, which displaces natural habitat and exacerbates negative feedback loops in coastal ecosystem functioning. Strategies adapted from root systems, and in particular the ecosystems supported by mangrove and other coastal forests, can serve to develop multifunctional coastal infrastructure. In particular, principles relating to root system architecture, surface texture, complex topology, material gradients, and adaptive soil penetration were abstracted and combined into several conceptual coastal infrastructure designs.

We conclude that bioinspired design concepts of built infrastructure should be part of the mosaic of solutions offered that provide protective, multifunctional, and livable spaces. Therefore, this review of biological root systems and the conceptualized biomimetic translations offers a new way of thinking about technical problems and vulnerabilities in engineering and broadly contributes to creating an improved understanding and intersection of the fields of biology and engineering.

AUTHOR CONTRIBUTIONS

ES wrote the largest share of this paper, including introduction, root as a biological model, application to coastal infrastructure, and discussion and conclusion. TH contributed to those parts and wrote root biomechanics, and application to building foundations. ES and TH together worked on the review of root biology. TH contributed the figures. ES compiled all texts and organized the writing. PG conceptualized the content, supervised the research, and revised the article.

FUNDING

The work on this paper was partially funded by the faculty startup fund of The University of Akron. Funding for Elena Stachew is provided by the National Oceanic and Atmospheric Administration (NOAA) Grant DNRH0902, distributed by ODNR Office of Coastal Management in Sandusky, Ohio and Cleveland Water Alliance.

ACKNOWLEDGMENTS

The shape change foundation concepts were created by in collaboration with undergraduate students Joshua Davis and Ashvi Shah. Contributions by Elena Stachew are a collaborative result supported by a Biomimicry Fellowship with sponsors Biohabitats and Cleveland Water Alliance. The authors would like to thank Dr. Jake Miesbauer for sharing his root biomechanics knowledge during inspiring discussions.

REFERENCES

- Abbe, T. B., Montgomery, D. R., Featherston, K., and McClure, E. (1993). *A Process-Based Classification of Woody Debris in a Fluvial Network; Preliminary Analysis of the Queets River*. Washington: EOS Transaction of the American Geophysical Union, 296.
- Abbe, T. B., Montgomery, D. R., and Petroff, C. (1997). "Design of Stable In-Channel Wood Debris Structures for Bank Protection and Habitat Restoration: An Example from the Cowlitz River, WA," in Proceedings of the Conference on Management Disturbed by Channel Incision. Oxford, MS: University of Mississippi, 16, 8.
- Abbe, T. B., and Montgomery, D. R. (1996). Large Woody Debris Jams, Channel Hydraulics and Habitat Formation in Large Rivers. *Regul. Rivers: Res. Mgmt.* 12 (2–3), 201–221. doi:10.1002/(sici)1099-1646(199603)12:2/3<201::aid-rrr390>3.0.co;2-a
- Abbe, T. B., and Montgomery, D. R. (2003). Patterns and Processes of Wood Debris Accumulation in the Queets River Basin, Washington. *Geomorphology* 51 (1), 81–107. doi:10.1016/s0169-555x(02)00326-4
- Alaoui, A., Rogger, M., Peth, S., and Blöschl, G. (2018). Does Soil Compaction Increase Floods? A Review. *J. Hydrol.* 557, 631–642. doi:10.1016/j.jhydrol.2017.12.052
- Amellal, N., Burtin, G., Bartoli, F., and Heulin, T. (1998). Colonization of Wheat Roots by an Exopolysaccharide-Producing *Pantoea Agglomerans* Strain and its Effect on Rhizosphere Soil Aggregation. *Appl. Environ. Microbiol.* 64 (10), 3740–3747. doi:10.1128/aem.64.10.3740-3747.1998
- Angermeier, P. L., and Karr, J. R. (1984). Relationships between Woody Debris and Fish Habitat in a Small Warmwater Stream. *Trans. Am. Fish. Soc.* 113 (6), 716–726. doi:10.1577/1548-8659(1984)113<716:RBWDAF>2.0.CO;2
- Arnone, E., Caracciolo, E., Noto, L. V., Preti, F., and Bras, R. L. (2016). Modeling the Hydrological and Mechanical Effect of Roots on Shallow Landslides. *Water Resour. Res.* 52 (11), 8590–8612. doi:10.1002/2015WR018227
- Bailey, P. H. J., Currey, J. D., and Fitter, A. H. (2002). The Role of Root System Architecture and Root Hairs in Promoting Anchorage against Uprooting Forces in Allium Cepa and Root Mutants of Arabidopsis Thaliana. *J. Exp. Bot.* 53 (367), 333–340. doi:10.1093/jexbot/53.367.333
- Ballard, J., Pasquale, C., and Howington, S. (2009). "A Heat and Fluid Transport Simulation of a Soil-Root-Stem System," in 39th AIAA Fluid Dynamics Conference. Reston, Virginia: American Institute of Aeronautics and Astronautics.
- Barbier, E. B., Koch, E. W., Silliman, B. R., Hacker, S. D., Wolanski, E., Primavera, J., et al. (2008). Coastal Ecosystem-Based Management with Nonlinear Ecological Functions and Values. *Science* 319 (5861), 321–323. doi:10.1126/science.1150349
- Baumann, V., and Bauer, G. E. A. (1974). The Performance of Foundations on Various Soils Stabilized by the Vibro-Compaction Method. *Can. Geotech. J.* 11 (4), 509–530. doi:10.1139/t74-056
- Bengough, A. G., McKenzie, B. M., Hallett, P. D., and Valentine, T. A. (2011). Root Elongation, Water Stress, and Mechanical Impedance: A Review of Limiting Stresses and Beneficial Root Tip Traits. *J. Exp. Bot.* 62 (1), 59–68. doi:10.1093/jxb/erq350
- Bengough, A. G., Mullins, C. E., and Wilson, G. (1997). Estimating Soil Frictional Resistance to Metal Probes and its Relevance to the Penetration of Soil by Roots. *Eur. J. Soil Sci.* 48 (4), 603–612. doi:10.1111/j.1365-2389.1997.tb00560.x
- Benke, A. C., Henry, R. L., III, Gillespie, D. L., and Hunter, R. J. (1985). Importance of Snag Habitat for Animal Production in Southeastern Streams. *Fisheries* 10 (5), 8–13. doi:10.1577/1548-8446(1985)010<0008:IOSHFA>2.0.CO;2
- Benyus, J. M. (2011). *A Biomimicry Primer*. London: The Biomimicry Institute and the Biomimicry Guild
- Bidlack, J. E., Jansky, S. H., and Stern, K. R. (2011). "Chapter 5: Roots and Soils," in *Stern's Introductory Plant Biology*. 12th ed. New York, NY: McGraw-Hill, 622.
- Blancaflor, E. B., and Masson, P. H. (2003). Plant Gravitropism. Unraveling the Ups and Downs of a Complex Process. *Plant Physiol.* 133 (4), 1677–1690. doi:10.1104/pp.103.032169
- Bloch, R. (1952). Wound Healing in Higher Plants. II. *Bot. Rev.* 18 (10), 655–679. doi:10.1007/bf02957556
- Bulleri, F., and Chapman, M. G. (2010). The Introduction of Coastal Infrastructure as a Driver of Change in Marine Environments. *J. Appl. Ecol.* 47 (1), 26–35. doi:10.1111/j.1365-2664.2009.01751.x
- Burrall, M., DeJong, J. T., Martinez, A., and Wilson, D. W. (2020). Vertical Pullout Tests of Orchard Trees for Bio-Inspired Engineering of Anchorage and Foundation Systems. *Bioinspiration Biomimetics* 16 (1), 016009. doi:10.1061/9780784482834.026
- Calderón, A. A., Ugalde, J. C., Chang, L., Zagal, J. C., and Pérez-Arancibia, N. O. (2016). "Design, Fabrication and Control of a Multi-Material-Multi-Actuator Soft Robot Inspired by Burrowing Worms," in 2016 IEEE International Conference on Robotics and Biomimetics (ROBIO). 31–38.
- Calderón, A. A., Ugalde, J. C., Chang, L., Zagal, J. C., and Pérez-Arancibia, N. O. (2019). An Earthworm-Inspired Soft Robot with Perceptive Artificial Skin. *Bioinspiration Biomimetics* 14 (5), 056012. doi:10.1088/1748-3190/ab1440
- Chen, R., Rosen, E., and Masson, P. H. (1999). Gravitropism in Higher Plants. *Plant Physiol.* 120 (2), 343–350. doi:10.1104/pp.120.2.343
- Cheshire, M. V. (1979). *Nature and Origin of Carbohydrates in Soils*. London; New York: Academic Press.
- Correa, J., Postma, J. A., Watt, M., and Wojciechowski, T. (2019). Soil Compaction and the Architectural Plasticity of Root Systems. *J. Exp. Bot.* 70 (21), 6019–6034. doi:10.1093/jxb/erz383
- Coutts, M. P. (1983). Root Architecture and Tree Stability. *Plant Soil* 71, 171–188. doi:10.1007/bf02182653
- Cremaldi, J. C., and Bhushan, B. (2018). Bioinspired Self-Healing Materials: Lessons from Nature. *Beilstein J. Nanotechnol.* 9 (1), 907–935. doi:10.3762/bjnano.9.85
- Crook, M., and Ennos, A. R. (1998). The Increase in Anchorage with Tree Size of the Tropical Tap Rooted Tree *Mallotus Wrayi*, King (Euphorbiaceae). *Ann. Bot.* 82 (3), 291–296. doi:10.1006/anbo.1998.0678
- Crook, M. J., Ennos, A. R., and Banks, J. R. (1997). The Function of Buttress Roots: a Comparative Study of the Anchorage Systems of Buttressed (*Aglaia* and *Nephelium* Ramboutanspecies) and Non-buttressed (*Mallotus Wrayi*) Tropical Trees. *J. Exp. Bot.* 48 (9), 1703–1716. doi:10.1093/jxb/48.9.1703
- Cucchi, V., Meredieu, C., Stokes, A., Berthier, S., Bert, D., Najjar, M., et al. (2004). Root Anchorage of Inner and Edge Trees in Stands of Maritime Pine (*Pinus Pinaster* Ait.) Growing in Different Podzolic Soil Conditions. *Trees* 18 (4), 460–466. doi:10.1007/s00468-004-0330-2
- Czarnes, S., Hallett, P. D., Bengough, A. G., and Young, I. M. (2000). Root- and Microbial-Derived Mucilages Affect Soil Structure and Water Transport. *Eur. J. Soil Sci.* 51 (3), 435–443. doi:10.1046/j.1365-2389.2000.00327.x
- Dade-Robertson, M., Mitrani, H., Corral, J. R., Zhang, M., Hernan, L., Guyet, A., et al. (2018). Design and Modelling of an Engineered Bacteria-Based, Pressure-Sensitive Soil. *Bioinspiration Biomimetics* 13 (4), 046004. doi:10.1088/1748-3190/aabe15
- Danjon, F., Barker, D. H., Drexhage, M., and Stokes, A. (2008). Using Three-Dimensional Plant Root Architecture in Models of Shallow-Slope Stability. *Ann. Bot.* 101 (8), 1281–1293. doi:10.1093/aob/mcm199
- Das, B. M. (2007). *Principles of Foundation Engineering*. 6th edition. Florence, KY, United States: Cengage Learning, Inc.
- DeJong, J. T., Fritzges, M. B., and Nüsslein, K. (2006). Microbially Induced Cementation to Control Sand Response to Undrained Shear. *J. Geotech. Geoenviron. Eng.* 132 (11), 1381–1392. doi:10.1061/(asce)1090-0241(2006)132:11(1381)
- DeJong, J., Tibbett, M., and Fourie, A. (2015). Geotechnical Systems that Evolve with Ecological Processes. *Environ. Earth Sci.* 73 (3), 1067–1082. doi:10.1007/s12665-014-3460-x
- Del Dottore, E., Sadeghi, A., Mondini, A., Mattoli, V., and Mazzolai, B. (2018). Toward Growing Robots: A Historical Evolution from Cellular to Plant-Inspired Robotics. *Front. Robotics AI* 5, 16. doi:10.3389/frobt.2018.00016
- Dinan, T. (2017). Projected Increases in Hurricane Damage in the United States: The Role of Climate Change and Coastal Development. *Ecol. Econ.* 138 (August), 186–198. doi:10.1016/j.ecolecon.2017.03.034
- Dottore, E. D., Mondini, A., Sadeghi, A., Mattoli, V., and Mazzolai, B. (2018). An Efficient Soil Penetration Strategy for Explorative Robots Inspired by Plant Root Circumnutation Movements. *Bioinspiration Biomimetics* 13 (1), 015003. doi:10.1088/1748-3190/AA9998
- Drew, M. C., and Saker, L. R. (1975). Nutrient Supply and the Growth of the Seminal Root System in Barley. *J. Exp. Bot.* 26 (1), 79–90. doi:10.1093/jxb/26.1.79

- Duarte, C. M. (2009). "Introduction," in *Global Loss of Coastal Habitats: Rates, Causes and Consequences*. Madrid, Spain: Fundación BBVA, 15–24.
- Dupray, S., and Roberts, J. (2009). Review of the Use of Concrete in the Manufacture of Concrete Armour Units. *Proc. Coasts, Mar. Struct. Breakwaters* 14, 260–271. doi:10.1680/cmsb.41301.0021
- Dupuy, L., Fourcaud, T., Lac, P., and Stokes, A. (2003). Modelling the Influence of Morphological and Mechanical Properties on the Anchorage of Root Systems." Proceedings of the International Conference Wind Effect on Trees, Karlsruhe, September 16–18, 2003. Universität Karlsruhe. Available at: https://agritrop.cirad.fr/531131/?fbclid=IwAR0ohEvINr-2nODiFiKm8x_9RsCMOJ8jdmfEfcMswbTSoHyipDHF7aI858.
- Duraiappah, A. K., Naeem, A., Agardy, T., Ash, N. J., Cooper, H. D., Diaz, S., et al. (2005). Ecosystems and Human Well-Being: Biodiversity Synthesis; a Report of the Millennium Ecosystem Assessment. Available at: <https://experts.umn.edu/en/publications/ecosystems-and-human-well-being-biodiversity-synthesis-a-report-o>
- Ennos, A. R., Crook, M. J., and Grimshaw, C. (1993). The Anchorage Mechanics of Maize, *Zea Mays*. *J. Exp. Bot.* 44 (258), 147–153. doi:10.1093/jxb/44.1.147
- Ennos, A. R., and Fitter, A. H. (1992). Comparative Functional Morphology of the Anchorage Systems of Annual Dicots. *Funct. Ecol.* 6 (1), 71–78. doi:10.2307/2389773
- Ennos, A. R. (1989). The Mechanics of Anchorage in Seedlings of Sunflower, *Helianthus Annuus* L. *New Phytol.* 113 (2), 185–192. doi:10.1111/j.1469-8137.1989.tb04705.x
- Ennos, A. R. (2000). The Mechanics of Root Anchorage. *The Mech. Root Anchorage* 33, 133–157. doi:10.1016/s0065-2296(00)33042-7
- Ennos, A. (1991). The Mechanics of Anchorage in Wheat *Triticum Aestivum* L.: II. Anchorage of Mature Wheat against Lodging. *J. Exp. Bot.* 42 (245), 1607–1613. doi:10.1093/jxb/42.12.1607
- Fayemi, P. E., Wanieck, K., Zollfrank, C., Maranzana, N., and Aoussat, A. (2017). Biomimetics: Process, Tools and Practice. *Bioinspiration Biomimetics* 12, 101002. doi:10.1088/1748-3190/12/1/011002
- Ferrario, F., Beck, M. W., Storlazzi, C. D., Micheli, F., Shepard, C. C., and Airoldi, L. (2014). The Effectiveness of Coral Reefs for Coastal Hazard Risk Reduction and Adaptation. *Nat. Commun.* 5, 3794. doi:10.1038/ncomms4794
- Finkel, S., and Ido, S. (2017). Methods and Matrices for Promoting Fauna and Flora Growth. U.S. Patent Office 9,538,732. Issued January 10, 2017.
- Frost, D. J., Alejandro, M., Mallett, S. D., Roozbahani, M. M., and DeJong, J. T. (2017). Intersection of Modern Soil Mechanics with Ants and Roots. *Geotech. Front.* 14, 900–909. doi:10.1061/9780784480472.096
- Frost, J. D., DeJong, J. T., and Recalde, M. (2002). Shear Failure Behavior of Granular-Continuum Interfaces. *Eng. Fracture Mech.* 69 (17), 2029–2048. doi:10.1016/s0013-7944(02)00075-9
- Galloway, A. F., Knox, P., and Krause, K. (2020). Sticky Mucilages and Exudates of Plants: Putative Microenvironmental Design Elements with Biotechnological Value. *New Phytol.* 225 (4), 1461–1469. doi:10.1111/nph.16144
- Gippel, C. J., Finlayson, B. L., and O'Neill, I. C. (1992). *The Hydraulic Basis of Snag Management*. London: Centre for Environmental Applied Hydrology, Department of Civil and Agricultural Engineering.
- Goodsell, P., Chapman, M., and Underwood, A. (2007). Differences between Biota in Anthropogenically Fragmented Habitats and in Naturally Patchy Habitats. *Mar. Ecol. Prog. Ser.* 351 (December), 15–23. doi:10.3354/meps07144
- Graham, B. F., and Bormann, F. H. (1966). Natural Root Grafts. *Bot. Rev.* 32 (3), 255–292. doi:10.1007/bf02858662
- Grant, C., and Dexter, A. (1989). Generation of Microcracks in Molded Soils by Rapid Wetting. *Soil Res.* 27 (1), 169–182. doi:10.1071/sr9890169
- Greacen, E. L., Farrell, D. A., and Cockroft, B. (1968). "Soil Resistance to Metal Probes and Plant Roots," in *Transactions of the 9th International Congress on Soil Science*. Adelaide, SA. 769–779.
- Greer, J. D., Morimoto, T. K., Okamura, A. M., and Hawkes, E. W. (2019). A Soft, Steerable Continuum Robot that Grows via Tip Extension. *Soft Robotics* 6 (1), 95–108. doi:10.1089/soro.2018.0034
- Griggs, G. B., and Fulton-Bennett, K. (1988). Rip Rap Revetments and Seawalls and Their Effectiveness along the Central California Coast. *Shore Beach* 56 (2), 3–11.
- Grimm, N. B., Faeth, S. H., Golubiewski, N. E., Redman, C. L., Wu, J., Bai, X., et al. (2008). Global Change and the Ecology of Cities. *Science* 319 (5864), 756–760. doi:10.1126/science.1150195
- Hanson, H., and Lindh, G. (1993). Coastal Erosion: An Escalating Environmental Threat. *Ambio* 11, 188–195.
- Hart, J. W. (1990). *Plant Tropisms: And Other Growth Movements*. Netherlands: Springer.
- Hawkes, E. W., Blumenschein, L. H., Greer, J. D., and Okamura, A. M. (2017). A Soft Robot that Navigates its Environment through Growth. *Sci. Robotics* 2 (8), eaan3028. doi:10.1126/scirobotics.aan3028
- Hoad, S. P., Russell, G., Lucas, M. E., and Bingham, I. J. (2001). "The Management of Wheat, Barley, and Oat Root Systems," in *Advances in Agronomy*. Cambridge: Academic Press. 74, 193–246. doi:10.1016/s0065-2113(01)74034-5
- Hobst, L., and Zajíc, J. (1983). "Anchoring of Foundations," in *Anchoring of Rock and Soil, in Development of Geotechnical Engineering*, 33, 497–513.
- Hodge, A., Berta, G., Doussan, C., Merchan, F., and Crespi, M. (2009). Plant Root Growth, Architecture and Function. *Plant and Soil* 321 (1–2), 153–187. doi:10.1007/s11104-009-9929-9
- Hogarth, P. J. (2015). *The Biology of Mangroves and Seagrasses*. Oxford: Oxford University Press.
- Jernstedt, J. A. (1984). Root Contraction in Hyacinth. I. Effects of IAA on Differential Cell Expansion. *Am. J. Bot.* 71 (8), 1080–1089. doi:10.1002/j.1537-2197.1984.tb11960.x
- Johnsson, A. (1997). Circumnutations: Results from Recent Experiments on Earth and in Space. *Planta Suppl.* 1 (203), S147–S158. doi:10.1007/pl00008103
- Jonkers, H. M. (2007). "Self Healing Concrete: A Biological Approach," in *Springer Series in Materials Science*. Berlin: Springer-Verlag, 100, 195–204. doi:10.1007/978-1-4020-6250-6_9
- Kazemi, A., Van de Riet, K., and Curet, O. M. (2017). Hydrodynamics of Mangrove-type Root Models: The Effect of Porosity, Spacing Ratio and Flexibility. *Bioinspiration Biomimetics* 12 (5), 056003. doi:10.1088/1748-3190/aa7ccf
- Keeley, J. E. (1988). Population Variation in Root Grafting and a Hypothesis. *Oikos* 52 (3), 364–366. doi:10.2307/3565212
- Khosravi, A., Martinez, A., DeJong, J., and Wilson, D. (2018). "Discrete Element Simulations of Bio-Inspired Self-Burrowing Probes in Sands of Varying Density," in *Proceeding of Biomediated and Bioinspired Geotechnics (B2G) Conference*. Atlanta, GA.
- Kiss, J. Z. (2006). Up, Down, and All Around: How Plants Sense and Respond to Environmental Stimuli. *Proc. Natl. Acad. Sci.* 103 (4), 829–830. doi:10.1073/pnas.05104711102
- Koch, E. W., Barbier, E. B., Silliman, B. R., Reed, D. J., Perillo, G. M., Hacker, S. D., et al. (2009). Non-linearity in Ecosystem Services: Temporal and Spatial Variability in Coastal Protection. *Front. Ecol. Environ.* 7 (1), 29–37. doi:10.1890/080126
- Kumar, H., Kulkarni, D., and Srimathi, R. A. (1985). Natural Grafts in Sandal. *Indian J. For.* 12, 33.
- Larson, M. G., Booth, D. B., and Morley, S. A. (2001). Effectiveness of Large Woody Debris in Stream Rehabilitation Projects in Urban Basins. *Ecol. Eng.* 18 (2), 211–226. doi:10.1016/s0925-8574(01)00079-9
- Lecompte, F., and Pagès, L. (2007). Apical Diameter and Branching Density Affect Lateral Root Elongation Rates in Banana. *Environ. Exp. Bot.* 59 (3), 243–251. doi:10.1016/j.envexpbot.2006.01.002
- Lenau, T. A., Metz, A. L., and Hesselberg, T. (2018). Paradigms for Biologically Inspired Design. *Bioinspiration, Biomimetics, and Bioreplication VIII* 11, 1059302. doi:10.1117/12.2296560
- Li, Q. (2018). *Forest Bathing: How Trees Can Help You Find Health and Happiness*. Oxford: Viking.
- Li, V. C., and Yang, E.-H. (2007). "Self Healing in Concrete Materials," in *Springer Series in Materials Science*. Berlin: Springer-Verlag, 100, 161–193. doi:10.1007/978-1-4020-6250-6_8
- Liang, T., Knappett, J. A., Bengough, A. G., and Ke, Y. X. (2017). Small-Scale Modelling of Plant Root Systems Using 3D Printing, with Applications to Investigate the Role of Vegetation on Earthquake-Induced Landslides. *Landslides* 14 (5), 1747–1765. doi:10.1007/s10346-017-0802-2
- Linkohr, B. I., Williamson, L. C., Fitter, A. H., and Leyser, H. M. O. (2002). Nitrate and Phosphate Availability and Distribution Have Different Effects on Root System Architecture of Arabidopsis. *Plant J.* 29 (6), 751–760. doi:10.1046/j.1365-3113.2002.01251.x

- Lotze, H. K., Lenihan, H. S., Bourque, B. J., Bradbury, R. H., Cooke, R. G., Kay, M. C., et al. (2006). Depletion, Degradation, and Recovery Potential of Estuaries and Coastal Seas. *Science* 312 (5781), 1806–1809. doi:10.1126/science.1128035
- Lynch, J. P., and Brown, K. M. (2001). “Topsoil Foraging—An Architectural Adaptation of Plants to Low Phosphorus Availability. *Plant and Soil* 237 (2), 225–237. doi:10.1023/a:1013324727040
- Malamy, J. E. (2005). Intrinsic and Environmental Response Pathways that Regulate Root System Architecture. *Plant Cell Environ* 28 (1), 67–77. doi:10.1111/j.1365-3040.2005.01306.x
- Manandhar, S., and Yasufuku, N. (2012). Analytical Model for the End-Bearing Capacity of Tapered Piles Using Cavity Expansion Theory. *Adv. Civil Eng.* 2012, 1–9. doi:10.1155/2012/749540
- Mao, Y., Wang, Y., McCormack, M. L., Rowe, N., Deng, X., Yang, X., et al. (2018). Mechanical Traits of Fine Roots as a Function of Topology and Anatomy. *Ann. Bot.* 122 (7), 1103–1116. doi:10.1093/aob/mcy076
- Martinez, A., O'Hara, K., Sinha, S. M., Wilson, D., and Ziotopoulou, K. (2018). “Monotonic and Cyclic Centrifuge Testing of Snake Skin-Inspired Piles,” in *Proceeding of Biomediated and Bioinspired Geotechnics (B2G) Conference*. Atlanta, GA.
- Martinez, A., Palumbo, S., and Todd, B. D. (2019). Bioinspiration for Anisotropic Load Transfer at Soil-Structure Interfaces. *J. Geotech. Geoenviron. Eng.* 145 (10), 04019074. doi:10.1061/(asce)gt.1943-5606.0002138
- Martinez, A., and Frost, J. D. (2017). The Influence of Surface Roughness Form on the Strength of Sand-Structure Interfaces. *Géotechnique Lett.* 7 (1), 104–111. doi:10.1680/jgele.16.00169
- Mattheck, C., Sörensen, J., and Bethge, K. (2006). A Graphic Way for Notch Shape Optimization. *WIT Trans. Ecol. Environ.* 87, 13–21. doi:10.2495/DN060021
- Mattheck, C., Bethge, K., and Erb, D. (1993). Failure Criteria for Trees. *Arboricultural J.* 17 (2), 201–209. doi:10.1080/03071375.1993.9746963
- Mayer-Pinto, M., Dafforn, K. A., and Johnston, E. L. (2019). A Decision Framework for Coastal Infrastructure to Optimize Biotic Resistance and Resilience in a Changing Climate. *Bioscience* 69 (10), 833–843. doi:10.1093/biosci/biz092
- Mayer-Pinto, M., Johnston, E. L., Bugnot, A. B., Glasby, T. M., Airolidi, L., Mitchell, A., et al. (2017). Building ‘blue’: An Eco-Engineering Framework for Foreshore Developments. *J. Environ. Manage.* 189, 109–114. doi:10.1016/j.jenvman.2016.12.039
- Mazda, Y., Magi, M., Kogo, M., and Hong, P. N. (1997). Mangroves as a Coastal Protection from Waves in the Tong King Delta, Vietnam. *Mangroves and Salt Marshes* 1 (2), 127–135. doi:10.1023/a:1009928003700
- McLachlan, A., and Defeo, O. (2018). “Chapter 15—Human Impacts,” in *The Ecology of Sandy Shores*. Third Edition, Editor A. McLachlan and O. Defeo (Academic Press), 375–420. doi:10.1016/B978-0-12-809467-9.00015-1
- Menges, A., and Reichert, S. (2015). Performative Wood: Physically Programming the Responsive Architecture of theHygroScopeand HygroSkin Projects. *Archit. Des.* 85 (5), 66–73. doi:10.1002/ad.1956
- Migliaccio, F., Tassone, P., and Fortunati, A. (2013). Circumnutation as an Autonomous Root Movement in Plants. *Am. J. Bot.* 100 (1), 4–13. doi:10.3732/ajb.1200314
- Minorsky, P. V. (2003). The Hot and the Classic. *Plant Physiol.* 132 (4), 1779–1780. doi:10.1104/pp.900085
- Mirzaali, M. J., Janbaz, S., Strano, M., Vergani, L., and Zadpoor, A. A. (2018). Shape-Matching Soft Mechanical Metamaterials. *Sci. Rep.* 8 (1), 1–7. doi:10.1038/s41598-018-19381-3
- Montgomery, D. R., Collins, B. D., Buffington, J. M., and Abbe, T. B. (2003). Geomorphic Effects of Wood in Rivers. *Am. Fish. Soc. Symp.* 37, 21–47.
- Mugnai, S., Azzarello, E., Masi, E., Pandolfi, C., and Mancuso, S. (2007). “Nutation in Plants,” in *Rhythms in Plants: Phenomenology, Mechanisms, and Adaptive Significance*. Editor S. Mancuso and S. Shabala (Berlin, Heidelberg: Springer Berlin Heidelberg), 77–90. doi:10.1007/978-3-540-68071-0_4
- Narayan, S., Beck, M. W., Reguero, B. J., Losada, I. J., Van Wesenbeeck, B., Pontee, N., et al. (2016). The Effectiveness, Costs and Coastal Protection Benefits of Natural and Nature-Based Defences. *PLoS One* 11 (5), e0154735. doi:10.1371/journal.pone.0154735
- Nicoll, B. C., and Dunn, A. J. (2000). “The Effects of Wind Speed and Direction on Radial Growth of Structural Roots,” in *The Supporting Roots of Trees and Woody Plants: Form, Function and Physiology*. Dordrecht: Springer Netherlands, 219–225. doi:10.1007/978-94-017-3469-1_21
- Nicoll, B. C., Achim, A., Mochan, S., and Gardiner, B. A. (2005). Does Steep Terrain Influence Tree Stability? A Field Investigation. *Can. J. For. Res.* 35 (10), 2360–2367. doi:10.1139/x05-157
- Nicoll, B. C., and Ray, D. (1996). Adaptive Growth of Tree Root Systems in Response to Wind Action and Site Conditions. *Tree Physiol.* 16 (11–12), 891–898. doi:10.1093/treephys/16.11-12.891
- Nicoll, B. C. (2006). *Effects of Soil, Terrain and Wind Climate on Tree Root System Development and Anchorage*. Holyrood: The University of Edinburgh. doi:10.1201/b13374
- North, G. B., Brinton, E. K., and Garrett, T. Y. (2008). Contractile Roots in Succulent Monocots: Convergence, Divergence and Adaptation to Limited Rainfall. *Plant Cell Environ.* 31 (8), 1179–1189. doi:10.1111/j.1365-3040.2008.01832.x
- Ohira, W., Honda, K., Nagai, M., and Ratanasuwana, A. (2013). Mangrove Stilt Root Morphology Modeling for Estimating Hydraulic Drag in Tsunami Inundation Simulation. *Trees* 27 (1), 141–148. doi:10.1007/s00468-012-0782-8
- Ozkan-Aydin, Y., Murray-Cooper, M., Aydin, E., McCaskey, E. N., Naclerio, N., Hawkes, E. W., et al. (2019). “Nutation AIDS Heterogeneous Substrate Exploration in a Robophysical Root,” in *RoboSoft 2019–2019 IEEE International Conference on Soft Robotics*. New York: Institute of Electrical and Electronics Engineers Inc, 172–177.
- Perkol-Finkel, S., and Sella, I. (2015). “Harnessing Urban Coastal Infrastructure for Ecological Enhancement,” in *Proceedings of the Institution of Civil Engineers-Maritime Engineering*. Westminster: Thomas Telford Ltd, 168, 102–110.
- Pierret, A., Moran, C. J., and Pankhurst, C. E. (1999). Differentiation of Soil Properties Related to the Spatial Association of Wheat Roots and Soil Macropores. *Plant and Soil* 211 (1), 51–58. doi:10.1023/a:1004490800536
- Pütz, N. (2002). “Contractile Roots,” in *Plant Roots. The Hidden Half*. 3rd ed. Editors Y. Waisel, A. Eshel, and U. Kafkafi (New York, NY: Marcel Dekker), 975–987. doi:10.1201/9780203909423.ch54
- Rella, A. J., and Miller, J. K. (2012). “Engineered Approaches for Limiting Erosion Along Sheltered Shorelines: A Review of Existing Methods,” in *Mitigating Shoreline Erosion Along the Hudson River Estuary's Sheltered Coasts*. Hudson River Valley Greenway Hudson River National Estuarine Research Reserve.
- Reubens, B., Poesen, J., Danjon, F., Geudens, G., and Muys, B. (2007). The Role of Fine and Coarse Roots in Shallow Slope Stability and Soil Erosion Control with a Focus on Root System Architecture: A Review. *Trees Struct. Funct.* 21 (4), 385–402. doi:10.1007/s00468-007-0132-4
- Rigg, G. B., and Harrar, E. S. (1931). The Root Systems of Trees Growing in Sphagnum. *Am. J. Bot.* 18 (6), 391–397. doi:10.1002/j.1537-2197.1931.tb09598.x
- Robertson, A. I., and Alongi, D. M. (1992). *Tropical Mangrove Ecosystems. Coastal and Estuarine Studies*. 41. Washington, DC: American Geophysical Union.
- Sadeghi, A., Tonazzini, A., Popova, L., and Mazzolai, B. (2014). A Novel Growing Device Inspired by Plant Root Soil Penetration Behaviors. *PLoS ONE* 9 (2), e90139. doi:10.1371/journal.pone.0090139
- Sadeghi, A., Mondini, A., and Mazzolai, B. (2017). Toward Self-Growing Soft Robots Inspired by Plant Roots and Based on Additive Manufacturing Technologies. *Soft Robotics* 4 (3), 211–223. doi:10.1089/soro.2016.0080
- Scape/Landscape Architecture PLLC; Parsons Brinckerhoff, ; Stevens Institute of Technology; Ocean and Coastal Consultants, Searc Consulting; The New York Harbor School; LOT-EK, MTWTF; Paul Greenberg (2014). *Living Breakwaters: Staten Island and Raritan Bay*. IP Edition. Rebuild by Design. Available at: <http://www.rebuildbydesign.org/our-work/all-proposals/winning-projects/ny-living-breakwaters>
- Silvester, R. (1972). Technical Note. Wave Reflection at Sea Walls and Breakwaters. *Proc. Inst. Civil Eng.* 51 (1), 123–131. doi:10.1680/iicep.1972.5988
- Steeves, T. A., and Sussex, I. M. (1989). “The Root,” in *Patterns in Plant Development*. Cambridge: Cambridge University Press, 229–254. doi:10.1017/cbo9780511626227.013
- Stokes, A., Atger, C., Bengough, A. G., Fourcaud, T., and Sidle, R. C. (2009). Desirable Plant Root Traits for Protecting Natural and Engineered Slopes against Landslides. *Plant and Soil* 324 (1–2), 1–30. doi:10.1007/s11104-009-0159-y
- Stokes, A. (2002). “Biomechanics of Tree Root Anchorage,” in *Plant Roots*. Boca Raton, Florida: CRC Press, 297–314.

- Stokes, A., Fitter, A. H., and Courts, M. P. (1995). Responses of Young Trees to Wind and Shading: Effects on Root Architecture. *J. Exp. Bot.* 46 (9), 1139–1146. doi:10.1093/jxb/46.9.1139
- Stokes, A., Nicoll, B. C., Coutts, M. P., and Fitter, A. H. (1997). Responses of Young Sitka Spruce Clones to Mechanical Perturbation and Nutrition: Effects on Biomass Allocation, Root Development, and Resistance to Bending. *Can. J. For. Res.* 27 (7), 1049–1057. doi:10.1139/x97-041
- Stolzy, L. H., and Barley, K. P. (1968). Mechanical Resistance Encountered by Roots Entering Compact Soils. *Soil Sci.* 105 (5), 297–301. doi:10.1097/00010694-196805000-00003
- Strain, E. M. A., OlabarriaMayer-Pinto, C. M., Mayer-Pinto, M., Cumbo, V., Morris, R. L., Bugnot, A. B., et al. (2018). Eco-Engineering Urban Infrastructure for Marine and Coastal Biodiversity: Which Interventions Have the Greatest Ecological Benefit?. *J. Appl. Ecol.* 55, 426–441. doi:10.1111/1365-2664.12961
- Suedel, B., Banks, C., Friona, T., Bijhouwer, P., and Ruby, R. (2016). “Making Sound Infrastructure Investments: Increasing Value on Great Lakes Breakwaters through the USACE Engineering with Nature Initiative,” in Presented at the TRB-CMTS 2016 Conference, June.
- Svoboda, C. D., and Russell, K. (2011). “Flume Analysis of Engineered Large Wood Structures for Scour Development and Habitat,” in World Environmental and Water Resources Congress 2011. Palm Springs, California, United States: American Society of Civil Engineers, 2572–2581.
- Tamasi, E., Stokes, A., Lasserre, B., Danjon, F., Berthier, S., Fourcaud, T., et al. (2005). Influence of Wind Loading on Root System Development and Architecture in Oak (*Quercus Robur* L.) Seedlings. *Trees* 19 (4), 374–384. doi:10.1007/s00468-004-0396-x
- Tamura, Y., and Cao, S. (2010). Climate Change and Disaster Risk Reduction,” in Proceedings of the 2010 APEC-WW and IG-WRDRR Joint Workshop Wind-Related Disaster Risk Reduction (WRDRR) Activities in Asia-Pacific Region and Cooperative Actions, Incheon, Korea.
- Tatsumi, J., Yamauchi, A., and Kono, Y. (1989). Fractal Analysis of Plant Root Systems. *Ann. Bot.* 64 (5), 499–503. doi:10.1093/oxfordjournals.aob.a087871
- Tisdall, J., Cockroft, B., and Uren, N. (1978). The Stability of Soil Aggregates as Affected by Organic Materials, Microbial Activity and Physical Disruption. *Soil Res.* 16 (1), 9–17. doi:10.1071/sr9780009
- Tomlinson, P. B. (2016). *The Botany of Mangroves*. Cambridge: Cambridge University Press. doi:10.1017/cbo9781139946575
- Twilley, R. R., and Day, J. W. (2013). “Mangrove Wetlands,” in *Estuarine Ecology*. 2a Ed. Hoboken, New Jersey: Wiley-Blackwell, John Wiley & Sons, Inc. Publications, 165–202.
- USACE; Army Engineer Waterways Experiment Station Coastal Engineering Research Center (1984). *Shore Protection Manual*. Washington, D.C.: US Government Printing Office.
- USBR and ERDC (2016). National Large Wood Manual: Assessment, Planning, Design, and Maintenance of Large Wood in Fluvial Ecosystems: Restoring Process, Function, and Structure.
- Van Tittelboom, K., Wang, J., Araújo, M., Snoeck, D., Gruyaert, E., Debbaut, B., et al. (2016). Comparison of Different Approaches for Self-Healing Concrete in a Large-Scale Lab Test. *Construction Building Mater.* 107, 125–137. doi:10.1016/j.conbuildmat.2015.12.186
- Van Wijngaarden, W. K., Vermolen, F. J., van Meurs, G. A. M., and Vuijk, C. (2011). Modelling Biogrout: A New Ground Improvement Method Based on Microbial-Induced Carbonate Precipitation. *Transp. Porous Med.* 87 (2), 397–420. doi:10.1007/s11242-010-9691-8
- Vincent, J. F. V., Bogatyreva, O. A., Bogatyrev, N. R., Bowyer, A., and Pahl, A.-K. (2006). Biomimetics: Its Practice and Theory. *J. R. Soc. Interf.* 3 (9), 471–482. doi:10.1098/rsif.2006.0127
- Waldron, L. J. (1977). The Shear Resistance of Root-Permeated Homogeneous and Stratified Soil. *Soil Sci. Soc. America J.* 41 (5), 843–849. doi:10.2136/sssaj1977.03615995004100050005x
- Wallace, J. B., and Benke, A. C. (1984). Quantification of Wood Habitat in Subtropical Coastal Plain Streams. *Can. J. Fish. Aquat. Sci.* 41 (11), 1643–1652. doi:10.1139/f84-203
- Whiffin, V. S., van Paassen, L. A., and Harkes, M. P. (2007). Microbial Carbonate Precipitation as a Soil Improvement Technique. *Geomicrobiol. J.* 24 (5), 417–423. doi:10.1080/01490450701436505
- Woodruff, Z. J., Brenner, P., Buccellato, A. P. C., and Go, D. B. (2014). Environmentally Opportunistic Computing: A Distributed Waste Heat Reutilization Approach to Energy-Efficient Buildings and Data Centers. *Energy Buildings* 69, 41–50. doi:10.1016/j.enbuild.2013.09.036
- Wright, J. P., Jones, C. G., and Flecker, A. S. (2002). An Ecosystem Engineer, the Beaver, Increases Species Richness at the Landscape Scale. *Oecologia* 132 (1), 96–101. doi:10.1007/s00442-002-0929-1
- Yang, J.-L., and Zhang, G.-L. (2011). Water Infiltration in Urban Soils and its Effects on the Quantity and Quality of Runoff. *J. Soils Sediments* 11 (5), 751–761. doi:10.1007/s11368-011-0356-1
- Young, T. P., and Perkocha, V. (1994). Treefalls, Crown Asymmetry, and Buttresses. *J. Ecol.* 82 (2), 319–324. doi:10.2307/2261299

Conflict of Interest: The authors declare that the research was conducted in the absence of any commercial or financial relationships that could be construed as a potential conflict of interest.

Copyright © 2021 Stachew, Houette and Gruber. This is an open-access article distributed under the terms of the Creative Commons Attribution License (CC BY). The use, distribution or reproduction in other forums is permitted, provided the original author(s) and the copyright owner(s) are credited and that the original publication in this journal is cited, in accordance with accepted academic practice. No use, distribution or reproduction is permitted which does not comply with these terms.

Advantages of publishing in Frontiers



OPEN ACCESS

Articles are free to read
for greatest visibility
and readership



FAST PUBLICATION

Around 90 days
from submission
to decision



HIGH QUALITY PEER-REVIEW

Rigorous, collaborative,
and constructive
peer-review



TRANSPARENT PEER-REVIEW

Editors and reviewers
acknowledged by name
on published articles

Frontiers

Avenue du Tribunal-Fédéral 34
1005 Lausanne | Switzerland

Visit us: www.frontiersin.org

Contact us: frontiersin.org/about/contact



REPRODUCIBILITY OF RESEARCH

Support open data
and methods to enhance
research reproducibility



DIGITAL PUBLISHING

Articles designed
for optimal readership
across devices



FOLLOW US

@frontiersin



IMPACT METRICS

Advanced article metrics
track visibility across
digital media



EXTENSIVE PROMOTION

Marketing
and promotion
of impactful research



LOOP RESEARCH NETWORK

Our network
increases your
article's readership